In-silico evaluation of mutations in GSK-3β related to wound physiology and fabrication of sustainable biomaterials and therapies for improved wound healing and soft tissue engineering

Thesis submitted by

Pratik Das

(Registration No.: D-7/ISLM/30/21 dated: 13th April, 2021)

For Completion & the Requirement for the Degree Of
Doctor of Philosophy
(Engineering)

Under the Guidance of

Dr. Piyali Basak
Director & Associate Professor,
School of Bioscience and Engineering,
Jadavpur University

&

Prof. Samit Kumar Nandi
ICAR National Professor
Department of Veterinary Surgery & Radiology,
West Bengal University of Animal & Fishery Sciences

School of Bioscience and Engineering
Faculty of Interdisciplinary Studies, Law & Management
Jadavpur University, Kolkata, West Bengal, India

2024

1. Title of the thesis:

In-silico evaluation of mutations in GSK-3β related to wound physiology and Fabrication of Sustainable Biomaterials and therapies for improved wound healing and soft tissue engineering

2. Name, Designation and Institution of Supervisors:

Dr.Piyali Basak

Associate Professor

School of Bio-Science and Engineering

Jadavpur University

Kolkata -700032

&

Dr. Samit Kumar Nandi

ICAR National Professor

Department of Veterinary Surgery & Radiology,

West Bengal University of Animal and Fishery Sciences

Kolkata-700037

3. List of Publications

Pratik Das, Debajyoti Pal, Sudipta Roy, Shubhamitra Chaudhuri, Shyam Sundar Kesh, Piyali Basak, and Samit Kumar Nandi. "Unveiling advanced strategies for therapeutic stem cell interventions in severe burn injuries: a comprehensive review." International Journal of Surgery (2024): 10-1097.

Mishra, Priyanka Priyadarsini, **Pratik Das**, Sukarna Paul, Piyali Das, Suvendu Manna, Piyali Basak, Nigamananda Das, and Ajaya Kumar Behera. "Graphene oxide dots-loaded chitin flask:

A sustainable adsorbent for separating multiple dyes from water." Environmental Quality Management (2024).

Adhikari, Jaideep, Shalini Dasgupta, **Pratik Das**, D. A. Gouripriya, Ananya Barui, Piyali Basak, Manojit Ghosh, and Prosenjit Saha. "Bilayer regenerated cellulose/quaternized chitosan-hyaluronic acid/collagen electrospun scaffold for potential wound healing applications." International Journal of Biological Macromolecules261(2024):129661.

Pratik Das, Ranabir Majumder, Nandita Sen, Samit Kumar Nandi, Arabinda Ghosh, Mahitosh Mandal, and Piyali Basak. "A computational analysis to evaluate deleterious SNPs of GSK3β, a multifunctional and regulatory protein, for metabolism, wound healing, and migratory processes." International Journal of Biological Macromolecules (2023): 128262.

Biswas, Shreya, Tuhin Kahali, Anwesha Mukherjee, Debasmita Chakraborty, Chayan Guha, Tathagata Adhikary ,**Pratik Das**, Nandan Kumar Jana, Suvendu Manna, and Piyali Basak. "Enzymes analysis, degradation kinetics, response surface optimization and heavy metal tolerance of the biodegradation of malachite green by Stenotrophomonas koreensis."Bioremediation Journal (2022): 1-23

Patra, Shamayita, Piyali Basak, **Pratik Das**, and Samrat Paul. "A novel observation: effect of anionic gelatin nanoparticle on stromal cells." Journal of Biomaterials Science, Polymer Edition (2023): 1-15

Pratik Das, Taranga Chakravarty, Arka Jyoti Roy, Suvendu Manna, Samit K. Nandi, and Piyali Basak. "Sustainable development of Draksha-Beeja extract loaded gelatin and starch-based green and biodegradable mats for potential tissue engineering applications." Sustainable Chemistry and Pharmacy 34(2023):101134.

Pratik Das, Suvendu Manna, Shivam Roy, Samit K. Nandi, and Piyali Basak. "Polymeric biomaterials-based tissue engineering for wound healing: a systemic review." Burns & Trauma 11 (2023): tkac058

Pratik Das, Suvendu Manna, Ajaya K. Behera, Moumita Shee, Piyali Basak, and Amit Kumar Sharma. "Current synthesis and characterization techniques for clay-based polymer nano-composites and its biomedical applications: A review. "Environmental Research (2022): 113534.

Majumder, Ranabir, Chandan Kanta Das, Indranil Banerjee, Bikash Chandra Jena, Anik Mandal, **Pratik Das**, Anjan Kumar Pradhan et al. "Screening of the Prime bioactive compounds from Aloe vera as potential anti-proliferative agents targeting DNA." Computers in Biology and Medicine (2021): 105052.

Pratik Das, Tanusree Dutta, Suvendu Manna, Sravanthi Loganathan, and Piyali Basak. "Facile green synthesis of-genotoxic, nonhemolytic organometallic silver nanoparticles using extract of crushed, wasted, and spent Humulus lupulus(hops): Characterization,anti-bacterial, and anti-cancer studies." Environmental Research 204 (2022): 111962.

Pratik Das, Ranabir Majumder, Mahitosh Mandal, and Piyali Basak. "In-Silico approach for identification of effective and stable inhibitors for COVID-19 main protease (Mpro) from flavonoid based phytochemical constituents of Calendula officinalis." Journal of Biomolecular Structure and Dynamics 39, no. 16 (2021): 6265-6280.

Pratik Das, Krishanu Ghosal, Nandan Kumar Jana, Anwesha Mukherjee, and Piyali Basak. "Green synthesis and characterization of silver nanoparticles using belladonna mother tincture and its efficacy as a potential antibacterial and anti-inflammatory agent. "Materials Chemistry and Physics 228 (2019): 310-317

4. List of Patent

PATENT PUBLISHED: A process for formulation and optimization of winery waste derived proanthocyanidin rich grape seed extract loaded into starch glycerite gel for effective wound healing by modulating the inflammatory responses. Application No.: 202331073970

5. Conferences

Conference Presentation: Gelatin & Starch-based mat loaded with Draksha Beeja supplements: toward Sustainable development of green and bio-degradable mat-based scaffold for Tissue Engineering applications, International Symposium on Sustainable Urban Environment,2022,UPES Dehradun

Conference article: Adhikari, Jaideep, Manojit Ghosh, Pratik Das, Piyali Basak, and Prosenjit Saha. "Polycaprolactone assisted electrospinning of honey/betel with chitosan for tissue engineering." Materials Today: Proceedings (2022).

6. Book Chapter

Subramanian, Bhuvaneshwaran, **Pratik Das**, Shreya Biswas, Arpita Roy, and Piyali Basak. "Polymers for additive manufacturing and 4D-printing for tissue regenerative applications." In Advances in Biomedical Polymers and Composites, pp. 159-182. Elsevier, 2023.

Basak P, Adhikary T, **Das P**, Shee M, Dutta T, Biswas S, Paul S, Manna S. Cellulases in paper and pulp, brewing and food industries: Principles associated with its diverse applications. In Current Status and Future Scope of Microbial Cellulases 2021 Jan 1 (pp. 275-293). Elsevier.

Certificate from Supervisor

This is to certify that the thesis entitled "In-silico evaluation of mutations in GSK-3β related to wound physiology and fabrication of sustainable bio-materials and therapies for improved wound healing and soft tissue engineering" submitted by Pratik Das who got registered (registration no D7/ISLM/30/21 dated 13.04.2021) his name under the Faculty of Interdisciplinary Studies, Law & Management for the award PhD (Arts/Science/Engineering/Pharmacy) degree of Jadavpur University is based upon his/her work under the supervision of Dr. Piyali Basak (Director, School of Bioscience and Engineering) and Dr. Samit Kumar Nandi(ICAR National Professor, West Bengal University of Animal and Fishery Sciences) that neither his/her thesis nor any part of the thesis has been submitted for any degree/diploma or any other academic award anywhere before.

Signature of the Supervisor/s

Piyali Basak
12th July 2024

Dr. Piyali Basak
Director & Associate Professor,
School of Bioscience and Engineering,
Jadavpur University

DR. PIYALI BASAK
ASSOCIATE PROFESSOR
SCHOOL OF BIOSCIENCE & ENGG.
JADAVPUR UNIVERSITY
KOLKATA - 700032

Samit Kumar Nandi 12/07/2024

Prof. Samit Kumar Nandi
ICAR National Professor
Department of Veterinary Surgery & Radiology,
West Bengal University of Animal & Fishery Sciences

Prof. S. K. Nandi
ICAR National Professor
Dept. of Vety. Surgery & Radiology
Faculty of Veterinary. & Animal Sciences
West Bengal University of Animal & Fishery Sciences
37,.K. B. Sarani. Belgachia, Kolkata-700037

Statement of Originality

I, Pratik Das (D7/ISLM/30/21) registered on 13.04.2021 do hereby declare that this thesis entitled *"In-silico evaluation of mutations in GSK-3β related to wound physiology and fabrication of sustainable bio-materials and therapies for improved wound healing and soft tissue engineering"* contains literature survey and original research work done by the undersigned candidates as part of Doctoral studies.

All information in this thesis has been obtained and presented in accordance with existing academic rules and ethical conduct. I declare that, as required by thesis rules and conduct, I have fully cited and referred all materials and results that are not original to this work.

I also declare that I have checked this thesis as per the "Policy on Anti Plagiarism, Jadavpur University, 2019", and the level of similarity as checked by iThenticate software is 7% excluding self plagarsim.

Signature of the candidate with date:

Pratik Das
12.07.2024

Signature of the Supervisor with date and seal:

Piyali Basak
12th July 2024

DR. PIYALI BASAK
ASSOCIATE PROFESSOR
SCHOOL OF BIOSCIENCE & ENGG.
JADAVPUR UNIVERSITY
KOLKATA - 700032

1. **Dr. Piyali Basak**
   Director & Associate Professor,
   School of Bioscience and Engineering,
   Jadavpur University

Samit Kumar Nandi 12/07/2024

Prof. S. K. Nandi
ICAR National Professor
Dept. of Vety. Surgery & Radiology
Faculty of Veterinary & Animal Sciences
West Bengal University of Animal & Fishery Sciences
37, K. B. Sarani. Belgachia. Kolkata-700037

2. **Prof. Samit Kumar Nandi**
   ICAR National Professor
   Department of Veterinary Surgery & Radiology,
   West Bengal University of Animal & Fishery Sciences

Declaration & Compliance of Academic Ethics

I hereby declare that this thesis entitled *"In-silico evaluation of mutations in GSK-3β related to wound physiology and fabrication of sustainable bio-materials and therapies for improved wound healing and soft tissue engineering"* contain review article conducted through literature survey and original research work that was carried out by me, as a part of my research work, essentially required for the **Degree of Doctor of Philosophy**. All the information regarding this thesis and the research work was achieved and presented in accordance with academic rules and ethical conduct.

➢ All the study designs and research protocols were evaluated carefully and sanctioned by the Doctoral Research Committee, School of Bioscience & Engineering, Jadavpur University and Research Advisory Committee.

➢ The research work was conducted as per appropriate guidelines of the University (Especially UGC regulation 2017, and its amendment version), guidelines of Govt of India for conducting Bio-medical Research as per globally accepted standards.

➢ The Ethical permission for using animals was appreciated and approved as per ethical committee of WBUAFS - 763/GO/Re/SL/03/CPCSEA/05/2021-22 dated 26.04.2022 approval no. of IAEC of West Bengal University of Animal and Fishery Sciences

➢ iThenticate: Plagiarism Detection Software was used for scrutinizing piracy and it was found a 7% similarity index excluding self-plagiarism.

Name: Pratik Das

Registration no: D-7/ISLM/30/21 dated 13th April, 2021

Date:
Place: Kolkata   **Signature**

CONTENTS

CHAPTER 2: In-silico Prediction and Analysis of GSK-3β Deleterious SNPs and their Impact on Wound Healing

CHAPTER 4: Development of winery waste-derived Proanthocyanidin-Rich Grape Seed Extract-Based Gel for Modulating Inflammatory Responses in Wound Healing

*CHAPTER 5: Fabrication and Characterization of Starch-PVA Thin Films Crosslinked
with Proanthocyanidin rich Grape Seed Extract for wound healing application*

List of Figures

wound closure by the treatments (b); Quantification of hydroxyproline in wound-healing tissues on days 7, 14, and 21 after wound creation. (c)

CHAPTER 5: Fabrication and Characterization of Starch-PVA Thin Films Crosslinked with Proanthocyanidin rich Grape Seed Extract for wound healing application

List of Tables

Acknowledgement

I would like to express my heartfelt gratitude to several individuals who have been instrumental in the completion of my PhD thesis.

First and foremost, I extend my deepest appreciation to Dr. Piyali Basak, Director of the School of Bioscience and Engineering, for her invaluable guidance and support throughout my research journey. Her wisdom, encouragement, and unwavering belief in my capabilities have been the cornerstone of my academic progress. Without her insightful feedback and steadfast support, this thesis would not have reached its current form.

I am equally grateful to Dr. Samit Kumar Nandi, ICAR National Professor at WBUAFS Kolkata, for his expert advice and encouragement. His profound knowledge and thoughtful mentorship have been pivotal in shaping the direction of my research. Dr. Nandi's patience, willingness to listen, and constructive criticism have significantly enhanced the quality of my work.

I am sincerely thankful to Prof. Manisha Chakraborty, Professor at the School of Bioscience and Engineering, for her constant support and insights which greatly enriched my work. Her enthusiasm for science and her dedication to her students have been a tremendous source of motivation for me. Prof. Chakraborty's guidance has been invaluable in navigating the complexities of my research.

I would also like to acknowledge Prof. Dr. Mahitosh Mondal from SMST, IIT KGP, whose expertise and advice have been instrumental in the successful completion of my research. His encouragement and insightful discussions have helped me overcome numerous challenges throughout my journey.

Dr. Samiran Mondal from the Department of Veterinary Pathology, WBUAFS, also deserves heartfelt thanks for his vital contributions and guidance. His support and constructive feedback have been crucial in refining my research methodology and analysis. I would like to thank Dr. Abhra Chanda, Secretary Faculty of Interdisciplinary Studies, Law & Management for his continuous support during the submission.

I owe a deep debt of gratitude to Ms. Koyel Bhowmik. I thank her for always taking care. Her incessant motivation and wisdom have shaped and moulded my understanding of this research work. Her immeasurable patience, endurance, motivation, and unflagging support are undeniably my greatest strengths, without which this work would not have been completed. I take this moment to express my unwavering love and respect for her.

Additionally, I would like to thank my friends Mr. Soumya Mondal and Mr. Souvik Pal for their moral support and help during my PhD work. Their encouragement, advice, and camaraderie have been invaluable throughout this journey. Their steadfast belief in my abilities and their willingness to help in times of need has provided me with the strength to persevere. I am truly fortunate to have such wonderful friends.

I owe my heartfelt gratitude to the innocent rabbits who endured the pain for my research work. I also take a moment to acknowledge that I shall forever cherish the moments spent in the Research Lab of my department. I would like to thank Swami Vivekananda Merit-cum-Means Scholarship Government of West Bengal for providing me with some scholarships during my PhD tenure.

Lastly, I thank the Almighty for giving me all the strength and perseverance needed to complete this journey.

Preface

The present thesis work entitled ***"In-silico evaluation of mutations in GSK-3β related to wound physiology and fabrication of sustainable bio-materials and therapies for improved wound healing and soft tissue engineering"*** is the outcome of the work done by the author in the School of Bioscience and Engineering, Jadavpur university. This research work was pursued under the guidance of Dr. Piyali Basak, Director & Associate Professor, the School of Bioscience and Engineering, Jadavpur University, and Prof. Samit Kumar Nandi, ICAR National Professor Department of Veterinary Surgery & Radiology, West Bengal University of Animal & Fishery Sciences, The research work embodied in this thesis has been submitted to Faculty of Interdisciplinary Studies, Law & Management, Jadavpur University, for the accomplishment of the degree of Doctor of Philosophy. No part of this thesis has already been or is being concurrently submitted for any degree, diploma or other qualification.

Abbreviations

%	Percentage
&	And
@	at the rate of
µl	Microliter
µm	Micrometer
ANOVA	Analysis of variance
Avg.	Average
ECM	Extra Cellular Matrix
FDA	Fluorescein diacetate
FDA	Food and drug administration
Fig	Figure
FTIR	Fourier-transform infrared spectroscopy
g/l	Gram per litre
gm	Gram
HCl	Hydrochloric acid
i.e.	'Id est'/ that is
I.U.	International Unit
IAEC	Institutional Animal Ethics Committee
mg	Milligram
mg/kg	milligram per kilogram
MICs	Minimum inhibitory concentrations
min	Minute(s)
ml	Millilitre
mM	Millimolar

MTT	3-(4,5-dimethylthiazol-2-yl)-2,5-diphenyl tetrazolium bromide
N	Normal
Na$_2$HPO$_4$	Disodium hydrogen phosphate
NaCl	Sodium chloride
NaOH	Sodium hydroxide
ng	Nanogram
nm	Nanometer
NO	Nitric oxide
O.D.	Optical density
℃	Degree celcius
PVA	Polyvinyl alcohol
SEM	Scanning Electron Microscopy
XRD	X-ray diffractometer
μg/μl	microgram per microlitre
μg	Microgram
FACS	Flow-cytometry
PBS	Phosphate Buffer Saline
ROS	Reactive Oxygen Species
DMEM	Dulbecco's Modified Eagle Medium.

Abstract

This study presents an integrated approach of advanced biomedical applications through the exploration of single nucleotide polymorphisms (SNPs) within the GSK-3β protein and its effect on wound healing, the development of biopolymer-based materials for wound healing, and the utilization of winery waste-derived grape seed extract (GSE) for its anti-inflammatory and wound healing properties. By intertwining genetic analysis with material science and bioactive compound optimization, the research offers a cohesive methodology to tackle complex biomedical challenges.

The first objective focused on GSK-3β, a critical serine/threonine kinase with diverse cellular functions. However, there is limited understanding of the impact of non-synonymous single nucleotide polymorphisms (nsSNPs) on its structure and function. Through an exhaustive in-silico investigation 12 harmful nsSNPs were predicted from a pool of 172 acquired from the NCBI dbSNP database using 12 established tools that detects deleterious SNPs. Consistently, these nsSNPs were discovered in locations with high levels of conservation. Notably, the three harmful nsSNPs F67C, A83T, and T138I were situated in the active/binding site of GSK-3β, which may affect the protein's capacity to bind to substrates and other proteins. Molecular dynamics simulations revealed that the F67C and T138I mutants had stable structures, indicating rigidness, whereas the A83T mutant was unstable. Analysis of secondary structures revealed different modifications in all mutant forms, which may affect the stability, functioning, and interactions of the protein. These mutations appear to alter the structural dynamics of GSK-3β, which may have functional ramifications, such as the formation of novel secondary structures and variations in coil-to-helix transitions. In conclusion, this study illuminates the possible structural and functional ramifications of these GSK-3 nsSNPs, revealing how protein compactness, stiffness, and interactions may affect biological activities. Thus, various possibilities might cause a non-healing wound. In the following work, we will try to study how to achieve better and faster wound healing using various therapeutics. We also aim to create therapeutics agents which would control the inflammatory cytokines after the onset of the wound and also promote angiogenesis and neovascularization thus nullifying the effect of dysregulated GSK-3β.

The second objective was the preparation of starch-gelatin composite mats incorporating grape seed extract (GSE). The composite mats were created by heating potato starch and gelatin, followed by the addition of grape seed extract and ethanol to form a polymer lump, which was

then pressed into a film. Material characterization included FTIR, AFM, SEM, mechanical testing, swelling studies, in-vitro degradation, thermal analysis, and contact angle measurements. The biological evaluation involved culturing L929 mouse fibroblast cells on the mats, assessing cell viability with the MTT assay, and hemocompatibility using a hemolysis test. In-vivo biocompatibility was tested by implanting mats in Wistar rats and conducting histological examination after 14 days. Results indicated that a balanced ratio of starch and gelatin (1:1) produced mats with optimal properties, including enhanced mechanical strength, smooth surface morphology, high swelling capacity, rapid degradation, and excellent biocompatibility and hemocompatibility. These composite mats serve as a promising platform for integrating bioactive compounds such as GSE, leveraging their properties for enhanced wound healing applications. However the material developed was not mechanically very stable and was of brittle nature which is not mostly suitable for wound dressing material.

In the third objective, the study delved into optimizing the extraction of proanthocyanidins from grape seeds and evaluating their biological effects. Grape seeds were cleaned, dried, crushed, and extracted using ethanol gradients, followed by cold maceration and centrifugation. UV-VIS spectroscopy, FTIR, and LCMS/MS characterized the extract, revealing high proanthocyanidin and total phenolic content. In-vitro assays on L929 cells demonstrated high cell viability and significant cell migration at optimal concentrations of GSE. Anti-inflammatory and antioxidant properties were confirmed through reduced expression of NF-κB, IL-6, TNF-alpha, and ROS levels in LPS-stimulated RAW cells. A GSE-loaded starch-glycerite gel was formulated and characterized, showing significant wound healing potential in rabbit models, enhanced collagen deposition, and improved epidermal regeneration. This objective highlighted the therapeutic potential of GSE, derived from winery waste, as a potent bioactive compound for wound healing applications.

The fourth objective connected these findings by developing and characterizing PVA-starch composite films loaded with GSE for wound healing applications. The GSE not only acted as an active component but also participated as a crosslinking agent by inducing hydrogen bonds between polymers. Three composites with varying PVA and starch ratios were fabricated using solvent casting, followed by material characterization through FTIR, XRD, SEM, AFM, thermal analysis, mechanical testing, contact angle measurements, nano-indentation, swelling index, and degradation studies. Antibacterial efficacy against Staphylococcus aureus and Escherichia coli, hemocompatibility, cytocompatibility, and in-vivo wound healing in rabbits were assessed. The PS@2:1 composite exhibited superior properties, including antibacterial activity, biocompatibility, and enhanced wound healing, with significant collagen deposition

and minimal inflammation in treated wounds. This final objective underscored the successful integration of genetic insights, material science, and bioactive compound optimization, resulting in a holistic approach to developing advanced wound healing materials.

In brief, this comprehensive study successfully identified deleterious SNPs within the GSK-3β gene, developed effective starch-gelatin composite mats, optimized grape seed extract for anti-inflammatory and wound healing applications, and fabricated PVA-starch composites with promising wound healing properties and overcame the limitations of the starch-gelatin mats. The therapies hence developed controlled inflammation and also promoted angiogenesis which is a common problem during dysregulation of GSK-3β. These therapies and wound dressing thus have a high potential in nullifying the adverse effect of deleterious mutation of GSK-3β related to wound healing. These interconnected objectives provide valuable insights into SNP analysis, biopolymer-based wound healing materials, and the utilization of winery waste-derived extracts, offering potential avenues for innovative therapeutic approaches in biomedical applications.

Chapter I

Introduction and Literature Review
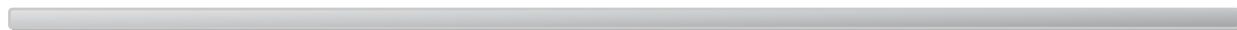
1. INTRODUCTION AND LITERATURE REVIEW

1.1 Introduction

1.1.1 Background in wound healing

Skin, the largest human organ forms the complex barrier separating internal and external environments. It is made up of three major layers such as epidermis, dermis, and hypodermis [1]. Positioned below epidermis, dermis is rich in different extracellular matrix proteins and collagen is one of the extracellular matrix proteins impart rigidity, elasticity along with structural support to dermis. The dermis layer is the hub for many blood capillaries, nervous system, hair follicles, and even the sweat glands. Besides these the lower underneath hypodermis layer is composed of adipose tissue, offering insulation and serving as protective padding [2].

Biologically, a wound is any injury to skin integrity or underlying tissues. This disruption can be caused by trauma, surgery, or pathological processes. Wounds can vary in severity and depth, ranging from superficial cuts and abrasions to deep lacerations or puncture wounds [3]. When the skin is damaged; such as in cases of injury or trauma; the wound healing process follows a dynamic sequence. The biological response to a wound involves a series of processes aimed at restoring tissue integrity and function, including inflammation, proliferation, and remodelling. The ultimate goal of wound healing is to close the wound, restore tissue strength, and minimize infection risk [4,5]. Initially, there is a clotting response to stop bleeding, followed by inflammation to remove microbes and debris. The subsequent proliferative phase includes granulation tissue formation, which includes blood vessels, fibroblasts, and extracellular matrix proteins. This tissue behaves as scaffold for cell migration and tissue repair. Finally, remodelling step includes maturation of scar tissue, where collagen fibers are re-oriented to enhance strength and flexibility. The complex composition and regenerative capabilities of the skin facilitates wound healing [2,6].

Various groups have delineated wound healing, yet they all covered the essential objective of repairing tissue defects. These categories include primary healing followed by delayed primary healing, healing by secondary intention, and finally the healing of partial-thickness wounds [7,8]. Primary healing involves rapid closure of a full-thickness surgical incision with minimal cellular damage, while delayed primary healing occurs when wound edges are

not promptly reapproximated, often seen in contaminated wounds. Healing by secondary intention entails allowing full-thickness wounds to close naturally, resulting in a more intense inflammatory response and pronounced wound contraction. Partial-thickness wounds predominantly heal through epithelialization, without significant wound contracture. The overall process of wound healing encompasses stages such as inflammation, fibroblastic phase, scar maturation, and wound contracture (Figure 1), which progress sequentially following injury. These phases, analogous to hemostasis, inflammation, granulation, and remodeling, involve complex interactions among cellular and extracellular components to achieve tissue repair [9,10].
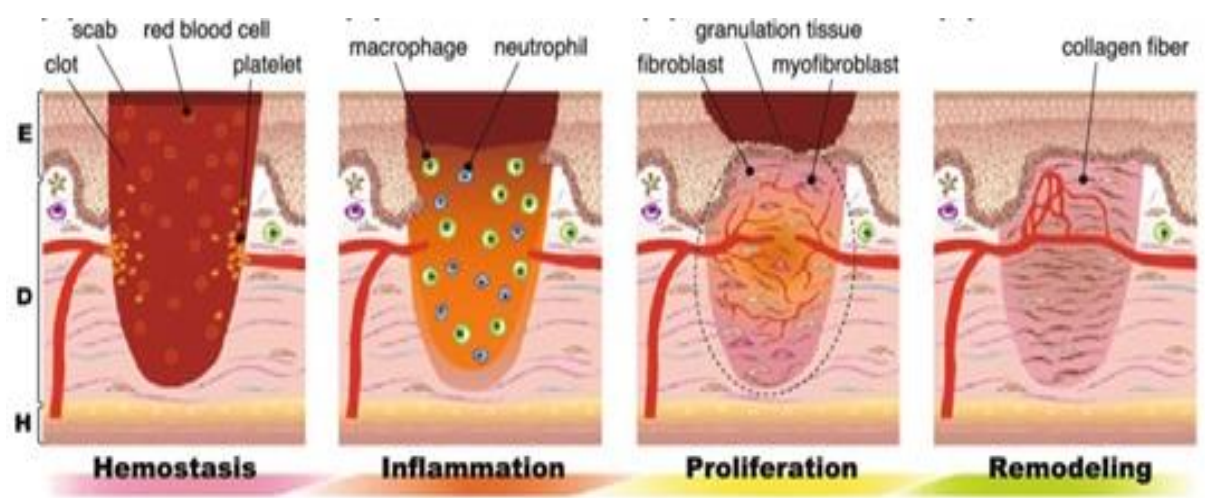
Figure 1.1: Stages showing wound healing mechanism

The inflammatory phase of wound healing initiates the influx of inflammatory cells and activates the local Wnt/β-catenin signaling pathway, which controls various physiological mechanisms such as proliferation, differentiation, migration, and cell fate determination [11]. Activation of the Wnt/β-catenin pathway further enhances wound repair by eliminating glycogen synthase kinase-3β (GSK), a crucial regulatory enzyme [12]. This leads to the promotion of proliferative step characterized by the initiation of re-epithelialization and eschar development. By this phase, cytoplasmic β-catenin deposition triggers the transcription of matrix metalloproteinase genes, facilitating angiogenesis, accumulation of extracellular matrix, and the development and proliferation of various cellular components such as fibroblasts and keratinocytes [13]. Subsequently, in the maturation and remodelling step, re-epithelialization of the epidermis occurs to restore protective barrier function. Transforming growth factor-β (TGF-β) promotes fibroblast proliferation, angiogenesis,

collagen organization, and extracellular matrix remodelling, thus facilitating the overall process of wound healing [14].

Wound healing requires several cells, growth factors, cytokines, extracellular matrix, and enzymes [15]. Fibroblasts are particularly crucial in wound healing [10]. Factors like microbial infection or biofilm can impact wound healing, as can ischemia and reperfusion, which are highlighted by Mustoe et al., (2006) in their discussion on the molecular biology underlying these processes. Ischemia-reperfusion injury involves a cascade of cellular processes leading to cell damage, including leukocyte and complement activation, and dysfunction of the microvasculature [7,16].

Similarly angiogenesis is crucial in wound healing, involving development of capillary sprouts that penetrate the extracellular matrix and form tube-like structures, ultimately extend and branch to create networks [17]. Various angiogenic stimulators, including vascular endothelial growth factor (VEGF), transforming growth factor-beta (TGF-ß), tumor necrosis alpha (TNFα), platelet-derived growth factor (PDGF), fibroblast growth factor (FGF), angiogenin, and angiopoietin-1, play roles in various stages of wound healing, like initiating angiogenesis, amplifying it, promoting vascular proliferation, stabilizing vessels, and maintaining angiogenesis [17]. Their activation starts wound healing, while disruptions in their interactions can prolong wound persistence. Understanding the mechanisms underlying altered expression of these molecular factors, leading to changes in cellular function, may reveal potential intervention points in wound healing [18].

Angiogenesis, development of new blood capillaries, is required for wound healing, and supplying injured tissue with oxygen and nutrients necessary for regeneration [19]. This process includes a sequence of intricate physiological events, initiated by released vascular endothelial growth factor (VEGF) and fibroblast growth factor (FGF) from various cell types including platelets and macrophages [20,21]. These growth factors stimulate endothelial cell proliferation and migration, leading to changes in existing blood vessels near the wound site. Endothelial cells undergo migration towards damaged site, then proliferate and the development of new capillaries takes place through sprouting and branching. Extracellular matrix components, integrins, and proteases guide endothelial cell migration, while matrix metalloproteinases (MMPs) facilitate extracellular matrix remodelling [22]. Newly formed blood vessels not only supply oxygen and nutrients but also aid in waste product removal and

support the recruitment of different cells in tissue repair, like fibroblasts and immune cells [23]. By ensuring an adequate blood supply, angiogenesis contributes to the establishment of a functional tissue network, thereby expediting the healing process and restoring the affected area to its normal physiological state.

Wound healing is influenced by various factors, which can be broadly categorized as either local or systemic. Local factors directly impact wound site, while systemic ones affect entire health and recovery capacity of individuals. Additionally, numerous factors can overlap between these categories [24]. Infection stands out as a crucial local factor, as microorganisms typically inhabit the skin's surface. However, when the skin is compromised, these microorganisms can infiltrate concerned tissues. The degree of infection, replication status, and microbial load within tissue determine the groups of wound infection, encompassing pathogenic infection, colonization, and systemic dissemination of invasion [25, 26]. Although the human body possesses significant natural healing capabilities, various cellular components involved in responding to injuries can weaken, leading to difficulties in wound closure (Figure 2). This weakening commonly occurs due to systemic changes associated with conditions like old age or diabetes. These two, in particular, are major contributors to chronic wounds, which are wounds that persist for longer than 3 months without healing [27–29]. Non-healing chronic wounds exhibit sustained myofibroblast activity, which contributes to tissue alterations, particularly notable in hypertrophic scars post-burn injury and in scleroderma's fibrotic stage [8, 30]. Myofibroblast-induced contractions are characteristic of fibrosis, impacting organs like the liver, heart, lung, and kidney [31]. Hypertrophic scars are marked by hypervascularization, abnormal ECM deposition, and excessive collagen build-up [32]. Prolonged exposure to toxic chemicals, including carcinogens, in chronic wounds can impair chemo-surveillance functionality. In cancer patients, wound healing may face hindrances due to factors like malnutrition, oncologic disorder, and its intervention [33].
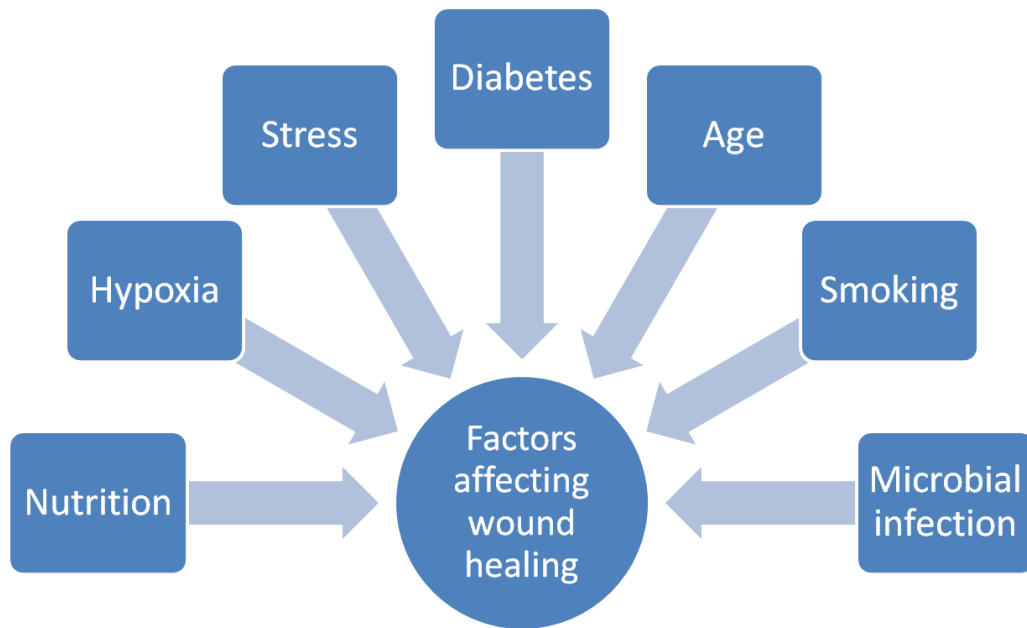
Figure1.2: Factors affecting wound healing process

Chronic wounds, often marked by infection or biofilm formation; lead to heightened development of inflammatory and proinflammatory cytokines. This heightened production triggers an increase in matrix metalloproteases and a decrease in their inhibitors. Sustained inflammation results in the breakdown of the ECM and inhibits fibroblast development. The reduced fibroblast production leads to insufficient collagen fibre production required for wound remodelling. Fibroblasts in the chronic wound environment exhibit signs of senescence. Furthermore, chronic wound environment hampers angiogenesis and retards epithelialization, contributing to slow healing. These characteristics collectively represent the environment of chronic wounds, which hinder timely healing. Intervening chronic wounds involve recognizing their molecular mechanisms present in clinically diverse wounds, examining their progression for healing steps.

1.1.2 Role of Glycogen synthase kinase-3 (GSK-3B) in Wound Healing

GSK-3 is linked with several signalling pathways like cyclic adenosine monophosphate Hedgehog, (cAMP) signalling, transforming growth factor-beta (TGF-β), Wnt, Notch, nuclear factor of activated T cells (NF-AT), and activators that stimulate phosphatidylinositol 3-kinase (PI3K) [34–36]. GSK-3 is linked in controlling numerous physiological processes such as metabolism, cell movement, programmed cell death, cell maturation, growth, and development of embryos. Its irregular activity is associated with various health conditions,

including diabetes and cancer [37, 38]. GSK-3, a widely expressed serine/threonine kinase, comprises two isoforms, namely GSK-3α and GSK-3β, which are encoded by separate genes. While both isoforms share a high degree of similarity, GSK-3α possesses a glycine-rich N-terminal extension, resulting in a larger molecular mass compared to GSK-3β (51/47 kDa) [39]. GSK-3 stands out among kinases for its preference for substrates that have undergone phosphorylation events C-terminal to GSK-3 phosphorylation site [40].

The absence of GSK-3β leads to heightened tissue repair and fibrogenesis *in vivo*, primarily attributed to increased levels of endothelin-1 (ET-1). GSK-3β, functions as a serine/threonine kinase for negative regulation of glucose homeostasis and is involved in various physiological methods, including the advancement of inflammation. Recent studies have suggested its involvement in controlling tumorigenesis by modulating autophagy pathways [41]. The phosphorylation of Ser9 at N-terminus of GSK-3β inhibits its activity, and phosphorylation of Tyr216 promotes it, indicating differential effects based on phosphorylation sites [42, 43]. GSK-3β also plays a critical role in angiogenesis, impacting advancement of diabetes associated wound healing. It induces break down of β-catenin, a pivotal factor for keratinocyte proliferation and migration, through the mechanism of phosphorylation and destabilization of β-catenin [44, 45].

GSK-3β facilitates wound healing processes by modulating various cellular mechanisms involved in tissue repair. GSK-3β is incorporated in control of cell proliferation, migration, inflammation, and apoptosis, required for proper wound healing. Specifically, GSK-3β down regulation promotes cell migration and proliferation, leading to accelerated wound closure and improved tissue regeneration. Moreover, GSK-3β activity regulates link between pro-inflammatory and anti-inflammatory cytokines, regulating inflammatory response during wound healing. Additionally, GSK-3β influences the differentiation of various cells required in wound repair, like fibroblasts and keratinocytes. Overall, targeting GSK-3β presents a promising therapeutic strategy to enhance wound healing processes [46]. Mutations or functional loss of GSK-3β could lead to fibrotic conditions in vivo, potentially regulated by ET-1. Findings suggest that GSK-3β help in regulation of excessive *in vivo* tissue repair, thereby reducing myofibroblast activity and fibrogenesis. This insight contributes to understanding method of tissue repair and its transition to fibrogenesis [39, 47, 48].

1.1.3 In-Silico Analysis

Process of wound repair is intricate and multifaceted, involving various cells and cytokines. Skin, serving as a vital barrier for the human body, can be compromised by a range of issues like ulcers, infections, scars, and chronic wounds [49]. This has underlined the necessity for enhancement of drugs oriented mechanism of healing process [50]. In-silico evaluation methodologies for wound healing leverage computational approaches to simulate and analyze the complex biological processes involved in tissue repair. These methods encompass various computational techniques, such as molecular modeling, bioinformatics, and systems biology, to elucidate the molecular mechanisms underlying wound healing [51]. Molecular modeling techniques, including molecular dynamics simulations and docking studies, enable researchers to investigate the interactions between biomolecules involved in wound healing, like growth factors, cytokines, and enzymes [52]. Molecular docking serves as a robust computational tool employed to predict potential binding configurations and elucidate the interaction mechanisms. Widely applied in drug discovery [53]; molecular docking aids in identifying the binding modes or forces governing ligand-protein complexes. Notably, binding energy stands as a critical criterion for assessing protein-ligand interactions, with lower binding energies indicative of greater stability. Epidermal growth factor receptor (EGFR1), matrix metalloproteinase (MMP-1) and fibroblast growth factor (FGFR1) are pivotal in regulating cell proliferation, and tissue remodelling, followed by wound healing processes [54].

By computationally predicting the binding affinities and structural changes of these molecules, researchers can gain insights into their roles in wound healing [55]. Additionally, bioinformatics tools are utilized to analyze large-scale omics data, like genomics, metabolomics, proteomics and transcriptomics to recognise key regulatory pathways and molecular signatures associated with wound healing. Integrative systems biology approaches further facilitate the construction of computational models that simulate the dynamic behaviour of biological networks involved in wound repair, allowing for the prediction of therapeutic targets and the optimization of treatment strategies [56–58].

In wound healing research, the utilization of in silico studies holds paramount importance for several reasons. Firstly, it is a biological mechanism-including several molecular interactions and cellular responses. In silico studies offer an economically friendly and time-efficient technique to explore these intricate mechanisms by simulating molecular interactions, predicting structural activities, and elucidating physicochemical properties of therapeutic

agents such as antimicrobial peptides (AMPs) [59]. Secondly, the design and optimization of novel wound-healing strategies, particularly those involving antimicrobial and wound-healing compounds, necessitate a comprehensive understanding of their structure-function relationships [60]. In silico analysis allows systematic characterization and classification, providing their mechanism of action. Furthermore, advancements in bioinformatics have enabled the prediction and screening of potential candidate peptides with enhanced efficacy and specificity. Therefore, in silico studies accelerates the development and optimization of innovative wound-healing therapies, addressing the urgent demand for effective solutions to chronic wounds [61, 62].

In silico research predicting the effects of GSK-3β mutations on wound-related pathways offer significant potential for precision medicine in wound healing. GSK-3β regulates various cellular processes implicated in wound repair, through inflammation, cell proliferation, and tissue remodelling. Mutations in GSK-3β gene have been linked to altered wound healing responses and susceptibility to chronic wounds [63]. Through computational modelling and bioinformatics approaches, researchers can analyze the structural and functional consequences of GSK-3β mutations, predicting their impact on key signalling pathways involved in tissue regeneration. By simulating the effects of specific mutations on protein-protein interactions, enzymatic activity, and downstream signalling cascades, in silico studies provide valuable insights into the molecular mechanisms underlying aberrant wound healing phenotypes associated with GSK-3β mutations [64].

Moreover, in silico studies enable recognition of potential targets and formulation of personalized treatment strategies for individuals with GSK-3β mutations affecting wound-related pathways. By integrating genomic data with computational models of wound healing processes, researchers can prioritize candidate drugs and interventions that modulate GSK-3β activity or target downstream effectors to regain basic wound healing mechanism [65]. Precision medicine approaches tailored to individual genetic profiles hold promise for optimizing treatment outcomes in wound healing, ensuring targeted and effective therapies for patients with specific GSK-3β mutations. Ultimately, in silico prediction of the effects of GSK-3β mutations on wound-related pathways represents a crucial step towards advancing personalized medicine in wound healing, offering novel insights into the pathogenesis of wound healing disorders and guiding innovative therapeutic practices [66].

1.1.4 Need for Advanced Therapies

The correct assessment and classification of wounds hold significant clinical significance due to their potential to prevent complications and provide valuable prognostic information regarding morbidity, mortality, and quality of life outcomes [67, 68]. Furthermore, an accurate assessment allows for development of a tailored therapeutic method and enables the concerned group to monitor healing progresses under normal parameters. Despite its importance, clinical evaluation of wounds is subject to a high degree of subjectivity, leading to change in wound assessment and management [69]. This change can be lead to several factors, including no or low clinical experience, inadequate understanding of contextual factors, inability to identify essential elements in wound assessment, limited knowledge of available treatment options, and difficulty in properly valuing clinical information [70,71]. Clinical evaluation typically encompasses a comprehensive approach that includes obtaining a detailed medical history, conducting a thorough clinical examination of the wound, and potentially utilizing wound assessment charts or tools. These tools aid in standardizing the assessment process and provide objective criteria for evaluating wound characteristics such as size, depth, tissue type, and presence of infection. Despite of the availability of such tools, the subjective interpretation of clinical findings and variability in clinical expertise contribute to inconsistencies in wound evaluation and management [72, 73]. Therefore, efforts to improve clinical training, enhance contextual understanding, and promote standardized wound assessment protocols are crucial for ensuring optimal patient outcomes in wound care settings. The need for innovative approaches to enhance wound treatment outcomes is increasingly recognized in healthcare settings due to several factors. Traditional wound care methods, while effective to some extent, may not always yield optimal outcomes, particularly in cases of chronic or complex wounds. Hence, it is necessitated for novel therapeutic mechanisms that can address challenges associated with wound healing and improve patient status [74, 75].

One of the primary drivers for innovative approaches in wound treatment is the rising incidence of chronic wounds, like diabetic ulcers, and pressure ulcers. Chronic wounds pose significant clinical challenges due to their prolonged healing time and susceptibility to complications such as infection and tissue necrosis. Conventional treatments often fall short in managing these wounds effectively, necessitating the development of new approaches that lead to more efficient healing and minimizes risk of complications [76,77]. Moreover, the

increasing prevalence of antibiotic-resistant bacteria and healthcare-associated infections further underscores the need for innovative wound treatment approaches. Conventional antimicrobial therapies may become less effective over time as bacteria develop resistance to commonly used antibiotics. Therefore, there is a pressing need to explore alternative antimicrobial strategies, such as antimicrobial peptides, nanoparticles, and bioactive dressings, which can offer broader antimicrobial coverage and reduce the risk of resistance development [78]. Furthermore, old age, risk of diabetes and obesity contribute to complexity of wound care management. These factors can impair the body's natural healing processes and increase chance of chronic wound development. Innovative approaches that take into account the unique needs and challenges associated with these patient populations are essential for achieving better treatment outcomes [79, 80].

Despite advancements in wound healing therapies, several gaps and limitations persist in current clinical practice. Traditional approaches often focus on symptom management rather than addressing the underlying biological mechanisms of wound healing. Additionally, there is a lack of personalized treatment strategies tailored to individual patient characteristics, such as genetic predispositions, which can significantly impact wound healing outcomes. Furthermore, the emergence of antibiotic-resistant bacteria poses challenges for infection management, while the high cost and accessibility of advanced wound care products limit their widespread use. Moreover, there is a need for more standardized and objective methods for wound assessment and monitoring to optimize treatment efficacy and minimize variations in clinical practice. Addressing these gaps requires innovative approaches that integrate advancements in biomaterials, regenerative medicine, and personalized medicine to improve patient status and enhance the quality of wound care delivery.
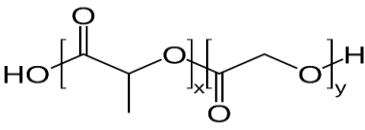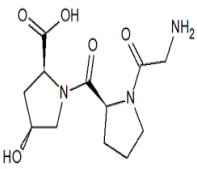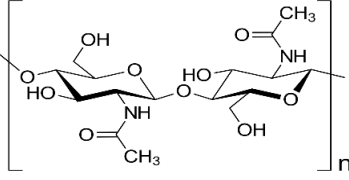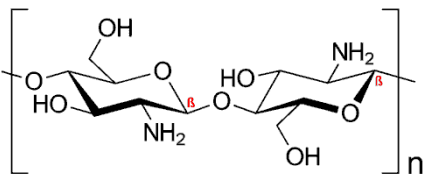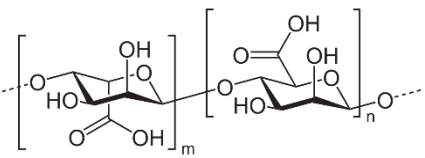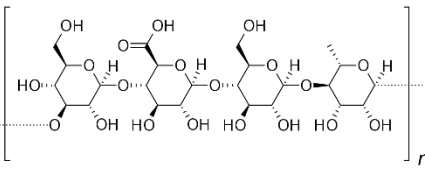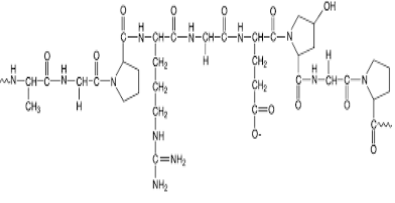
1.1.5 Role of Biomaterials and specialized ointments for Wound healing
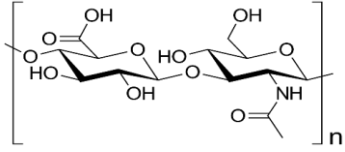
Deep wounds, incapable of self-regeneration, necessitate the origin of specialised scaffolds to facilitate healing by giving mechanical support to new tissue. It not only serves as a structural base offering support and attachment but also keeps on interacting with cells, initiating the cellular mechanisms crucial for tissue regeneration [81, 82]. Essential attributes of scaffolds include porosity, surface area and volume ratio, pliable nature and geometry. Biomaterial types and processing techniques play pivotal roles in determining scaffold properties, with bioresorbable or pro-regenerative scaffolds being preferred. These scaffolds can be used with

various agents to increase physiological reactions and expedite wound healing [83, 84]. Techniques like electrospinning or 3D printing enable the fabrication of scaffolds with tailored properties suitable for wound repair [85, 86]. Biomaterials elevate the regenerative potential of human tissues, facilitating the restoration of damaged states and re-establishing normal biological function. Various fabrication techniques enable the incorporation of biomaterials within the body, serving as scaffold to regenerate tissues. The primary objective is to provide support for cellular attachment, proliferation, migration, and differentiation, thereby promoting the generation of functional tissue [87]. Furthermore, biomaterials function as temporary scaffolds mimicking ECM, facilitating cell regeneration. Several biomaterials are extensively used in tissue engineering due to their bioavailability and biocomaptibility (Table 1). Their use in *in vitro* models demonstrated lesser toxic generation during degradation enhancing cell adhesion and function [88, 89].

Table 1.1: Biomaterials in wound healing [87,88]

Sl. No.	Examples	Details	General Structure
1.	Polyurethane and their derivatives.	Composed of organic substances linked together by carbamate	
2.	Poly Caprolactone	It is biodegradable polyester that has a low melting point of around	
3.	Polyvinyl Alcohol	Hydrophilic synthetic polymer	
4.	Silicone	Polymers made up of siloxane	

5.	Poly (lactide-co-glycolide)	Co-polymer made up of glycolic acid and lactic acid	
6.	Collagen	Bio based protein in ECM of connective tissue	
7.	Chitin	Chitin is bio based polysaccharide, with polymer of *N*-acetylglucosamine	
8.	Chitosan	Polysaccharide with β-(1→4)-linked D-glucosamine and *N*-acetyl-D-glucosamine.	
9.	Alginate	Anionic biopolymer in brown algae in linear format	
10.	Gellan	It is a linear, negatively charged polysaccharide	
11.	Gelatin	Skin, bones, and connective tissues	

12.	Hyaluronic acid	Bio based compound in articular cartilage	

These approaches encompass various aspects such as the types of biomaterials involved, the specific cells targeted for substitution, relevant growth factors, signalling molecules, and the fabrication methods employed. Numerous biomaterials have been explored for their potential in treating chronic wounds, each with its unique characteristics and mechanisms involved in wound healing. In-depth reviews of both natural and synthetic biomaterials highlight their applications in specific types of wound treatments and the underlying mechanisms driving their efficacy in wound healing [90–92]. Skin substitutes are used for enhancing the wound healing process by providing scaffold that mimics the ECM of the skin. Various skin constructs are formed by utilizing biomolecules such as collagen, hyaluronan, and others [93]. The electrospun quaternary crosslinked ammonium silane collagen demonstrated their biocompatibility in dermal fibroblasts [94]. Poly glycerol sebacate is utilized in wound healing due to its biostability, nontoxicity and bioavailability [95].Studies show its applications in skin healing and tissue regeneration processes [96]. Biodegradable "Poly (glycerol sebacate)/polyhydroxybutyrate scaffold loaded with simvastatin (SIM) and ciprofloxacin (CIP)" were evaluated for wound healing, showing regulated release of CIP to control wound infections and delayed release of SIM to facilitate wound healing [97]. Similarly, studies shows an injectable "catechol–Fe^{3+} cross-linked poly (glycerol sebacate)-co-poly (ethylene glycol)-g-catechol prepolymer hydrogel" system for treating bacterial infections and skin wounds, demonstrating its self-healing-properties-and antibacterial activity against Methicillin-resistant Staphylococcus aureus (MRSA) [80]. Despite advancements in biomaterial-based therapies, the extent of wound penetration complicates the selection of appropriate therapy and its impact on the wound-healing process[89]. Therefore, the utilization of specific biomaterials tailored to these criteria holds promise for accelerating cell regeneration [87].

The utilization of biomaterials in wound healing offers numerous advantages and can lead to improved treatment outcomes. Biomaterials provide a scaffold that mimics bio based ECM of

the skin, for cell attachment, proliferation, and tissue regeneration. Additionally, they can deliver bioactive molecules, growth factors, and antimicrobial agents to the wound site, promoting wound closure and preventing infections. Biomaterials also possess tunable properties that allow for customization based on specific wound characteristics, like size, depth, and location, enabling personalized treatment approaches. Furthermore, biomaterial-based dressings can provide protection from external contaminants and maintain a moist wound environment, which is contributing to optimal wound healing. Overall, the use of biomaterials in wound healing can enhance the efficiency of process and minimize healing time [98, 99].

Studies showed positive outcomes linked to utilization of biomaterials in wound healing. Biomaterial-based dressings have been shown to accelerate wound closure, promote tissue regeneration, and reduce the risk of infection. Additionally, they can minimize scarring and improve the cosmetic appearance of healed wounds. Furthermore, biomaterials can facilitate the integration of newly formed tissue with the surrounding skin, resulting in improved wound strength and functionality. Importantly, biomaterials provide a versatile platform for the delivery of therapeutics, enabling targeted and regulated dispersal of bioactive agents to the wound site. This targeted delivery approach enhances the efficacy of treatment while minimizing systemic side effects. Overall, utilisation of biomaterials in wound healing has great promise for improving patient outcomes and advancing the field of wound care [100,101].

Similarly hydrogel possesses a myriad of desirable properties that make it highly advantageous for wound healing. It's excellent anti-oxidation capability facilitate obdurate the wound healing and exacerbate tissue damage. Hydrogel's responsiveness to near-infrared (NIR) and pH changes facilitates controlled dispersal of therapeutic agents, enhancing its efficacy in promoting wound healing. Additionally, its flexibility near wound site ensures optimal contact and coverage, facilitating the healing process. The faster self-healing property of hydrogel further contributes to its longevity and durability upon application to the wound [75, 80]. Hydrogel exhibits good tissue adhesion, which helps to securely seal the wound and prevent leakage of fluids. Its degradability ensures that it is gradually absorbed by the body as the wound heals, reducing the need for frequent dressing changes and minimizing patient discomfort [102,103]. The photothermal antibacterial activity of the hydrogel, combined with its ability to be removed through irradiation and/or acidic solution washing,

provides an effective means of combating infections, particularly those caused by drug-resistant bacteria. *In vivo* experiments have demonstrated the ability of different gels and ointments to promote haemostasis, prevent infections, and accelerate closure of different skin wounds [76].

Creams facilitate wound healing due to their ability to deliver emollients and moisturizers directly to the skin [104]. Emollients and moisturizers are essential for maintaining skin hydration, softness, and flexibility. Properly hydrated skin helps to create an optimal environment for cell migration, proliferation, and tissue regeneration, promoting faster wound closure and reducing risk of complications such as infection and scarring. The structural and functional characteristics of creams facilitate wound care applications. As emulsions containing water and oil phases, creams can provide hydration to the skin while also forming a protective barrier against external contaminants [105]. Their non-greasy to mildly greasy textures allow for easy application and absorption into the skin, ensuring that the active ingredients are effectively delivered to the wound site. Additionally, the ability of creams to incorporate both aqueous and oleaginous ingredients enables the formulation of products with diverse therapeutic attributes like antimicrobial agents, anti-inflammatory compounds, and growth factors having diverse solubility range, essential for promoting wound healing [106]. Moreover, creams offer advantages in terms of drug release and absorption, allowing for controlled delivery of medications to the wound site for managing pain, preventing infection, and promoting tissue repair during wound healing. Rheological attributes of creams can be tailored to optimize their performance, ensuring that they adhere well to the wound area and provide sustained release of therapeutic agents over time. Overall, creams represent a versatile and effective vehicle for delivering essential components of wound care, making them indispensable in the management of various types of wounds and skin injuries [75].

1.1.6 Significance of Sustainable Material/Biomaterials

"Biomaterials are materials meant to interface with biological systems to augment, treat, or replace tissues, organs, or bodily functions illustrated by European Society for Biomaterials Consensus Conference-II" [107]. These materials encompass a diverse range of bio-based or synthetic substances, like metals, ceramics, and their composites, which exhibit biocompatibility with living tissues. Biopolymers are deduced from various natural biological

sources including plants, animals, microorganisms, and agricultural residues [108,109]. For instance, biopolymers from plant sources like rice, corn, sorghum, wheat, potatoes, cotton, yams, banana, cassava, tapioca, and barley can be chemically developed from their constituent monomers like oils, amino acids and sugars[110,111]. Classification of biomaterials is based on their material properties and their interaction with living tissues, with categories including bioactive, functionally inactive and biodegradable materials. In various medical procedures such as hand surgery, bone reconstruction, and joint replacement, biomaterials play a crucial role by interacting with body organs, facilitating tissue regeneration and functional restoration. Selection of appropriate biomaterials ensures compatibility with biological systems, promoting successful surgical outcomes and patient recovery [112].

Eco-friendly biomaterials produced using green technology or derived from various biological resources, have emerged as promising alternatives to traditional materials in biomedical and non-biomedical applications. These biomaterials are sustainable and environmentally friendly, addressing concerns about the ecological impact of conventional materials. In the biomedical field, eco-friendly biomaterials have found widespread applications in various areas such as breast implants, nerve regeneration therapy, ligament and tendon repair, orthopedics, wound healing, and ophthalmology for contact lens design [113]. These materials offer biocompatibility and promote tissue integration, enhancing patient outcomes and reducing the risk of adverse reactions. Furthermore, eco-friendly biomaterials contribute to the conservation of natural resources and minimize environmental pollution, aligning with the principles of sustainable development and responsible manufacturing practices [114]. Beyond biomedical applications, eco-friendly biomaterials also serve numerous non-biomedical applications (Table 2) due to their versatile properties and eco-conscious manufacturing processes.

Table 1.2: Different biomaterials & their medical applications

Sl. No.	Name of Biomaterial	Medical Applications
1	Fibrin	wound healing, Haemostatic agent, tissue reconstruction
2	Elastin	cell encapsulation, tissue reconstruction
3	Starch	Bone regeneration
4	Collagen	tissue regeneration, wound treatment
5	Hyaluronic acid	wound treatment
6	Alginate	tissue regeneration, wound treatment

Recently, a variety of medicinal applications have emerged for biopolymers, including suturing, repairing, promoting adhesion, providing coverage, occluding, isolating, maintaining contact elimination, promoting cell proliferation, guiding tissue growth, and facilitating regulated drug delivery [115–117]. To explore and replicate vital functional and structural characteristics of natural tissues, numerous techniques and processes for biomaterial production have been developed [118]. These materials are utilized in fields such as packaging, construction, textiles, and consumer goods manufacturing. By replacing conventional materials with eco-friendly alternatives, industries can reduce their carbon footprint and minimize waste generation. Additionally, eco-friendly biomaterials offer opportunities for innovative product design and development, fostering a shift towards more sustainable manufacturing practices across various sectors. Overall, the adoption of eco-friendly biomaterials represents a proactive approach towards achieving environmental sustainability and promoting a circular economy, where materials are reused, recycled, or composted at the end of their lifecycle, contributing to a healthier planet for future generations [119].

Biopolymers have garnered significant attention across various applications due to the growing need for sustainable and biodegradable solutions. One critical area where

biopolymers are utilized is in drug delivery processes to enhance efficacy of bioactive molecules for therapeutic purposes. Advances in this field are essential for improving illness treatment. In enhancement of drug delivery mechanisms, synthetic and/or natural and/or semi-natural polymers are frequently used[120]. However, frequent utilization of chemical-based polymers in industries like food and medicine raises environmental concerns. There is a growing cognizance of environmental sustainability, regulations on toxicants, and the management of medical waste. Consequently, there is a push towards developing packaging materials based on biopolymers. The adoption of biopolymers offers several environmental benefits, including the reduction of CO_2 emissions, medical wastes, and the dependence on non-biodegradable-based resources. This shift towards biopolymer usage aligns with efforts to create more sustainable practices in medical industries [121,122].

1.2 Literature review

1.2.1 Molecular Mechanisms of wound healing

Wound healing is a sophisticated mechanism including various tissues working together in a well-coordinated manner. It encompasses cell migration, proliferation, ECM deposition, inflammation, and angiogenesis. While minor skin wounds can heal relatively quickly, more extensive damages derived through any kind of external pressure and/or surgery may take longer and often result in scar formation [123]. To develop effective therapies for preventing scarring and promoting wound repair, understanding intricate cellular and molecular mechanisms involved in wound repair, is required. This understanding can aid in optimizing treatments for chronic wounds and improving tissue function post-injury. Various stages of wound healing, like clot development to re-epithelialization, angiogenesis, and eventual scar formation are involved with various intrinsic mechanisms [124]. Each phase also involves complex interactions between fibroblasts, cutaneous nerves, immune cells, endothelial cells, melanocytes, keratinocytes and adipocytes [125,126].

Wound healing process is a meticulously organized cascade mechanism designed to repair the skin [127]. In acute cutaneous wound healing, a series of systematic cellular processes occur, beginning with haemostasis to stop bleeding, followed by inflammation to clear debris and fight infection. Subsequently, proliferation ensues, involving migration and proliferation of various cell types like fibroblasts, keratinocytes, and endothelial cells, leading to development of tissue and blood vessels. Finally, tissue remodelling occurs, characterized by

the restructuring and maturation of the newly formed tissue, ultimately resulting in wound closure [128,129]. Hemostasis is primary step to skin injury, where blood vessel constriction and platelet activation occurs. It leads to release of granules containing various cytokines, including TGF-β and PDGF [130,131]. These cytokines serve to recruit neutrophils and macrophages, for inflammatory step to be activated [132]. Former arrive first at wound site, while macrophages, derived from activated monocytes. They contribute to phagocytosis and form additional growth factors for proliferation, angiogenesis, and keratinocyte migration [133,134].

After skin damage occurs, various cell signalling pathways are triggered in response of defence mechanisms. However, due to skin complexity and divergent healing strategies of acute and chronic wounds, diverse range of approaches is required for betterment of respective condition [135]. Acute wounds typically heal within 3-4 weeks relying on parameters like size, location, patient characteristics, and underlying health conditions. In contrast, chronic wounds are attributed with infections, development of pathogenic biofilms, and failure of concerned epidermal cells to capture reparative signals [136]. In acute wounds, PDGF and TGF A1 and TGF A2 are released, attracting inflammatory cells that clean bacterial wound through release of reactive oxygen species. Subsequently, growth factors promote cellular proliferation and migration, leading to granulation tissue development to support epithelialisation [137]. Proliferative step facilitates granulation tissue development, re-epithelialization, and angiogenesis for blood supply to nascent skin. Several signalling pathways, like "Wingless-related integration (Wnt)/β-catenin, nuclear factor erythroid 2–related factor 2 (Nrf2), phosphoinositide-3-kinase (PI3K)/protein kinase B (AKT), hypoxia-inducible factor 1 (HIF-1), transforming growth factor-β (TGF-β) and Notch" are identified as regulators of different steps of wound healing, viz cellular proliferation, migration, angiogenesis, inflammation, and tissue remodelling [138–140]. However, dysregulated signalling in these pathways can spoil wound healing and lead to complexity [141].

Overexpression of Wnt signaling molecules enhances cellular proliferation and extracellular matrix degradation, reflecting key aspects of wound regeneration. This observation suggested vitality of Wnt signaling in orchestrating fundamental phases of wound healing [142,143]. The canonical Wnt/β-catenin signalling pathway activates hypoxia-induced expression of Wnt ligands and it's binding with "frizzled trans-membrane receptors and lipoprotein receptor-related protein 5/6 (LRP5/6) co-receptor complex". It regulates function of

dishevelled with the recruitment of axin, leading to the segregation and finally the destruction complex. Consequently, β-catenin binds to T-cell factors/lymphoid transcription factors (TCFs/LEFs) and regulates gene expression within nucleus. Notably, inhibiting this pathway with overexpression of Pigment epithelium-derived factor (PEDF), leads to impaired wound healing due to inhibited angiogenesis [140,144].

Similarly, Notch signalling pathway modulates various cellular functions crucial for effective tissue repair [145]. During early stages, lower Notch signalling permit IL-36α expression, enhancing inflammation, while its activation in the late stages promotes M2 macrophages [146]. Notably, the application of collagen triple helix repeat containing 1 (CTHRC1) lead to M2 macrophage addition via Notch pathway activation, emphasizing its importance in this process[147]. In keratinocytes and endothelial cells, Notch signaling promotes proliferation and angiogenesis, as demonstrated by reduced proliferation upon DAPT treatment and enhanced migration and vessel formation with Jag1 activation. Additionally, Notch1 signalling controls proliferation and distinction of epidermal stem cells, inhibiting their differentiation into myofibroblasts. Importantly, Notch signalling inhibits scar development by blocking EpSC differentiation into myofibroblasts. Loss of Notch signalling promotes endothelial-to-myofibroblast transition, leading to fibrosis and impaired wound healing. These findings underscore the diverse and critical roles of the Notch pathway in orchestrating various aspects of wound healing mechanism [148,149].

Several studies have investigated therapeutic strategies aimed at enhancing wound healing by triggering PI3K/AKT pathway [137,140,150]. This pathway, activated by attachment of PDGF and EGF to receptor tyrosine kinases (RTKs), triggers a cascade of events leading to cellular proliferation, angiogenesis, and reduced inflammation. After triggered, "PI3K phosphorylates phosphatidylinositol 4,5-bisphosphate (PIP2) to phosphatidylinositol-3,4,5-triphosphate (PIP3), subsequently activating AKT by kinases such as PDK1 and mTORC2". This activation of AKT promotes downstream signalling, by activating mTORC1 that stimulates pro-migratory and proliferative RNA transcripts crucial for completion of the mechanism. The PI3K/AKT pathway is particularly active at inflammation and proliferation steps. Therefore, interventions aimed at enhancing PI3K/AKT signalling represent a promising approach to promote effective wound healing [151–153].

TGF-β signalling pathway facilitates wound healing, orchestrating various phases of the process. Upon attaching of TGF-β to its receptor, TβRII a heterotetrameric complex involving TβRII and TβRI, facilitates the triggering of downstream signalling cascades. Phosphorylation of suppressor of mothers' gene against decapentaplegic (Smad2 and Smad3) through activated TβRI initiates their interaction with Smad4, facilitating nuclear translocation and regulation of target gene expression, including "c-Myc, integrins, IL-6 and E-cadherin. TGF-β1 bound to latency-associated peptide prodomain (LAP)", becomes activated through cleavage by matrix metalloproteinases and structural alterations accelerated by integrin activities. Throughout wound healing, TGF-β acts as a chemokine during the inflammatory phase, promoting fibroblast proliferation and migration. In the proliferative phase, TGF-β1 facilitates keratinocyte migration, angiogenesis, and development of granulation tissue. In remodelling step, TGF-β1 drives fibroblast distinction into myofibroblasts, enhancing wound contraction and collagen production. Hence TGF-β signalling is crucial in coordinating various cellular processes for effective wound repair [154,155].

GSK-3β regulates various cellular mechanisms, including glucose homeostasis, inflammation and energy metabolism [156]. Recent research has highlighted its involvement in tumorigenesis by blocking autophagy pathways. Phosphorylation at different sites of GSK-3β, such as Ser9 and Tyr216, can have opposing effects on its activity. GSK-3β is intricately linked to inflammation through multiple signalling pathways, including Wnt/GSK-3β/NF-κB/β-catenin axis [157] and GSK-3β-Nrf2/AKT/NF-κB axis [158]. Studies suggest that GSK-3β/NF-κB signalling facilitates inflammation progression, as evidenced by decreased secretion of HO-1, p-Akt, p-Nrf2 and p-GSK-3β in rats, which were restored upon attenuation of kidney injury and inflammation [159,160]. Suppression of GSK-3β expression activates AMP-activated protein kinase, lowering pro-inflammatory reactions along with elevating anti-inflammatory immune activities in the liver. Moreover, inhibiting GSK-3β activity inhibits transcription of NF-κB while enhancing[161] cAMP response element binding protein(CREB1) activity, thereby attenuating inflammation and hepatocyte apoptosis caused by liver injury[162].

In one of the study involving Gsk3β-conditional-KO mice (Gsk3β-CKO mice) imparts crucial activities of GSK-3β in wound healing and fibrogenesis. Gsk3b-CKO mice displayed enhanced wound closure, heightened fibrogenesis, and scarring in comparison with controls,

indicating GSK-3β's regulatory function in these processes. Increased collagen formation, reduced cell apoptosis, increased profibrotic alpha-SMA levels, and enhanced myofibroblast development were observed in Gsk3b-CKO mice during wound healing. Importantly, antagonizing ET-1 altered Gsk3b-CKO fibroblasts phenotype, underscoring the role of GSK-3β in modulating ET-1 levels to regulate wound healing and fibrosis progression [163].

Wound healing process relies heavily on the intricate balance of matrix metalloproteinase (MMPs), crucial for ECM remodelling and cell migration [164]. During the proliferative stage, MMPs enhances the rebuilding of new granulation tissue and synthesizing ECM components. However, dysregulation of MMP activity, leading to excessive degradation, is implicated in the non-healing nature of wounds, especially the diabetic ulcers [165]. To maintain this balance, MMP inhibitors (MMPIs) are essential, with numerous naturally occurring and synthetic inhibitors explored for their potential in wound healing. Natural MMPIs such as curcumin, resveratrol, theaflavin, and catechin derivatives hold promise in regulating MMP activity and promoting effective wound repair, underscoring their potential therapeutic value in managing diabetic ulcers and other wound healing complications [166,167].

Elevated levels of MMPs, particularly MMP-1, -2, and -9, due to factors like oxidative stress, lead significantly to the afflicted wound healing process. The imbalance between ECM breakdown and repair caused by MMP activity prolongs wound and exacerbates skin damage. Additionally, absence of skin inhibitors of metalloproteinases (TIMPs) results in the upregulation of MMPs; further exacerbating the wound healing delay. To address this imbalance, strategies aiming to suppress MMP-2 and MMP-9 while enhancing TIMP-1 and TIMP-2 expression are crucial. Additionally promoting MMP-8 activity, while inhibiting MMP-9 could facilitate wound healing. Cleaving the MMP-3 zymogen to prevent MMP-9 activation represents another potential therapeutic target. These approaches seek to restore MMP balance and improve healing process, highlighting the importance of targeted interventions in managing wounds [168,169].

Studies emphasize intricate interplay between signalling pathways in regulating cellular behaviour during wound healing and underscore their potential as therapeutic targets for enhancing tissue regeneration. However, chronic wounds exhibit minimal densities of growth factor receptors, reducing the mitogenic potential of dermal and epidermal cells. Despite

elevated cell cycle-associated genes expression in chronic wound-derived keratinocytes, indicating a hyperproliferative state, these cells exhibit impaired migratory potential, necessitating periodic clinical interventions to avoid complexity [136,170,171].

1.2.2 GSK-3B Mutations in Health and Disease

GSK-3β overexpression is implicated in promoting various malignancies by enhancing cancer cell survival, invasion, and angiogenesis, while also influencing tumor differentiation through increased kinase activity and nuclear accumulation [172]. Notably, GSK-3β's role extends to wound healing, where it modulates levels of endothelin-1 (ET-1), critical for wound repair and fibrosis. Additionally, GSK-3β regulates Wnt/β-catenin signalling cascade, phosphorylating key proteins such as β-catenin, Axin, and APC, which regulate this pathway's activity. In fibroblast activation and collagen release, inhibition of GSK-3β may have implications for wound healing by regulating fibrotic activity and enhancing tissue repair. This suggests that targeting GSK-3β could offer therapeutic benefits in managing wound healing processes and potentially mitigating scar formation [173]. GSK3β helps in organizing cytoskeleton, establishing cell polarity, and facilitating cellular motility and migration [174].

GSK-3β facilitates angiogenesis and diabetic wound healing by regulating key factors involved in keratinocyte proliferation, migration, and invasion [175]. It induces breakdown of β-catenin, required for keratinocyte functions. Treatment with lucidone promotes keratinocyte proliferation, migration, and invasion, accompanied by increased β-catenin activities and decreased GSK-3β levels, suggesting that GSK-3β inhibition contributes to enhanced angiogenesis. Additionally, increased expression of Nrf2 and reduced ROS levels in angiogenesis highlight the significance of GSK-3β/Nrf2 axis in suppressing angiogenesis. These findings underscore vitality of GSK-3β in modulating angiogenesis and diabetic wound healing processes [44,175,176]. The wound healing process is intricate and involves numerous proteins, with GSK3-β emerging as a key regulator due to its involvement in the Wnt-beta catenin pathway, known to influence cell division and accelerate wound healing. Many literatures suggest that inhibition of GSK3-β can enhance wound healing [177].

GSK-3β mutations can significantly impact the process by influencing various cellular functions involved in tissue repair. For instance, dysregulation of GSK-3β activity can affect the proliferation and migration of fibroblasts, required for wound closure [172,173].

Additionally, GSK-3β controls inflammatory responses during healing, influencing the connection between pro-inflammatory and anti-inflammatory signals required for proper tissue repair. Furthermore, GSK-3β mutations changes expression and activity of key molecules in wound healing pathways, like TGF-β, Wnt/β-catenin, and NF-κB, thereby impact the overall healing outcome. Depending on the nature of the mutation and its effects on GSK-3β function, individuals with these mutations may exhibit variations in wound healing kinetics, susceptibility to infection, and scar formation [178,179].

1.2.3 In-silico studies related to wound healing

"In silico modelling" refers to use of "computational methodologies and mathematical models" to simulate and explore biological processes, diseases, and pharmacological reactions. These models are constructed based on existing biological data and aim to duplicate the biological systems, like tissues, or organs. By developing virtual models, researchers can generate predictions, test hypotheses, and gain deep insights into complex biological phenomena. In wound healing research, in silico modelling provides a valuable approach for understanding the underlying mechanisms and exploring potential therapeutic interventions. While traditional treatment methods for wounds, like grafting and dressings, have shown tissue regeneration efficiencies, the development of specific guidelines in clinical set up requires further research [178,180].

Various models are studied for mechanisms of cutaneous wound healing. Each model has its own pros and cons. *In vitro* mechanisms offer insights into specific cellular populations and mechanisms but may not fully capture the broader tissue matrix's complexity. In contrast, *in vivo* models can duplicate patho-physiology of entire mechanism but fails during translating the results to clinical scenarios. Similarly in *ex vivo* models transitory validation of cellular effects could be done but requires proper optimization. There is an increasing demand to improve the translational approach in wound healing research by integrating various knowledge sources. This aims to uncover underlying mechanisms and create effective tests for new therapeutic innovations [181,182].

In-silico studies helps in understanding and advancing wound healing research by providing insights into molecular interactions and identifying potential therapeutic targets. Through molecular docking and simulation techniques, researchers can model the interactions between small molecules and proteins involved in it, like cytokines, and MMPs. By elucidating

binding modes and affinity of tiny molecules within protein binding domain, in-silico studies develops the design and optimization of new drug candidates for wound healing[167,183]. Furthermore, computational approaches enable the prediction of ligand-receptor complex structures, binding energies, and kinetics, offering valuable information for drug discovery and development processes. These in-silico investigations complement studies, providing best way to explore a wide range of potential therapeutic interventions for improving wound healing outcomes [184].

In addition to drug discovery, in-silico studies are instrumental in elucidating the underlying molecular mechanisms for wound healing processes. Through network studies, pathway modeling, and molecular dynamics simulations, researchers can gain idea of complexity between various cellular and molecular components in wound healing cascades. Molecular docking is used for structure-based drug analysis, enabling the best conformational prediction within the target binding domain. A lower binding energy indicates a higher stability, suggesting prolonged contact between the molecules. This computational approach recognises potent drug molecules by finding binding affinities and interactions with target proteins, facilitating the rational design and optimization of therapeutic agents [185]. This comprehensive understanding enables the identification of key regulatory nodes and critical pathways that can be targeted for therapeutic intervention. Moreover, in-silico studies facilitate the prediction of potential side effects, drug interactions of candidate molecules, aiding in selection of promising candidates for further experimental validation. Overall, in-silico approaches serve as invaluable tools for accelerating novel therapeutic strategies for enhancing tissue regeneration [186].

The molecular docking approach facilitates the investigation of small molecule interactions with proteins at the atomic level, offering insights into their behaviour within binding sites and elucidating fundamental biochemical processes. This method involves predicting the conformation and positioning of ligands within binding sites, known as poses, and assessing binding affinity. By employing computation methods, molecular docking predicts ligand-receptor complex structures, binding energies, and affinities. In the context of MMP modulation, molecular docking results reveal strong interactions and affinities between compounds and MMPs, indicating their potential to modulate MMP activity. Pharmacologically, higher binding affinities correlate with increased target occupancy and activation potential, aligning with observed outcomes such as collagen synthesis and re-

epithelization, indicative of MMP activation [167,183,187]. The following table suggested some of the in silico studies have been done till now related to wound physiology and wound healing (Table 2).

Table 1.3: In silico studies on wound physiology and wound healing

Sl no	In silico study	Type of wound	References
1	"Use of berberine as wound healing agent via network pharmacology, molecular docking, and molecular dynamics simulation"	Chronic wound	[188]
2	"Wound Healing Potential of Phenylethanoid Glycoside in Inhibiting the Receptor for Advanced Glycation End Products"	Diabetic wound	[183]
3	"In Silico of Peptides with Wound Healing properties"	Chronic wounds	[59]
4	"*In vitro* human skin models for wound healing mechanism"	Chronic wounds	[182]
5	"*In Vivo, In Vitro*, and In Silico Wound Healing Potential of *Pinctada martensii* Purified Peptides"	Chronic wounds	[12]
6	"Wound Healing Potential and In Silico Appraisal of *Convolvulus arvensis* L. Methanolic Extract"	Chronic wounds	[58]
7	"In silico and antibacterial evaluation of curcumin derivatives loaded nanofiber"	Chronic wound	[189]
8	"In silico wound healing properties of 1-betasitosterol, 2-stigmasterol, microcarpin, ramosin, chrysophanol, asphodelin, and emodin with GSK3-β protein"	Chronic wound	[177]
9	"In silico wound healing properties curcuminoids from *Curcuma longa* as positive regulators of Wnt/β-catenin signaling pathway in wound healing"	Chronic wound	[185]

10	"In silico wound healing potential of isosakuratenin isolated from *Chromolaena odorata*"	Chronic wounds	[187]
11	"In silico Study of *Trianthema portulacastrum* Embedded Iron Oxide Nanoparticles on Gsk-3β for wound healing"	Chronic wounds	[190]
12	"In silico, *in vitro, ex vivo,* and *invivo* models of wounds and scars in human skin"	Chronic wounds	[191]
13	"Wound healing phytoconstituents from seed kernel of *Entada pursaetha* DC. and their molecular docking studies with Gsk3-β"	Chronic & acute wounds	[12]
14	"Wound healing activity and docking of glycogen-synthase-kinase-3-beta-protein with isolated triterpenoid lupeol in rats"	Chronic & acute wounds	[11]

The future of in silico mechanism for wound healing holds great promise as computational methodologies continue to advance, offering new insights and approaches for understanding the complex biological processes involved. With the increasing availability of high-performance computing resources and sophisticated algorithms, researchers can develop more comprehensive models that accurately simulate the intricate interactions between cells, tissues, and biomolecules during wound repair. Additionally, the integration of multi-scale modelling techniques, such as agent-based modelling and molecular dynamics simulations, enables the exploration of wound healing dynamics at various levels of complexity, from molecular interactions to tissue-level responses [192]. By harnessing the power of in silico approaches, researchers can accelerate the discovery and development of innovative wound healing therapies, ultimately improving patient outcomes and quality of life [193,194].

1.2.4 Challenges in Wound Healing Therapies

Skin wound treatment has evolved to incorporate a combination of regenerative strategies and conventional treatments such as debridement, aiming to address the challenges associated with wound healing [90]. Conventional methods like skin grafts, while effective, present

limitations including difficulty in securing them to the wound site and the potential for invasive surgical procedures leading to complications [195]. "Regenerative skin wound healing", a burgeoning field in biomedicine, seeks to overcome these challenges by restoring skin function and minimizing scarring through innovative approaches focused on enhancing the natural regeneration process. By leveraging reparative strategies that mimic physiological wound healing mechanisms, regenerative approaches hold promise for wound care [196]. Various factors affect this process for development of chronic wounds. These factors encompass both local and systemic aspects that disrupt the intricate cascade of events involved in tissue repair [27,30,197]. Local parameters include issues like tissue maceration, biofilm formation, ischemia, hypoxia and wound infection, all of which create an unfavorable environment for healing. Systemic factors, including conditions like old age and malnutrition further exacerbate the healing impairment. Despite adhering to good clinical practices, it remains challenging to completely mitigate the impact of these factors. Additionally, lowered growth factors, heightened levels of enzymes elevated inflammatory factors and accumulation of senescent cells serve as indicative of chronic wounds, underscoring the multifaceted nature of healing impairment [198].

Chronic wounds present a formidable challenge due to the complex environment they create, hindering the natural healing processes and leading to non-healing conditions. To effectively address this issue, it becomes crucial to delve deep into the underlying mechanisms contributing to the pathology of chronic wounds. This necessitates the identification of clinically relevant biological markers that play pivotal roles in perpetuating the chronicity of wounds. By pinpointing these biomarkers and understanding their functions, it becomes feasible to develop targeted interventions aimed at reversing the chronic status of wounds. These interventions could serve various purposes, including prognostic assessments, diagnostic tools, or treatment options tailored to address the specific underlying mechanisms identified. Ultimately, the identification and targeting of such biomarkers hold significant promise in improving the outcomes of chronic wound management, offering new avenues for therapeutic interventions and enhancing overall wound management [199]. The proteolytic degradation of ECM impedes wound progression and perpetuates the inflammatory cycle by attracting more inflammatory cells. This vicious cycle of inflammation and protease-mediated ECM destruction contributes to the chronicity of wounds, highlighting the importance of addressing protease dysregulation in wound healing interventions [200].

Managing chronic wounds involves a systematic approach that begins with validation of wound. This assessment provides crucial insights into underlying issues that may impede healing and guides subsequent treatment strategies. By addressing patient-specific factors such as hyperglycemia, renal insufficiency, and nutritional deficits alongside wound management, clinicians can optimize healing outcomes [201]. Additionally, a multidisciplinary approach involving various healthcare professionals ensures comprehensive care tailored to the individual needs of the patient. For example, vascular examinations help identify vascular insufficiency, enabling timely interventions to improve blood flow and facilitate wound healing. By integrating medical management with wound care and leveraging a multidisciplinary team, clinicians can navigate the complexities of chronic wound management more effectively, ultimately leading to favourable patient outcomes [202,203].

Dysregulation of microRNA (miRNA) expression influences several steps of wound healing mechanism. Reduced levels of miR-132 contribute to delayed wound healing by upregulating inflammatory pathways regulated by NF-κB, TLR and TNF signalling [204]. This prolonged inflammatory phase, driven by increased secretion of inflammatory mediators impedes change to proliferative step [205]. Conversely, overexpression of miR-155 provides detrimental effects such as increased myeloperoxidase-positive cells and decreased angiogenic markers, ultimately contributing to excessive ECM accumulation, which can hinder wound healing. Additionally, elevated levels of miR-200, miR-191, miR-26a, miR-15b, miR-200b and miR-205-5p are associated with impaired wound healing processes through various mechanisms, including inhibition of angiogenesis and VEGF pathways. These findings underscore intricate regulatory roles of miRNAs in modulating key pathways involved in wound healing, highlighting their potential as therapeutic targets for managing delayed wound repair [206,207].

Various types of wound dressings have their own limitations and challenges, which may hinder their effectiveness in promoting wound healing. Traditional dressings require frequent replacement and can leave particulates behind upon removal, potentially causing re-injury to the wound bed [100,208]. Moreover, the mechanical removal of gauze dressings may also remove healthy tissues along with unhealthy ones, making it less ideal for wound management. Similarly, foam-based dressings and adherent contact layer-based dressings may dry out quickly and require secondary dressings, while also posing discomfort during

removal and developing infection [98,209]. Film-based dressings address some of these issues. Hydrocolloid-based dressings, while effective in some cases, may also have drawbacks such as ineffectiveness against high exudate, frequent changing requirements, pain upon removal, and potential for wound maceration. These limitations underscore the need for continued innovation and development of wound dressing materials that can address the diverse needs of different types of wounds while minimizing discomfort and complications [210,211]

The traditional techniques have limitations including need for surgical treatments, minimal donor availability and potential alterations in functions. In contrast, regenerative healing approaches leverage developing methodologies to overcome these challenges without scarring [213]. These approaches encompass a range of strategies including smart wound dressings, stem cell and/or gene therapy, bioactive biomaterial matrices and bioengineered skin grafts [214]. However, further advancements are needed to optimize the cellular composition and spatial distribution of these skin substitutes to better recapitulate the complex microarchitecture of native skin tissues, highlighting ongoing efforts to develop innovative strategies for wound healing that preserve functional properties [215].

1.2.5 Natural Products in Wound Healing

Bio-based products are recognized for their potency in skin healing due to their diverse biological activities and minimal side effects. Plant-derived compounds, like flavonoids, alkaloids, terpenoids, and phenols, exhibit various pharmacological properties that promote tissue regeneration and wound closure. For instance, flavonoids possess antioxidant, anti-inflammatory, and antimicrobial properties, making them effective in reducing oxidative stress, and inflammation, and preventing infection in wounds. Additionally, alkaloids have been found to enhance angiogenesis facilitating generation of blood capillaries and ECM components essential for wound healing. Terpenoids, including essential oils, demonstrate antimicrobial activity and promote epithelialization, while phenolic compounds contribute to wound contraction and scar reduction by modulating the inflammatory response and enhancing collagen deposition [216].

Dysregulation of wound healing mechanism is a multifaceted issue involving various factors such as microbial biofilms, increased free radicals, and an imbalance in inflammatory cytokines. These parameters disrupt normal steps of wound healing, contributing to

persistence of chronic wounds. Overactive matrix metalloproteinases (MMPs) have also been implicated in delayed wound healing, as they degrade extracellular matrix components necessary for tissue repair [178]. These challenges underscore the need for effective wound healing solutions that address the underlying pathophysiological mechanisms involved in chronic wounds while minimizing adverse effects.

Despite the advancements in synthetic wound healing products, concerns regarding their safety and environmental impact persist. Synthetic materials often contain additives, preservatives, or chemical compounds that may trigger allergic reactions or tissue irritation, posing risks to patients' health. Moreover, the long-term biocompatibility and environmental consequences of synthetic materials are not always well understood, raising concerns about their sustainability and posing potential ecological harm [217]. To mitigate these issues, there is a growing interest in exploring alternative, more natural approaches to wound care. By harnessing the therapeutic properties of natural compounds and materials, such as plant extracts, bioactive molecules, and biopolymers, researchers aim to develop safer, biocompatible, and environmentally friendly wound healing solutions [218]. These natural approaches offer promising avenues for enhancing wound healing outcomes while minimizing risks to both patients and the environment.

Numerous researchers have investigated the potential of various bioactive products for healing activity along with higher anti-inflammation and anti-microbial activity and antioxidant potency. These attributes are often due to bioactive compounds present in these natural products, which belong to diverse chemical families such as phenols, saponins, coumarins etc [219]. Saponins shown to elevate pro-collagen level, thereby aiding in tissue regeneration, similarly tannins and flavonoids exhibit antimicrobial attribute, crucial for preventing infections in wounds [220]. Given their potent wound-healing properties, natural products and their bioactive constituents help in wound care management [216,221]. For instance polymers such as polycaprolactone are utilized in the fabrication of healing material, often supplemented with biological materials to imitate dermal matrix. Additionally, taking antimicrobial compounds can enhance the antimicrobial properties of these dressings, resulting reduction in infection [222–224].

Bio-based molecules offer a promising alternative for elevating healing mechanisms. Most of these compounds possess antimicrobial and antioxidant properties, along with other healing

bioactive constituents, which promote blood coagulation and combat infection due to the presence of abundant phytochemicals and bio-active compounds.[225,226]. Extensive literature reports highlight the potential of various bioactive compounds to enhance wound healing across different phases of the process. Compared to synthetic molecules, natural compounds are generally safer, better tolerated, and more cost-effective, making them attractive options for wound therapy. Natural polymer-based dressings for wound healing, including alginate, chitosan, collagen, and cellulose, offer several advantages in wound management [227]. Natural-based biomaterials promote biocompatible and biodegradable wound healing, enhancing cell proliferation and collagen synthesis while maintaining a moist environment. They are non-toxic, often antimicrobial, and reduce infection risk. Alginate-based dressings, for example, are preferred over hydrocolloid dressings due to their ability to control pain, ease of use, and capacity to absorb exudate effectively. However, these dressings may be associated with higher costs and can potentially lead to wound maceration. On the other hand, iodine-based dressings, while commonly used for their antimicrobial properties, pose certain limitations [228,229].

The utilization of natural products for wound healing offers several potential advantages over conventional therapies. Natural compounds derived from plants often exhibit diverse biological activities, including antimicrobial, antioxidant, and wound-healing attributes [230]. For example, plant extracts such as aloe vera and curcumin are studied for effective wound-healing mechanism [231]. These natural products can modulate various steps of wound healing, leading to improved outcomes. Furthermore, natural products have no or minimum side effects as compared to other drugs commonly used in wound management [197,232]. They are biocompatible with human tissues and are less likely to cause adverse reactions, making them suitable for long-term use, particularly in chronic wound care.

Moreover, natural products often offer a cost-effective alternative to traditional wound therapies. Many natural remedies can be easily sourced from botanicals and herbs, making them more accessible and affordable, especially in resource-limited settings (Saini et al., 2016). Additionally, the cultivation and extraction of natural compounds require fewer synthetic processes and chemicals, reducing the environmental impact associated with manufacturing pharmaceuticals. Furthermore, the use of natural products aligns with the growing trend towards holistic and integrative medicine, where the focus is on promoting overall health and wellness rather than just treating symptoms [226]. The potential

advantages of natural products in wound healing lie not only in their efficacy and safety but also in their sustainability and compatibility with complementary therapeutic approaches [227,233].

1.2.6 Waste-Derived Biomaterials

Researchers worldwide are increasingly exploring innovative and eco-friendly technologies for the management of biological waste, focusing on its holistic utilization beyond traditional methods like composting and biogas production [156,234]. Among these advancements, the preparation of biomaterials such as scaffolds from animal waste has garnered significant attention. Biomaterials derived from livestock waste, including, hyaluronic acid and collagen, have emerged as valuable resources [234]. For instance, eggshells are repurposed for calcium citrate nanosheets, which hold promise as bone graft substitutes [235]. These approaches highlight the potential of biological methods in waste management, for converting waste into valuable products, offering a green synthesis approach. Utilizing animal waste for biomaterial fabrication not only addresses environmental pollution but also contributes to the development of sustainable solutions for various biomedical applications [236].

Allografts and autografts represent two primary approaches in tissue transplantation for wound repair, each with distinct advantages and limitations. Allografts, derived from donors of the same species as the recipient, offer a readily available source of tissue for transplantation. In contrast, autografts involve the transplantation of tissues from the individual's own body, reducing rejection chance but often limited by donor site availability and increased surgical complexity. However, advancements in tissue engineering have expanded the options for wound repair, with scaffolds serving as temporary biologic structures to support tissue regeneration [237,238]. Tailoring the mechanical properties of biomaterials ensures optimal wound healing outcomes by enabling them to withstand mechanical stress, conform to the wound's shape, and support cell growth and tissue regeneration. By integrating advanced biomaterials with tissue engineering techniques, researchers can develop innovative ideas to address the diverse challenges linked to wound repair and enhance patient outcomes [239]. By employing sophisticated fabrication techniques, these bioactive molecules are transformed into scaffolds and dressing materials with remarkable biocompatibility and tissue regeneration attributes. Furthermore, utilization of waste-derived biomaterials not only addresses environmental concerns by reducing waste

accumulation in landfills and water bodies but also presents a cost-effective and sustainable solution for healthcare systems [240].

Similarly in another study by Sing et al., decellularized extracellular matrix (ECM) derived from the submucosa of goat small intestines was investigated as a potential scaffold [241]. Initially, biowaste from the goat small intestines was collected and underwent a decellularization process to remove cellular components. The resulting decellularized ECM was then repurposed as a scaffold for controlled release applications. Specifically, the researchers explored its potential for delivering curcumin, a compound renowned for its antioxidant properties and ability to enhance wound contractures. By incorporating curcumin into the decellularized goat small intestine scaffold, the study aimed to harness the therapeutic benefits of curcumin for wound healing purposes while utilizing the ECM scaffold to provide structural support and facilitate controlled release of the bioactive compound [241].

Similarly the study by [242], keratin from chicken feathers was utilized to develop wound dressings, including "three different combinations: keratin alone (CFK), keratin-chitosan (CFK-C), and keratin-sodium alginate (CFK-SA)". The research suggested CFK-C and CFK-SA had antimicrobial activity. Moreover, these fabricated materials showed biocompatibility [242]. In another study "a porous scaffold was developed by blending agar with chicken feather-derived keratin. The scaffold fabrication involved mixing 5% ground feather and 5% agar solution, followed by employing the freeze extraction technique. This method resulted in the formation of an interconnected porous structure characterized by 94.40% porosity and pore sizes ranging from 50 to 300 nm. The scaffold exhibited hydrophobic properties along with 160% water retention capacity, 16.33% elongation until breakage, and a tensile strength of 0.154 MPa. Additionally, the scaffold demonstrated favourable antimicrobial properties, excellent cell viability, and negative cytotoxicity. These attributes suggest that the developed scaffold holds significant potential for applications in tissue engineering, particularly in skin regeneration and wound healing"[243].

Similarly the egg membrane, known for its favourable morphology and mechanical properties, has been explored for its potential in fabricating biomaterials for wound dressing [244]. Various extraction processes, including manual peeling, as well as the use of EDTA or acetic acid, have been employed to isolate the eggshell membrane [244]. Biobrane, a

biomaterial composed of a porcine collagen-coated nylon net, offers a convenient solution for wound management by enabling topical application to the wound site and easy removal upon re-epithelialization [245]. This innovative approach not only simplifies wound care procedures but also enhances patient comfort and reduces the risk of disturbance to the healing process. With its unique properties and practical application, Biobrane represents a promising advancement in wound management strategies [245].

The utilization of biomaterials in wound healing offers multifaceted benefits, like a scaffold that imitates bio based ECM of skin, facilitating cell attachment, proliferation, and tissue regeneration. Moreover, biomaterials can deliver bioactive molecules and antimicrobial agents, aiding in wound closure and infection prevention. Their tunable properties allow for customization to specific wound characteristics. Studies, have demonstrated the positive outcomes associated with biomaterial use, including accelerated wound closure, tissue regeneration, reduced scarring, and improved cosmetic appearance [98][99]. Additionally, biomaterials enable targeted delivery of therapeutics, enhancing treatment efficacy while minimizing systemic side effects [100,101]. Overall, biomaterials play a pivotal role in advancing wound care, promising improved patient outcomes and contributing to the evolution of wound healing strategies.

Biomaterials used for wound healing often possess sustainable and eco-friendly characteristics, contributing to their suitability for medical applications while minimizing environmental impact. These biomaterials are frequently derived from renewable sources, reducing reliance on non-renewable resources [244]. Additionally, many biomaterials used in wound healing are biodegradable, meaning they can be broken down naturally by biological processes over time, thus reducing waste accumulation and environmental pollution. Furthermore, the production processes for these biomaterials often involve environmentally friendly methods, such as green chemistry principles or low-energy fabrication techniques, further minimizing their ecological footprint [246]. Overall, the sustainable and eco-friendly characteristics of biomaterials used for wound healing align with the broader goals of promoting environmental stewardship and conservation while advancing medical treatment modalities [247]

1.2.7 Different therapies for wound healing

Biomaterials enhance the regenerative potential of tissues by facilitating the restoration of damaged states and the re-establishment of biological function. Their primary objective is to provide mechanical support for crucial cellular processes such as adhesion, proliferation, migration, and differentiation, thereby fostering the generation of functional tissue. Natural biomaterials are extensively studied due to their biocompatibility enabling enhanced cell adhesion and function within in vitro biological models. Through interdisciplinary collaboration and continuous advancements in biomaterial design and fabrication, tissue engineering holds significant promise for developing innovative solutions to promote tissue regeneration and wound healing [87, 88].

Starch, due to its easily modifiable nature through chemical procedures, has emerged as a versatile material for applications in drug delivery and tissue engineering. Researchers have developed innovative starch-based hydrogels for drug delivery purposes, such as the injectable starch-chitosan hydrogel[253], which demonstrated potential for delivering chondrocytes. Starch's non-ionic nature allows it to be blended with other polymers, enhancing properties like pore size and water uptake in resulting polymer blends [254], who achieved excellent mechanical properties and increased porosity in gelatine-starch scaffolds. Moreover, starch-based scaffolds exhibit favourable characteristics for tissue engineering applications, including biodegradation and substrate suitability for cell adhesion, [255]. These attributes make starch-based scaffolds promising candidates for wound healing applications, [256], where increased fibroblast cell growth and proliferation were observed with low toxicity, and [257], who successfully treated chronic ulcers using starch-based nanocomposite hydrogel scaffolds without eliciting hypersensitivity reactions. Additionally reported on the development of starch-gelatine scaffolds, showcasing their ability to accelerate wound closure and promote tissue reorganization and remodelling, further underscoring the potential of starch-based materials in wound healing therapies [258].

Similarly Hyaluronic acid and chitosan are commonly used polysaccharides in the fabrication of hydrogels for wound healing applications. Hydrogels containing Hyaluronic acid and chitosan have demonstrated angiogenic promotion, enhanced vascular endothelial growth factor secretion, and increased antibacterial activity, making them promising therapeutic options for wound healing [259,260]. Additionally, Hyaluronic acid -based hydrogels have been shown to promote blood clotting and exhibit antibacterial properties, further supporting their efficacy in wound management. Chitosan-based hydrogels have also been utilized for

wound healing, with studies showing interactions with mucin to inhibit bacterial growth and enhance fibroblast proliferation. In burn wounds, chitosan-based hydrogels have demonstrated accelerated re-epithelialization, collagen fiber deposition, and wound healing[158]. Moreover, composite hydrogels combining Hyaluronic acid and chitosan, along with other materials such as PLGA microspheres or collagen, have been developed to enhance angiogenesis and antibacterial activity, contributing to improved wound healing outcomes. Overall, these studies highlight the potential of Hyaluronic acid and chitosan-based hydrogels as effective wound healing therapeutics, offering biocompatibility, enhanced cell adhesion, proliferation, migration, and wound protection [261].

Similarly bacterial cellulose possesses a porous structure akin to skin and is highly hydrophilic, making it well-suited for wound dressings to maintain a moist wound environment, which is crucial for effective healing. [263] developed a 3D printed carboxymethyl cellulose scaffold loaded with platelet-rich plasma, demonstrating sustained release of growth factors that enhanced angiogenesis, granulation, and re-epithelialization in diabetic wounds. This active dressing showed promise for diabetic patients by promoting wound healing. Additionally, cellulose can be combined with other components to augment its efficacy [264] incorporated cellulose with zinc oxide nanoparticles, resulting in improved mechanical and antibacterial properties of the wound dressing. These findings underscore the potential of cellulose-based materials in wound management, offering versatility and enhanced therapeutic effects for promoting wound healing.

In the context of treating wound disorders, topical gels represent a preferred therapeutic option due to their efficacy and safety profile, minimizing adverse effects at the site of application. Within pharmaceutical topical formulations, semisolids, liquids, sprays, and solid powders are commonly utilized, with gels, creams, and ointments falling under the category of semisolid treatments. Gels exhibit unique properties, forming an interlacing three-dimensional network of particles in the dispersed phase, facilitated by strong communication between the solid and fluid components. This interlacing and internal friction contributes to the semisolid state of gels, making them less oily and easier to remove from the skin, thereby enhancing patient compliance. Gels can be categorized based on the nature of the colloid phase and the nature of the solvent, offering versatile options for topical drug delivery strategies [265–267].

An optimal penetration enhancer should possess a range of characteristics to effectively facilitate the delivery of drugs through the skin barrier. These include chemical stability, pharmacological and chemical inertness, non-toxicity, lack of irritancy and allergenicity, rapid onset and consistent duration of action, reversibility, absence of odor, taste, or color, affordability, acceptance from both pharmaceutical and cosmetic perspectives, compatibility with skin solubility, absence of pharmacological activity within the body, aesthetic appeal, and versatility for incorporation into various topical formulations [268,269]. Additionally, penetration enhancers like gels find diverse applications, serving as drug delivery systems for oral medications, facilitating topical drug administration to the skin, eyes, or mucous membranes, providing long-acting drug formulations for intramuscular injection, and contributing to various cosmetic products such as shampoos, fragrances, dentifrices, and skincare preparations [270]. These attributes collectively ensure the efficacy, safety, and versatility of penetration enhancers in pharmaceutical and cosmetic applications.

Similarly, ointments have garnered attention for their potential benefits in wound healing, attributed to their anti-inflammatory, antimicrobial, and wound-healing properties derived from natural ingredients [271,272]. These ointments provide a natural alternative to conventional pharmaceutical products, particularly for minor wounds and skin irritations. While ointments may offer promising therapeutic effects, it's essential to acknowledge that scientific evidence supporting their efficacy can vary. Thus, consulting healthcare professionals is advisable to ensure safe and effective use, especially for more serious injuries or medical conditions [273]. Typically, ointments are topically applied directly to the wound site, facilitating targeted delivery of their active ingredients for localized treatment [274]. This targeted application makes them suitable for addressing various skin issues and promoting wound healing.

Decellularized ECM represents a promising approach in tissue engineering by providing scaffold with native architecture and biochemical cues of the tissue while removing cellular components. Research on dECMs has shown their potential as ideal tissue scaffolds due to their tissue-oriented construction, complex vascular meshwork composite for enhancing tissue regeneration. These matrices provide optimistic surrounding conducive to functions of stem cells, offering opportunities for applications in involuntary tissue engineering and skin regeneration. However, challenges such as edema, scar development and inflammatory are common, suggesting further optimization in utilization of dECMs *in vivo* through animal

experiments and address potential limitations in human applications [273,275,276]. Despite these challenges, refunctionalizing dECMs holds significant promise as a strategy to boost tissue engineering efforts, offering opportunities to address a wide range of clinical needs and improve patient outcomes.

1.2.8 Integration of Sustainable Practices in Soft Tissue Engineering

In tissue engineering, biomaterials facilitate tissue regeneration and restoring normal biological function in damaged tissues. These biomaterials are utilized within body using various fabrication techniques to serve like scaffolds for tissue reconstruction. Their primary function is to provide mechanical support for crucial cellular mechanisms like adhesion, proliferation, migration, and differentiation, thereby promoting tissue generation. Biomaterials also serve as temporary scaffolds imitating ECM and acting as a template for tissue development. Both bio-based and synthetic biomaterials are used in tissue engineering for their biocompatibility. When applied in *in vitro* biological models, these biomaterials produce fewer toxic by-products and enhance bio-recognition for improved cell adhesion (Greenwood et al., 2018).

Soft tissue engineering for wound healing involves the development of biomaterial-based approaches to promote the regeneration and repair of damaged tissues, particularly in cases of chronic wounds or extensive injuries. This field integrates principles from materials science, biology, and engineering to design scaffolds, dressings, and other therapeutic constructs imitating native ECM and backing cellular activities crucial for tissue regeneration. These biomaterials are often engineered to possess specific attributes like biocompatibility, bioavailability, porosity, and bioactivity to facilitate various steps required for wound healing. Several bio based and synthetic polymers, including hydrogels and collagen, are frequently used in soft tissue engineering as they manage a conducive microenvironment for healing processes [277,278].

Researchers in soft tissue engineering aim to develop advanced biomaterial-based solutions that not only accelerate wound closure but also enhance the functional restoration of injured tissues. Strategies like incorporating bioactive molecules, and stem cells into biomaterial matrices aim to promote angiogenesis, tissue regeneration, and remodelling for improved wound healing outcomes. Additionally, innovative fabrication mechanisms like electro-spinning offer precision on scaffold for development of tailored constructs for particular

wound types and patient needs. Through interdisciplinary collaboration and continuous advancements in biomaterial design and fabrication, soft tissue engineering holds promise for revolutionizing wound care by providing effective, biocompatible, and sustainable solutions for tissue repair [279–281].

Healing process of wounds which affect skin upper layer extensively is often prolonged and challenging due to diminished restoration, due to injury depth [282,283]. To address these challenges, traditional remedies derived from regional plants, animals, and natural products have long been relied upon, especially in regions like Asia and Latin America, where they serve as primary sources of wound care for many individuals [284]. Natural products have historically played a crucial role in medicine, offering a diverse array of bioactive compounds derived from plants with various biological functions [285]. These compounds are valued for their comprehensive structural composition, broad-spectrum antimicrobial activity, target-specific reactivity, and minimal to no side effects, making them important resources for both traditional and modern medicine formulations [286]. Utilization of natural compounds in wound healing has gained significant traction, reflecting their widespread application for wound management.

There has been an upsurge emphasis on adopting sustainable practices in fabrication process for healing remedies. One approach involves utilizing renewable and biodegradable resources as raw materials for biomaterial synthesis. For instance, bio based polymers like alginate, and chitosan, derived from sources like crustacean shells, seaweed, and plant fibers, respectively, offer excellent biocompatibility and wound healing properties while being environmentally friendly [287]. Additionally, utilisation of waste materials from several industrial by-products to develop biomaterials has been increasing. By repurposing these waste streams, not only can the environmental burden of waste disposal be reduced, but valuable resources can also be extracted for biomaterial production, contributing to a more sustainable circular economy [288].

Another sustainable approach involves the development of fabrication processes that minimize energy consumption, waste generation, and environmental impact. Green synthesis methods, such as solvent-free techniques, microwave-assisted synthesis, and enzymatic reactions, are being increasingly employed to produce biomaterials with reduced environmental footprint [289]. Moreover, the use of eco-friendly solvents and biocompatible

crosslinkers further enhances the sustainability profile of biomaterial fabrication processes [290]. Furthermore, advances in additive manufacturing technologies, such as 3D printing, enable precise control over material usage and offer opportunities for on-demand, customized fabrication of biomaterials, thereby minimizing material waste and energy consumption [291]. By integrating these sustainable practices into biomaterial fabrication processes, researchers can facilitate eco-friendly solutions for healing practices.

The shift towards sustainable biomaterials in biomedical applications has opened up new avenues for therapeutic interventions, particularly in fields such as 3D bioprinting, tissue engineering, even drug delivery process. The sources of these biomaterials are algae, plants, and animals, offer numerous advantages over their non-ecological counterparts. They are biodegradable and bioavailable, making them suitable for scaffold applications where cells can grow and thrive. For instance, animal waste, a byproduct of industries such as meat and leather production, is being repurposed to extract valuable biomaterials like collagen, gelatine, and chitosan. Moreover, even human skin with its redundant property is utilized as a scaffold for tissue engineering, thereby substitutes the synthesized ones, contributing to improved healing practices [98,292].

Chemically, sustainable biomaterials can be classified into polysaccharides and proteins, both of which offer unique properties and applications in skin burn treatment. Polysaccharides like chitosan, alginate, and hyaluronic acid, along with keratin, are explored in scaffold fabrication for tissue engineering. Additionally, synthetic biodegradable polymers are being developed and integrated with antimicrobial agents, antioxidants, and growth factors to accelerate healing practices. This interdisciplinary approach leverages the natural resources available in abundance while advancing innovations in tissue engineering, drug delivery, transplantation, and molecular medicine. Overall, the utilization of sustainable biomaterials holds promise for addressing challenges in skin burn treatment and improving patient care outcomes through multifunctional scaffold designs and targeted therapeutic interventions [98,292].

In soft tissue engineering realm, environmental impact and ethical considerations associated with biomaterials are gaining increasing attention. Biomaterials used in tissue engineering often involve complex fabrication processes, which can consume significant energy and resources, leading to environmental implications such as pollution and waste generation. To

mitigate these impacts, researchers are exploring sustainable alternatives and green fabrication techniques. For instance, biofabrication methods that utilize renewable resources, such as plant-derived polymers or waste materials, can reduce environmental pressure [293]. Additionally, biodegradable biomaterials offer the advantage of reducing long-term environmental pollution by naturally degrading after fulfilling their intended function, minimizing the accumulation of synthetic materials in ecosystems [294]. Furthermore the ethical considerations in soft tissue engineering involve ensuring the responsible and equitable use of biomaterials, particularly in the context of human experimentation and clinical translation. This includes ensuring efficacy of biomaterial-based therapies and adherence to ethical guidelines for human trials [295]. Moreover, there is a growing emphasis on transparency and informed consent in research involving biomaterials, ensuring that participants fully understand the risks and benefits of experimental treatments. Additionally, there is a need to address potential social and economic disparities in access to advanced tissue engineering therapies, promoting equitable distribution and affordability to ensure that benefits are accessible to all segments of society [296]. By integrating environmental sustainability and ethical considerations into soft tissue engineering practices, researchers can develop biomaterial-based therapies that not only advance medical treatment but also uphold principles of social responsibility and environmental stewardship [297].

Eco-friendly biomaterials, developed through green technology or derived from various biological sources, represent a promising shift toward sustainable alternatives in both biomedical and non-biomedical applications. As highlighted by [113] these materials have gained significant traction in the biomedical field, finding diverse applications ranging from breast implants to wound healing and ophthalmology. Offering biocompatibility and promoting tissue integration, eco-friendly biomaterials contribute to improved patient outcomes while reducing the risk of adverse reactions. Moreover, their eco-friendly nature addresses concerns about the ecological impact of conventional materials, as emphasized by [114]. By conserving natural resources and minimizing environmental pollution, these biomaterials align with the principles of sustainable development and responsible manufacturing practices, making them a promising choice for use in both healthcare and beyond [297]

1.3 Problem statement

Wound healing is crucial for tissue repair and restoration, encompassing multiple cellular and molecular pathways. Single nucleotide polymorphisms (SNPs) are genetic variations that can influence individual susceptibility to diseases and response to treatments, including wound healing [58,298,299]. Interpreting the role of SNPs in wound healing pathways is essential for preparing personalized therapeutic approaches. With recent advancements in bioinformatics, utilizing a computational approach to validate SNPs role on wound healing pathways offers a promising avenue for elucidating genetic determinants of wound healing variability. By analyzing datasets of genetic variants and their association with wound healing outcomes, bioinformatics tools can identify SNPs that modulate key pathways involved in tissue repair, offering insights into potential therapeutic targets for enhancing wound healing efficacy (Velnar et al., 2009; Wu et al., 2019).

Of particular interest is the GSK-3β gene, which is related to wound-related pathways. Mutations in GSK-3β have shown major impact in other disorders and conditions, including impaired wound healing. GSK-3β regulates multiple cellular processes associated with wound healing, like inflammation, cell proliferation, and migration [39,298,299]. Therefore, investigating the impact of GSK-3β mutations on wound-related pathways using bioinformatics approaches holds significant potential for identifying novel therapeutic targets. By comprehensively analyzing genetic data and correlating GSK-3β mutations with wound healing outcomes, researchers can uncover specific genetic variants that influence GSK-3β activity and downstream signalling pathways relevant to wound repair. This could facilitate the exploitation of specific therapeutics for regulating GSK-3β activity to promote more effective wound healing. It has been evident from various studies that the dysregulation of GSK-3β has a direct impact on inflammation angiogenesis hence affecting the healing process. Thus it is necessary to develop formulations or therapies which can directly control the inflammatory cytokines after the onset of the wound and also promote angiogenesis and neovascularization thus nullifying the effect of dysregulated GSK-3β. However, the utilization of sustainable biomaterials for wound healing is paramount, not only for their therapeutic efficacy but also for addressing pressing environmental concerns. By incorporating eco-friendly biomaterials derived from renewable sources such as cellulose, collagen, chitin, alginate etc., we can mitigate the environmental impact linked to traditional wound healing materials [88, 92]. Sustainable biomaterials offer a promising avenue for reducing carbon footprint and minimizing waste generation in wound care practices. Moreover, their biodegradable nature aligns with the principles of eco-consciousness,

fostering a greener approach to healthcare. Embracing sustainable biomaterials for wound healing not only benefits patients but also contributes to the global effort towards environmental sustainability.

1.4 Rationale of research

The recovery of wounds involves a complex cascade of physiological processes, including homeostasis, inflammation, proliferation, and tissue remodelling, as highlighted [300]. These phases are orchestrated by numerous cellular events, regulated by various growth factors, cytokines, and signalling pathways. Factors like age, health status, and other underlying conditions play critical roles in influencing the efficiency and success of wound healing mechanism [301,302]. Any disruption or imbalance in these processes, brought on by a loss of the body's self-healing ability, can pose challenges to wound-healing circumstances. Microorganisms, particularly bacteria, are significant contributors to wound infections, which can impede healing and lead to tissue deterioration. The normal progression of wound infection is through several stages, including contamination, colonization, acute colonization, and infection [303]. These microbial infections disrupt the natural healing process, causing distracted healing and further complicating the wound management process. Therefore, proper wound management is essential for promoting optimal wound healing results.

The rationale for studying the vitality of SNPs in wound healing and the fabrication of effective therapeutics using a bioinformatics approach is multifaceted. Firstly, SNPs represent genetic variations that can influence individual susceptibility to diseases and response to treatments, including wound healing. By employing bioinformatics tools, systematic analyze genetic data to identify SNPs associated with altered wound healing outcomes, providing valuable insights into the genetic determinants underlying wound healing variability. Moreover integrating information on biomaterials, particularly hydrogels, into this study is crucial. Hydrogels are frequently used materials for wound healing processes for their higher water content, biocompatibility, and tunability. Understanding how SNPs interact with hydrogel-based therapeutics and influence wound healing pathways by optimizing new biomaterial-based wound care strategies, ultimately enhancing treatment efficacy and patient outcomes [304].

Furthermore, investigating the interplay between SNPs and hydrogels in wound healing pathways is required in regenerative medicine. Hydrogels can serve as versatile platforms for

delivering bioactive molecules, cells, and growth factors required for a well-managed wound closure [304]. By elucidating the molecular mechanisms underlying the interaction between SNPs and hydrogel-based therapeutics, researchers can identify key genetic factors that influence therapeutic responses and tailor treatment strategies to individual patient profiles. This personalized approach holds significant promise for improving wound healing outcomes and reducing healthcare costs associated with chronic wound management. Ultimately, integrating bioinformatics analysis with biomaterials research, particularly hydrogels, offers a comprehensive framework for advancing our understanding of wound healing pathways and developing innovative therapeutic interventions for effective wound care [305].

1.5 Scope of Study

The scope of the study on bioinformatics approaches to evaluate SNPs importance in wound healing and fabrication of effective therapeutics encompasses several key areas. Firstly, the study aims to elucidate the genetic determinants underlying variability in wound healing outcomes, particularly focusing on the influence of SNPs on wound-related GSK-3B pathways. By utilizing bioinformatics tools and datasets for in silico study of GSK-3B mutant variants, researchers can identify SNPs associated with altered wound healing responses, providing valuable insights into the molecular mechanisms driving individual differences in wound healing efficiency. Moreover, the study seeks to integrate information on biomaterials, gels, and ointments into the analysis, acknowledging their pivotal role in wound healing interventions. Understanding how specific SNPs interact with biomaterial-based therapeutics, can inform the development of personalized treatment strategies tailored to individual genetic profiles. It also aims to explore the potential of biomaterials, gels, and ointments as effective therapeutic modalities for wound healing. Biomaterials offer versatile platforms for delivering bioactive molecules, growth factors, and antimicrobial agents to wound sites, enhancing tissue regeneration and subsequent wound closure. Ultimately, the scope of the study extends to advancing our understanding of the complex interplay between genetic factors, biomaterial-based therapies, and wound healing processes, for overarching aim of wound management.

1.6 Aims and Objectives

1.6.1 Aim:

To investigate the impact of deleterious SNPs in GSK-3β on wound healing and to develop and characterize proanthocyanidin-rich grape seed extract-based biomaterials and formulations for enhanced wound healing applications with the potential to control chronic inflammation and promote angiogenesis during the process and thus nullifying the effect of de-regulated GSK-3β due to presence of SNPs .

1.6.2 Objectives:

Objective 1: In-silico Prediction and Analysis of GSK-3β Deleterious SNPs and Their Impact on Wound Healing

1. Predict deleterious SNPs in the GSK-3β gene.

2. Re-confirm the deleterious nature of the identified SNPs using multiple prediction servers: Meta SNPs, PHD-SNP, SNPs & GO, PREDICT SNP, and Pmut.

3. Assess the effect of these nsSNPs on GSK-3β protein stability.

4. Predict conserved domains within GSK-3β.

5. Model the GSK-3β protein and its mutants.

6. Conduct secondary structure prediction for GSK-3β and its mutants.

7. Perform molecular dynamic simulation analysis.

8. Analyze and predict secondary structural changes resulting from the SNPs.

Objective 2: Fabrication and Characterization of Starch-Gelatin MAT loaded with commercially available Proanthocyanidin-Rich Grape Seed Extract

1. Fabricate different compositions of Starch-Gelatin MAT based on varying ratios of Gelatin and Starch.

2. Conduct detailed physiochemical characterization of the fabricated films, including:

   o Scanning Electron Microscopy (SEM)

   o Thermogravimetric Analysis (TGA)

- Differential Scanning Calorimetry (DSC)

- Fourier Transform Infrared Spectroscopy (FTIR)

- Tensile Strength Study

- Atomic Force Microscopy (AFM)

- Contact Angle Study

3. Perform swelling and degradation studies.

4. Evaluate in-vitro cellular interactions using fibroblast cells, including:

- Cellular Proliferation Assay (MTT Assay)

- Live/Dead Assay

5. Conduct in-vivo biocompatibility studies using a rat model.

Objective 3: Development of winery waste-derived Proanthocyanidin-Rich Grape Seed Extract-Based Gel for Modulating Inflammatory Responses in Wound Healing

1. Extract and optimize proanthocyanidin-rich grape seed extract from winery waste.

2. Analyze proanthocyanidin content.

3. Conduct LCMS analysis for compound characterization.

4. Perform in-vitro studies on fibroblast cells, including:

- Cellular Proliferation Assay (MTT Assay)

- Scratch Assay

- Cellular Morphology Analysis

- Cell Cycle Analysis

- Anti-inflammatory Assay

5. Fabricate starch glycerite gel containing the grape seed extract.

6. Assess the cellular and hemolytic properties of the formulated gel.

7. Conduct in-vivo critical wound healing studies using a rabbit model.

Objective 4: Fabrication and Characterization of Starch-PVA Thin Films Crosslinked with Proanthocyanidin-Rich Grape Seed Extract for wound healing application

1. Develop different compositions of Starch-PVA thin films by varying the ratios of PVA and Starch.

2. Perform detailed physiochemical characterization of the films, including:

   o Scanning Electron Microscopy (SEM)

   o Thermogravimetric Analysis (TGA)

   o Differential Scanning Calorimetry (DSC)

   o Fourier Transform Infrared Spectroscopy (FTIR)

   o Tensile Strength Study

   o Atomic Force Microscopy (AFM)

   o X-ray Diffraction (XRD) Study

   o Contact Angle Study

3. Conduct swelling and degradation studies.

4. Evaluate in-vitro cellular interactions with fibroblast cells, including:

   o Cellular Proliferation Assay (MTT Assay)

   o Scratch Assay

   o Cellular Morphology Analysis

   o Cellular Attachment Study

5. Perform in-vivo wound healing studies using a rabbit model.

This structured approach aims to comprehensively study the genetic and material science aspects of wound healing, contributing to the development of innovative therapeutic strategies and biomaterials for enhanced wound care.

References

[1] D. Chicharro-Alcantara, M. Rubio-Zaragoza, E. Damia-Gimenez, J.M. Carrillo-Poveda, B. Cuervo-Serrato, P. Pelaez-Gorrea, Platelet rich plasma: new insights for cutaneous wound healing management, J Funct Biomater 18 (2018) 1–10.

[2] H. Sorg, C.G.G. Sorg, Skin Wound Healing: Of Players, Patterns, and Processes, European Surgical Research 64 (2023) 141–157. https://doi.org/10.1159/000528271.

[3] A. Nourian Dehkordi, F. Mirahmadi Babaheydari, M. Chehelgerdi, S. Raeisi Dehkordi, Skin tissue engineering: wound healing based on stem-cell-based therapeutic strategies, Stem Cell Res Ther 10 (2019) 111. https://doi.org/10.1186/s13287-019-1212-2.

[4] J.L. Liesveld, N. Sharma, O.S. Aljitawi, Stem cell homing: From physiology to therapeutics, Stem Cells 38 (2020) 1241–1253. https://doi.org/10.1002/stem.3242.

[5] L. Ye, X. He, E. Obeng, D. Wang, D. Zheng, T. Shen, J. Shen, R. Hu, H. Deng, The CuO and AgO co-modified ZnO nanocomposites for promoting wound healing in Staphylococcus aureus infection, Mater Today Bio 18 (2023) 100552. https://doi.org/10.1016/j.mtbio.2023.100552.

[6] R. Fitridge, M. Thompson, Mechanisms of Vascular Disease, University of Adelaide Press, 2011. https://doi.org/10.1017/UPO9781922064004.

[7] R.G. Frykberg, J. Banks, Challenges in the Treatment of Chronic Wounds, Adv Wound Care (New Rochelle) 4 (2015) 560–582. https://doi.org/10.1089/wound.2015.0635.

[8] P. Monika, M.N. Chandraprabha, A. Rangarajan, P.V. Waiker, K.N. Chidambara Murthy, Challenges in Healing Wound: Role of Complementary and Alternative Medicine, Front Nutr 8 (2022). https://doi.org/10.3389/fnut.2021.791899.

[9] P.G. Bowler, B.I. Duerden, D.G. Armstrong, Wound Microbiology and Associated Approaches to Wound Management, Clin Microbiol Rev 14 (2001) 244–269. https://doi.org/10.1128/CMR.14.2.244-269.2001.

[10] P. Monika, P.V. Waiker, M.N. Chandraprabha, A. Rangarajan, K.N.C. Murthy, Myofibroblast progeny in wound biology and wound healing studies, Wound Repair and Regeneration 29 (2021) 531–547. https://doi.org/10.1111/wrr.12937.

[11] B.G. Harish, V. Krishna, H.S. Santosh Kumar, B.M. Khadeer Ahamed, R. Sharath, H.M. Kumara Swamy, Wound healing activity and docking of glycogen-synthase-kinase-3-β-protein with isolated triterpenoid lupeol in rats, Phytomedicine 15 (2008) 763–767. https://doi.org/10.1016/j.phymed.2007.11.017.

[12] S.M. Vidya, V. Krishna, B.K. Manjunatha, B.R. Bharath, K.P. Rajesh, H. Manjunatha, K.L. Mankani, Wound healing phytoconstituents from seed kernel of Entada pursaetha DC. and their molecular docking studies with glycogen synthase kinase 3-β, Medicinal Chemistry Research 21 (2012) 3195–3203. https://doi.org/10.1007/s00044-011-9860-5.

[13]   M. Kulac, C. Aktas, F. Tulubas, R. Uygur, M. Kanter, M. Erboga, M. Ceber, B. Topcu, O.A. Ozen, The effects of topical treatment with curcumin on burn wound healing in rats, J Mol Histol 44 (2013) 83–90. https://doi.org/10.1007/s10735-012-9452-9.

[14]   X.-J. Wang, G. Han, P. Owens, Y. Siddiqui, A.G. Li, Role of TGFβ-Mediated Inflammation in Cutaneous Wound Healing, Journal of Investigative Dermatology Symposium Proceedings 11 (2006) 112–117. https://doi.org/10.1038/sj.jidsymp.5650004.

[15]   K.G. Harding, Science, medicine, and the future: Healing chronic wounds, BMJ 324 (2002) 160–163. https://doi.org/10.1136/bmj.324.7330.160.

[16]   T.A. Mustoe, K. O??Shaughnessy, O. Kloeters, Chronic Wound Pathogenesis and Current Treatment Strategies: A Unifying Hypothesis, Plast Reconstr Surg 117 (2006) 35S-41S. https://doi.org/10.1097/01.prs.0000225431.63010.1b.

[17]   M.G. Tonnesen, X. Feng, R.A.F. Clark, Angiogenesis in Wound Healing, Journal of Investigative Dermatology Symposium Proceedings 5 (2000) 40–46. https://doi.org/10.1046/j.1087-0024.2000.00014.x.

[18]   P. Kumar, S. Kumar, E.P. Udupa, U. Kumar, P. Rao, T. Honnegowda, Role of angiogenesis and angiogenic factors in acute and chronic wound healing, Plast Aesthet Res 2 (2015) 243. https://doi.org/10.4103/2347-9264.165438.

[19]   D.B. Gurevich, C.E. Severn, C. Twomey, A. Greenhough, J. Cash, A.M. Toye, H. Mellor, P. Martin, Live imaging of wound angiogenesis reveals macrophage orchestrated vessel sprouting and regression, EMBO J 37 (2018). https://doi.org/10.15252/embj.201797786.

[20]   N.M. Kofler, M. Simons, Angiogenesis versus arteriogenesis: neuropilin 1 modulation of VEGF signaling, F1000Prime Rep 7 (2015). https://doi.org/10.12703/P7-26.

[21]   S.I. Blaber, J. Diaz, M. Blaber, Accelerated healing in <scp>NONcNZO10/LtJ</scp> type 2 diabetic mice by <scp>FGF</scp> -1, Wound Repair and Regeneration 23 (2015) 538–549. https://doi.org/10.1111/wrr.12305.

[22]   Y.C. Chan, S. Roy, Y. Huang, S. Khanna, C.K. Sen, The MicroRNA miR-199a-5p Down-regulation Switches on Wound Angiogenesis by Derepressing the v-ets Erythroblastosis Virus E26 Oncogene Homolog 1-Matrix Metalloproteinase-1 Pathway, Journal of Biological Chemistry 287 (2012) 41032–41043. https://doi.org/10.1074/jbc.M112.413294.

[23]   A.P. Veith, K. Henderson, A. Spencer, A.D. Sligar, A.B. Baker, Therapeutic strategies for enhancing angiogenesis in wound healing, Adv Drug Deliv Rev 146 (2019) 97–125. https://doi.org/10.1016/j.addr.2018.09.010.

[24]   F. Royaniyan, A. Mohammad, T.A. Fereshte, R. Fatemeh, A. FATEMEH, A.R. HOSSEIN, A. Shervin, D. ALI, Effect of lipogel containing extracts of eryngium campestre L. and satureja hortensis L. on wound healing in male wistar rats, Journal of Mazandaran University of Medical Sciences 31 (2021) 152–162.

[25]   A. Daemi, M. Lotfi, M.R. Farahpour, A. Oryan, S.J. Ghayour, A. Sonboli, Topical application of *Cinnamomum* hydroethanolic extract improves wound healing by enhancing re-epithelialization and keratin biosynthesis in streptozotocin-induced diabetic mice, Pharm Biol 57 (2019) 799–806. https://doi.org/10.1080/13880209.2019.1687525.

[26] S.G. Seyed Ahmadi, M.R. Farahpour, H. Hamishehkar, Topical application of *Cinnamon verum* essential oil accelerates infected wound healing process by increasing tissue antioxidant capacity and keratin biosynthesis, Kaohsiung J Med Sci 35 (2019) 686–694. https://doi.org/10.1002/kjm2.12120.

[27] R.F. Diegelmann, Wound healing: an overview of acute, fibrotic and delayed healing, Frontiers in Bioscience 9 (2004) 283. https://doi.org/10.2741/1184.

[28] M. Olsson, K. Järbrink, U. Divakar, R. Bajpai, Z. Upton, A. Schmidtchen, J. Car, The humanistic and economic burden of chronic wounds: A systematic review, Wound Repair and Regeneration 27 (2019) 114–125. https://doi.org/10.1111/wrr.12683.

[29] H.N. Wilkinson, M.J. Hardman, Wound healing: cellular mechanisms and pathological outcomes, Open Biol 10 (2020). https://doi.org/10.1098/rsob.200223.

[30] V. Sarrazy, F. Billet, L. Micallef, B. Coulomb, A. Desmoulière, Mechanisms of pathological scarring: Role of myofibroblasts and current developments, Wound Repair and Regeneration 19 (2011). https://doi.org/10.1111/j.1524-475X.2011.00708.x.

[31] G.D. Marconi, L. Fonticoli, T.S. Rajan, S.D. Pierdomenico, O. Trubiani, J. Pizzicannella, F. Diomede, Epithelial-Mesenchymal Transition (EMT): The Type-2 EMT in Wound Healing, Tissue Regeneration and Organ Fibrosis, Cells 10 (2021) 1587. https://doi.org/10.3390/cells10071587.

[32] D. Zhao, Y. Wang, C. Du, S. Shan, Y. Zhang, Z. Du, D. Han, Honokiol Alleviates Hypertrophic Scar by Targeting Transforming Growth Factor-β/Smad2/3 Signaling Pathway, Front Pharmacol 8 (2017). https://doi.org/10.3389/fphar.2017.00206.

[33] W.G. Payne, D.K. Naidu, C.K. Wheeler, D. Barkoe, M. Mentis, R.E. Salas, D.J. Smith Jr, M.C. Robson, Wound healing in patients with cancer, Eplasty 8 (2008).

[34] S. FRAME, P. COHEN, GSK3 takes centre stage more than 20 years after its discovery, Biochemical Journal 359 (2001) 1–16. https://doi.org/10.1042/bj3590001.

[35] B.W. Doble, J.R. Woodgett, GSK-3: tricks of the trade for a multi-tasking kinase, J Cell Sci 116 (2003) 1175–1186. https://doi.org/10.1242/jcs.00384.

[36] K.W. Cormier, J.R. Woodgett, Recent advances in understanding the cellular roles of GSK-3, F1000Res 6 (2017) 167. https://doi.org/10.12688/f1000research.10557.1.

[37] R.S. Jope, C.J. Yuskaitis, E. Beurel, Glycogen Synthase Kinase-3 (GSK3): Inflammation, Diseases, and Therapeutics, Neurochem Res 32 (2007) 577–595. https://doi.org/10.1007/s11064-006-9128-5.

[38] J.A. McCubrey, D. Rakus, A. Gizak, L.S. Steelman, S.L. Abrams, K. Lertpiriyapong, T.L. Fitzgerald, L. V. Yang, G. Montalto, M. Cervello, M. Libra, F. Nicoletti, A. Scalisi, F. Torino, C. Fenga, L.M. Neri, S. Marmiroli, L. Cocco, A.M. Martelli, Effects of mutations in Wnt/β-catenin, hedgehog, Notch and PI3K pathways on GSK-3 activity—Diverse effects on cell growth, metabolism and cancer, Biochimica et Biophysica Acta (BBA) - Molecular Cell Research 1863 (2016) 2942–2976. https://doi.org/10.1016/j.bbamcr.2016.09.004.

[39] M. Kapoor, S. Liu, X. Shi-wen, K. Huh, M. McCann, C.P. Denton, J.R. Woodgett, D.J. Abraham, A. Leask, GSK-3β in mouse fibroblasts controls wound healing and fibrosis through an

endothelin-1–dependent mechanism, Journal of Clinical Investigation (2008). https://doi.org/10.1172/JCI35381.

[40] F. Takahashi-Yanaga, Activator or inhibitor? GSK-3 as a new drug target, Biochem Pharmacol 86 (2013) 191–199. https://doi.org/10.1016/j.bcp.2013.04.022.

[41] R.J. Vidri, T.L. Fitzgerald, GSK-3: An important kinase in colon and pancreatic cancers, Biochimica et Biophysica Acta (BBA) - Molecular Cell Research 1867 (2020) 118626. https://doi.org/10.1016/j.bbamcr.2019.118626.

[42] J. Ren, T. Liu, Y. Han, Q. Wang, Y. Chen, G. Li, L. Jiang, GSK-3β inhibits autophagy and enhances radiosensitivity in non-small cell lung cancer, Diagn Pathol 13 (2018) 33. https://doi.org/10.1186/s13000-018-0708-x.

[43] X. Fan, Z. Zhao, D. Wang, J. Xiao, Glycogen synthase kinase-3 as a key regulator of cognitive function, Acta Biochim Biophys Sin (Shanghai) 52 (2020) 219–230. https://doi.org/10.1093/abbs/gmz156.

[44] Q. Lv, J. Deng, Y. Chen, Y. Wang, B. Liu, J. Liu, Engineered Human Adipose Stem-Cell-Derived Exosomes Loaded with miR-21-5p to Promote Diabetic Cutaneous Wound Healing, Mol Pharm 17 (2020) 1723–1733. https://doi.org/10.1021/acs.molpharmaceut.0c00177.

[45] X. Zhang, L. Wang, Y. Qu, Targeting the β-catenin signaling for cancer therapy, Pharmacol Res 160 (2020) 104794. https://doi.org/10.1016/j.phrs.2020.104794.

[46] E. Beurel, R.S. Jope, The paradoxical pro- and anti-apoptotic actions of GSK3 in the intrinsic and extrinsic apoptosis signaling pathways, Prog Neurobiol 79 (2006) 173–189. https://doi.org/10.1016/j.pneurobio.2006.07.006.

[47] L. Hoffmeister, M. Diekmann, K. Brand, R. Huber, GSK3: A Kinase Balancing Promotion and Resolution of Inflammation, Cells 9 (2020) 820. https://doi.org/10.3390/cells9040820.

[48] S.M. Arciniegas Ruiz, H. Eldar-Finkelman, Glycogen Synthase Kinase-3 Inhibitors: Preclinical and Clinical Focus on CNS-A Decade Onward, Front Mol Neurosci 14 (2022). https://doi.org/10.3389/fnmol.2021.792364.

[49] D. Chouhan, N. Dey, N. Bhardwaj, B.B. Mandal, Emerging and innovative approaches for wound healing and skin regeneration: Current status and advances, Biomaterials 216 (2019) 119267. https://doi.org/10.1016/j.biomaterials.2019.119267.

[50] F. Yang, X. Qin, T. Zhang, C. Zhang, H. Lin, Effect of Oral Administration of Active Peptides of Pinctada Martensii on the Repair of Skin Wounds, Mar Drugs 17 (2019) 697. https://doi.org/10.3390/md17120697.

[51] J. Li, J. Li, Recent advances in computational modeling of the wound healing process, Quantitative Biology 6 (2018) 95–105.

[52] T. Zhang, F. Yang, X. Qin, X. Yang, C. Zhang, Z. Wan, H. Lin, Investigation of the In Vivo, In Vitro, and In Silico Wound Healing Potential of Pinctada martensii Purified Peptides, Mar Drugs 20 (2022) 417. https://doi.org/10.3390/md20070417.

[53] D. St-Cyr, D.F. Ceccarelli, S. Orlicky, A.M. van der Sloot, X. Tang, S. Kelso, S. Moore, C. James, G. Posternak, J. Coulombe-Huntington, T. Bertomeu, A. Marinier, F. Sicheri, M. Tyers,

Identification and optimization of molecular glue compounds that inhibit a noncovalent E2 enzyme–ubiquitin complex, Sci Adv 7 (2021). https://doi.org/10.1126/sciadv.abi5797.

[54] J. Xu, S. Zhang, T. Wu, X. Fang, L. Zhao, Discovery of TGFBR1 (ALK5) as a potential drug target of quercetin glycoside derivatives (QGDs) by reverse molecular docking and molecular dynamics simulation, Biophys Chem 281 (2022) 106731. https://doi.org/10.1016/j.bpc.2021.106731.

[55] F. Akbari, M. Azadbakht, A. Bagheri, L. Vahedi, In Silico, In Vitro, and In Vivo Wound Healing Activity of Astragalus microcephalus Willd., Adv Pharmacol Pharm Sci 2022 (2022) 1–16. https://doi.org/10.1155/2022/2156629.

[56] O. Mashinchian, A.R. Pishevar, M. Mashinchian, Role of bioinformatics and computational biology in wound healing research: a systematic review, Wound Repair and Regeneration 27 (2019) 432–441.

[57] M. Karamanou, S.P. Karabela, Computational models of wound healing: methods and applications, Wound Medicine 31 (2020).

[58] U. Saleem, S. Khalid, S. Zaib, F. Anwar, M.F. Akhtar, L. Hussain, A. Saleem, B. Ahmad, Wound Healing Potential and In Silico Appraisal of Convolvulus arvensis L. Methanolic Extract, Biomed Res Int 2022 (2022) 1–16. https://doi.org/10.1155/2022/1373160.

[59] M. Trejos, Y. Aristizabal, A. Aragón-Muriel, J. Oñate-Garzón, Y. Liscano, Characterization and Classification In Silico of Peptides with Dual Activity (Antimicrobial and Wound Healing), Int J Mol Sci 24 (2023) 13091. https://doi.org/10.3390/ijms241713091.

[60] Y. Liscano, J. Oñate-Garzón, J.P. Delgado, Peptides with Dual Antimicrobial–Anticancer Activity: Strategies to Overcome Peptide Limitations and Rational Design of Anticancer Peptides, Molecules 25 (2020) 4245. https://doi.org/10.3390/molecules25184245.

[61] R.K. Thapa, D.B. Diep, H.H. Tønnesen, Topical antimicrobial peptide formulations for wound healing: Current developments and future prospects, Acta Biomater 103 (2020) 52–67. https://doi.org/10.1016/j.actbio.2019.12.025.

[62] S. Yin, Y. Wang, X. Yang, Amphibian-derived wound healing peptides: chemical molecular treasure trove for skin wound treatment, Front Pharmacol 14 (2023). https://doi.org/10.3389/fphar.2023.1120228.

[63] B. Balboni, M. Masi, W. Rocchia, S. Girotto, A. Cavalli, GSK-3β Allosteric Inhibition: A Dead End or a New Pharmacological Frontier?, Int J Mol Sci 24 (2023) 7541. https://doi.org/10.3390/ijms24087541.

[64] J. Shang, Y. Xu, H. Jiang, Y. Bai, J. Zheng, Impact of glycogen synthase kinase-3β polymorphism on the susceptibility of type 2 diabetes mellitus: A meta-analysis., BMC Med Genet 20 (2019).

[65] Y. Lee, S.-B. Yoon, H. Hong, H.Y. Kim, D. Jung, B.-S.Moon, W.-K. Park, S. Lee, H. Kwon, J. Park, H. Cho, Discovery of GSK3β Inhibitors through In Silico Prediction-and-Experiment Cycling Strategy, and Biological Evaluation, Molecules 27 (2022) 3825. https://doi.org/10.3390/molecules27123825.

[66]   A.P. Saraswati, S.M. Ali Hussaini, N.H. Krishna, B.N. Babu, A. Kamal, Glycogen synthase kinase-3 and its inhibitors: Potential target for various therapeutic conditions, Eur J Med Chem 144 (2018) 843–858. https://doi.org/10.1016/j.ejmech.2017.11.103.

[67]   C. Dealey, The Care of Wounds: A Guide for Nurses, 4th ed., Wiley-Blackwell, 2012.

[68]   S. Patel, A. Maheshwari, A. Chandra, Biomarkers for wound healing and their evaluation, J Wound Care 25 (2016) 46–55. https://doi.org/10.12968/jowc.2016.25.1.46.

[69]   A.D. Widgerow, Chronic wounds – is cellular 'reception' at fault? Examining integrins and intracellular signalling, Int Wound J 10 (2013) 185–192. https://doi.org/10.1111/j.1742-481X.2012.00967.x.

[70]   K.F. Cutting, R.J. White, P. Mahoney, DEVELOPING CLINICAL CRITERIA FOR WOUND INFECTION—A DELPHI APPROACH, Journal of Wound, Ostomy and Continence Nursing 32 (2005) S26. https://doi.org/10.1097/00152192-200505002-00085.

[71]   G. Logan, Clinical judgment and decision-making in wound assessment and management: is experience enough?, Br J Community Nurs 20 (2015) S21–S28. https://doi.org/10.12968/bjcn.2015.20.Sup3.S21.

[72]   J. Fletcher, Wound assessment and the TIME framework, British Journal of Nursing 16 (2007) 462–466. https://doi.org/10.12968/bjon.2007.16.8.23415.

[73]   L.M. Mioton, S.W. Jordan, P.J. Hanwright, K.Y. Bilimoria, J.Y. Kim, The Relationship between Preoperative Wound Classification and Postoperative Infection: A Multi-Institutional Analysis of 15,289 Patients, Arch Plast Surg 40 (2013) 522–529. https://doi.org/10.5999/aps.2013.40.5.522.

[74]   A. Shamloo, M. Sarmadi, Z. Aghababaie, M. Vossoughi, Accelerated full-thickness wound healing via sustained bFGF delivery based on a PVA/chitosan/gelatin hydrogel incorporating PCL microspheres, Int J Pharm 537 (2018) 278–289. https://doi.org/10.1016/j.ijpharm.2017.12.045.

[75]   D. Stan, C. Tanase, M. Avram, R. Apetrei, N. Mincu, A.L. Mateescu, D. Stan, Wound healing applications of creams and "smart" hydrogels, Exp Dermatol 30 (2021) 1218–1232. https://doi.org/10.1111/exd.14396.

[76]   N.K. Preman, S.P. E. S., A. Prabhu, S.B. Shaikh, V. C., R.R. Barki, Y.P. Bhandary, P.D. Rekha, R.P. Johnson, Bioresponsive supramolecular hydrogels for hemostasis, infection control and accelerated dermal wound healing, J Mater Chem B 8 (2020) 8585–8598. https://doi.org/10.1039/D0TB01468K.

[77]   A.J.M. Boulton, Diabetic foot – what can we learn from leprosy? Legacy of Dr Paul W. Brand, Diabetes Metab Res Rev 28 (2012) 3–7. https://doi.org/10.1002/dmrr.2230.

[78]   S. Wang, X. Zeng, Q. Yang, S. Qiao, Antimicrobial Peptides as Potential Alternatives to Antibiotics in Food Animal Industry, Int J Mol Sci 17 (2016) 603. https://doi.org/10.3390/ijms17050603.

[79]   J. Lazaro-Martinez, J. Aragon-Sanchez, E. Garcia-Morales, Antibiotics versus conservative surgery for treating diabetic foot osteomyelitis: a randomized comparative trial, Diabetes Care 37 (2014) 789–795.

[80]   X. Zhao, Y. Liang, Y. Huang, J. He, Y. Han, B. Guo, Physical Double-Network Hydrogel Adhesives with Rapid Shape Adaptability, Fast Self-Healing, Antioxidant and NIR/pH Stimulus-Responsiveness for Multidrug-Resistant Bacterial Infection and Removable Wound Dressing, Adv Funct Mater 30 (2020). https://doi.org/10.1002/adfm.201910748.

[81]   A. Chaudhari, K. Vig, D. Baganizi, R. Sahu, S. Dixit, V. Dennis, S. Singh, S. Pillai, Future Prospects for Scaffolding Methods and Biomaterials in Skin Tissue Engineering: A Review, Int J Mol Sci 17 (2016) 1974. https://doi.org/10.3390/ijms17121974.

[82]   V.A. Solarte David, V.R. Güiza-Argüello, M.L. Arango-Rodríguez, C.L. Sossa, S.M. Becerra-Bayona, Decellularized Tissues for Wound Healing: Towards Closing the Gap Between Scaffold Design and Effective Extracellular Matrix Remodeling, Front Bioeng Biotechnol 10 (2022). https://doi.org/10.3389/fbioe.2022.821852.

[83]   A.C. Panayi, V. Haug, Q. Liu, M. Wu, M. Karvar, S. Aoki, C. Ma, R. Hamaguchi, Y. Endo, D.P. Orgill, Novel application of autologous micrografts in a collagen-glycosaminoglycan scaffold for diabetic wound healing, Biomedical Materials 16 (2021) 035032. https://doi.org/10.1088/1748-605X/abc3dc.

[84]   A. Mariconda, A. Agovino, M. Sirignano, L. Guadagno, Strong Interaction with Carbon Filler of Polymers Obtained by Pyrene Functionalized Hoveyda-Grubbs 2nd Generation Catalyst, Polymers (Basel) 11 (2019) 1261. https://doi.org/10.3390/polym11081261.

[85]   F. Yao, Y. Zheng, Y. Gao, Y. Du, F. Chen, Electrospinning of peanut protein isolate/poly-L-lactic acid nanofibers containing tetracycline hydrochloride for wound healing, Ind Crops Prod 194 (2023) 116262. https://doi.org/10.1016/j.indcrop.2023.116262.

[86]   B. Akar, B. Jiang, S.I. Somo, A.A. Appel, J.C. Larson, K.M. Tichauer, E.M. Brey, Biomaterials with persistent growth factor gradients in vivo accelerate vascularized tissue formation, Biomaterials 72 (2015) 61–73. https://doi.org/10.1016/j.biomaterials.2015.08.049.

[87]   R.Z. Murray, Z.E. West, A.J. Cowin, B.L. Farrugia, Development and use of biomaterials as wound healing therapies, Burns Trauma 7 (2019). https://doi.org/10.1186/s41038-018-0139-7.

[88]   X. Deng, M. Gould, M.A. Ali, A review of current advancements for wound healing: Biomaterial applications and medical devices, J Biomed Mater Res B Appl Biomater 110 (2022) 2542–2573. https://doi.org/10.1002/jbm.b.35086.

[89]   S. Bhat, A. Kumar, Biomaterials in Regenerative Medicine, Journal of Postgraduate Medicine, Education and Research 46 (2012) 81–89. https://doi.org/10.5005/jp-journals-10028-1018.

[90]   E. Tottoli, R. Dorati, I. Genta, E. Chiesa, S. Pisani, Skin and tissue engineering in wound healing, in: P.B. Malafaya, A.M.S.P.S.P. Marques (Eds.), Advanced Strategies for Wound Dressings, Woodhead Publishing, 2020: pp. 83–114.

[91]   J. Su, J. Li, J. Liang, K. Zhang, J. Li, Hydrogel Preparation Methods and Biomaterials for Wound Dressing, Life 11 (2021) 1016. https://doi.org/10.3390/life11101016.

[92]   S. Prete, M. Dattilo, F. Patitucci, G. Pezzi, O.I. Parisi, F. Puoci, Natural and Synthetic Polymeric Biomaterials for Application in Wound Management, J Funct Biomater 14 (2023) 455. https://doi.org/10.3390/jfb14090455.

[93] M.I. Avila Rodríguez, L.G. Rodríguez Barroso, M.L. Sánchez, Collagen: A review on its sources and potential cosmetic applications, J Cosmet Dermatol 17 (2018) 20–26. https://doi.org/10.1111/jocd.12450.

[94] C. Dhand, Y. Balakrishnan, S.T. Ong, N. Dwivedi, J.R. Venugopal, S. Harini, C.M. Leung, K.Z.W. Low, X.J. Loh, R.W. Beuerman, S. Ramakrishna, N.K. Verma, R. Lakshminarayanan, Antimicrobial quaternary ammonium organosilane cross-linked nanofibrous collagen scaffolds for tissue engineering, Int J Nanomedicine Volume 13 (2018) 4473–4492. https://doi.org/10.2147/IJN.S159770.

[95] L. Vogt, L. Liverani, J. Roether, A. Boccaccini, Electrospun Zein Fibers Incorporing Poly(glycerol sebacate) for Soft Tissue Engineering, Nanomaterials 8 (2018) 150. https://doi.org/10.3390/nano8030150.

[96] A. Tamayol, A. Hassani Najafabadi, P. Mostafalu, A.K. Yetisen, M. Commotto, M. Aldhahri, M.S. Abdel-wahab, Z.I. Najafabadi, S. Latifi, M. Akbari, N. Annabi, S.H. Yun, A. Memic, M.R. Dokmeci, A. Khademhosseini, Biodegradable elastic nanofibrous platforms with integrated flexible heaters for on-demand drug delivery, Sci Rep 7 (2017) 9220. https://doi.org/10.1038/s41598-017-04749-8.

[97] P. Heydari, J. Varshosaz, A. Zargar Kharazi, S. Karbasi, Preparation and evaluation of poly glycerol sebacate/poly hydroxy butyrate core-shell electrospun nanofibers with sequentially release of ciprofloxacin and simvastatin in wound dressings, Polym Adv Technol 29 (2018) 1795–1803. https://doi.org/10.1002/pat.4286.

[98] J.S. Boateng, K.H. Matthews, H.N.E. Stevens, G.M. Eccleston, Wound Healing Dressings and Drug Delivery Systems: A Review, J Pharm Sci 97 (2008) 2892–2923. https://doi.org/10.1002/jps.21210.

[99] S. Guo, L.A. DiPietro, Factors Affecting Wound Healing, J Dent Res 89 (2010) 219–229. https://doi.org/10.1177/0022034509359125.

[100] V. Jones, J.E. Grey, K.G. Harding, Wound dressings, BMJ 332 (2006) 777–780. https://doi.org/10.1136/bmj.332.7544.777.

[101] P.T. Thevenot, D.W. Baker, H. Weng, M.-W. Sun, L. Tang, The pivotal role of fibrocytes and mast cells in mediating fibrotic reactions to biomaterials, Biomaterials 32 (2011) 8394–8403. https://doi.org/10.1016/j.biomaterials.2011.07.084.

[102] Z. Ma, W. Song, Y.He, H. Li, Multilayer Injectable Hydrogel System Sequentially Delivers Bioactive Substances for Each Wound Healing Stage, ACS Appl Mater Interfaces (2020) acsami.0c06360. https://doi.org/10.1021/acsami.0c06360.

[103] E. Calo, L. Ballamy, V.V. Khutoryanskiy, Hydrogels in wound management. In Hydrogels: Design, Synthesis and Application, Drug Delivery and Regenerative Medicine (2018).

[104] J.N. Mayba, M.J. Gooderham, Review of Atopic Dermatitis and Topical Therapies, J Cutan Med Surg 21 (2017) 227–236. https://doi.org/10.1177/1203475416685077.

[105] V. Gounden, M. Singh, Hydrogels and Wound Healing: Current and Future Prospects, Gels 10 (2024) 43. https://doi.org/10.3390/gels10010043.

[106] Y.A. Prakoso, Kurniasih, The Effects of *Aloe vera* Cream on the Expression of CD4 [+] and CD8 [+] Lymphocytes in Skin Wound Healing, J Trop Med 2018 (2018) 1–5. https://doi.org/10.1155/2018/6218303.

[107] T. Biswal, S.K. BadJena, D. Pradhan, Sustainable biomaterials and their applications: A short review, Mater Today Proc 30 (2020) 274–282. https://doi.org/10.1016/j.matpr.2020.01.437.

[108] Y.M. Awad, E. Blagodatskaya, Y.S. Ok, Y. Kuzyakov, Effects of polyacrylamide, biopolymer and biochar on the decomposition of <scp>[14] C </scp> -labelled maize residues and on their stabilization in soil aggregates, Eur J Soil Sci 64 (2013) 488–499. https://doi.org/10.1111/ejss.12034.

[109] M.K. Lauer, A.G. Tennyson, R.C. Smith, Inverse vulcanization of octenyl succinate-modified corn starch as a route to biopolymer–sulfur composites, Mater Adv 2 (2021) 2391–2397. https://doi.org/10.1039/D0MA00948B.

[110] N.M. Aguilar, F. Arteaga-Cardona, M.E. de Anda Reyes, J.J. Gervacio-Arciniega, U. Salazar-Kuri, Magnetic bioplastics based on isolated cellulose from cotton and sugarcane bagasse, Mater Chem Phys 238 (2019) 121921. https://doi.org/10.1016/j.matchemphys.2019.121921.

[111] C. Redondo-Gómez, M. Rodríguez Quesada, S. Vallejo Astúa, J.P. Murillo Zamora, M. Lopretti, J.R. Vega-Baudrit, Biorefinery of Biomass of Agro-Industrial Banana Waste to Obtain High-Value Biopolymers, Molecules 25 (2020) 3829. https://doi.org/10.3390/molecules25173829.

[112] D. Campoccia, L. Montanaro, C.R. Arciola, A review of the biomaterials technologies for infection-resistant surfaces, Biomaterials 34 (2013) 8533–8554. https://doi.org/10.1016/j.biomaterials.2013.07.089.

[113] J. Baranwal, B. Barse, A. Fais, G.L. Delogu, A. Kumar, Biopolymer: A Sustainable Material for Food and Medical Applications, Polymers (Basel) 14 (2022) 983. https://doi.org/10.3390/polym14050983.

[114] P. Pesode, S. Barve, S. V. Wankhede, A. Ahmad, Sustainable Materials and Technologies for Biomedical Applications, Advances in Materials Science and Engineering 2023 (2023) 1–22. https://doi.org/10.1155/2023/6682892.

[115] C.-H.Tsai, P.-Y.Wang, I.-C.Lin, H. Huang, G.-S.Liu, C.-L. Tseng, Ocular Drug Delivery: Role of Degradable Polymeric Nanocarriers for Ophthalmic Application, Int J Mol Sci 19 (2018) 2830. https://doi.org/10.3390/ijms19092830.

[116] Y. Chen, S.-T.Hung, E. Chou, H.-S. Wu, Review of Polyhydroxyalkanoates Materials and other Biopolymers for Medical Applications, Mini Rev Org Chem 15 (2018) 105–121. https://doi.org/10.2174/1570193X14666170721153036.

[117] S.-B.Park, E. Lih, K.-S. Park, Y.K. Joung, D.K. Han, Biopolymer-based functional composites for medical applications, Prog Polym Sci 68 (2017) 77–105. https://doi.org/10.1016/j.progpolymsci.2016.12.003.

[118] E.B. Yahya, A.A. Amirul, A.K. H.P.S., N.G. Olaiya, M.O. Iqbal, F. Jummaat, A.S. A.K., A.S. Adnan, Insights into the Role of Biopolymer Aerogel Scaffolds in Tissue Engineering and Regenerative Medicine, Polymers (Basel) 13 (2021) 1612. https://doi.org/10.3390/polym13101612.

[119] G. Kumar Gupta, S. De, A. Franco, A. Balu, R. Luque, Sustainable Biomaterials: Current Trends, Challenges and Applications, Molecules 21 (2015) 48. https://doi.org/10.3390/molecules21010048.

[120] J.M. Ruso, P.V. Messina, Biopolymers for Medical Applications, CRC Press, 2017.

[121] A. Farooq, M.K. Patoary, M. Zhang, H. Mussana, M. Li, M.A. Naeem, M. Mushtaq, A. Farooq, L. Liu, Cellulose from sources to nanocellulose and an overview of synthesis and properties of nanocellulose/zinc oxide nanocomposite materials, Int J Biol Macromol 154 (2020) 1050–1073. https://doi.org/10.1016/j.ijbiomac.2020.03.163.

[122] N. Peelman, P. Ragaert, B. De Meulenaer, D. Adons, R. Peeters, L. Cardon, F. Van Impe, F. Devlieghere, Application of bioplastics for food packaging, Trends Food Sci Technol 32 (2013) 128–141. https://doi.org/10.1016/j.tifs.2013.06.003.

[123] R. Vu, M. Dragan, P. Sun, S. Werner, X. Dai, Epithelial–Mesenchymal Plasticity and Endothelial–Mesenchymal Transition in Cutaneous Wound Healing, Cold Spring Harb Perspect Biol 15 (2023) a041237. https://doi.org/10.1101/cshperspect.a041237.

[124] O.A. Peña, P. Martin, Cellular and molecular mechanisms of skin wound healing, Nat Rev Mol Cell Biol (2024). https://doi.org/10.1038/s41580-024-00715-1.

[125] S. Chhabra, N. Chhabra, A. Kaur, N. Gupta, Wound Healing Concepts in Clinical Practice of OMFS, J Maxillofac Oral Surg 16 (2017) 403–423. https://doi.org/10.1007/s12663-016-0880-z.

[126] Y.H. Almadani, J. Vorstenbosch, P.G. Davison, A.M. Murphy, Wound Healing: A Comprehensive Review, Semin Plast Surg 35 (2021) 141–144. https://doi.org/10.1055/s-0041-1731791.

[127] P.-H.Wang, B.-S.Huang, H.-C.Horng, C.-C.Yeh, Y.-J. Chen, Wound healing, Journal of the Chinese Medical Association 81 (2018) 94–101. https://doi.org/10.1016/j.jcma.2017.11.002.

[128] K.M.K. Ozgok, J.P. Regan, Treasure Island, StatPearls Publishing LLC, 2021.

[129] H.A. Wallace, B.M. Basehore, P.M. Zito, Treasure Island, StatPearls Publishing LLC;, 2021.

[130] S. Barrientos, O. Stojadinovic, M.S. Golinko, H. Brem, M. Tomic-Canic, PERSPECTIVE ARTICLE: Growth factors and cytokines in wound healing, Wound Repair and Regeneration 16 (2008) 585–601. https://doi.org/10.1111/j.1524-475X.2008.00410.x.

[131] L. Cañedo-Dorantes, M. Cañedo-Ayala, Skin Acute Wound Healing: A Comprehensive Review, Int J Inflam 2019 (2019) 1–15. https://doi.org/10.1155/2019/3706315.

[132] L. Chen, H. Deng, H. Cui, J. Fang, Z. Zuo, J. Deng, Y. Li, X. Wang, L. Zhao, Inflammatory responses and inflammation-associated diseases in organs, Oncotarget 9 (2018) 7204–7218. https://doi.org/10.18632/oncotarget.23208.

[133] C. Qing, The molecular biology in wound healing & non-healing wound, Chinese Journal of Traumatology 20 (2017) 189–193. https://doi.org/10.1016/j.cjtee.2017.06.001.

[134] P. Krzyszczyk, R. Schloss, A. Palmer, F. Berthiaume, The Role of Macrophages in Acute and Chronic Wound Healing and Interventions to Promote Pro-wound Healing Phenotypes, Front Physiol 9 (2018). https://doi.org/10.3389/fphys.2018.00419.

[135] R. Zeng, C. Lin, Z. Lin, H. Chen, W. Lu, C. Lin, H. Li, Approaches to cutaneous wound healing: basics and future directions, Cell Tissue Res 374 (2018) 217–232. https://doi.org/10.1007/s00441-018-2830-1.

[136] T.N. Demidova-Rice, M.R. Hamblin, I.M. Herman, Acute and Impaired Wound Healing, Adv Skin Wound Care 25 (2012) 304–314. https://doi.org/10.1097/01.ASW.0000416006.55218.d0.

[137] L. Bonnici, S. Suleiman, P. Schembri-Wismayer, A. Cassar, Targeting Signalling Pathways in Chronic Wound Healing, Int J Mol Sci 25 (2023) 50. https://doi.org/10.3390/ijms25010050.

[138] B.J. Goggins, K. Minahan, S. Sherwin, W.S. Soh, J. Pryor, J. Bruce, G. Liu, A. Mathe, D. Knight, J.C. Horvat, M.M. Walker, S. Keely, Pharmacological HIF-1 stabilization promotes intestinal epithelial healing through regulation of α-integrin expression and function, American Journal of Physiology-Gastrointestinal and Liver Physiology 320 (2021) G420–G438. https://doi.org/10.1152/ajpgi.00192.2020.

[139] S. Choi, M. Yoon, K.-Y. Choi, Approaches for Regenerative Healing of Cutaneous Wound with an Emphasis on Strategies Activating the Wnt/β-Catenin Pathway, Adv Wound Care (New Rochelle) 11 (2022) 70–86. https://doi.org/10.1089/wound.2020.1284.

[140] X. Wu, Q. Sun, S. He, Y. Wu, S. Du, L. Gong, J. Yu, H. Guo, Ropivacaine inhibits wound healing by suppressing the proliferation and migration of keratinocytes via the PI3K/AKT/mTOR Pathway, BMC Anesthesiol 22 (2022) 106. https://doi.org/10.1186/s12871-022-01646-0.

[141] P. Basu, M. Martins-Green, Signaling Pathways Associated with Chronic Wound Progression: A Systems Biology Approach, Antioxidants 11 (2022) 1506. https://doi.org/10.3390/antiox11081506.

[142] R. Ghadially, 25 Years of Epidermal Stem Cell Research, Journal of Investigative Dermatology 132 (2012) 797–810. https://doi.org/10.1038/jid.2011.434.

[143] K.A. Bielefeld, S. Amini-Nik, B.A. Alman, Cutaneous wound healing: recruiting developmental pathways for regeneration, Cellular and Molecular Life Sciences 70 (2013) 2059–2081. https://doi.org/10.1007/s00018-012-1152-9.

[144] A.L. Carre, M.S. Hu, A.W. James, K. Kawai, M.G. Galvez, M.T. Longaker, H.P. Lorenz, β-Catenin–Dependent Wnt Signaling: A Pathway in Acute Cutaneous Wounding [RETRACTED], Plast Reconstr Surg 141 (2018) 669–678. https://doi.org/10.1097/PRS.0000000000004170.

[145] Y. Shi, B. Shu, R. Yang, Y. Xu, B. Xing, J. Liu, L. Chen, S. Qi, X. Liu, P. Wang, J. Tang, J. Xie, Wnt and Notch signaling pathway involved in wound healing by targeting c-Myc and Hes1 separately, Stem Cell Res Ther 6 (2015) 120. https://doi.org/10.1186/s13287-015-0103-4.

[146] Y. Takazawa, E. Ogawa, R. Saito, R. Uchiyama, S. Ikawa, H. Uhara, R. Okuyama, Notch down-regulation in regenerated epidermis contributes to enhanced expression of interleukin-36α and suppression of keratinocyte differentiation during wound healing, J Dermatol Sci 79 (2015) 10–19. https://doi.org/10.1016/j.jdermsci.2015.04.003.

[147] S. Qin, J. Zheng, Z. Xia, J. Qian, C. Deng, S. Yang, CTHRC1 promotes wound repair by increasing M2 macrophages via regulating the TGF-β and notch pathways, Biomedicine & Pharmacotherapy 113 (2019) 108594. https://doi.org/10.1016/j.biopha.2019.01.055.

[148] P. Wang, B. Shu, Y. Xu, J. Zhu, J. Liu, Z. Zhou, L. Chen, J. Zhao, X. Liu, S. Qi, K. Xiong, J. Xie, Basic fibroblast growth factor reduces scar by inhibiting the differentiation of epidermal stem cells to myofibroblasts via the Notch1/Jagged1 pathway, Stem Cell Res Ther 8 (2017) 114. https://doi.org/10.1186/s13287-017-0549-7.

[149] J. Patel, B. Baz, H.Y. Wong, J.S. Lee, K. Khosrotehrani, Accelerated Endothelial to Mesenchymal Transition Increased Fibrosis via Deleting Notch Signaling in Wound Vasculature, Journal of Investigative Dermatology 138 (2018) 1166–1175. https://doi.org/10.1016/j.jid.2017.12.004.

[150] J. Ruttanapattanakul, N. Wikan, S. Okonogi, M. Na Takuathung, P. Buacheen, P. Pitchakarn, S. Potikanond, W. Nimlamool, Boesenbergia rotunda extract accelerates human keratinocyte proliferation through activating ERK1/2 and PI3K/Akt kinases, Biomedicine & Pharmacotherapy 133 (2021) 111002. https://doi.org/10.1016/j.biopha.2020.111002.

[151] W. Xiao, H. Tang, M. Wu, Y. Liao, K. Li, L. Li, X. Xu, Ozone oil promotes wound healing by increasing the migration of fibroblasts via PI3K/Akt/mTOR signaling pathway, Biosci Rep 37 (2017). https://doi.org/10.1042/BSR20170658.

[152] B. Hou, W. Cai, T. Chen, Z. Zhang, H. Gong, W. Yang, L. Qiu, Vaccarin hastens wound healing by promoting angiogenesis via activation of MAPK/ERK and PI3K/AKT signaling pathways in vivo, Acta Cir Bras 34 (2019). https://doi.org/10.1590/s0102-865020190120000002.

[153] T. Yu, M. Gao, P. Yang, D. Liu, D. Wang, F. Song, X. Zhang, Y. Liu, Insulin promotes macrophage phenotype transition through PI3K/Akt and PPAR-γ signaling during diabetic wound healing, J Cell Physiol 234 (2019) 4217–4231. https://doi.org/10.1002/jcp.27185.

[154] S. Liarte, Á. Bernabé-García, F.J. Nicolás, Role of TGF-β in Skin Chronic Wounds: A Keratinocyte Perspective, Cells 9 (2020) 306. https://doi.org/10.3390/cells9020306.

[155] A.B. Baba, B. Rah, Gh.R. Bhat, I. Mushtaq, S. Parveen, R. Hassan, M. Hameed Zargar, D. Afroze, Transforming Growth Factor-Beta (TGF-β) Signaling in Cancer-A Betrayal Within, Front Pharmacol 13 (2022). https://doi.org/10.3389/fphar.2022.791272.

[156] P. Sharma, V.K. Gaur, S.-H.Kim, A. Pandey, Microbial strategies for bio-transforming food waste into resources, Bioresour Technol 299 (2020) 122580. https://doi.org/10.1016/j.biortech.2019.122580.

[157] J. Li, Y. Liu, Y. Gao, L. Zhong, Q. Zou, X. Lai, Preparation and properties of calcium citrate nanosheets for bone graft substitute, Bioengineered 7 (2016) 376–381. https://doi.org/10.1080/21655979.2016.1226656.

[158] B. Huang, J. Liu, T. Meng, Y. Li, D. He, X. Ran, G. Chen, W. Guo, X. Kan, S. Fu, W. Wang, D. Liu, Polydatin Prevents Lipopolysaccharide (LPS)-Induced Parkinson's Disease via Regulation of the AKT/GSK3β-Nrf2/NF-κB Signaling Axis, Front Immunol 9 (2018). https://doi.org/10.3389/fimmu.2018.02527.

[159] D. Li, R. Zhang, L. Cui, C. Chu, H. Zhang, H. Sun, J. Luo, L. Zhou, L. Chen, J. Cui, S. Chen, B. Mai, S. Chen, J. Yu, Z. Cai, J. Zhang, Y. Jiang, M. Aschner, R. Chen, Y. Zheng, W. Chen, Multiple organ injury in male C57BL/6J mice exposed to ambient particulate matter in a real-ambient PM exposure system in Shijiazhuang, China, Environmental Pollution 248 (2019) 874–887. https://doi.org/10.1016/j.envpol.2019.02.097.

[160] C. Zhang, Q. Xiao, J. Sheng, T. Liu, Y. Cao, Y. Xue, M. Shi, Z. cao, L. Zhou, X. Luo, K. Deng, C. Chen, Gegen Qinlian Decoction abates nonalcoholic steatohepatitis associated liver injuries via anti-oxidative stress and anti-inflammatory response involved inhibition of toll-like receptor 4 signaling pathways, Biomedicine & Pharmacotherapy 126 (2020) 110076. https://doi.org/10.1016/j.biopha.2020.110076.

[161] H. Zhang, J. Wang, Y. Wang, C. Gao, Y. Gu, J. Huang, J. Wang, Z. Zhang, Salvianolic Acid A Protects the Kidney against Oxidative Stress by Activating the Akt/GSK-3 β /Nrf2 Signaling Pathway and Inhibiting the NF- κ B Signaling Pathway in 5/6 Nephrectomized Rats, Oxid Med Cell Longev 2019 (2019) 1–16. https://doi.org/10.1155/2019/2853534.

[162] H. Zhou, H. Wang, M. Ni, S. Yue, Y. Xia, R.W. Busuttil, J.W. Kupiec-Weglinski, L. Lu, X. Wang, Y. Zhai, Glycogen synthase kinase 3β promotes liver innate immune activation by restraining AMP-activated protein kinase activation, J Hepatol 69 (2018) 99–109. https://doi.org/10.1016/j.jhep.2018.01.036.

[163] M. Kapoor, S. Liu, X. Shi-wen, K. Huh, M. McCann, C.P. Denton, J.R. Woodgett, D.J. Abraham, A. Leask, GSK-3β in mouse fibroblasts controls wound healing and fibrosis through an endothelin-1–dependent mechanism, Journal of Clinical Investigation (2008). https://doi.org/10.1172/JCI35381.

[164] S. GILL, W. PARKS, Metalloproteinases and their inhibitors: Regulators of wound healing, Int J Biochem Cell Biol 40 (2008) 1334–1347. https://doi.org/10.1016/j.biocel.2007.10.024.

[165] S.M. Ayuk, H. Abrahamse, N.N. Houreld, The Role of Matrix Metalloproteinases in Diabetic Wound Healing in relation to Photobiomodulation, J Diabetes Res 2016 (2016) 1–9. https://doi.org/10.1155/2016/2897656.

[166] P.K. Mukherjee, N. Maity, N.K. Nema, B.K. Sarkar, Natural Matrix Metalloproteinase Inhibitors, in: 2013: pp. 91–113. https://doi.org/10.1016/B978-0-444-62615-8.00003-5.

[167] A. Balachandran, S.B. Choi, M.-M. Beata, J. Małgorzata, G.R.A. Froemming, C.A. Lavilla, M.P. Billacura, S.N. Siyumbwa, P.N. Okechukwu, Antioxidant, Wound Healing Potential and In Silico Assessment of Naringin, Eicosane and Octacosane, Molecules 28 (2023) 1043. https://doi.org/10.3390/molecules28031043.

[168] T.C. Appleby, A.E. Greenstein, M. Hung, A. Liclican, M. Velasquez, A.G. Villaseñor, R. Wang, M.H. Wong, X. Liu, G.A. Papalia, B.E. Schultz, R. Sakowicz, V. Smith, H.J. Kwon, Biochemical characterization and structure determination of a potent, selective antibody inhibitor of human MMP9, Journal of Biological Chemistry 292 (2017) 6810–6820. https://doi.org/10.1074/jbc.M116.760579.

[169] M.A. Shah, A. Starodub, S. Sharma, J. Berlin, M. Patel, Z.A. Wainberg, J. Chaves, M. Gordon, K. Windsor, C.B. Brachmann, X. Huang, G. Vosganian, J.D. Maltzman, V. Smith, J.A. Silverman, H.-J. Lenz, J.C. Bendell, Andecaliximab/GS-5745 Alone and Combined with mFOLFOX6 in Advanced Gastric and Gastroesophageal Junction Adenocarcinoma: Results from a Phase I Study, Clinical Cancer Research 24 (2018) 3829–3837. https://doi.org/10.1158/1078-0432.CCR-17-2469.

[170] P. Martin, R. Nunan, Cellular and molecular mechanisms of repair in acute and chronic wound healing, British Journal of Dermatology 173 (2015) 370–378. https://doi.org/10.1111/bjd.13954.

[171] O. Krizanova, A. Penesova, J. Sokol, A. Hokynkova, A. Samadian, P. Babula, Signaling pathways in cutaneous wound healing, Front Physiol 13 (2022). https://doi.org/10.3389/fphys.2022.1030851.

[172] W.J. Ryves, R. Dajani, L. Pearl, A.J. Harwood, Glycogen Synthase Kinase-3 Inhibition by Lithium and Beryllium Suggests the Presence of Two Magnesium Binding Sites, Biochem Biophys Res Commun 290 (2002) 967–972. https://doi.org/10.1006/bbrc.2001.6305.

[173] P. Das, R. Majumder, N. Sen, S.K. Nandi, A. Ghosh, M. Mandal, P. Basak, A computational analysis to evaluate deleterious SNPs of GSK3β, a multifunctional and regulatory protein, for metabolism, wound healing, and migratory processes, Int J Biol Macromol 256 (2024) 128262. https://doi.org/10.1016/j.ijbiomac.2023.128262.

[174] T. Sun, M. Rodriguez, L. Kim, Glycogen synthase kinase 3 in the world of cell migration, Dev Growth Differ 51 (2009) 735–742. https://doi.org/10.1111/j.1440-169X.2009.01141.x.

[175] H. Zhao, J. Mao, Y. Yuan, J. Feng, H. Cheng, G. Fan, Y. Zhang, T. Li, Sodium Dichloroacetate Stimulates Angiogenesis by Improving Endothelial Precursor Cell Function in an AKT/GSK-3β/Nrf2 Dependent Pathway in Vascular Dementia Rats, Front Pharmacol 10 (2019). https://doi.org/10.3389/fphar.2019.00523.

[176] H. Zhang, J. Wang, Y. Wang, C. Gao, Y. Gu, J. Huang, J. Wang, Z. Zhang, Salvianolic Acid A Protects the Kidney against Oxidative Stress by Activating the Akt/GSK-3 β /Nrf2 Signaling Pathway and Inhibiting the NF- κ B Signaling Pathway in 5/6 Nephrectomized Rats, Oxid Med Cell Longev 2019 (2019) 1–16. https://doi.org/10.1155/2019/2853534.

[177] H. Aksoy, T. Şekerler, N. Mert, In silico investigation of wound healing potential of some compounds in tubers of Asphodelus species with GSK3-β protein, J Res Pharm 25 (2021).

[178] G. Han, R. Ceilley, Chronic Wound Healing: A Review of Current Management and Treatments, Adv Ther 34 (2017) 599–610. https://doi.org/10.1007/s12325-017-0478-y.

[179] J.A. McCubrey, L.S. Steelman, F.E. Bertrand, N.M. Davis, S.L. Abrams, G. Montalto, A.B. D'Assoro, M. Libra, F. Nicoletti, R. Maestro, J. Basecke, L. Cocco, M. Cervello, A.M. Martelli, Multifaceted roles of GSK-3 and Wnt/β-catenin in hematopoiesis and leukemogenesis: opportunities for therapeutic intervention, Leukemia 28 (2014) 15–33. https://doi.org/10.1038/leu.2013.184.

[180] Y. Adib, A. Bensussan, L. Michel, Cutaneous Wound Healing: A Review about Innate Immune Response and Current Therapeutic Applications, Mediators Inflamm 2022 (2022) 1–16. https://doi.org/10.1155/2022/5344085.

[181] L. Geris, R. Schugart, H. Van Oosterwyck, *In silico* design of treatment strategies in wound healing and bone fracture healing, Philosophical Transactions of the Royal Society A: Mathematical, Physical and Engineering Sciences 368 (2010) 2683–2706. https://doi.org/10.1098/rsta.2010.0056.

[182] F. Hofmann, M. Jaeger-Erben, Organizational transition management of circular business model innovations, Bus Strategy Environ 29 (2020) 2770–2788. https://doi.org/10.1002/bse.2542.

[183] R. Baidya, B. Sarkar, An In Silico Approach to Evaluate the Diabetic Wound Healing Potential of Phenylethanoid Glycoside in Inhibiting the Receptor for Advanced Glycation End Products (RAGE), in: The 2nd International Electronic Conference on Biomedicines, MDPI, Basel Switzerland, 2023: p. 24. https://doi.org/10.3390/ECB2023-14137.

[184] V. Singh, A. Bali, In silico drug design: A review, J Adv Pharm Technol Res 10 (2019) 45–50.

[185] R.A.I. Reshad, S. Alam, H.B. Raihan, K.N. Meem, F. Rahman, F. Zahid, Md.I. Rafid, S.M.O. Rahman, S. Omit, Md.H. Ali, In silico investigations on curcuminoids from Curcuma longa as positive regulators of the Wnt/β-catenin signaling pathway in wound healing, Egyptian Journal of Medical Human Genetics 22 (2021) 65. https://doi.org/10.1186/s43042-021-00182-9.

[186] V. De-Pasquale, L.M. Pavone, Hurdles in drug design and discovery of novel therapeutic agents: A special emphasis on in silico methods, Curr Med Chem 26 (2019) 6406–6418.

[187] N.A. Mokhtar, F.M. Tap, S.Z.A. Talib, N.A. Khairudin, Docking study for assessment of wound healing potential of isosakuratenin isolated from Chromolaena odorata: An In-silico approach, IOP Conf Ser Mater Sci Eng 1051 (2021) 012078. https://doi.org/10.1088/1757-899X/1051/1/012078.

[188] R. SACHDEO, C. KHANWELKAR, A. SHETE, IN SILICO EXPLORATION OF BERBERINE AS A POTENTIAL WOUND HEALING AGENT VIA NETWORK PHARMACOLOGY, MOLECULAR DOCKING, AND MOLECULAR DYNAMICS SIMULATION, International Journal of Applied Pharmaceutics (2024) 188–194. https://doi.org/10.22159/ijap.2024v16i2.49922.

[189] A.Y.M. Alabdali, R. Khalid, M. Kzar, M.O. Ezzat, G.M. Huei, T.W. Hsia, R. Mogana, H. Rahman, B.M.A. Razik, P.K. Issac, S. Chinnappan, S.I. Khalivulla, Design, synthesis, in silico and antibacterial evaluation of curcumin derivatives loaded nanofiber as potential wound healing agents, J King Saud Univ Sci 34 (2022) 102205. https://doi.org/10.1016/j.jksus.2022.102205.

[190] E. Yadav, P. Yadav, A. Verma, In silico Study of Trianthema portulacastrum Embedded Iron Oxide Nanoparticles on Glycogen Synthase Kinase-3β: A Possible Contributor to its Enhanced in vivo Wound Healing Potential, Front Pharmacol 12 (2021). https://doi.org/10.3389/fphar.2021.664075.

[191] S. Ud-Din, A. Bayat, Non-animal models of wound healing in cutaneous repair: In silico, in vitro, ex vivo, and in vivo models of wounds and scars in human skin, Wound Repair and Regeneration 25 (2017) 164–176. https://doi.org/10.1111/wrr.12513.

[192] T. Otsuka, H.-M. Kan, C.T. Laurencin, Regenerative Engineering Approaches to Scar-Free Skin Regeneration, Regen Eng Transl Med 8 (2022) 225–247. https://doi.org/10.1007/s40883-021-00229-8.

[193] L. Guo, Y. Feng, J. Ding, Integrating computational modeling and experiments to develop effective wound healing strategies, Adv Drug Deliv Rev (2020) 82–106.

[194] E. Zgheib, C.X. Lim, D.I. Shreiber, In silico models of wound healing., Curr Opin Biomed Eng 10 (2019) 170–176.

[195] C.S.J. Dunkin, J.M. Pleat, P.H. Gillespie, M.P.H. Tyler, A.H.N. Roberts, D.A. McGrouther, Scarring Occurs at a Critical Depth of Skin Injury: Precise Measurement in a Graduated Dermal Scratch

in Human Volunteers, Plast Reconstr Surg 119 (2007) 1722–1732. https://doi.org/10.1097/01.prs.0000258829.07399.f0.

[196] S.T. Boyce, A.L. Lalley, Tissue engineering of skin and regenerative medicine for wound care, Burns Trauma 6 (2018). https://doi.org/10.1186/s41038-017-0103-y.

[197] P. Monika, M.N. Chandraprabha, A. Rangarajan, P.V. Waiker, K.N. Chidambara Murthy, Challenges in Healing Wound: Role of Complementary and Alternative Medicine, Front Nutr 8 (2022). https://doi.org/10.3389/fnut.2021.791899.

[198] R.J. Langdon, P. Yousefi, C.L. Relton, M.J. Suderman, Epigenetic modelling of former, current and never smokers, Clin Epigenetics 13 (2021) 206. https://doi.org/10.1186/s13148-021-01191-6.

[199] K. Järbrink, G. Ni, H. Sönnergren, A. Schmidtchen, C. Pang, R. Bajpai, J. Car, The humanistic and economic burden of chronic wounds: A protocol for a systematic review, Syst Rev 6 (2017).

[200] S.M. McCarty, S.L. Percival, Proteases and Delayed Wound Healing, Adv Wound Care (New Rochelle) 2 (2013) 438–447. https://doi.org/10.1089/wound.2012.0370.

[201] A.J.M. Boulton, D.G. Armstrong, S.F. Albert, R.G. Frykberg, R. Hellman, M.S. Kirkman, L.A. Lavery, J.W. LeMaster, J.L. Mills, M.J. Mueller, P. Sheehan, D.K. Wukich, Comprehensive Foot Examination and Risk Assessment, Diabetes Care 31 (2008) 1679–1685. https://doi.org/10.2337/dc08-9021.

[202] R.G. Frykberg, J. Banks, Challenges in the Treatment of Chronic Wounds, Adv Wound Care (New Rochelle) 4 (2015) 560–582. https://doi.org/10.1089/wound.2015.0635.

[203] J.A. Molnar, M.J. Underdown, W.A. Clark, Nutrition and Chronic Wounds, Adv Wound Care (New Rochelle) 3 (2014) 663–681. https://doi.org/10.1089/wound.2014.0530.

[204] D. Li, A. Wang, X. Liu, F. Meisgen, J. Grünler, I.R. Botusan, S. Narayanan, E. Erikci, X. Li, L. Blomqvist, L. Du, A. Pivarcsi, E. Sonkoly, K. Chowdhury, S.-B. Catrina, M. Ståhle, N.X. Landén, MicroRNA-132 enhances transition from inflammation to proliferation during wound healing, Journal of Clinical Investigation 125 (2015) 3008–3026. https://doi.org/10.1172/JCI79052.

[205] J. Ye, Y. Kang, X. Sun, P. Ni, M. Wu, S. Lu, MicroRNA-155 Inhibition Promoted Wound Healing in Diabetic Rats, Int J Low Extrem Wounds 16 (2017) 74–84. https://doi.org/10.1177/1534734617706636.

[206] S. Dangwal, B. Stratmann, C. Bang, J.M. Lorenzen, R. Kumarswamy, J. Fiedler, C.S. Falk, C.J. Scholz, T. Thum, D. Tschoepe, Impairment of Wound Healing in Patients With Type 2 Diabetes Mellitus Influences Circulating MicroRNA Patterns via Inflammatory Cytokines, Arterioscler Thromb Vasc Biol 35 (2015) 1480–1488. https://doi.org/10.1161/ATVBAHA.114.305048.

[207] D. Ozdemir, M.W. Feinberg, MicroRNAs in diabetic wound healing: Pathophysiology and therapeutic opportunities, Trends Cardiovasc Med 29 (2019) 131–137. https://doi.org/10.1016/j.tcm.2018.08.002.

[208] S. Dhivya, V.V. Padma, E. Santhini, Wound dressings – a review, Biomedicine (Taipei) 5 (2015) 22. https://doi.org/10.7603/s40681-015-0022-9.

[209] C. Weller, G. Sussman, Wound Dressings Update, Journal of Pharmacy Practice and Research 36 (2006) 318–324. https://doi.org/10.1002/j.2055-2335.2006.tb00640.x.

[210] F. Wahid, X.-J.Zhao, X.-Q.Zhao, X.-F.Ma, N. Xue, X.-Z.Liu, F.-P. Wang, S.-R. Jia, C. Zhong, Fabrication of Bacterial Cellulose-Based Dressings for Promoting Infected Wound Healing, ACS Appl Mater Interfaces 13 (2021) 32716–32728. https://doi.org/10.1021/acsami.1c06986.

[211] H. Agarwal, A.K. Gupta, N. Gupta, S. Mukharjee, C.K. Durga, Comparison of results of silver-impregnated dressing with povidone iodine based-dressing in patients with diabetic foot, Hellenic Journal of Surgery 87 (2015) 465–467. https://doi.org/10.1007/s13126-015-0258-6.

[212] D. Díaz-García, A. Filipová, I. Garza-Veloz, M.L. Martinez-Fierro, A Beginner's Introduction to Skin Stem Cells and Wound Healing, Int J Mol Sci 22 (2021) 11030. https://doi.org/10.3390/ijms222011030.

[213] M. Hosseini, A. Shafiee, Engineering Bioactive Scaffolds for Skin Regeneration, Small 17 (2021). https://doi.org/10.1002/smll.202101384.

[214] L. Liu, Y. Yu, Y. Hou, J. Chai, H. Duan, W. Chu, H. Zhang, Q. Hu, J. Du, Human Umbilical Cord Mesenchymal Stem Cells Transplantation Promotes Cutaneous Wound Healing of Severe Burned Rats, PLoS One 9 (2014) e88348. https://doi.org/10.1371/journal.pone.0088348.

[215] J.W. Kim, M.J. Kim, C.S. Ki, H.J. Kim, Y.H. Park, Fabrication of bi-layer scaffold of keratin nanofiber and gelatin-methacrylate hydrogel: Implications for skin graft, Int J Biol Macromol 105 (2017) 541–548. https://doi.org/10.1016/j.ijbiomac.2017.07.067.

[216] N. Ibrahim, S. Wong, I. Mohamed, N. Mohamed, K.-Y. Chin, S. Ima-Nirwana, A. Shuid, Wound Healing Properties of Selected Natural Products, Int J Environ Res Public Health 15 (2018) 2360. https://doi.org/10.3390/ijerph15112360.

[217] T. Velnar, T. Bailey, V. Smrkolj, The Wound Healing Process: An Overview of the Cellular and Molecular Mechanisms, Journal of International Medical Research 37 (2009) 1528–1542. https://doi.org/10.1177/147323000903700531.

[218] A. Shedoeva, D. Leavesley, Z. Upton, C. Fan, Wound Healing and the Use of Medicinal Plants, Evidence-Based Complementary and Alternative Medicine 2019 (2019) 1–30. https://doi.org/10.1155/2019/2684108.

[219] R. Thakur, N. Jain, R. Pathak, S.S. Sandhu, Practices in Wound Healing Studies of Plants, Evidence-Based Complementary and Alternative Medicine 2011 (2011) 1–17. https://doi.org/10.1155/2011/438056.

[220] D.E. Tsala, D. Amadou, S. Habtemariam, Natural wound healing and bioactive natural products , Phytopharmacology 4 (2013) 532–560.

[221] T. Kurahashi, J. Fujii, Roles of Antioxidative Enzymes in Wound Healing, J Dev Biol 3 (2015) 57–70. https://doi.org/10.3390/jdb3020057.

[222] N. Tra Thanh, M. Ho Hieu, N. Tran Minh Phuong, T. Do Bui Thuan, H. Nguyen Thi Thu, V.P. Thai, T. Do Minh, H. Nguyen Dai, V.T. Vo, H. Nguyen Thi, Optimization and characterization of electrospun polycaprolactone coated with gelatin-silver nanoparticles for wound healing application, Materials Science and Engineering: C 91 (2018) 318–329. https://doi.org/10.1016/j.msec.2018.05.039.

[223] E.S. Permyakova, J. Polčak, P. V. Slukin, S.G. Ignatov, N.A. Gloushankova, L. Zajíčková, D. V. Shtansky, A. Manakhov, Antibacterial biocompatible PCL nanofibers modified by COOH-anhydride plasma polymers and gentamicin immobilization, Mater Des 153 (2018) 60–70. https://doi.org/10.1016/j.matdes.2018.05.002.

[224] A. Ehterami, M. Salehi, S. Farzamfar, A. Vaez, H. Samadian, H. Sahrapeyma, M. Mirzaii, S. Ghorbani, A. Goodarzi, In vitro and in vivo study of PCL/COLL wound dressing loaded with insulin-chitosan nanoparticles on cutaneous wound healing in rats model, Int J Biol Macromol 117 (2018) 601–609. https://doi.org/10.1016/j.ijbiomac.2018.05.184.

[225] S. Vitale, S. Colanero, M. Placidi, G. Di Emidio, C. Tatone, F. Amicarelli, A.M. D'Alessandro, Phytochemistry and Biological Activity of Medicinal Plants in Wound Healing: An Overview of Current Research, Molecules 27 (2022) 3566. https://doi.org/10.3390/molecules27113566.

[226] Y.L. Ti, F. Song, Z. Fang, P. Zhang, Plants and phytochemicals inhibit scar formation: A systematic review, Ind. Crops Prod 185 (2022).

[227] M.S. Criollo-Mendoza, L.A. Contreras-Angulo, N. Leyva-López, E.P. Gutiérrez-Grijalva, L.A. Jiménez-Ortega, J.B. Heredia, Wound Healing Properties of Natural Products: Mechanisms of Action, Molecules 28 (2023) 598. https://doi.org/10.3390/molecules28020598.

[228] D. Hu, Q. Ren, Z. Li, L. Zhang, Chitosan-Based Biomimetically Mineralized Composite Materials in Human Hard Tissue Repair, Molecules 25 (2020) 4785. https://doi.org/10.3390/molecules25204785.

[229] L.J. Borda, F.E. Macquhae, R.S. Kirsner, Wound Dressings: A Comprehensive Review, Curr Dermatol Rep 5 (2016) 287–297. https://doi.org/10.1007/s13671-016-0162-5.

[230] Y. Liang, J. He, B. Guo, Functional Hydrogels as Wound Dressing to Enhance Wound Healing, ACS Nano 15 (2021) 12687–12722. https://doi.org/10.1021/acsnano.1c04206.

[231] N.A. Mohd Zaid, M. Sekar, S.R. Bonam, S.H. Gan, P.T. Lum, M.Y. Begum, N.N.I. Mat Rani, J. Vaijanathappa, Y.S. Wu, V. Subramaniyan, N.K. Fuloria, S. Fuloria, Promising Natural Products in New Drug Design, Development, and Therapy for Skin Disorders: An Overview of Scientific Evidence and Understanding Their Mechanism of Action, Drug Des Devel Ther Volume 16 (2022) 23–66. https://doi.org/10.2147/DDDT.S326332.

[232] L. Melguizo-Rodríguez, E. de Luna-Bertos, J. Ramos-Torrecillas, R. Illescas-Montesa, V.J. Costela-Ruiz, O. García-Martínez, Potential Effects of Phenolic Compounds That Can Be Found in Olive Oil on Wound Healing, Foods 10 (2021) 1642. https://doi.org/10.3390/foods10071642.

[233] E. Liu, H. Gao, Y. Zhao, Y. Pang, Y. Yao, Z. Yang, X. Zhang, Y. Wang, S. Yang, X. Ma, J. Zeng, J. Guo, The potential application of natural products in cutaneous wound healing: A review of preclinical evidence, Front Pharmacol 13 (2022). https://doi.org/10.3389/fphar.2022.900439.

[234] M.F.M.A. Zamri, R. Bahru, R. Amin, M.U. Aslam Khan, S.I.A. Razak, S.A. Hassan, M.R.A. Kadir, N.H.M. Nayan, Waste to health: A review of waste derived materials for tissue engineering, J Clean Prod 290 (2021) 125792. https://doi.org/10.1016/j.jclepro.2021.125792.

[235] J. Li, Y. Liu, Y. Gao, L. Zhong, Q. Zou, X. Lai, Preparation and properties of calcium citrate nanosheets for bone graft substitute, Bioengineered 7 (2016) 376–381. https://doi.org/10.1080/21655979.2016.1226656.

[236] A. Tarafdar, V.K. Gaur, N. Rawat, P.R. Wankhade, G.K. Gaur, M.K. Awasthi, N.A. Sagar, R. Sirohi, Advances in biomaterial production from animal derived waste, Bioengineered 12 (2021) 8247–8258. https://doi.org/10.1080/21655979.2021.1982321.

[237] P.X. Ma, J.-W. Choi, Biodegradable Polymer Scaffolds with Well-Defined Interconnected Spherical Pore Network, Tissue Eng 7 (2001) 23–33. https://doi.org/10.1089/107632701300003269.

[238] A.B.M. Hilmi, Vital roles of stem cells and biomaterials in skin tissue engineering, World J Stem Cells 7 (2015) 428. https://doi.org/10.4252/wjsc.v7.i2.428.

[239] A.-G. Niculescu, A.M. Grumezescu, An Up-to-Date Review of Biomaterials Application in Wound Management, Polymers (Basel) 14 (2022) 421. https://doi.org/10.3390/polym14030421.

[240] S. Jana, P. Das, J. Mukherjee, D. Banerjee, P.R. Ghosh, P. Kumar Das, R.N. Bhattacharya, S.K. Nandi, Waste-derived biomaterials as building blocks in the biomedical field, J Mater Chem B 10 (2022) 489–505. https://doi.org/10.1039/D1TB02125G.

[241] H. Singh, S.D. Purohit, R. Bhaskar, I. Yadav, S. Bhushan, M.K. Gupta, N.C. Mishra, Curcumin in decellularized <scp>goat small intestine submucosa</scp> for wound healing and skin tissue engineering, J Biomed Mater Res B Appl Biomater 110 (2022) 210–219. https://doi.org/10.1002/jbm.b.34903.

[242] M. Shanmuganathan, Behavioural finance in an era of artificial intelligence: Longitudinal case study of robo-advisors in investment decisions, J Behav Exp Finance 27 (2020). https://doi.org/10.1016/j.jbef.2020.100297.

[243] K.K. Nayak, P. Gupta, In vitro biocompatibility study of keratin/agar scaffold for tissue engineering, Int J Biol Macromol 81 (2015) 1–10. https://doi.org/10.1016/j.ijbiomac.2015.07.025.

[244] R.A. Mensah, F. Trotta, E. Briggs, N.S. Sharifulden, L.V.B. Silva, Z. Keskin-Erdogan, S. Diop, A.K. Kureshi, D.Y.S. Chau, A Sustainable, Green-Processed, Ag-Nanoparticle-Incorporated Eggshell-Derived Biomaterial for Wound-Healing Applications, J Funct Biomater 14 (2023) 450. https://doi.org/10.3390/jfb14090450.

[245] Herndon D., Total burn care, 3rd ed., Saunder Elsevier, 2007.

[246] O.L. Shanmugasundaram, K. Syed Zameer Ahmed, K. Sujatha, P. Ponnmurugan, A. Srivastava, R. Ramesh, R. Sukumar, K. Elanithi, Fabrication and characterization of chicken feather keratin/polysaccharides blended polymer coated nonwoven dressing materials for wound healing applications, Materials Science and Engineering: C 92 (2018) 26–33. https://doi.org/10.1016/j.msec.2018.06.020.

[247] K.G. Grønlien, M.E. Pedersen, K.W. Sanden, V. Høst, J. Karlsen, H.H. Tønnesen, Collagen from Turkey (Meleagris gallopavo) tendon: A promising sustainable biomaterial for pharmaceutical use, Sustain Chem Pharm 13 (2019) 100166. https://doi.org/10.1016/j.scp.2019.100166.

[248] A. Barbu, B. Neamtu, M. Zăhan, G.M. Iancu, C. Bacila, V. Mireșan, Current Trends in Advanced Alginate-Based Wound Dressings for Chronic Wounds, J Pers Med 11 (2021) 890. https://doi.org/10.3390/jpm11090890.

[249] L. Suamte, A. Tirkey, P.J. Babu, Design of 3D smart scaffolds using natural, synthetic and hybrid derived polymers for skin regenerative applications, Smart Mater Med 4 (2023) 243–256. https://doi.org/10.1016/j.smaim.2022.09.005.

[250] ter Horst B, N.S. Moiemen, Grover L. M., 6 - natural polymers: Biomaterials for skin scaffolds, Biomaterials for Skin Repair and Regeneration (2019) 151–192.

[251] Y. Gao, Y. Kang, T. Wang, C. Li, S. Shen, C. Qu, S. Gong, P. Liu, L. Yang, J. Liu, B. Han, C. Li, Alginate microspheres-collagen hydrogel, as a novel 3D culture system, enhanced skin wound healing of hUCMSCs in rats model, Colloids Surf B Biointerfaces 219 (2022) 112799. https://doi.org/10.1016/j.colsurfb.2022.112799.

[252] M. Mobaraki, D. Bizari, M. Soltani, H. Khshmohabat, K. Raahemifar, M. Akbarzade Amirdehi, The Effects of Curcumin Nanoparticles Incorporated into Collagen-Alginate Scaffold on Wound Healing of Skin Tissue in Trauma Patients, Polymers (Basel) 13 (2021) 4291. https://doi.org/10.3390/polym13244291.

[253] J. Ngoenkam, A. Faikrua, S. Yasothornsrikul, J. Viyoch, Potential of an injectable chitosan/starch/β-glycerol phosphate hydrogel for sustaining normal chondrocyte function, Int J Pharm 391 (2010) 115–124. https://doi.org/10.1016/j.ijpharm.2010.02.028.

[254] J. Sundaram, T.D. Durance, R. Wang, Porous scaffold of gelatin–starch with nanohydroxyapatite composite processed via novel microwave vacuum drying, Acta Biomater 4 (2008) 932–942. https://doi.org/10.1016/j.actbio.2008.01.019.

[255] M.R. Roslan, N.F.M. Nasir, E.M. Cheng, N.A.M. Amin, Tissue engineering scaffold based on starch: A review, in: 2016 International Conference on Electrical, Electronics, and Optimization Techniques (ICEEOT), IEEE, 2016: pp. 1857–1860. https://doi.org/10.1109/ICEEOT.2016.7755010.

[256] V.S. Waghmare, P.R. Wadke, S. Dyawanapelly, A. Deshpande, R. Jain, P. Dandekar, Starch based nanofibrous scaffolds for wound healing applications, Bioact Mater 3 (2018) 255–266. https://doi.org/10.1016/j.bioactmat.2017.11.006.

[257] H. Salehi, M. Mehrasa, B. Nasri-Nasrabadi, M. Doostmohammadi, R. Seyedebrahimi, N. Davari, M. Rafienia, M. Hosseinabadi, M. Agheb, M. Siavash, Effects of nanozeolite/starch thermoplastic hydrogels on wound healing, Journal of Research in Medical Sciences 22 (2017) 110. https://doi.org/10.4103/jrms.JRMS_1037_16.

[258] R. Chhabra, V. Peshattiwar, T. Pant, A. Deshpande, D. Modi, S. Sathaye, A. Tibrewala, S. Dyawanapelly, R. Jain, P. Dandekar, *In Vivo* Studies of 3D Starch–Gelatin Scaffolds for Full-Thickness Wound Healing, ACS Appl Bio Mater 3 (2020) 2920–2929. https://doi.org/10.1021/acsabm.9b01139.

[259] Q. Shi, H. Liu, D. Tang, Y. Li, X. Li, F. Xu, Bioactuators based on stimulus-responsive hydrogels and their emerging biomedical applications, NPG Asia Mater 11 (2019) 64. https://doi.org/10.1038/s41427-019-0165-3.

[260] L. Zhu, K.M. Bratlie, pH sensitive methacrylated chitosan hydrogels with tunable physical and chemical properties, Biochem Eng J 132 (2018) 38–46. https://doi.org/10.1016/j.bej.2017.12.012.

[261] Q.-Q.Ouyang, Z. Hu, Z.-P.Lin, W.-Y.Quan, Y.-F.Deng, S.-D.Li, P.-W.Li, Y. Chen, Chitosan hydrogel in combination with marine peptides from tilapia for burns healing, Int J Biol Macromol 112 (2018) 1191–1198. https://doi.org/10.1016/j.ijbiomac.2018.01.217.

[262] I.P. Murray, M.B. Gregoire, R.G. Downey, Organizational Commitment of Management Employees in Restaurant Operations, Hospitality Research Journal 14 (1990) 339–348. https://doi.org/10.1177/109634809001400236.

[263] L. Diaz-Gomez, I. Gonzalez-Prada, R. Millan, A. Da Silva-Candal, A. Bugallo-Casal, F. Campos, A. Concheiro, C. Alvarez-Lorenzo, 3D printed carboxymethyl cellulose scaffolds for autologous growth factors delivery in wound healing, Carbohydr Polym 278 (2022) 118924. https://doi.org/10.1016/j.carbpol.2021.118924.

[264] M. Alavi, A. Nokhodchi, Antimicrobial and Wound Treatment Aspects of Micro- and Nanoformulations of Carboxymethyl, Dialdehyde, and TEMPO-Oxidized Derivatives of Cellulose: Recent Advances, Macromol Biosci 20 (2020). https://doi.org/10.1002/mabi.201900362.

[265] S. Suvarnalata, R.Y. Chaudhari, Transdermal Gel: As a Novel Drug Delivery System, International Journal of Pharmacy & Life Sciences 7 (2016).

[266] M.M. Ahmed, M.M. Ali, SEMISOLID DOSAGE FORM: TOPICAL GEL FORMULATION A REVIEW, World J Pharm Res 5 (2016) 1256–1268.

[267] P.B. Patil, S.K. Datir, R.B. Saudagar, A Review on Topical Gels as Drug Delivery System, Journal of Drug Delivery and Therapeutics 9 (2019).

[268] D.E. Lee, N. Ayoub, D.K. Agrawal, Mesenchymal stem cells and cutaneous wound healing: novel methods to increase cell delivery and therapeutic efficacy, Stem Cell Res Ther 7 (2016) 37. https://doi.org/10.1186/s13287-016-0303-6.

[269] P. Karande, A. Jain, K. Ergun, V. Kispersky, S. Mitragotri, Design principles of chemical penetration enhancers for transdermal drug delivery, Proceedings of the National Academy of Sciences 102 (2005) 4688–4693. https://doi.org/10.1073/pnas.0501176102.

[270] R. Supraja, An overall review on topical preparation-gel, Innovat International Journal of Medical & Pharmaceutical Sciences 1 (2016).

[271] B. Nagoba, M. Davane, Studies on wound healing potential of topical herbal formulations- do we need to strengthen study protocol?, J Ayurveda Integr Med 10 (2019) 316–318. https://doi.org/10.1016/j.jaim.2019.09.002.

[272] S. Gunasekaran, A.A.J. Nayagam, R. Natarajan, Wound healing potentials of herbal ointment containing Calendula officinalis Linn.on the alteration of immunological markers and biochemical parameters in excision wounded animals, Clinical Phytoscience 6 (2020) 77. https://doi.org/10.1186/s40816-020-00215-7.

[273] A.A. John N, S. G, K. K, K. M, WOUND HEALING EFFICACY OF HERBAL OINTMENT CONTAINING OLDENLANDIA HERBACEA ROXB. ON EXCISION WOUNDED ANIMALS, International Research Journal Of Pharmacy 9 (2018) 95–99. https://doi.org/10.7897/2230-8407.098172.

[274] O. Yazarlu, M. Iranshahi, H.R.K. Kashani, S. Reshadat, S. Habtemariam, M. Iranshahy, M. Hasanpour, Perspective on the application of medicinal plants and natural products in wound healing: A mechanistic review, Pharmacol Res 174 (2021) 105841. https://doi.org/10.1016/j.phrs.2021.105841.

[275] A. Ullah, M. Jang, H. Khan, H.J. Choi, S.An, D. Kim, Y.-R.Kim, U.-K.Kim, G.M. Kim, Microneedle array with a pH-responsive polymer coating and its application in smart drug delivery for wound healing, Sens Actuators B Chem 345 (2021) 130441. https://doi.org/10.1016/j.snb.2021.130441.

[276] J. Liang, L. Cui, J. Li, S. Guan, K. Zhang, J. Li, *Aloe vera* : A Medicinal Plant Used in Skin Wound Healing, Tissue Eng Part B Rev 27 (2021) 455–474. https://doi.org/10.1089/ten.teb.2020.0236.

[277] C. Oliveira, D. Sousa, J.A. Teixeira, P. Ferreira-Santos, C.M. Botelho, Polymeric biomaterials for wound healing, Front Bioeng Biotechnol 11 (2023). https://doi.org/10.3389/fbioe.2023.1136077.

[278] C. Chong, Y. Wang, A. Fathi, R. Parungao, P.K. Maitz, Z. Li, Skin wound repair: Results of a pre-clinical study to evaluate electropsun collagen–elastin–PCL scaffolds as dermal substitutes., Burns 45 (2019) 1639–1648. https://doi.org/10.1016/j.burns.2019.04.014.

[279] M. Downer, C.E. Berry, J.B. Parker, L. Kameni, M. Griffin, Current Biomaterials for Wound Healing, Bioengineering 10 (2023) 1378. https://doi.org/10.3390/bioengineering10121378.

[280] P. Chandika, F. Khan, S.-Y.Heo, Y.-M.Kim, M. Yi, W.-K. Jung, Enhanced wound-healing capability with inherent antimicrobial activities of usnic acid incorporated poly(ε-caprolactone)/decellularized extracellular matrix nanofibrous scaffold, Biomaterials Advances 140 (2022) 213046. https://doi.org/10.1016/j.bioadv.2022.213046.

[281] A. Chaudhari, K. Vig, D. Baganizi, R. Sahu, S. Dixit, V. Dennis, S. Singh, S. Pillai, Future Prospects for Scaffolding Methods and Biomaterials in Skin Tissue Engineering: A Review, Int J Mol Sci 17 (2016) 1974. https://doi.org/10.3390/ijms17121974.

[282] M. Hesketh, K.B. Sahin, Z.E. West, R.Z. Murray, Macrophage Phenotypes Regulate Scar Formation and Chronic Wound Healing, Int J Mol Sci 18 (2017) 1545. https://doi.org/10.3390/ijms18071545.

[283] A. Budovsky, L. Yarmolinsky, S. Ben-Shabat, Effect of medicinal plants on wound healing, Wound Repair and Regeneration 23 (2015) 171–183. https://doi.org/10.1111/wrr.12274.

[284] WHO, WHO Traditional Medicine Strategy, 2023.

[285] M. Reza Farahpour, Medicinal Plants in Wound Healing, in: Wound Healing - Current Perspectives, IntechOpen, 2019. https://doi.org/10.5772/intechopen.80215.

[286] C.C. Barua, A. Talukdar, A.G. Barua, A. Chakraborty, R.K. Sarma, R.S. Bora, EVALUATION OF THE WOUND HEALING ACTIVITY OF METHANOLIC EXTRACT OF AZADIRACHTA INDICA (NEEM) AND TINOSPORA CORDIFOLIA (GUDUCHI) IN RATS , Pharmacologyonline 1 (2010) 70–77.

[287] V.T. Tchemtchoua, G. Atanasova, A. Aqil, P. Filée, N. Garbacki, O. Vanhooteghem, C. Deroanne, A. Noël, C. Jérome, B. Nusgens, Y. Poumay, A. Colige, Development of a Chitosan Nanofibrillar Scaffold for Skin Repair and Regeneration, Biomacromolecules 12 (2011) 3194–3204. https://doi.org/10.1021/bm200680q.

[288] Y. Wang, K. Liu, M. Zhang, T. Xu, H. Du, B. Pang, C. Si, Sustainable polysaccharide-based materials for intelligent packaging, Carbohydr Polym 313 (2023) 120851. https://doi.org/10.1016/j.carbpol.2023.120851.

[289] R. Saberi Riseh, Y.A. Skorik, V.K. Thakur, M. Moradi Pour, E. Tamanadar, S.S. Noghabi, Encapsulation of Plant Biocontrol Bacteria with Alginate as a Main Polymer Material, Int J Mol Sci 22 (2021) 11165. https://doi.org/10.3390/ijms222011165.

[290] X. Zhang, X. Wu, J. Zhang, A Novel and Facile Method to Prepare Uniform Alginate Chitosan Microspheres, PLoS One 13 (2018).

[291] A. Tariq, Z.U. Arif, M.Y. Khalid, M. Hossain, P.I. Rasool, R. Umer, S. Ramakrishna, Recent Advances in the Additive Manufacturing of Stimuli-Responsive Soft Polymers, Adv Eng Mater 25 (2023). https://doi.org/10.1002/adem.202301074.

[292] N. Chaudhari, A.D. Findlay, A.W. Stevenson, T.D. Clemons, Y. Yao, A. Joshi, S. Sayyar, G. Wallace, S. Rea, P. Toshniwal, Z. Deng, P.E. Melton, N. Hortin, K.S. Iyer, W. Jarolimek, F.M. Wood, M.W. Fear, Topical application of an irreversible small molecule inhibitor of lysyl oxidases ameliorates skin scarring and fibrosis, Nat Commun 13 (2022) 5555. https://doi.org/10.1038/s41467-022-33148-5.

[293] P.S. Gungor-Ozkerim, I. Inci, Y.S. Zhang, A. Khademhosseini, M.R. Dokmeci, Bioinks for 3D bioprinting: an overview, Biomater Sci 6 (2018) 915–946. https://doi.org/10.1039/C7BM00765E.

[294] S. V Murphy, A. Atala, 3D bioprinting of tissues and organs, Nat Biotechnol 32 (2014) 773–785. https://doi.org/10.1038/nbt.2958.

[295] L.M. Thoma, C.L. DeLaughter, P.K. Mandal, Decellularized extracellular matrix for cardiac repair: A review, Biomater Res 23 (2019).

[296] C. Jensen, , J Wilm, D.G. Harkin, 3D printing: Making headway in tackling the COVID-19 pandemic, J 3D Print Med 5 (2021) 61–69.

[297] L.A. Elfawy, C.Y. Ng, I.N. Amirrah, Z. Mazlan, A.P.Y. Wen, N.I.M. Fadilah, M. Maarof, Y. Lokanathan, M.B. Fauzi, Sustainable Approach of Functional Biomaterials–Tissue Engineering for Skin Burn Treatment: A Comprehensive Review, Pharmaceuticals 16 (2023) 701. https://doi.org/10.3390/ph16050701.

[298] E. Yadav, P. Yadav, A. Verma, In silico Study of Trianthema portulacastrum Embedded Iron Oxide Nanoparticles on Glycogen Synthase Kinase-3β: A Possible Contributor to its Enhanced in vivo Wound Healing Potential, Front Pharmacol 12 (2021). https://doi.org/10.3389/fphar.2021.664075.

[299] N. Abu Bakar, R.B.S.M.N. Mydin, N. Yusop, J. Matmin, N.F. Ghazalli, Understanding the ideal wound healing mechanistic behavior using in silico modelling perspectives: A review, J Tissue Viability 33 (2024) 104–115. https://doi.org/10.1016/j.jtv.2023.11.001.

[300] A.S. MacLeod, J.N. Mansbridge, The Innate Immune System in Acute and Chronic Wounds, Adv Wound Care (New Rochelle) 5 (2016) 65–78. https://doi.org/10.1089/wound.2014.0608.

[301] S.M. Riha, M. Maarof, M.B. Fauzi, Synergistic Effect of Biomaterial and Stem Cell for Skin Tissue Engineering in Cutaneous Wound Healing: A Concise Review, Polymers (Basel) 13 (2021) 1546. https://doi.org/10.3390/polym13101546.

[302] A. Sharma, S. Khanna, G. Kaur, I. Singh, Medicinal plants and their components for wound healing applications, Futur J Pharm Sci 7 (2021) 53. https://doi.org/10.1186/s43094-021-00202-w.

[303] I.E. Cock, S.F. Van Vuuren, A review of the traditional use of southern African medicinal plants for the treatment of fungal skin infections, J Ethnopharmacol 251 (2020) 112539. https://doi.org/10.1016/j.jep.2019.112539.

[304] K. Lee, E.A. Silva, D.J. Mooney, Growth factor delivery-based tissue engineering: general approaches and a review of recent developments, J R Soc Interface 8 (2011) 153–170. https://doi.org/10.1098/rsif.2010.0223.

[305] C.M. Agrawal, R.B. Ray, Biodegradable polymeric scaffolds for musculoskeletal tissue engineering, J Biomed Mater Res 55 (2001) 141–150. https://doi.org/10.1002/1097-4636(200105)55:2<141::AID-JBM1000>3.0.CO;2-J.

Chapter II

In-silico Prediction and Analysis of GSK-3β Deleterious SNPs and their Impact on Wound Healing

2.1 Background

Single nucleotide polymorphisms (SNPs) stand out as important change-agents in the intriguing world of genetic variants that genetics has revealed. SNPs, commonly referred to as "snips," are small changes in the nucleotide sequence of the genome that have the potential to affect the structures and functions of proteins.[1]. Single-Nucleotide Polymorphisms (SNPs) play an essential role in modifying the amino acid sequence of proteins. The majority of the genome's SNPs are located in the coding regions, where they occur at a rate of one per 300 base pairs and with a minor allele frequency (MAF) value greater than 1% [2–4]. Up to this point, there have been around 5,00,000 SNPs recorded in the coding sections of the human genome[5]. Synonymous and non-synonymous (nsSNP) SNPs are the most common types of SNPs found in these samples. Synonymous single-nucleotide polymorphisms (SNPs) are changes in the DNA sequences that do not cause major alteration in the amino acid sequences, in contrast to non-synonymous SNPs like missense SNPs, which is majorly instrumental in amino acid substitutions and thus protein variations in humans [6,7]. nsSNPs account for almost half of the mutations that cause a wide range of genetic illnesses, as well as a number of autoimmune and degenerative diseases[8]. Using nsSNPs for structural and functional study may aid in the development of genomic-based customized therapy[9,10]. Thus, this field of research has been gaining immense popularity in recent times. It is time-consuming and expensive to apply experimental methods to determine the impact of many nsSNPs. These methodologies may be substituted for experiments to study how nsSNPs affect protein integrity, function and stability in a computational manner. In fact, a number of in-silco investigations have shown that detrimental nsSNPs have a negative impact on the structure and function of numerous proteins[11,12].

Shifting the focus to a specific protein of interest, Glycogen synthase kinase-3 (GSK-3) initially discovered in mammals, emerges as a conserved serine/threonine kinase with a multifaceted role [13,14]. GSK-3 has been demonstrated to phosphorylate approximately 100 substrates and has been proven to impact diverse cellular functions, including cellular proliferation and the control of several metabolic and signalling pathways[15]. Initially, it is identified as a regulator of glycogen production through inactivating phosphorylation of glycogen synthase. Then it has recently been discovered to control a wide variety of activities via Wnt and other signalling pathways. After the initial isolation of GSK-3 from rabbit skeletal muscle, additional analysis revealed two

homologous isomers of GSK-3, namely GSK-3α and GSK-3β[16]. Both the isomers showed high expression in the brain[17,18] and were found to be 98 percent identical in the internal kinase domain. GSK-3β depletion results in embryo mortality in mice, demonstrating that the other homolog cannot compensate for the loss of GSK-3β[19].

GSK-3β overexpression promotes a wide range of malignancies. GSK-3β overexpression promotes cancer cell survival, invasion, and angiogenesis. GSK-3β expression and nuclear accumulation boosted kinase activity and tumour differentiation [20]. As an independent prognostic indicator, GSK-3β activity is inversely linked with patient survival in glioblastoma multiforme (GBM), a deadly brain tumour [21], cancers of the pancreas, colon, and kidney benefit from GSK-3 activation when pSer9GSK-3 is reduced. Pharmacological inhibition of GSK-3 in these cancers resulted in decreased proliferation and increased apoptosis[22].

GSK-3β is also crucial to the healing of wounds[23,24]. Reports suggest that GSK-3β controls the levels of ET-1, which is involved in wound healing and fibrosis[25]. Proteins in the Wnt/-catenin signalling cascade are phosphorylated by CK1and GSK-3β, including β-catenin, Axin, and APC (adenomatous polyposis coli), which operate as either positive or negative regulators of the process[26–28]. Injury sites attract anti-inflammatory cells like keratinocytes and fibroblasts. Consequently, the wound heals, and scars form as a result. As a result, it's possible that inhibiting GSK-3β has a role in wound healing.

With all these facts this research utilizes an advanced in silico molecular dynamics approach to evaluate the impact of harmful Single Nucleotide Polymorphisms (SNPs) on GSK3β, a pivotal protein involved in metabolism, wound healing, and migration. By combining sequence- and structure-based bioinformatics, we pinpoint deleterious SNPs within the GSK3β gene, providing precise insights into their effects on protein structure and function. Employing molecular modelling and simulation techniques, we uncover how mutant proteins alter structures and protein-protein interactions, shedding light on GSK3β's intricate regulatory pathways. Our findings hold potential for tailored treatment strategies, as SNPs affecting GSK3β's structure relate to cellular dysfunctions and wound healing. This study's implications for personalized medicine could reshape approaches to GSK3-related conditions and other SNP-influenced genes, presenting a comprehensive in-silico understanding of harmful nsSNPs' consequences on GSK3β's structure, stability, and function.

2.2 Methodology

2.2.1 Datasets

The SNPs linked with GSK-3β were derived from the National Center for Biotechnology Information (NCBI) dbSNP database:

(https://www.ncbi.nlm.nih.gov/snp/?LinkName=gene_snp&from_uid=2932).

A complete list of SNPs is given in Supplementary data. The fasta sequence of the targeted Gene (Gene ID: 2932) and the targeted protein sequence (P49841) have been extracted from www.ncbi.nlm.nih.gov.

2.2.2 Predication of Deleterious SNPs of GSK3B

The two primary methods for analyzing SNPs are sequence-based and structure-based. Sequence-based methods are founded on evolutionary dialogue and structural homology, whereas structure-based methods take into account the effect of mutations in individual amino acids on protein phenotype [29]. Thus methods covering both approaches take into account the wide feature coverages of SNPs. To find the most harmful SNPs, we used a combination of the two approaches. Many online resources were examined to speculate on the potential harm caused by SNPs related to GSK3B. The major tools used are:

Protein **V**ariation **E**ffect **An**alyser (PROVEAN) (web application available at www.provean.jcvi.org/) is a sequence homology-based prediction tool and is mostly operated as an online tool. The functional impact of a missense mutation could be predicted using this tool. It predicts the nature of SNP, i.e., whether it is natural or deleterious in nature. The scoring system indicates if the score is less than or equal to -2.5, then the mutation is expected to be deleterious, and a score above it is estimated as neutral[30].

Protein **An**alysis **th**rough **E**volutionary **R**elationship (PANTHER) (web application available at http://www.pantherdb.org/tools/csnpScoreForm.jsp) majorly identifies the influence of non-synonymous genetic variations on the function of Protein based on evolutionary preservation time. The application computes the time scale (in millions of years) a particular amino acid has gone preservation in the heredity leading to the generation of the Protein of interest[31].

Polymorphism **Phen**otyping version **2** (PolyPhen-2) (web application available at www.genetics.bwh.harvard.edu/pph2/) is a method that is a combined approach and includes multiple homologous sequence alignments and protein 3D structures. This web-based tool can predict the impact of the amino acid change on both the function and structure of the Protein. The prediction gives the user an idea about the difference in the position-specific independent count (PSIC) scores of the two variants, in which one includes wild-type amino acids and the other with the substituted amino acid. The score gives us a clear idea regarding the impact of amino acid substitution on the Protein. PSIC score ranges from 0 to 1, with values above 0.5 indicating possible damage and values above 0.9 indicating probable damage[32].

Screening for **N**on**a**cceptable **P**olymorphism (SNAP2) (web application available at https://www.rostlab.org/services/SNAP/) examines a wide range of sequence and variant properties to distinguish between variations with an effect and variants with no effect. The input query for SNAP2 is a protein sequence in FASTA format. An overall score was generated, ranging between zero (no change) and one hundred percent (high effect prediction), revealing the likelihood that a specific mutation will disrupt the native Protein's function with expected precision[33].

The sorting **Intolerant **f**rom **T**olerant (SIFT) (web application available at https://sift.bii.a-star.edu.sg/) program is based on sequence homology, and it identifies the deleterious (probability score <0.05) and tolerated SNPs. To better understand the impact of amino acid variation on Protein phenotypic and functional changes, this prediction can be useful. The db SNP rsIDs were utilized as an input query for this server because they were obtained from the database [34].

The Disease-**Su**sceptibility-based **S**AV **P**henotype Predi**ct**ion (SuSPect) (web application available at www.sbg.bio.ic.ac.uk/suspect) is used to find disease-associated and neutral variants in a protein or domain; the tool applies the disease-propensity technique, which compares the observed numbers to random expectations using a binomial test. Predictions are compiled based on protein sequences and the central chain protein as inputs (IBP). Sequence, structural, and system biology properties are used by SusPect [35] to estimate the impact of missense mutations. There are threshold values of 50 between neutral and disease-causing variations, with scores ranging from 0 to 100.

In order to validate the assumptions, all the common Deleterious SNPs were subjected to analyse using different applications like META-SNP (http://snps.biofold.org/meta-snp)[36], PHD-SNP (https://snps.biofold.org/phd-snp/phd-snp.html) [37], SNP & GO (https://snps-and-go.biocomp.unibo.it/snps-and-go/) [38] Predict SNP (https://loschmidt.chemi.muni.cz/predictsnp1/)[39], and PMUT (http://mmb.irbbarcelona.org/PMut/analyses/new/) [40].

2.2.3 Investigation of the oncogenic effect of the Selected Mutation

For the determination of cancer-associated mutation, the C-Scape server was used, which is a well-known accepted application for the identification of Cancer-associated mutation. Point mutations in the genome's coding and noncoding regions may be tested for oncogenicity using C-Scape, an online combinatorial platform [41]. Based on P values ranging from 0 to 1, the C-Scape available at http://cscape.biocompute.org.uk/ classifies a mutation as either neutral or cancer driver. It is projected that a value above [0.5] is oncogenic, whereas values below [0.5] are considered benign.

All the selected mutations were cross-checked using a web-based application based on cancer-specific model Functional Analysis through Hidden Markov Models available at http://fathmm.biocompute.org.uk. When a single nucleotide variation (nsSNV) occurs in the human genome, the FATHMM server can predict the functional effects of both the variant and its non-synonymous counterparts. The prediction is capable of distinguishing between cancer-promoting/driver mutations and other germline polymorphisms[42].

2.2.4 Investigating the Stability of the Mutant and the Native Protein

The stability of the mutated proteins was tested using different servers. **I-Mutant2.0** (http://folding.biofold.org/i-mutant/i-mutant2.0.html) is a tool that is available online for the prediction of protein stability changes with single amino acid replacement from protein sequences[43]. **MUpro (** https://mupro.proteomics.ics.uci.edu/ **)** applies support vector machine algorithms to predict alteration in the stability of the Protein [44]. **SAAFEC-SEQ (**http://compbio.clemson.edu/SAAFEC-SEQ/**)** uses the PsePSSM algorithm to envisage the stability of the Protein due to mutation[45]. **AggreRATE-Disc(** https://www.iitm.ac.in/bioinfo/aggrerate-disc/) is a server by IIT Madras that tries to predict

whether a mutation will boost or alleviate a protein's aggregation and thus point towards protein stability[46].

2.2.5 Conservation analysis

The ConSurf server was used to determine the evolutionary dialogue of the GSK-3β protein's amino acid residues (http://consurf.tau.ac.il/2016/).ConSurf uses sequence similarity to make predictions about which amino acid residues are conserved in proteins across evolutionary time. Amino acid residues are predicted to have a conservation score between 1 and 9, with 9 indicating a highly conserved residue[47]. To determine which amino acid residues in the GSK3B protein are likely to have been conserved throughout evolutionary time, the ConSurf server was fed the Protein's sequence in FASTA format.

2.2.6 Finding active sites | binding sites of the Protein

The active sites or site of protein binding was predicted using different tools, including COACH (https://zhanggroup.org/COACH/)[48], RaptorX (http://raptorx6.uchicago.edu/) [49], CASTp (http://sts.bioe.uic.edu/castp/index.html?3trg) [50] & P2RANK (https://prankweb.cz/) [51]. The FASTA amino acid sequence of GSK-3β was used as input for all the servers, and the output was analyzed. The Common binding sites from all the servers were finally considered for further studies. By comparing binding-specific substructure and sequence profiles, the COACH servers identify ligand-binding templates from the BioLiP protein function database. Final ligand binding site predictions will be made by combining these predictions with those from other approaches (such as COFACTOR, FINDSITE, and ConCavity).

2.2.7 Modelling of the complete GSK-3β protein and the Mutants

Three-dimensional structures of native and single-point mutated proteins were modelled using the I-TASSER (Iterative Threading ASSEmbly Refinement) server (https://zhanggroup.org/I-TASSER/). I-TASSER is a meta-server for predicting the tertiary structure of proteins [52]. To predict protein structures and annotate their functions based on those predictions, Zhang Lab has developed I-TASSER (Iterative Threading ASSEmbly Refinement), a hierarchical method. LOMETS, a multithreaded method, first locates structural templates in the PDB; then, using these templates as a starting point, it builds iterative fragment assembly simulations to create full-length atomic models. I-TASSER uses replica-exchanged Monte Carlo simulations to construct a full-

length model of a protein by first generating pieces of that Protein through threading alignments. Replicas (decoys) created at low temperatures in the simulation are clustered using SPICKER, and the centres of the top five clusters are used to create entire atomic models. The confidence score is a reflection of how well the anticipated model performed (C-score). Between 5 and 2, C-scores can be obtained. The projected mode is more reliable with a higher C-score. For each query protein, the model with the highest C-score was chosen as the most accurate prediction. Each protein structure was calculated using the same set of default parameters. Server predictions of normal and mutant models were made using FASTA-formatted protein sequences as input. In order to see the molecular structures in high-quality 3D photos, we used Discovery Studio.

2.2.8 Energy minimization and validation of the native and mutant protein model

Models of both wild-type and mutant proteins were improved using the atomic-level protein structure refinement programme ModRefiner (https://zhanglab.ccmb.med.umich.edu/ModRefiner/) [53]. Ramachandran Plot Server (https://zlab.umassmed.edu/bu/rama/), a structural validation tool for the evaluation of the Ramachandran Plot of proteins, was then used to assess the quality of the energy-minimised models [54].

2.2.9 Evaluating Protein Domains and Secondary Structure

SOPMA is a modified version of the Self-Optimised Prediction technique (SOPM) that uses a three-state description of the alignment of amino acids in a protein to identify the secondary structure (α-helix, b-sheet, and coil) [55]. The prediction is based on an amino acid sequence query and numerous alignments of protein sequences that are relevant to the query. SOPMA and PHD, a neural network-based technique, both predict 82.2 percent of residues for 74.2 percent of co-predicted amino acids with high precision. It is possible to connect to the web server at https://npsa-prabi.ibcp.fr/cgi-bin/npsa_automat.pl?page=/NPSA/npsa_sopma.html

2.2.10 Evaluation of functional and structural properties of the Mutated Protein

MutPred v1.2 and HOPE were used to predict the structural and functional properties of selected nsSNPs. In humans, amino acid substitutions can be reliably classified as either disease-causing or disease-neutral using the web programme MutPred (http://mutpred.mutdb.org/). This method also assists in determining the detrimental amino acid substitution or molecular etiology of

disease[56]. It emphasizes an extensive range of structural and functional features and properties, including secondary structure, signal peptide and trans-membrane topology, macromolecular binding, PTMs, metal binding, catalytic activity and allostery106. The protein sequences (in FASTA format), including the discovered genetic variations and their corresponding amino acid substitutions, were provided. MutPred v1.2 gave output scores indicating the probability of harmful or disease-associated amino acid replacement. There would be a list of the top five features based on their P value that affected the structural and functional properties. Predicted scores were sorted into three groups according to three hypotheses: (i) actionable hypotheses with g > 0.5 and p 0.05; (ii) confident hypotheses with g > 0.75 and p 0.05; and (iii) extremely confident hypotheses with g > 0.75 and p 0.01.

The HOPE web service tool (www.cmbi.ru.nl/hope)[57] was used to determine the structural consequences of a point mutation in a human protein sequence. All of the submitted nsSNP protein sequences were hand-picked. HOPE produced output by collecting and combining data from a wide variety of online sources. The algorithm's first iteration made use of BLAST searches against the Protein Data Bank and the Universal Protein Resource in order to gather information on the tertiary structure necessary to construct a homology model. Distributed Annotation System was then used to predict protein characteristics[57].

2.2.11 Molecular dynamics simulation

The molecular dynamics simulation of the Native and the mutated protein was conducted to analyze the conformational behaviour and protein stability of the mutated protein with reference to the native protein. GROMACS v.2019.4 packages have been used to perform a 250ns MD simulation on the Native and mutated proteins. The topology of the biomolecular systems was generated through the AMBER99SB-ILDN force field[58]. This system was solved using a standard Tip3p water model, where a cubic periodic boundary box shape with a distance of 10Å has been allocated to all sides to maintain a certain volume. Explicit water molecules are employed in the solvation mechanism, which is then neutralized by the addition of the counter ion NA+. Using the steepest descent minimization algorithm, the energy reduction process was carried out until it reaches stability with maximum force <100 kJ mol^{-1} nm^{-1}. Later on, all the proteins were equilibrated by NVT (0–300 K) and NPT (1 bar at 300 K) ensemble for 100ps[59]. After the equilibration process, a 250ns MD production run was carried out for all the proteins. After

completing the MD simulation of each system, the trajectories were analyzed to learn more about the system's dynamics using tools like the root mean square deviation (RMSD), root mean square fluctuation (RMSF), the radius of gyration (Rg), number of internal hydrogen bonds, Gibbs free landscape, and density analysis. The PCA analysis and the secondary structure analysis were also carried out to point out the structural conformational change in Mutated Proteins compared to that of the Native one[60].

2.3. Results and Discussion

2.3.1 Retrieval of Non-synonymous coding SNPs(nsSNPs)from dbSNP database (NCBI)

The human GSK3β gene in the dbSNP database has been found to include a total of 68492 SNPs. Out of the total number of reported SNPs, 172 were novel or missense variants, 115 were coding-synonymous variants, 440 were located in the 5' Untranslated Region (UTR), 1,407 were found in the 3' UTR, 64,355 were found in the intron region, and the remaining SNPs belonged to various other categories. In Fig. 2.1a, we can see how widely spread out GSK3B SNPs are. To better understand how GSK3B's structure, stability, and function are affected by nsSNPs, missense SNPs were chosen for this work.

2.3.2 Prediction of deleterious nsSNPs

The selected 172 missense SNPs were tested to investigate their effect on protein structure. Out of the 172 nsSNPs, 94 nsSNPs were predicted as 'deleterious' using the PROVEAN server; 163 were predicted as 'deleterious' by the PANTHER server; The PolyPhen pointed out 66 nsSNPs to be 'deleterious'. Analysis using SNAP showed that 61 nsSNPs were 'deleterious'; 52 nsSNPS were predicted to be 'deleterious' by the SIFT server, and finally the SuSpect predicted 19 nsSNPs to be highly 'deleterious'. After predicting potentially harmful nsSNPs with six well-established web-tools, we ran a prediction-matching study to find nsSNPs that were predicted with 100% concordance by all six. There were 12 extremely harmful nsSNPs that were shared by all of the servers, as determined by a screening of 172 nsSNPs using six in silico techniques. The intersection of the results is depicted in Figure 2.1b. The 12 damaging nsSNPs predicted were rs201448262(T235P), rs201450363(I182T), rs747385360(P225L), rs748461608(T138I), rs750723548(H337R), rs758696011(Y161C), rs767657425(N108H), rs944354549(K86N), rs1334056340(P184L), rs1576402131(K197N), rs1576533875(A83T), rs1576533961(F67C).

The details of all these 12 SNPs along with the detailed scoring from the six different serves are given in Table 2.1. There is a possibility that these harmful SNPs alter the Protein's structure, stability, and/or function. These potentially harmful SNPs were thus factored into the study's overall design.

Table 2.1: Prelection of Deleterious Mutations using PROVEAN, PANTHER ,POLYPHEN-2,SNAP2,SIFT and SuSpect for most Deleterious 12 SNPs

Sl No.	Mutation	PROVEAN	PANTHER	Pdel || Preservation Time	POLYPHEN-2	SNAP2	Score || Accuracy(%)	SIFT	Sift Score || Sift Median	SuSpect
1	T235P	-5.809	Probably Damaging	0.85||1237	0.977	Effect	79 || 85	DELETERIOUS	0.001 || 2.24	80
2	I182T	-4.806	Probably Damaging	0.89||1628	1	Effect	63 || 80	DELETERIOUS	0 2 || .25	96
3	P225L	-9.749	Probably Damaging	0.89||1628	1	Effect	73 || 85	DELETERIOUS	0 || 3.04	98
4	T138I	-5.696	Probably Damaging	0.89||1628	1	Effect	67 || 80	DELETERIOUS	0 || 3.04	93
5	H337R	-7.287	Probably Damaging	0.89||1628	0.998	Effect	88 ||91	DELETERIOUS	0.01 || 3.04	95
6	Y161C	-8.383	Probably Damaging	0.89||1628	1	Effect	22 || 63	DELETERIOUS	0 || 3.04	85
7	N108H	-4.914	Probably Damaging	0.89||1628	1	Effect	15 || 59	DELETERIOUS	0 || 3.04	89
8	K86N	-4.931	Probably Damaging	0.89||1628	1	Effect	58 || 71	DELETERIOUS	0 || 3.04	92
9	P184L	-9.711	Probably Damaging	0.89||1628	1	Effect	43 || 71	DELETERIOUS	0 || 3.04	96
10	K197N	-4.689	Probably Damaging	0.89||1628	1	Effect	88 || 91	DELETERIOUS	0.01 || 3.04	98
11	A83T	-3.943	Probably Damaging	0.89||1628	1	Effect	52 || 75	DELETERIOUS	0 || 3.04	98
12	F67C	-7.869	Probably Damaging	0.89||1628	1	Effect	77 || 85	DELETERIOUS	0 || 3.04	98
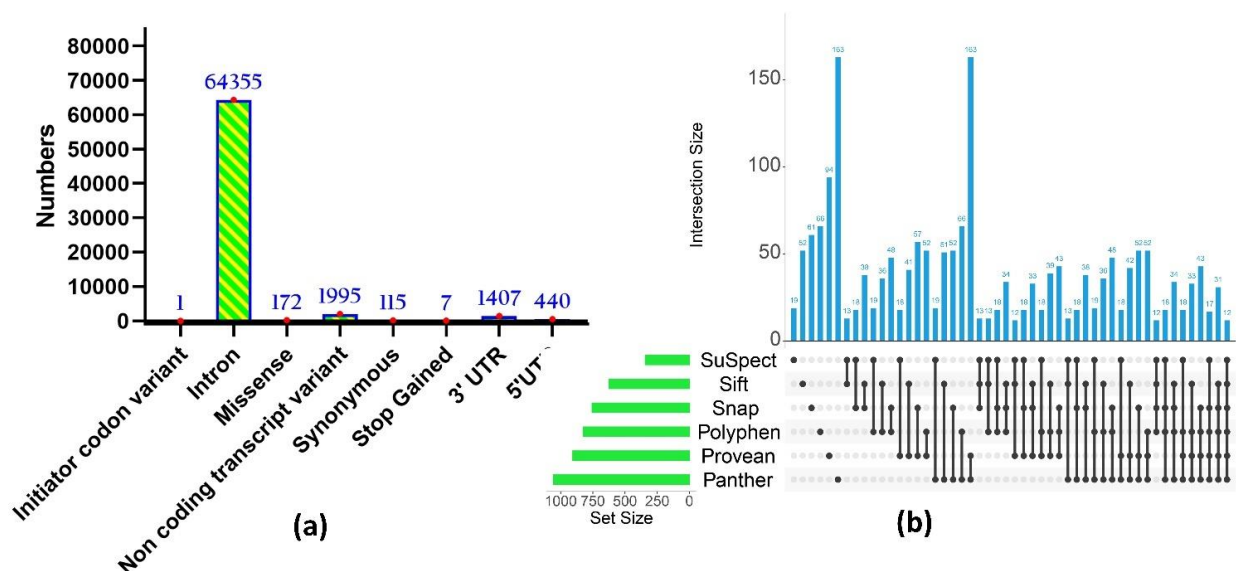
Figure 2.1: Numbers of mutations in GSK -3β (a), Intersection size of deleterious SNPs using 6 different detection servers (b)

2.3.3 Re-evaluation of selected Missense Mutation

The 12 selected nsSNPs were re-evaluated using a few available servers to support the earlier prediction. All the selected nsSNPs were reanalyzed using **Meta SNP, PHD-SNP, SNPs & GO, Predict-SNP** and **Pmut** servers. All the servers predicted that the selected 12 nsSNPs were all 'deleterious' in nature. The detailed scoring and indications are given in Table 2.2. Hence re-evaluation pointed out that all common deleterious nsSNPs were selected initially from 6 different server analyses, and all of these can be potentially harmful as they were also found to be deleterious using all the servers. Thus all further studies were carried out using these 12 nsSNPs.

Table 2.2: Confirmation of Deleterious SNPs using Servers Meta SNPs, PHD-SNP,SNPs & GO, PREDICT SNP and Pmut

Sl No.	Mutation	Meta SNP	RI	PHD-SNP	RI || Probability	SNPs & GO	RI || Probability	Predict SNP	Accuracy	Pmut	Score || Prediction()
1	T235P	Disease	4	Disease	7 || 0.86	Disease	6 || 0.79	DELETERIOUS	0.87	Disease	0.92 || 94
2	I182T	Disease	4	Disease	3 || 0.64	Disease	4 || 0.68	DELETERIOUS	0.72	Disease	0.93 || 94
3	P225L	Disease	8	Disease	8 || 0.88	Disease	6 || 0.79	DELETERIOUS	0.87	Disease	0.93 || 94
4	T138I	Disease	4	Disease	3 || 0.64	Disease	2 || 0.62	DELETERIOUS	0.61	Disease	0.93 || 94
5	H337R	Disease	5	Disease	5 || 0.77	Neutral	2 || 0.41	DELETERIOUS	0.87	Disease	0.92 || 94
6	Y161C	Disease	7	Disease	8 || 0.90	Disease	6 || 0.79	DELETERIOUS	0.72	Disease	0.93 || 94
7	N108H	Disease	5	Disease	7 || 0.86	Disease	5 || 0.73	DELETERIOUS	0.72	Disease	0.74 || 87
8	K86N	Disease	4	Disease	6 || 0.80	Disease	4 || 0.68	DELETERIOUS	0.76	Disease	0.86 || 91
9	P184L	Disease	6	Disease	7 || 0.86	Disease	6 || 0.78	DELETERIOUS	0.87	Disease	0.93 || 94
10	K197N	Disease	4	Disease	6 || 0.79	Disease	4 || 0.69	DELETERIOUS	0.87	Disease	0.93 || 94
11	A83T	Disease	3	Disease	6 || 0.81	Disease	3 || 0.64	DELETERIOUS	0.87	Disease	0.92 || 94
12	F67C	Disease	8	Disease	8 || 0.92	Disease	7 || 0.87	DELETERIOUS	0.87	Disease	0.54 || 80

2.3.4 Prediction of Cancer-Causing nsSNPs

Two cancer prediction pipelines, CScape and the FATHMM service, were used to further screen the functionally detrimental, disease-associated mutations for their oncogenic status. There were a total of 12 mutations analyzed, and four of them (T235P, Y161C, P184L, and A83T) were identified as possible cancer drivers due to their high confidence in reflecting oncogenic status using CScape with a score > 0.9. Aside from this, all other nsSNPs were indicated to be carcinogenic, with a score of 0.85 or higher. Similarly, the FATHMM server also pointed out all the mutations to be cancerous with a threshold score below -0.75. The detailed results can be observed in Table 2.3. This means that all 12 of these nsSNPS have the potential to trigger genetic alterations that might eventually result in cancer.

2.3.5 SNPs and their predicted impact on protein stability

Effects of nsSNPs in the stability of GSK3B protein were predicted using I-Mutant3.0, MUpro, SAAFEC-SEQ and AggreRATE-Disc. I-Mutant server predicted 10 nsSNPS out of 12 to have decreased stability. nsSNPs like T235P, I182T, P225L, T138I, H337R, Y161C, N108H, P184L, A83T, and F67C showed decreased stability using I-Mutant servers, whereas MUPRO servers pointed out 11 nsSNPs (Except P184L) to have decreased stability. SAAFEC-SEQ server pointed all the nsSNPs to be destabilizing. On the other hand, AggreRATE-Disc pointed T235P, I182T, P225L, T138I, Y161C, P184L, and F67C to have decreased protein stability and the others to have an increase in protein stability. Detailed reports of the servers are given in Table 2.4 and Table 2.5. Several reports demonstrated that Protein misfolding and breakdown resulted in alterations in protein stability[61,62]. Thus, these polymorphism-caused changes in protein stability may have consequences for protein structure and function. Protein structure is linked to function. Denatured proteins lose their native three-dimensional structure as a result of mutations or other changes to their amino acid building blocks[63]. The denaturation of the Protein prevents it from performing its biological role. The effect of single-residue mutations on protein stability is represented by a spectrum of structural consequences, including but not limited to a decrease in hydrophobic area, backbone strain, and the elimination of electrostatic connections[64]. On the other hand, an increase in protein stability is highly desirable, although, in terms of down-regulating protein action by drug, this stability might cause a big hindrance.

Table 2.3: Prediction of Cancer-causing mutations

	C-SCAPE						FATHOM				
	# Chromosome	Position	Ref. Base	Mutant Base	Coding Score	Warning	Prediction	Score	HMM Pos.	HMM, Prob. W.	HMM, Prob. M.
T235P	3	119912716	T	G	0.958239	oncogenic (high conf.)	CANCER	-1.25	201	0.178262	0.022082938
I182T	3	119916107	A	G	0.865025	oncogenic	CANCER	-1.53	148	0.308014	0.003887535
P225L	3	119912745	G	A	0.88734	oncogenic	CANCER	-3.87	191	0.865178	0.015114511
T138I	3	119923437	G	A	0.886095	oncogenic	CANCER	-1.14	105	0.093045	0.00286167
H337R	3	119863505	T	C	0.804378	oncogenic	CANCER	-1.5	303	0.318214	0.032466061
Y161C	3	119916170	T	C	0.891062	oncogenic (high conf.)	CANCER	-1.18	127	0.130315	0.014508799
N108H	3	119947312	T	G	0.872145	oncogenic	CANCER	-1.53	74	0.363509	0.082645079
K86N	3	120002070	T	G	0.787282	oncogenic	CANCER	-1.15	52	0.110649	0.015898985
P184L	3	119916101	G	A	0.906849	oncogenic (high conf.)	CANCER	-1.73	150	0.439846	0.07371345
K197N	3	119916061	T	G	0.851109	oncogenic	CANCER	-1.78	163	0.426633	0.014388586
A83T	3	120002081	C	T	0.94015	oncogenic (high conf.)	CANCER	-2.84	49	0.72753	0.021330656
F67C	3	120002128	A	C	0.873562	oncogenic	CANCER	-1.57	33	0.333111	0.01243948

Table 2.4: The effect of the nsSNPs on GSK-3β protein's stability

		Imutatnt 3.0			MUPRO					
SI No.	Mutation	SVM2 Prediction Effect	SVM3 Prediction Effect	DDG Value Prediction (Kcal/mol)	Stability	Delta G	Method 1	Confidence Score	Method 2	Confidence Score
1	T235P	Decrease RI: 4	Large Decrease RI: 2	-0.65	DECREASE stability	-0.95	DECREASE	-0.55	DECREASE	-0.93
2	I182T	Decrease RI: 9	Large Decrease RI: 8	-2.28	DECREASE stability	-1.75	DECREASE	-1	DECREASE	-0.88
3	P225L	Decrease RI: 6	Large Decrease RI: 5	-0.55	DECREASE stability	-0.01	INCREASE	0.51	INCREASE	0.93
4	T138I	Decrease RI: 6	Large Decrease RI: 6	-0.54	DECREASE stability	-0.26	DECREASE	-0.8	DECREASE	-0.56
5	H337R	Decrease RI: 2	Large Decrease RI: 1	-0.04	DECREASE stability	-0.62	DECREASE	0.08	DECREASE	-0.68
6	Y161C	Decrease RI: 4	Large Decrease RI: 4	-1.27	DECREASE stability	-0.5	DECREASE	-1	DECREASE	-0.71
7	N108H	Decrease RI: 9	Large Decrease RI: 6	-1.01	DECREASE stability	-0.81	DECREASE	-0.57	DECREASE	-0.76
8	K86N	Increase RI: 1	Neutral RI: 1	-0.38	DECREASE stability	-0.32	DECREASE	-0.98	DECREASE	-0.94
9	P184L	Decrease RI: 7	Large Decrease RI: 2	-0.8	INCREASE stability	0.61	INCREASE	0.07	INCREASE	0.71
10	K197N	Increase RI: 4	Neutral RI: 1	-0.09	DECREASE stability	-0.8	DECREASE	-0.81	DECREASE	-0.91
11	A83T	Decrease RI: 3	Large Decrease RI: 6	-0.43	DECREASE stability	-0.91	DECREASE	-0.42	DECREASE	-0.79
12	F67C	Decrease RI: 7	Large Decrease RI: 5	-1.78	DECREASE stability	-1.44	INCREASE	0.11	INCREASE	0.55

Table 2.5: Protein structure stability prediction using **SAAFEC-SEQ** and **AggreRATE-Disc**

| SNPs | SAAFEC-SEQ | | AggreRATE-Disc | |
	Predicted Effect	ddG (unit)	Effect on aggregation	Prediction probability
T235P	Destabilising	-0.4	DECREASE	0.999
I182T	Destabilising	-2.17	DECREASE	1
P225L	Destabilising	-1.34	DECREASE	0.658
T138I	Destabilising	-1.14	DECREASE	0.91
H337R	Destabilising	-0.5	INCREASE	0.996
Y161C	Destabilising	-2.31	DECREASE	0.824
N108H	Destabilising	-1.07	INCREASE	0.898
K86N	Destabilising	-1.03	INCREASE	0.98
P184L	Destabilising	-0.88	DECREASE	0.967
K197N	Destabilising	-0.91	INCREASE	0.997
A83T	Destabilising	-1.49	INCREASE	0.999
F67C	Destabilising	-2.78	DECREASE	0.976

2.3.6 Prediction of Conserved Domain

The most harmful nsSNP's possible effects were further examined using ConSurf. Each amino acid residue's level of evolutionary conservation within the Protein was calculated using this method. By combining evolutionary conservation information with estimates of solvent accessibility, it pinpoints amino acid locations that are known to be crucial for both structural and functional reasons. In this study, scores ranging from 1 to 9 were used to rate the conservation levels of all residues from each Protein that were taken from Consurf. We focused only on residues that corresponded to the positions of the twelve (12) high-risk nsSNPs that we had previously found. The server predicted the functional and structural significance of all the mutated amino acid positions. All 12 mutations were highly conserved and of structural and functional importance (Table 2.6). The results also showed that these eight high-risk nsSNPs were undoubtedly harmful to the protein structures and activities. Understanding the possible effects of mutations on human health requires knowledge of evolution[65]. At the molecular level, the evolution of amino acids has an impact on their properties, such as size, form, hydrophobicity, and charge[66]. Biological processes depend on the functional sites of proteins, such as protein-protein interaction sites, DNA interaction sites, and enzymatic sites. This could imply that the nsSNPs in these conserved regions have more harmful consequences than other nsSNPs identified in non-conservative regions and may have a major impact on biological activities[67,68].

Table 2.6: Amino acid conservation profiles in proteins with high-risk nsSNPs, as determined using ConSurf.

nsSNPs	Score	Prediction	Comment
T235P	7	Conserved	An exposed residue
I182T	9	Highly Conserved	A buried residue | A predicted structural residue (highly conserved and buried).
P225L	9	Highly Conserved	The residue is predicted to be highly functional residue (highly conserved and exposed)
T138I	9	Highly Conserved	The residue is predicted to be highly functional residue (highly conserved and exposed)
H337R	8	Highly Conserved	A predicted functional residue
Y161C	7	Conserved	A buried residue
N108H	9	Highly Conserved	The residue is predicted to be highly functional residue (highly conserved and exposed)
K86N	8	Highly Conserved	The residue is predicted to be highly functional residue (highly conserved and exposed)
P184L	8	Highly Conserved	The residue is predicted to be highly functional residue (highly conserved and exposed)

K197N	8	Highly Conserved	The residue is predicted to be highly functional residue (highly conserved and exposed)	
A83T	9	Highly Conserved	The residue is predicted to be highly functional residue (highly conserved and exposed)	
F67C	9	Highly Conserved	The residue is predicted to be highly functional residue (highly conserved and exposed)	

2.3.7 Finding Active Sites

The presence of ligand binding sites or Active Sites in the mutant residues may alter the ligand's ability to bind to the GSK-3B protein, which may then alter the Protein's functionality. Residues on active sites have a variety of functions. They might participate in substrate binding and catalysis, stabilize reaction intermediates, or affect the shape of the binding cleft[69]. Among the 12 different nsSNPs, the COACH server detected two residues at A83 and T138; the RaptorX binding server predicted F67, A83, and T138. In order to get more confirmation, the GSK3B protein was evaluated using the CASTp server, which detected 67PHE, 83ALA, and 138THR as the active site residue and sever P2RANK also detected F67, A83 and T138 as the active site residue. All the servers majorly pointed out to 3 residues, i.e. 67PHE, 83ALA, 138THR, to be the residues of the active sites. The active site Domains from all servers are depicted in Figure 2.2, and a detailed list of all the residues of the active sites predicted by the servers is given in Table 2.7. The same analysis was done on four different servers to get a more accurate prediction, and the residues which were common from most of the servers were taken into consideration for further studies. Based on the findings, we found that F67, A83, and T138 are some of the binding site residues. This finding is in agreement with previous studies of GSK-3β's active site residue. Various research findings have demonstrated that residues F67, A83, and T138 indeed function as crucial binding sites residues within the protein, facilitating the binding of ligands for the inhibition of GSK3β[70–72]. This is also evident from previous research that A83 serves as an "adenine pocket" and T138 serves as a "Near adenine N3" pocket[73]. The data obtained from this investigation aligns with previously established findings, emphasizing the significance of validating mutations in these residues and assessing their impact on protein function.

Table 2.7: Active /Binding site prediction using different Servers

Calculation Method	POCKET COORDINATES			SCORE	RESIDUE Numbers	OTHER PARAMETERS
COACH	X	Y	Z	C-Score: 1		Cluster Size: 3891

	46.658	-7.655	-38.190		62,63,64,65,70,83,85,110,132, 133,134,135,137,138,185,186, 188,199,200	
RaptorX	-	-	-	P Value : 6.01 x 10 $^{-13}$	I62 G63 F67 V70 A83 K85 V110 L132 D133 Y134 V135 P136 T138 Q185 L188 C199 D200	Multiplicity : 85, **uGDT(GDT)**: 320(76) **uSeqId(SeqId):** 350(83)
CASTp	-	-	-	POCKET ID: 2	62ILE, 63GLY, 64ASN, 65GLY, 66SER, 67PHE, 68GLY, 70VAL, 83ALA, 85LYS, 87VAL, 93PHE, 94LYS, 97GLU, 101MET, 110VAL, 112LEU, 130LEU, 132LEU, 133ASP, 134TYR, 135VAL, 137GLU, 138THR, 141ARG, 179HIS, 180ARG, 181ASP, 183LYS, 185GLN, 186ASN, 188LEU, 199CYS, 200ASP, 201PHE, 202GLY, 203SER, 216TYR, 217ILE, 218CYS, 223ARG	Area (SA): 463.338 Volume (SA): 407.237
P2RANK	25.908	-47.399	31.540	**RANK**:1 SCORE: 34.1	101, 112 ,132,134 ,135 ,137 ,138 ,140 ,180 ,181 ,183 ,185 ,186 ,188 ,199 ,200 ,201 ,202 ,203 ,217 ,218 ,219 ,62 ,63 ,64 ,65 ,66 ,67 ,70 ,83 ,85 ,87 ,90,93 ,94 ,97	SAS Points: 190

COACH

P2RANK

P2RANK

CASTp
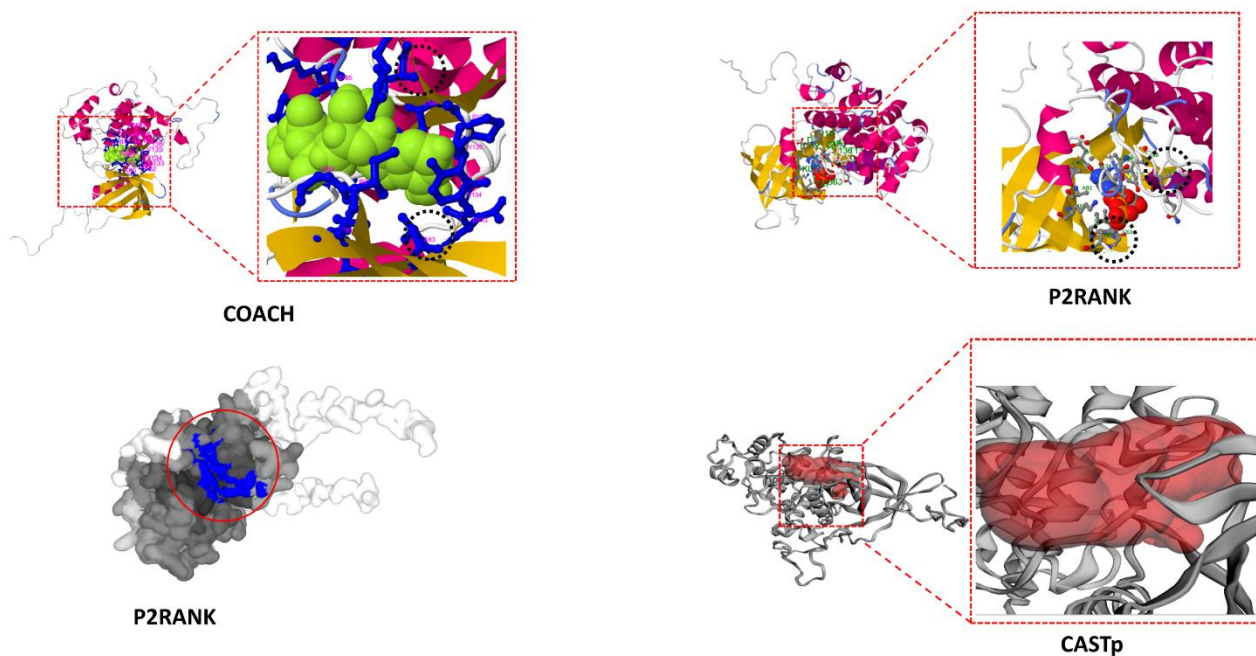
Figure 2.2: Active /Binding Site Pockets predicted by different Servers

2.3.8 Modelling of GSKβ protein and Mutants

The three-dimensional (3D) structures of the native and three selected point mutant proteins were predicted and modelled using I-TASSER. In generating the mutant models, all FASTA sequences were submitted to the I-TASSER, where each nsSNP was substituted into the native sequence. The native and mutant GSK-3B proteins were modelled using I-TASSER, utilizing the top 10 protein models available as templates in PDB that most closely resemble the target protein sequence structurally. The PBD template with maximum confidence and alignment, which were taken into consideration, is 3i4b (A GSK-3β Protein). The best model was chosen based on the greatest confidence score out of the five projected models for each Protein (C-score). The C-score ranges from -5 to 2 and represents the degree of confidence in the prediction of pairwise comparison. A model with a greater C-score indicates greater confidence. Discovery Studio Visualizer was used to visualize the generated Protein. Modelling of the whole Protein (Figure 2.3a) along with the mutants (Figure 2.3b-d) was important for accessing the protein structural information and also for carrying out molecular dynamic simulation. The majority of the GSK-3β protein present in the Protein Data Bank lacked N and C-terminal regions or had missing amino acid residues in between. These limitations can indeed affect the accuracy of molecular simulations and our understanding of protein function. The N- and C-terminal regions of a protein are frequently essential for upholding its structural stability and can exert a significant influence on protein-protein interactions [75]. Consequently, we endeavored to generate a comprehensive protein model using existing crystal structure of GSK-3β from the Protein Data Bank (PDB ID: 3i4b) as a templete. To validate our model, we aligned it with the crystal structure. Remarkably, the root mean square deviation (RMSD) value between the two structures was remarkably low at 0.59 Å (as depicted in Figure 2.3e). Additionally, we conducted a sequence alignment to identify any gaps or missing residues, as illustrated in Figure 2.3f.
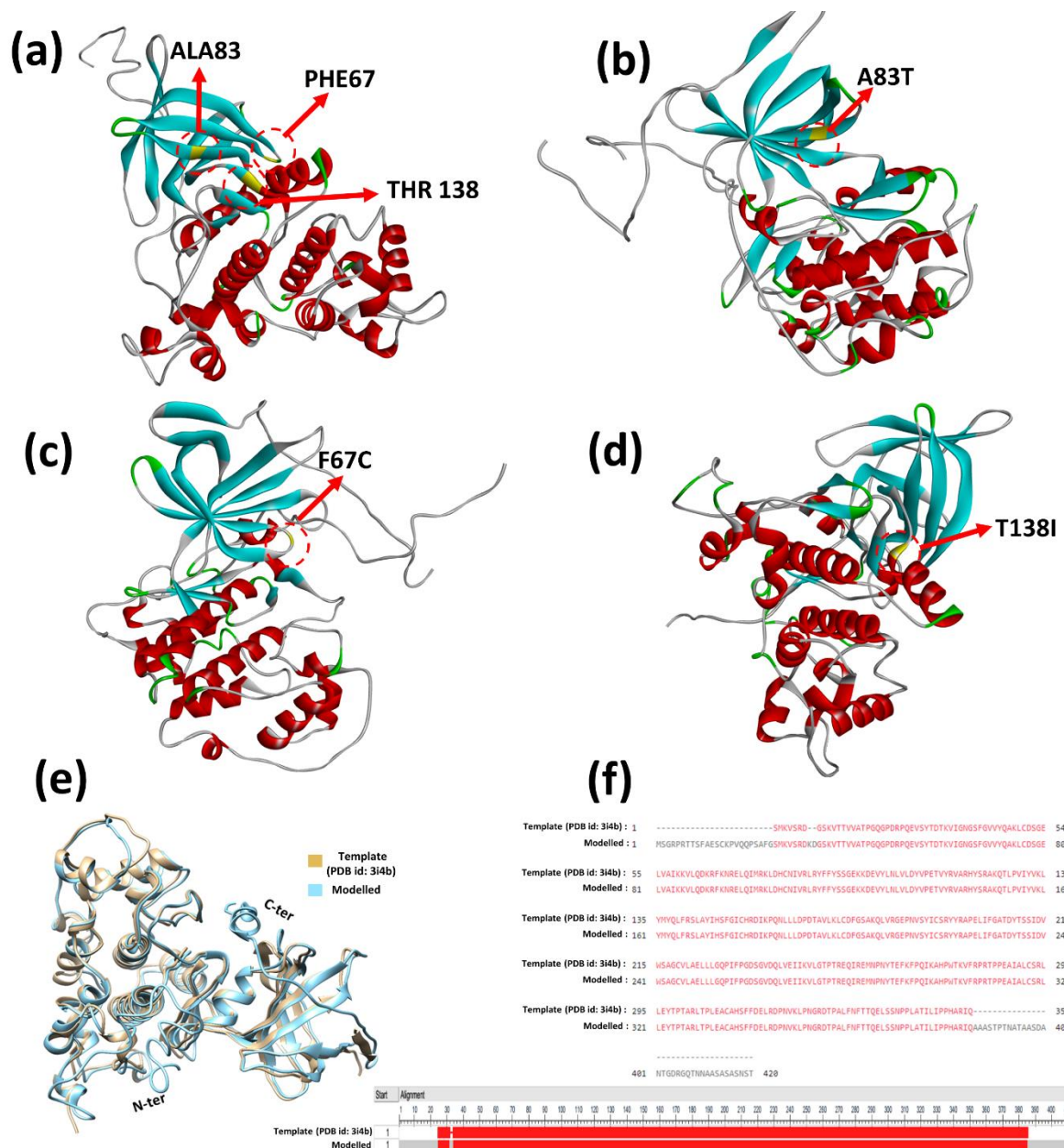
Figure 2.3: Refined model of the Native (a) and Mutated Protein A83T(b), F67C(c), T138I(d), Superimposing of GSK3β (PBD ID: 3i4b) protein crystal structure and modelled GSK3β protein (e), Amino acid sequence alignment between GSK3β (PBD ID: 3i4b) protein crystal structure and modelled GSK3β protein.

2.3.9 Energy minimization and validation of the modelled native and mutant protein

All the modelled proteins were refined using the ModRefiner tool. The main aim of the refinement is to improve the physical quality of protein structure very significantly. The refined models all had a TM-Score of more than 0.9, pointing to the fact that the initial and final models were in the same fold (Figure 2.3). The modelled structures of the Protein and the mutated versions were further validated using the Ramachandran Plot Server to check the reliability of predicted protein structures. Ramachandran plots for the native and mutant GSK3B protein models showed more than 90% of the residues were located in the allowed regions, and only a few amino acids deviated. The Detailed report of the plot is given in Table 2.8 and Figure 2.4. The results from the Ramachandran Plot pointed out that all the refined protein models were highly reliable and consistent.
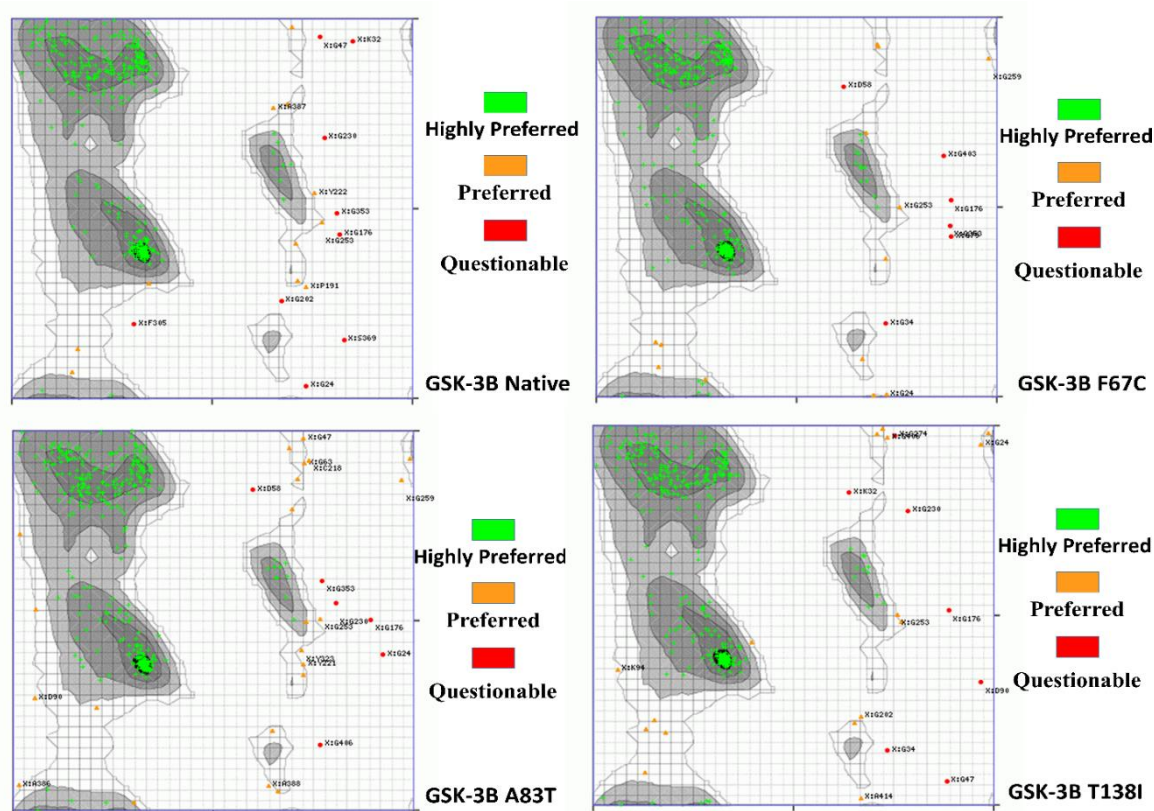
Figure2.4: Ramachandran Plot of the modelled Native and Mutated Protein

Table 2.8: Observations from the Ramachandran Plot

Protein	Amino Acids	Highly Preferred Observations	Preferred observations	Questionable observations
GSK-3B Native	420	398 (95.215%)	11 (2.632%)	9 (2.153%)
GSK-3B (F67C)	420	399 (95.455%)	13 (3.110%)	6 (1.435%)
GSK-3B (A83T)	420	390 (93.301%)	22 (5.263%)	6 (1.435%)
GSK-3B (T138I)	420	395 (94.498%)	16 (3.828%)	7 (1.675%)

2.3.10 Secondary Structure Prediction

The secondary structure of GSK-3β and the mutants were predicted by SOPMA, which explained the distributions of alpha helix, beta sheet, and coil and how mutation has changed the secondary structure of the Protein. The result indicated a large number of random coils that are (46.67 %), followed by 128 alpha helixes (43.59%), 67 extended strands (15.95 %), and 29 beta turns (6.90%) in the projected secondary structure of the Native GSK-3β protein. All the mutated structures showed certain variations from that of the native. All the Mutated Proteins showed a decrease in the number of Random coils and an increase in the number of the alpha helix. The number of beta-turns was also reduced in the mutated proteins. The detailed report is provided in Figure 2.5. It was noticed that the nsSNP A83T was in the extended strand, F67C in the random coil, and T138I in the alpha helix. Because secondary structures make up between 25 and 75 percent of the length of proteins, changes in their confirmation have an immediate impact on protein structure. The nsSNPs altered the secondary structure of the Protein and thus can result in altered stability of the Protein.

Mutations in GSK-3β's secondary structure may have many effects:

Secondary structural changes can affect protein stability. Alpha helices may boost stability, but random coils may limit structural flexibility.

GSK-3β is a signalling pathway kinase enzyme[74]. Secondary structural changes may affect the catalytic activity and substrate recognition, altering phosphorylation events and signalling. Secondary structural elements determine protein binding sites and interaction surfaces[75,76]. These components may impact the protein's interaction with other proteins, regulators, or substrates. Secondary structural modifications may affect the protein's subcellular localization and availability to substrates or regulatory factors[77].

These structural modifications to GSK-3β may alter downstream signalling pathways, impacting cell growth, proliferation, differentiation, and death. These changes may cause phenotypic differences linked with mutations, depending on the pathways impacted.
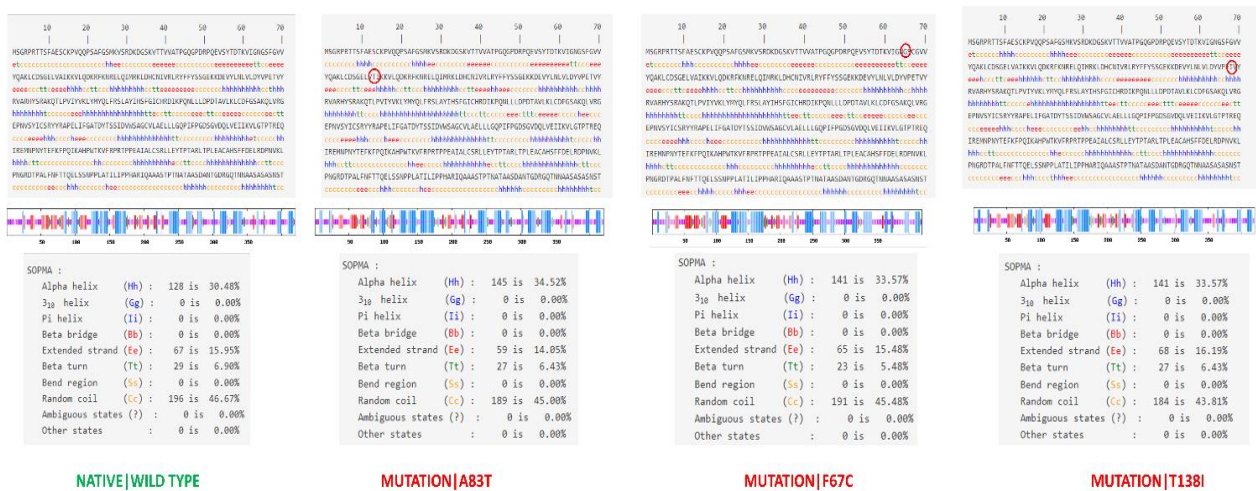
Figure 2.5: Secondary structure of the native and mutated Protein

2.3.11 Functional and structural modifications of genetic variants

The selected mutations were analysed using MutPred2 and Hope server to predict the effect of the mutation on the structure and function of the Protein. MutPred2 can forecast the removal or gain of allosteric sites, metal binding sites, DNA binding sites, and transmembrane proteins, among other structural and functional protein modifications. The HOPE server, on the other hand, detects the effect of amino acid substitution and predicts the consequence of such substitution. Detailed results of the MutPred2 and Hope servers are given in Table 2.9.

Table 2.9: Functional and structural modifications of genetic variants as predicted by MUTPRED and HOPE

Substitution	Structural Change	Properties	Predicted Significances	Predicted Features	SCORE
A83T		• The mutant residue is much bigger than its non-mutant equivalent. • When compared to the mutant residue, the wild-type residue has elevated hydrophobicity.	• The changed residue is located in close proximity to other residues in a region that plays a vital role in the binding of other molecules. It is also located in a binding-critical domain. If the mutation affects these link between two domains, the protein's function could be altered. • Hydrophobic interactions in the protein's core will be abolished due to the mutation.	• Acetylation depletion at K85 • Methylation at position K86 is lost. • Altered Metal-binding due to site distortion • Alteration in DNA binding	0.9
F67C		• Wild-type amino acids are smaller than their mutant counterparts. • The mutant residue at the position is reduced in size compared to its wild-type counterpart.	• This mutation may interfere with the binding domain's ability to send signals to the activity domain.	• Alteration in Ordered interface • Allosteric site loss at position F67 • Relative loss of solvent accessibility • Altered DNA binding • Altered Metal binding • Altered Transmembrane Protein	0.956

	• This could lead to less contact with the outside world.		• The catalytic site at F67 is lost. • Loss of Pyrrolidone carboxylic acid at Q72 • Glycosylation at position N64 is lost.
T138I	• Compared to its wild-type counterpart, the mutant residue is much larger. • Because of its proximity to the mutated region as a protein's surface protein kinase domain. UniProt classifies the mutation of this residue may affect how the protein interacts with other molecules and with its own components. The mutation alters the function of this domain by introducing a new amino acid with unusual properties. • The hydrophobicity of the wild-type and mutant residues are different.		• Altered Ordered interface • The Y-134 Allosteric Site Has Been Lost. • Modified binding with metal • Loss of Catalytic site at D133 • Loss of Sulfation at Y134 .906

Based on the results, all the amino acid mutations showed a probability score greater than 0.9. An amino acid substitution is predicted as pathogenic if a probability score is 0.50 and above. Mutation A83T showed altered DNA and metal binding. Similar alterations were predicted in F67C and T138I. The HOPE server predicted that all the mutated amino acids were of different sizes than those of the native. For mutation F67C and T138I, it predicted that the change in sequence might lead to potential loss in external interactions. Protein networks are known to be sensitive to changes in charge, mass, and hydrophobicity[78,79]. Thus, these changes can affect how proteins interact with one another. On the basis of these findings, we postulated that a number of nsSNPs would affect the Protein's function and structure, leading to an increased risk of various metabolic diseases and possibly potentially causing other disorders linked to this Protein.

2.3.12 Molecular Dynamic Simulation Analysis

Molecular dynamics and simulation (MD) studies were carried out to determine the stability and convergence of GSK-3β (Native protein) and its mutants A83T, F67C, and T138I. The root means square deviation (RMSD), the root means square fluctuation (RMSF), radius of gyration (Rg), and Solvent accessible surface area (SASA) during 250 ns were analyzed to detect the stability, flexibility, and compactness of the Native and the mutant protein during the simulation. The average RMSD values for the native and the mutant A83T, F67C, and T138I protein were 0.434 ±0.05 nm, 0.572 ±0.08, 0.436±0.02 and 0.400 ±0.03 nm respectively **(Figure 2.6a)**. The A83T mutant exhibited a much higher RMSD value of 0.572 nm whereas the mutant F67C showed fewer fluctuations having similar RMSD values with that of the Native protein. On the other hand, mutant T138I displayed a lesser RMSD of 0.4 nm as compared to the native/wild-type protein **(Figure 2.6a)**. RMSD values remained relatively constant for both native GSK-3β and F67C and T138I mutants, demonstrating that these mutants are likely to create a stable structure under physiological settings; however, the A83T mutant's persistently increased RMSD values throughout the MD simulation suggest that this mutation may render the protein structure less stable.[80]. The native protein showed some fluctuations (increase in RMSD) during the period 60-90ns thus pointing to some instability and a similar trend was also observed during 140-160ns. Mutant proteins T138I and F67C showed some initial spike in RMSD but after 100ns the protein remained overall stable. The mutant A83T showed fluctuations throughout the simulation with the maximum spike of 0.7 nm at around 70 ns, such spikes point to the presence of more than one conformation throughout the whole MD simulation which signifies A83T to be unstable during the

simulation. The larger RMSD value observed for the A83T mutant relative to the wild-type protein suggests that significant structural changes have been generated by the mutation.

The plot for root means square fluctuations (RMSF) of the wild Protein and the mutant (A83T, F67C, and T138I) structures during the simulations were analyzed to check the flexibility of the proteins **(Figure 2.6b)**. RMSF values in all the proteins were quite high in the N and C terminals. The average RMFS values for the native and the mutant A83T, F67C, and T138I protein were 0.182 ± 0.14nm, 0.188 ± 0.1nm, 0.161 ± 0.09nm, and 0.154 ± 0.09 nm respectively. It was quite evident that the residues of the wild-type protein showed various fluctuations around the residue 210 and 275-310 and thus can be confirmed to have higher flexibility than that of the mutant protein. Mutant A83T showed some high fluctuations around residues 90 and 121; Mutant F67C showed fluctuations around residues 65 to 150; Mutant T138I showed fluctuations around residues 275-290. The overall comparison showed that the average RMFS value for the wild-type protein and A83T mutant were mostly in the same range whereas the Mutant F67C and T138I showed a lowering in the average RMFS value. The overall data suggested that the mutant F67C and T138I showed a comparatively rigid structure when compared to that of the Native.

The radius of gyration (Rg) measures the compactness of the Protein. The average RMFS values for the native and the mutant A83T, F67C, and T138I protein were 2.28 ± 0.014nm, 2.26 ± 0.15nm, 2.23 ± 0.015nm, and 2.26 ± 0.016 nm respectively **(Figure 2.6c)**. Significant lowering of gyration (Rg) indicates a highly compact orientation of the Protein. A similar lower Rg value was observed for the mutant F67C as compared to the wild type. Overall, the proteins showed a compact structure throughout the simulation.

Following Rg analysis, a similar pattern was also observed in Solvent accessible surface area (SASA) in both wild-type proteins and mutant proteins. The average SASA value of the wild type and the mutant A83T, F67C, and T138I was 220.24 ± 5.04 nm^2, 216.87 ± 5.74 nm^2, 207.77 ± 7.31 nm^2, and 214.11 ± 4.31 nm^2 respectively. It is visible from **Figure 2.6d** that the SASA value lowered to the maximum for F67C as compared to other mutants and wild-type proteins. The ability to get to a solvent area is the amount of a bimolecular surface that is accessible to the molecules of a solvent. A lower SASA value in mutant structures indicates that they are smaller than their wild-type counterparts. The reason for a greater change observed

in the SASA value of the mutant and that of native GSK3B could be the effect of amino acid substitution thus altering the size of the protein surface and other characteristics[81].
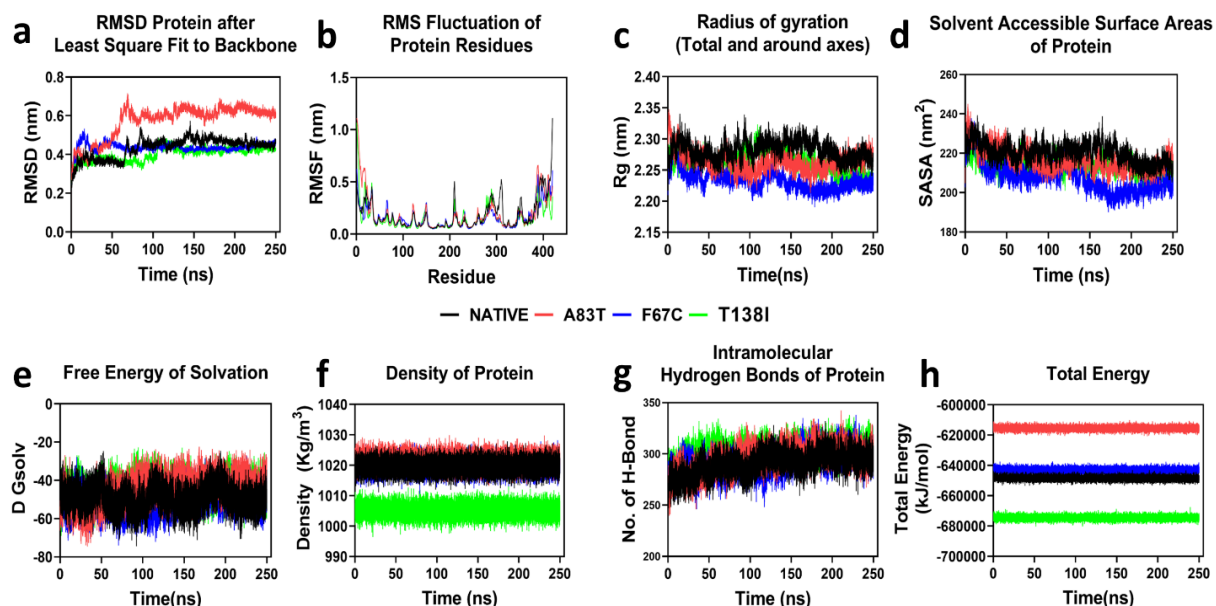
Figure 2.6: **Comparative Analysis of Structural Dynamics between Native and Mutated Proteins.** a) Root mean square deviation (RMSD), b) Root mean square fluctuation (RMSF),c) Radius of Gyration (Rg) of the Mutated and the native Protein, d) Solvent accessible surface area (SASA), e) Solvation Energy Contributions, f) Density Profiles, g) Comparison of Hydrogen Bonding Patterns, and h) Total Energy Calculations.

The solvation-free energy is an important thermodynamics parameter to estimate the impact of the solution on the Protein[82] [83]. The solvation energy of the system for all the mutant and wild-type proteins is estimated throughout the 250ns. Mutant F67C exhibited lower dG solvation energy and corroborated with wild-type protein, significantly indicating stable Protein **(Figure 2.6e)**. Mutant A83T and T138I showed slightly higher solvation energy as compared to that of the wild types indicating some instability. The total density of the system during the production run for 250 ns for A83T and F67C mutants and wild type was found to be consistent (~1020 Kg/m³) throughout the simulation process, indicating the equilibrated system **(Figure 2.6f)**. However, in the mutant T138, we observed a much lower density of around 1005Kg/m³. The average density for the native and the mutant A83T, F67C, and T138I protein were 1019.649 ±2.063, 1021.52± 2.13, 1019.80± 2.09 and 1005.206 ± 2.055 respectively.

The number of intra-molecular hydrogen bonds is depicted in **Figure 2.6g.** From the analysis, it can be noted that the native structure forms a lesser number of H-bonds with an average of ~290, while A83T, F67C & T138I mutants exhibit a greater number of H-bonds with an average of for each mutant ~295,291,302. Since the number of H-bonds was higher in the

mutant structures, protein stability will be affected. Mutations can cause rigidity in the Protein's structure, which can disrupt its normal functional behaviour. The total energy of the system is the indicator of the stability of the Protein **(Figure 2.6h)**. Mutant F67C and the native showed similar trends with an average total energy of around -648434.36 kJ/mol and -642868.69 kJ/mol respectively. Mutant A83T exhibited a higher energy level (-615481.62 kJ/mol), showing signs of instability, whereas T138I showed the least energy with an average value of -674523.60 kJ/mol thus suggesting more rigidity and stability.

The advanced analysis of the trajectories from the MD simulation was performed by essential dynamics (ED) or Principal component analysis (PCA). Through PCA, the motion of Protein was identified by extracting the concerted motion of the Protein in different frames during simulations[84]. The first two eigen vectors captured the maximum percentage of the total motions for the native and as well as for the mutant variant, hence a two-dimensional motion projection plot was constructed by contrasting the first two eigen vectors (PC1 and PC2) to observe the corrected movements of the residues of the Native and the mutated proteins. Dots that cluster together in the middle represent a protein structure with high stability, whereas dots that spread outward represent a structure with low stability. For native/wild-type proteins, the principal components PC1 and PC2 displayed scattered orientation of trajectories during the initial phase of the simulation, although during the ending phase the dots got clustered towards the centroid pointing to the stable confirmation of the protein. Mutation A83T showed similar distribution during the initial phase of the simulation although during the ending phase the clustering density got high but the movement got deviated from the centroid as compared to that of the native. In the A83T mutant, the variance needed more time to settle the global movement toward the centroid than the native protein **(**Figure 2.7b**).**

Interestingly, F67C exhibited fewer steps toward reducing covariance to achieve global motion of trajectories toward centroid than native and A83T mutants (Figure 2.7). In contrast, T138I exhibited a similar pattern of PC values with higher steps required for minimization of the covariance as compared to F67C. Mutant F67C exhibited clustering of the dots very close to the centroid during the end of the simulation pointing to a very stable confirmation of the protein. Mutant T138I showed stable confirmation although there was some deviation from the centroid than compared to the other mutants and the Native.
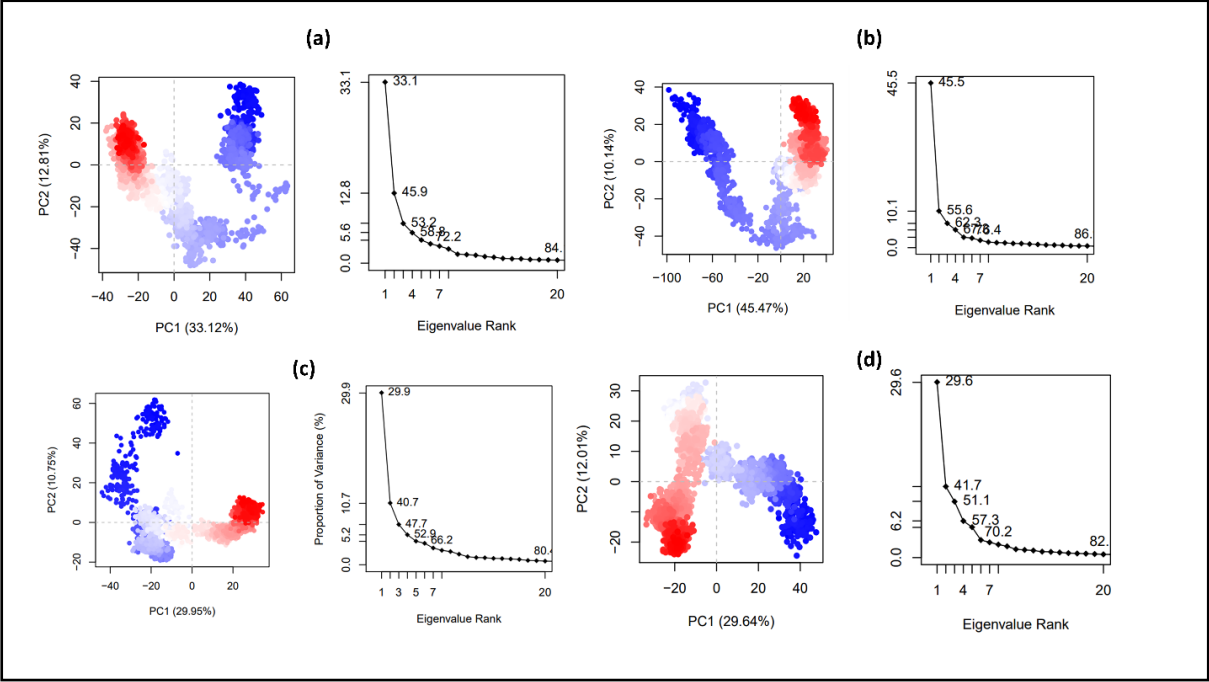
Figure 2.7: PCA Analysis (a) The projection of PC1 on PC2. The continuous colour spectrum from blue to white to red represents simulation time. The initial timescale is represented by blue, intermediate by white, and final by red. a)NATIVE ,b) Mutant A83T,c) Mutant F67C, d) Mutant T138I.

Dynamic cross correlation matrix (DCM) of the residual positions for individual mutant andnative/wild type proteins are carried out and depicted in **Figure 2.8**. The trace of the covariance matrix has been used to estimate the overall flexibility of the whole dynamic system.For native protein, the high degree of positive correlation observed among residues 50-130, 150-250 and 370-390 respectively (Figure 2.8a). Mutated Protein A83T showed high positive cross correlation in the residue region 150-300, with traces of negative cross-correlation at the N terminal of the protein. Mutant F67C showed increased anti-correlation and correlation in comparison to the native protein. It was observed that positively correlated motions are dominant in all the structures of all the dynamic systems except the T138I mutated protein (dominant white region). Mutant T138I also showed decreased correlated motions.
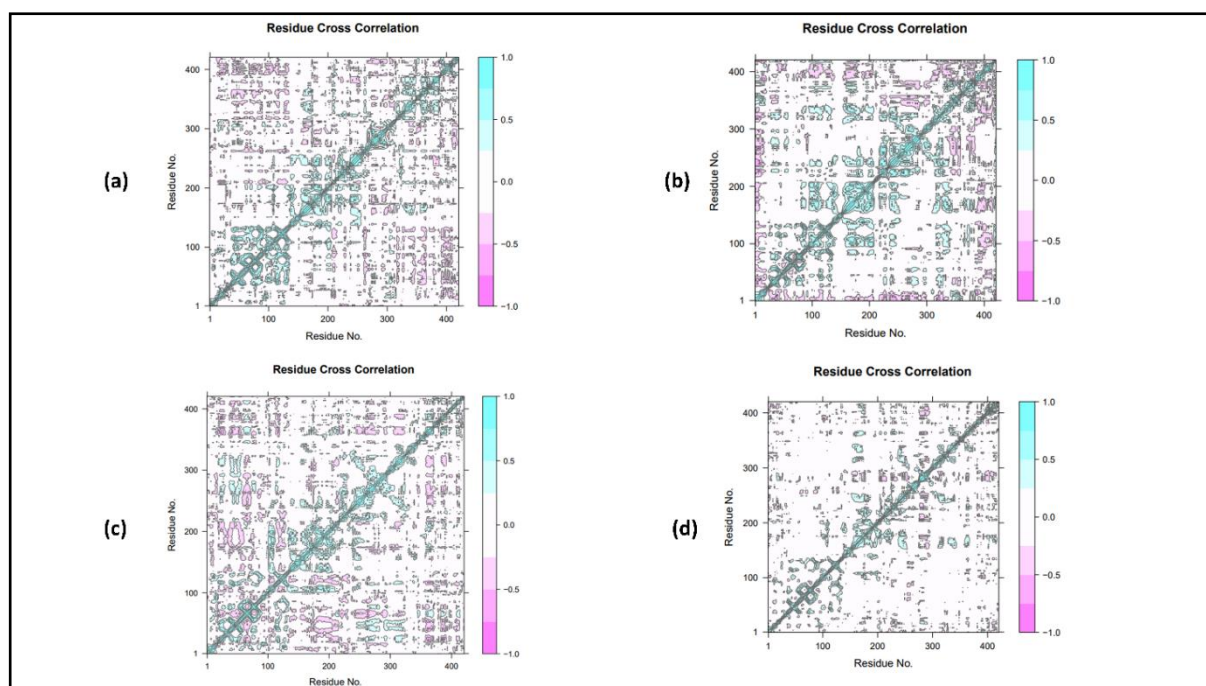
Figure 2.8 :Dynamic cross correlation matrix(DCCM) plots The positive value represents the positively correlated motions (cyan), whilenegative values represent the anti-correlated motions (pink).a)NATIVE ,b) Mutant A83T,c) Mutant F67C, d) Mutant T138I.

Secondary structure analysis during the 250 ns simulation for wild/native type and other mutants is displayed in **Figure 2.9**. In wild-type protein, the structure represented the presence of significant coil formation between 120-130 residues, β-sheets between 60-75 residues, β-bridges between 1-5 residues, and α-helices between 75-90 residues **(Figure 2.9a)**. However, mutant A83T displayed a similar arrangement except for the coil near 250 ns time turned into α-helix **(Figure 2.9b)**. The residue at around ~290 showed a significant change from bend to turn, also residue 260-265 showed a change from turn to the alpha helix. F67C displayed significant numbers of turns, and 5-helix formed between 50-75 residues **(Figure 2.9c)**. Turns were seen in significant numbers in the F67C mutant, indicating that the mutation may affect the local structural flexibility. Residues 50–75 came together to create a 5-helix. This implies that the wild-type protein does not include the particular helical structure that the F67C mutation may have caused to arise in this area. In the mutant protein T138I number of coils was reduced, and residue at 290-300 showed a significant change from bend to turn and the rest of the secondary structures appeared similar to the wild-type protein **(Figure 2.9d)**. This conformational change may have functional implications as it affects the local structure in that region. The information as a whole demonstrates that each mutation (A83T, F67C, and T138I)

has resulted in distinct modifications to the protein's secondary structure, which may have a substantial impact on the protein's overall stability, functionality, and relationships. The mutations appear to have changed the protein's structural dynamics, which may have functional repercussions, as evidenced by the emergence of novel secondary structures (such as the 5-helix) and modifications in coil-to-helix transitions.
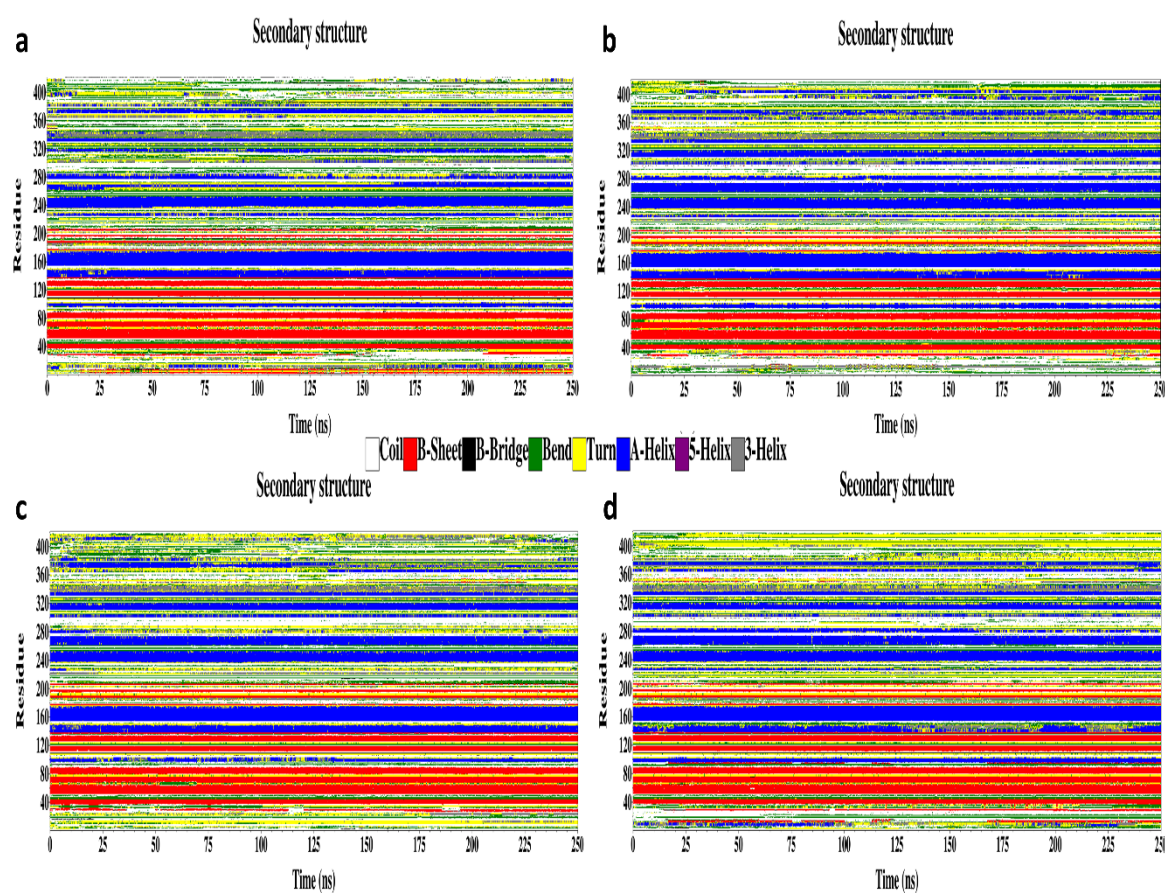
Figure 2.9: Comparative Analysis of Secondary Structure Changes in Native and Mutant Protein Variants: a) wild (native), b) A83T, c) F67C, and d) T138I.

Events of time frame for every 50 ns of MD trajectory were analyzed for Native and A83T, F67C, and T138I mutants depicted in **Figure 2.10**. An individual trajectory of each protein after 50ns is provided in **Fig 2.11** for a better understanding of the change in structure. In native Protein, the α-helix started diminishing after 50 ns and till 200 ns conformed into the loop. Later at 250 ns, the loop conformed back into α-helix. While in A83T there is no such helical loss or gain was observed like the former, but a turn and a β-sheet appeared at 100 ns and later at 150 ns disappeared which reappeared at 200 ns and again conformed into the loop at 250 ns **(Figure 2.10b)**. In A83T, the residues from 278 to 283 have shown significant change in

structure when compared to that of the native the loops and turns in the native have turned to the alpha helix in the mutated protein. The alpha-helix in the native turned into loops in the mutated variant (A83T) at the end of 250ns. In the F67C mutant, changes were observed during the formation of parallel β-sheets connected via a loop which were absent at the beginning of the simulation and 50 ns. But later, from 100 ns to 250 ns, the conformation is stable (Figure 8C). A significant change was observed in the residues from 260-265 where the loop in the native has turned into alpha-helix at the end of the simulation. In T138I, significant alteration similar to F67C and A83T was noticed including alterations at residue 260-264 from loop to alpha helix, and a similar trend was also noticed at residue 275-283.

The development of β-sheets, twists, and α-helices at various times during the simulations suggests that the GSK-3B protein mutations have significantly altered the secondary structure. The protein's stability, functionality, and interactions with other molecules may all be impacted by these structural alterations. This is only a brief overview of the findings; a more thorough examination would involve looking at the three-dimensional structure of the particular protein and its interactions with ligands, substrates, or other proteins.

These findings were further supported by molecular dynamics simulations, which simulate the protein's evolution. The structural modifications and their effects on the actual biological system would require experimental validation.
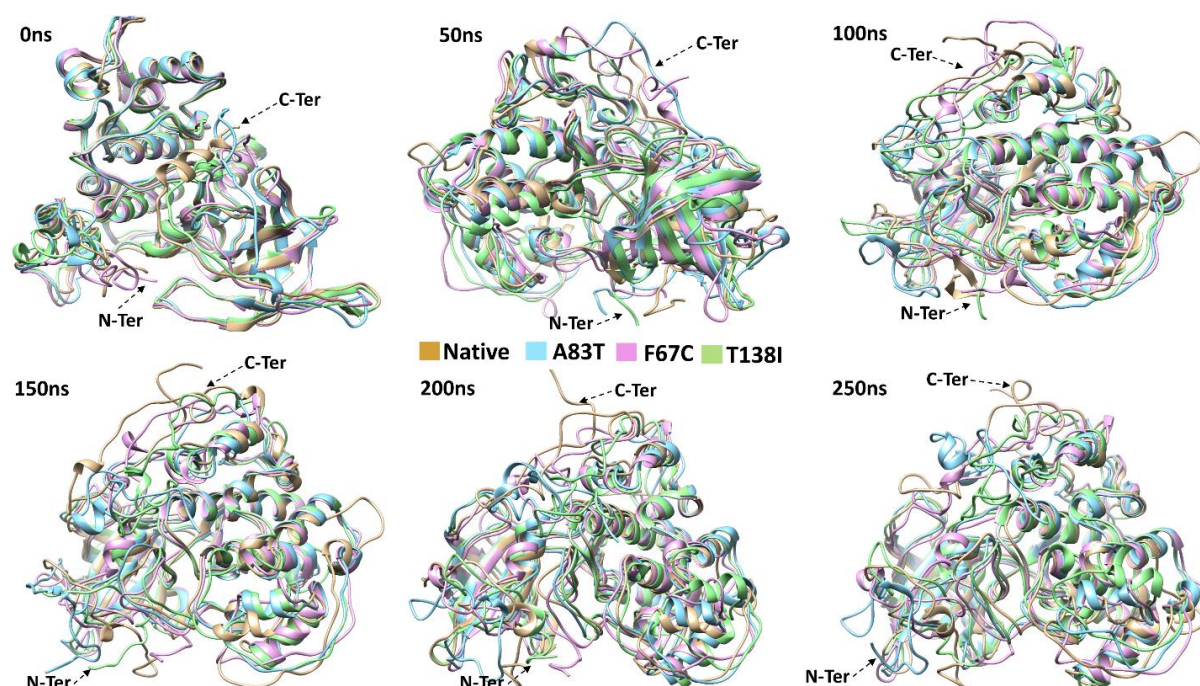
Figure 2.10: Analysis of Molecular Dynamics Trajectories at Different Time Intervals (50ns) for Native and Mutant Protein Structures.
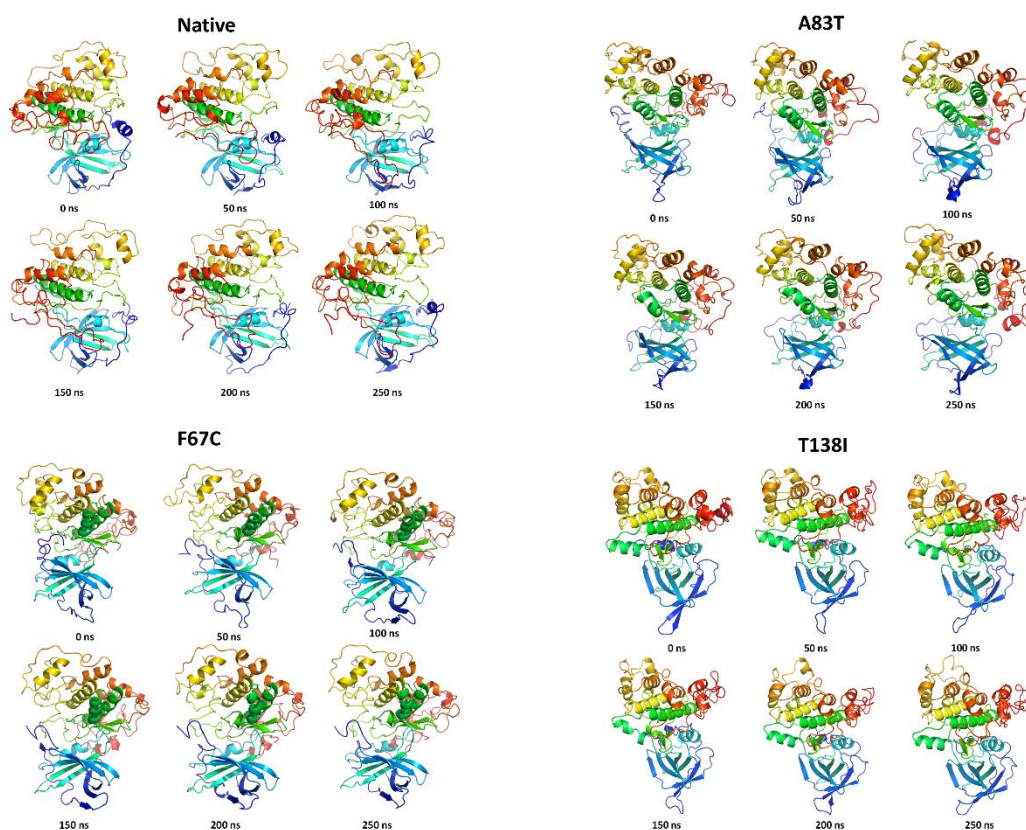
Fig 2.11: Analysis of Molecular Dynamics Trajectories at Different Time Intervals (50ns) for Native and Mutant Protein Structures represented individually.

The possible effect of the deleterious mutation in the Wnt/β-catenin pathway regulating the wound healing process

The study majorly points to the three major deleterious mutations out of several others which can be a potential threat. These three mutations are in the amino acids present in the active binding site of the protein. On the other hand, the mutations also have a significant impact on the overall structure of the protein which in turn can affect its interaction with other proteins in various metabolic reactions. One of the major findings of this study is the regulatory role of GSK-3β in wound healing. GSK-3β is an important protein in the Wnt/β-catenin pathway which controls various signaling pathways. Downregulation of β-catenin is facilitated by the serine/threonine kinase GSK-3β, which binds to and phosphorylates many proteins in the Wnt pathway. Since GSK-3β inhibits Wnt signalling, it may serve as a tumour suppressor as well[85]. In the absence of Wnt ligands β-catenin is phosphorylated by GSK-3β as it is retained in the degradation complex by APC; phosphorylated-catenin is a target of the E3 ubiquitin

ligase-Trcp. The ubiquitin proteasome-mediated pathway leads to the degradation of ubiquitinated β-catenin once Trcp has transferred the ubiquitin chain to β-catenin [86,87]. A schematic representation pointed out in **Figure 2.12** gives a better understanding of the role of GSK-3β in wound healing mechanisms. Wnt ligand is shown here binding to the Frizzled (FZD) receptor and LRP5/6 co-receptor on the cell surface after being produced in response to a wound. It does so by phosphorylating GSK-3β on serine 9, which in turn activates Disheveled (Dvl) and blocks the enzyme's action. As a result, beta-catenin accumulates in the cytoplasm and then moves into the nucleus, where it joins other transcription factors to regulate gene expression[88]. Genes involved in cell division, migration, and fate determination are among those whose transcription is stimulated by this complex [87]. Collaboratively, these processes facilitate the healing of damaged tissues and wounds. Aberrant accumulation of β-catenin in the nucleus and the constitutive activation of the β-catenin/TCF/LEF complex can contribute to tumour development and progression by activating genes that promote cell proliferation, survival, and invasion while suppressing genes that regulate apoptosis and cell differentiation.
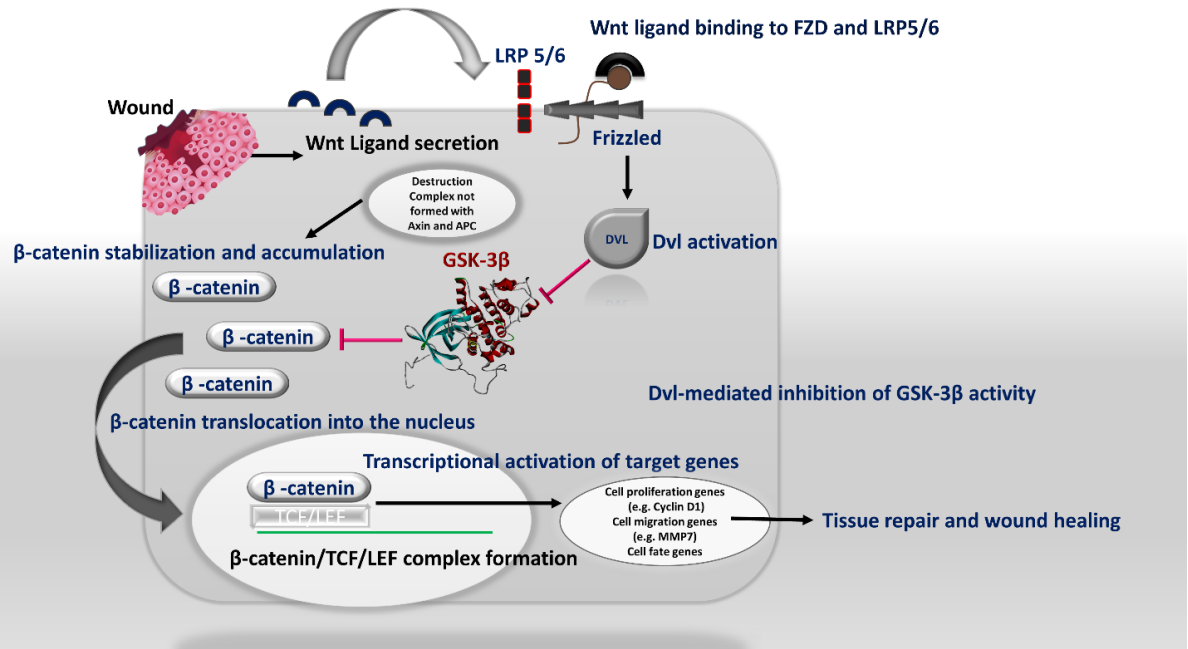
Figure 2.11: WNT signaling pathways in wound healing and role of GSK-3β in perspective wound healing.

GSK-3β helps in the phosphorylation of Axin. Phosphorylation enhances the stability and binding of Axin to β-catenin [89]. The Wnt ligand binds with its receptor and overpowers the phosphorylation of β-catenin. Phosphorylation results in the formation of the β-catenin-T-cell factor (TCF) complex which instigates the transcription of genes and might highly hinder the wound healing pathways. Two of the SNPs i.e. F67C and T138I showed stability in the GSK-

3β structure more than that of the native one, this stability in the structure might facilitate the stronger binding with Axin and in turn, can hinder the activity of the ligands. The axin and the GSK-3β majorly interact by a helical ridge composed of hydrophobic axin residues. Val263, Leu266, Val267, and Ile270 of GSK-3β create a helical groove, into which Phe388, Leu392, Leu396, and Val399 fit on the other side of the channel, Tyr288, Phe291, Phe293, Pro294, and Ile296 from the expanded GSK3 loop pack against Pro385, Ala389, Ile393, and Leu396 of axin [90]. Secondary structure analysis after 250ns simulation showed significant change in the GSK-3β residue region between 260-290. This region shows several changes in secondary structure and thus can alter axin binding. GSK-3β mutation in wound healing can vary depending on the context and the stage of wound healing. Inhibition of GSK-3β may be beneficial during the early stages of wound healing to promote cell migration and proliferation[91], while activation of GSK-3β may be beneficial during the later stages of wound healing to promote granulation tissue formation. The mutations have a high probability of altering the structure and hence the function of this highly important protein and thus further biological studies are needed to carry out to come to a proper conclusion. Although an initial indication through this work could be highly fruitful in the scientific community.

GSK3 β activation stimulates the generation of pro-inflammatory cytokines such IL-6, IL-1β, and IFNγ. Conversely, inhibiting GSK3β reduces the production of pro-inflammatory mediators and enhances IL-10 synthesis by immune cells[92]Gsk3β inhibition can also decrease the nuclear activity of the Nfkb1 pathway[93]. Destabilized or hyperactive GSK-3β can enhance NF-κB activity, increasing the transcription of pro-inflammatory genes. Active GSK-3β drives inflammation, as demonstrated in various animal models of inflammatory diseases[94,95]. GSK-3β inhibition reduces inflammation and tissue damage, evidenced by decreased cytokine production, immune cell infiltration, and inflammatory markers. Treatment with GSK-3β inhibitors, such as TDZD-8, LiCl, and SB216763, consistently mitigates inflammatory responses and promotes tissue healing[95]. GSK3 β has also been shown to play an important role in angiogenesis through its control of vascular cell migration and differentiation. GSK-3β is an important protein in the Wnt/β-catenin pathway which controls various signaling pathways. Downregulation of β-catenin is facilitated by the serine/threonine kinase GSK-3β, which binds to and phosphorylates many proteins in the Wnt pathway. Since GSK-3β inhibits Wnt signalling and inhibits beta-catenin from entering cytoplasm by degrading it. During the downregulation and deactivation of GSK-3β, the beta-catenin enters

the cytoplasm and then moves to the nucleus where it is stabilized by the fibroblast growth factor-2 and by the E4 region of adenovirus that promotes an angiogenic response[96].

Thus it is quite evident that GSK3 β has a negative impact on wounds by modulating the inflammatory responses. From the above study, it is prominent that deleterious mutations in GSK3B change the structure of the binding/active site of GSK3 β which in turn has a high possibility that inhibitors will not be able to inhibit GSK3 β. The activated or dysregulated GSK3 β can cause an increase in pro-inflammatory cytokines and can also demote angiogenic response during a wound. Thus we aim to create therapeutics agents which would control the inflammatory cytokines after the onset of the wound and also promote angiogenesis and neovascularization thus nullifying the effect of dysregulated GSK-3 β.

2.4 Inference

At the end of this study, we systematically evaluated the spectrum of single nucleotide polymorphisms (SNPs) located within the GSK-3β protein by employing a comprehensive amalgamation of distinct bioinformatics techniques accessed via numerous platforms. Twelve highly harmful non-synonymous single nucleotide polymorphisms (nsSNPs) were identified by this integrative strategy: rs201448262(T235P), rs201450363(I182T), rs747385360(P225L), rs748461608(T138I), rs750723548(H337R), rs758696011(Y161C) (F67C). These particular SNPs were identified as potential risk factors due to their clear effect on native protein structure and function. Among this subset, the A83T, F67C, and T138I mutations have been identified in the GSK-3β receptor's essential ligand binding domain. This strategic placement suggests the possibility of disrupting interactions with transcriptional co-activators and other ligands, with implications for many biological processes. We found that these mutations led to changes in the secondary structure of the protein as well as its overall instability. These mutation hotspots are crucial because they have both evolutionary conservation and functional importance. The dramatically different dimensions of the substituted amino acids highlight the profound functional impact they have on the entire protein structure. They may also be carcinogenic, as shown by predictive analysis.

The molecular dynamics simulations revealed that the A83T mutant exhibited structural instability with consistently higher RMSD values, while mutants F67C and T138I remained structurally stable, with F67C showing the most compact structure thus pointing to structural rigidity. Additionally, mutants A83T, F67C, and T138I displayed variations in flexibility, solvent accessibility, solvation energy, and total energy, suggesting distinct structural and

stability profiles compared to the native GSK-3β protein. Changes in the secondary protein structure were also shown by the simulations, opening the door to the possibility of altered interactions with partner molecules. Given GSK-3β's extensive involvement in cellular and metabolic networks, these results have important ramifications. Future efforts are needed to verify the clinical importance of these SNPs by experimental investigations, particularly with regard to those predicted to influence protein structure. This study expands our understanding of the complex molecular mechanisms that contribute to disease vulnerability and cellular malfunction. Finding harmful missense SNPs that may affect protein stability or binding site interactions opens the door to exploring new diagnostic and therapeutic approaches that specifically target these variants. Given the importance of GSK-3β across a variety of systems, our research has the potential to illuminate the practical ramifications of the SNPs found in this key enzyme. Our major objective from the findings is to develop therapeutics and formulations which would have a direct effect on inflammation and angiogenesis and thus curing wounds and simultaneously nullifying the effect of dysregulated GSK-3β.

GSK3 β has a negative impact on wounds by modulating the inflammatory responses. From the above study, it is prominent that deleterious mutations in GSK3B change the structure of the binding/active site of GSK3 β which in turn has a high possibility that inhibitors will not be able to inhibit GSK3 β. The activated or dysregulated GSK3 β can cause an increase in pro-inflammatory cytokines and can also demote angiogenic response during a wound. Thus we aim to create therapeutics agents which would control the inflammatory cytokines after the onset of the wound and also promote angiogenesis and neovascularization thus nullifying the effect of dysregulated GSK-3β.

References:

[1]   J.F. Abril, S. Castellano, Genome annotation, CRC Press, 2018. https://doi.org/10.1016/B978-0-12-809633-8.20226-4.

[2]   D.E. Reich, S.B. Gabriel, D. Altshuler, Quality and completeness of SNP databases, Nat Genet 33 (2003) 457–458.

[3]   J.C. Stephens, J.A. Schneider, D.A. Tanguay, J. Choi, T. Acharya, S.E. Stanley, R. Jiang, C.J. Messer, A. Chew, J.-H. Han, others, Haplotype variation and linkage disequilibrium in 313 human genes, Science (1979) 293 (2001) 489–493.

[4]   R.T. Brumfield, P. Beerli, D.A. Nickerson, S. V. Edwards, The utility of single nucleotide polymorphisms in inferences of population history, Trends Ecol Evol 18 (2003) 249–256. https://doi.org/10.1016/S0169-5347(03)00018-1.

[5]   P.M. Visscher, M.A. Brown, M.I. McCarthy, J. Yang, Five years of GWAS discovery, Am J Hum Genet 90 (2012) 7–24. https://doi.org/10.1016/j.ajhg.2011.11.029.

[6]   M. Naveed, S. Tehreem, S. Mubeen, F. Nadeem, F. Zafar, M. Irshad, In-silico analysis of non-synonymous-SNPs of STEAP2: To provoke the progression of prostate cancer, Open Life Sci 11 (2016) 402–416. https://doi.org/10.1515/biol-2016-0054.

[7]   K.K. Jacob, G. Radhika, T. V. Aravindakshan, An in silico evaluation of non-synonymous single nucleotide polymorphisms of mastitis resistance genes in cattle, Anim Biotechnol 31 (2020) 25–31. https://doi.org/10.1080/10495398.2018.1524770.

[8]   P.C. Ng, S. Levy, J. Huang, T.B. Stockwell, B.P. Walenz, K. Li, N. Axelrod, D.A. Busam, R.L. Strausberg, J.C. Venter, Genetic variation in an individual human exome, PLoS Genet 4 (2008) e1000160.

[9]   Á. Végvári, Mutant proteogenomics, Proteogenomics (2016) 77–91.

[10]   G. Sunil Krishnan, A. Joshi, V. Kaushik, Bioinformatics in personalized medicine, Adv Bioinformatics (2021) 303–315.

[11]   N.R. Ramayanam, R. Manickam, V.T. Mahalingam, K.W. Goh, C. Ardianto, P. Ganesan, L.C. Ming, R.M. Ganesan, Functional and Structural Impact of Deleterious Missense Single Nucleotide Polymorphisms in the NR3C1, CYP3A5, and TNF-$α$ Genes: An In Silico Analysis, Biomolecules 12 (2022) 1307.

[12]   L.T. Rozario, T. Sharker, T.A. Nila, In silico analysis of deleterious SNPs of human MTUS1 gene and their impacts on subsequent protein structure and function, PLoS One 16 (2021) e0252932.

[13]   D.B. RYLATT, A. AITKEN, T. BILHAM, G.D. CONDON, N. EMBI, P. COHEN, Glycogen Synthase from Rabbit Skeletal Muscle: Amino Acid Sequence at the Sites Phosphorylated by Glycogen Synthase Kinase-3, and Extension of the N-Terminal Sequence Containing the Site Phosphorylated by Phosphorylase Kinase, Eur J Biochem 107 (1980) 529–537. https://doi.org/10.1111/j.1432-1033.1980.tb06060.x.

[14]   N. EMBI, D.B. RYLATT, P. COHEN, Glycogen Synthase Kinase-3 from Rabbit Skeletal Muscle: Separation from Cyclic-AMP-Dependent Protein Kinase and Phosphorylase Kinase, Eur J Biochem 107 (1980) 519–527. https://doi.org/10.1111/j.1432-1033.1980.tb06059.x.

[15]   R. Mancinelli, G. Carpino, S. Petrungaro, C.L. Mammola, L. Tomaipitinca, A. Filippini, A. Facchiano, E. Ziparo, C. Giampietri, Multifaceted roles of GSK-3 in cancer and autophagy-related diseases, Oxid Med Cell Longev 2017 (2017). https://doi.org/10.1155/2017/4629495.

[16]   J.E. Forde, T.C. Dale, Glycogen synthase kinase 3: A key regulator of cellular fate, Cellular and Molecular Life Sciences 64 (2007) 1930–1944. https://doi.org/10.1007/s00018-007-7045-7.

[17]   W.J. Ryves, A.J. Harwood, R. Dajani, L. Pearl, Glycogen synthase kinase-3 inhibition by lithium and beryllium suggests the presence of two magnesium binding sites, Biochem Biophys Res Commun 290 (2002) 967–972. https://doi.org/10.1006/bbrc.2001.6305.

[18]   J.R. Woodgett, Molecular cloning and expression of glycogen synthase kinase-3/Factor A, EMBO Journal 9 (1990) 2431–2438. https://doi.org/10.1002/j.1460-2075.1990.tb07419.x.

[19]   D.C. Souder, R.M. Anderson, An expanding GSK3 network: implications for aging research, Geroscience 41 (2019) 369–382. https://doi.org/10.1007/s11357-019-00085-z.

[20]   A. V Ougolkov, M.E. Fernandez-Zapico, V.N. Bilim, T.C. Smyrk, S.T. Chari, D.D. Billadeau, Aberrant nuclear accumulation of glycogen synthase kinase-3beta in human pancreatic cancer: association with kinase activity and tumor dedifferentiation., Clin Cancer Res 12 (2006) 5074–5081. https://doi.org/10.1158/1078-0432.CCR-06-0196.

[21]   T. Furuta, H. Sabit, Y. Dong, K. Miyashita, M. Kinoshita, N. Uchiyama, Y. Hayashi, Y. Hayashi, T. Minamoto, M. Nakada, Biological basis and clinical study of glycogen synthase kinase- 3β-targeted therapy by drug repositioning for glioblastoma., Oncotarget 8 (2017) 22811–22824. https://doi.org/10.18632/oncotarget.15206.

[22]   V. Bilim, A. Ougolkov, K. Yuuki, S. Naito, H. Kawazoe, A. Muto, M. Oya, D. Billadeau, T. Motoyama, Y. Tomita, Glycogen synthase kinase-3: a new therapeutic target in renal cell carcinoma, Br J Cancer 101 (2009) 2005–2014.

[23]   Y. Chen, X. Liu, H. Wang, S. Liu, N. Hu, X. Li, Akt regulated phosphorylation of GSK-3β/cyclin D1, p21 and p27 contributes to cell proliferation through cell cycle progression from G1 to S/G2M phase in low-dose arsenite exposed HaCaT cells, Front Pharmacol 10 (2019) 1176. https://doi.org/10.3389/fphar.2019.01176.

[24]   S.M. Zhang, Z. Yang, F.Z. Qi, Alda-1, an Aldehyde Dehydrogenase 2 Agonist, Improves Cutaneous Wound Healing by Activating Epidermal Keratinocytes via Akt/GSK-3β/β-Catenin Pathway, Aesthetic Plast Surg 46 (2022) 126–127. https://doi.org/10.1007/s00266-021-02550-7.

[25]   M. Kapoor, S. Liu, S.W. Xu, K. Huh, M. McCann, C.P. Denton, J.R. Woodgett, D.J. Abraham, A. Leask, GSK-3β in mouse fibroblasts controls wound healing and fibrosis through an endothelin-1-dependent mechanism, Journal of Clinical Investigation 118 (2008) 3279–3290. https://doi.org/10.1172/JCI35381.

[26]   P. Mohapatra, N. Chandrasekaran, Wnt/β-catenin targeting in liver carcinoma through nanotechnology-based drug repurposing: A review, Biomedicine and Pharmacotherapy 155 (2022) 113713. https://doi.org/10.1016/j.biopha.2022.113713.

[27]   A. Aminuddin, P.Y. Ng, Promising druggable target in head and neck squamous cell carcinoma: Wnt signaling, Front Pharmacol 7 (2016) 244. https://doi.org/10.3389/fphar.2016.00244.

[28]   M. Majidinia, J. Aghazadeh, R. Jahanban-Esfahlani, B. Yousefi, The roles of Wnt/β-catenin pathway in tissue development and regenerative medicine, J Cell Physiol 233 (2018) 5598–5612. https://doi.org/10.1002/jcp.26265.

[29]   J.T.L. Mah, E.S.H. Low, E. Lee, In silico SNP analysis and bioinformatics tools: A review of the state of the art to aid drug discovery, Drug Discov Today 16 (2011) 800–809. https://doi.org/10.1016/j.drudis.2011.07.005.

[30]   Y. Choi, A.P. Chan, PROVEAN web server: A tool to predict the functional effect of amino acid substitutions and indels, Bioinformatics 31 (2015) 2745–2747. https://doi.org/10.1093/bioinformatics/btv195.

[31]   H. Tang, P.D. Thomas, PANTHER-PSEP: Predicting disease-causing genetic variants using position-specific evolutionary preservation, Bioinformatics 32 (2016) 2230–2232. https://doi.org/10.1093/bioinformatics/btw222.

[32]   I. Adzhubei, D.M. Jordan, S.R. Sunyaev, Predicting functional effect of human missense mutations using PolyPhen-2, Curr Protoc Hum Genet 76 (2013) 7–20. https://doi.org/10.1002/0471142905.hg0720s76.

[33]   M. Hecht, Y. Bromberg, B. Rost, Better prediction of functional effects for sequence variants, BMC Genomics 16 (2015) 1–12. https://doi.org/10.1186/1471-2164-16-S8-S1.

[34]   N.L. Sim, P. Kumar, J. Hu, S. Henikoff, G. Schneider, P.C. Ng, SIFT web server: Predicting effects of amino acid substitutions on proteins, Nucleic Acids Res 40 (2012) W452--W457. https://doi.org/10.1093/nar/gks539.

[35]   C.M. Yates, I. Filippis, L.A. Kelley, M.J.E. Sternberg, SuSPect: Enhanced prediction of single amino acid variant (SAV) phenotype using network features, J Mol Biol 426 (2014) 2692–2701. https://doi.org/10.1016/j.jmb.2014.04.026.

[36]   E. Capriotti, R.B. Altman, Y. Bromberg, Collective judgment predicts disease-associated single nucleotide variants., BMC Genomics 14 Suppl 3 (2013). https://doi.org/10.1186/1471-2164-14-s3-s2.

[37]   E. Capriotti, P. Fariselli, PhD-SNPg: A webserver and lightweight tool for scoring single nucleotide variants, Nucleic Acids Res 45 (2017) W247–W252. https://doi.org/10.1093/nar/gkx369.

[38]   E. Capriotti, R. Calabrese, P. Fariselli, P.L. Martelli, R.B. Altman, R. Casadio, WS-SNPs&GO: a web server for predicting the deleterious effect of human protein variants using functional annotation., BMC Genomics 14 Suppl 3 (2013) 1–7. https://doi.org/10.1186/1471-2164-14-s3-s6.

[39]   J. Bendl, J. Stourac, O. Salanda, A. Pavelka, E.D. Wieben, J. Zendulka, J. Brezovsky, J. Damborsky, PredictSNP: Robust and Accurate Consensus Classifier for Prediction of Disease-Related Mutations, PLoS Comput Biol 10 (2014) e1003440. https://doi.org/10.1371/journal.pcbi.1003440.

[40]   V. López-Ferrando, A. Gazzo, X. De La Cruz, M. Orozco, J.L. Gelpí, PMut: A web-based tool for the annotation of pathological variants on proteins, 2017 update, Nucleic Acids Res 45 (2017) W222–W228. https://doi.org/10.1093/nar/gkx313.

[41]   M.F. Rogers, H.A. Shihab, T.R. Gaunt, C. Campbell, CScape: A tool for predicting oncogenic single-point mutations in the cancer genome, Sci Rep 7 (2017) 1–10. https://doi.org/10.1038/s41598-017-11746-4.

[42]   H.A. Shihab, J. Gough, D.N. Cooper, P.D. Stenson, G.L.A. Barker, K.J. Edwards, I.N.M. Day, T.R. Gaunt, Predicting the Functional, Molecular, and Phenotypic Consequences of Amino Acid Substitutions using Hidden Markov Models, Hum Mutat 34 (2013) 57–65. https://doi.org/10.1002/humu.22225.

[43]   E. Capriotti, P. Fariselli, R. Casadio, I-Mutant2.0: Predicting stability changes upon mutation from the protein sequence or structure, Nucleic Acids Res 33 (2005) W306--W310. https://doi.org/10.1093/nar/gki375.

[44]   J. Cheng, A. Randall, P. Baldi, Prediction of protein stability changes for single-site mutations using support vector machines, Proteins: Structure, Function and Genetics 62 (2006) 1125–1132. https://doi.org/10.1002/prot.20810.

[45] G. Li, S.K. Panday, E. Alexov, Saafec-seq: A sequence-based method for predicting the effect of single point mutations on protein thermodynamic stability, Int J Mol Sci 22 (2021) 1–11. https://doi.org/10.3390/ijms22020606.

[46] P. Rawat, S. Kumar, M. Michael Gromiha, An in-silico method for identifying aggregation rate enhancer and mitigator mutations in proteins, Int J Biol Macromol 118 (2018) 1157–1167. https://doi.org/10.1016/j.ijbiomac.2018.06.102.

[47] H. Ashkenazy, S. Abadi, E. Martz, O. Chay, I. Mayrose, T. Pupko, N. Ben-Tal, ConSurf 2016: an improved methodology to estimate and visualize evolutionary conservation in macromolecules., Nucleic Acids Res 44 (2016) W344-50. https://doi.org/10.1093/nar/gkw408.

[48] J. Yang, A. Roy, Y. Zhang, Protein-ligand binding site recognition using complementary binding-specific substructure comparison and sequence profile alignment, Bioinformatics 29 (2013) 2588–2595. https://doi.org/10.1093/bioinformatics/btt447.

[49] M. Källberg, H. Wang, S. Wang, J. Peng, Z. Wang, H. Lu, J. Xu, Template-based protein structure modeling using the RaptorX web server, Nat Protoc 7 (2012) 1511–1522. https://doi.org/10.1038/nprot.2012.085.

[50] J. Dundas, Z. Ouyang, J. Tseng, A. Binkowski, Y. Turpaz, J. Liang, CASTp: Computed atlas of surface topography of proteins with structural and topographical mapping of functionally annotated residues, Nucleic Acids Res 34 (2006) W116--W118. https://doi.org/10.1093/nar/gkl282.

[51] R. Krivák, D. Hoksza, P2Rank: machine learning based tool for rapid and accurate prediction of ligand binding sites from protein structure, J Cheminform 10 (2018) 1–12. https://doi.org/10.1186/s13321-018-0285-8.

[52] Y. Zhang, I-TASSER server for protein 3D structure prediction, BMC Bioinformatics 9 (2008) 1–8. https://doi.org/10.1186/1471-2105-9-40.

[53] D. Xu, Y. Zhang, Improving the physical realism and structural accuracy of protein models by a two-step atomic-level energy minimization, Biophys J 101 (2011) 2525–2534. https://doi.org/10.1016/j.bpj.2011.10.024.

[54] R.J. Anderson, Z. Weng, R.K. Campbell, X. Jiang, Main-chain conformational tendencies of amino acids, Proteins: Structure, Function and Genetics 60 (2005) 679–689. https://doi.org/10.1002/prot.20530.

[55] C. Geourjon, G. Deléage, Sopma: Significant improvements in protein secondary structure prediction by consensus prediction from multiple alignments, Bioinformatics 11 (1995) 681–684. https://doi.org/10.1093/bioinformatics/11.6.681.

[56] V. Pejaver, J. Urresti, J. Lugo-Martinez, K.A. Pagel, G.N. Lin, H.-J. Nam, M. Mort, D.N. Cooper, J. Sebat, L.M. Iakoucheva, others, Inferring the molecular and phenotypic impact of amino acid variants with MutPred2, Nat Commun 11 (2020) 1–13.

[57] H. Venselaar, T.A.H. Te Beek, R.K.P. Kuipers, M.L. Hekkelman, G. Vriend, Protein structure analysis of mutations causing inheritable diseases. An e-Science approach with life scientist friendly interfaces, BMC Bioinformatics 11 (2010) 1–10.

[58] Y. Ouyang, L. Zhao, Z. Zhang, Characterization of the structural ensembles of p53 TAD2 by molecular dynamics simulations with different force fields, Physical Chemistry Chemical Physics 20 (2018) 8676–8684.

[59] P. Banik, R. Majumder, A. Mandal, S. Dey, M. Mandal, A computational study to assess the polymorphic landscape of matrix metalloproteinase 3 promoter and its effects on transcriptional activity, Comput Biol Med 145 (2022) 105404.

[60] R. Majumder, C.K. Das, I. Banerjee, B.C. Jena, A. Mandal, P. Das, A.K. Pradhan, S. Das, P. Basak, S.K. Das, others, Screening of the Prime bioactive compounds from Aloe vera as potential anti-proliferative agents targeting DNA, Comput Biol Med 141 (2022) 105052.

[61] S.M. Singh, N. Kongari, J. Cabello-Villegas, K.M.G. Mallela, Missense mutations in dystrophin that trigger muscular dystrophy decrease protein stability and lead to cross-β aggregates, Proc Natl Acad Sci U S A 107 (2010) 15069–15074. https://doi.org/10.1073/pnas.1008818107.

[62] M. Arshad, A. Bhatti, P. John, Identification and in silico analysis of functional SNPs of human TAGAP protein: A comprehensive study, PLoS One 13 (2018) e0188143. https://doi.org/10.1371/journal.pone.0188143.

[63] E. Martz, Introduction to protein science-architecture, function, and genomics: Lesk, Arthur M., Oxford university press, 2006. https://doi.org/10.1002/bmb.2005.494033022442.

[64] P. Yue, Z. Li, J. Moult, Loss of protein structure stability as a major causative factor in monogenic disease, J Mol Biol 353 (2005) 459–473. https://doi.org/10.1016/j.jmb.2005.08.020.

[65] V. Ramensky, P. Bork, S. Sunyaev, Human non-synonymous SNPs: Server and survey, Nucleic Acids Res 30 (2002) 3894–3900. https://doi.org/10.1093/nar/gkf493.

[66] W.R. Rudnicki, T. Mroczek, P. Cudek, Amino acid properties conserved in molecular evolution, PLoS One 9 (2014) e98983. https://doi.org/10.1371/journal.pone.0098983.

[67] A. Droit, G.G. Poirier, J.M. Hunter, Experimental and bioinformatic approaches for interrogating protein-protein interactions to determine protein function, J Mol Endocrinol 34 (2005) 263–280. https://doi.org/10.1677/jme.1.01693.

[68] M.P. Miller, S. Kumar, Understanding human disease mutations through the use of interspecific genetic variation, Hum Mol Genet 10 (2001) 2319–2328. https://doi.org/10.1093/hmg/10.21.2319.

[69] M. Kokkinidis, N.M. Glykos, V.E. Fadouloglou, C. Christo, K.C. Tatyana, Chapter 7—Protein Flexibility and Enzymatic Catalysis, Advances in Protein Chemistry and Structural Biology; Christov, C., Karabencheva-Christova, T., Eds (n.d.) 181–2018.

[70] M. Zhang, S. Zhou, N.H. Obaid, U.S. Altimari, M.A. Mohammed, A.K.O. Aldulaim, E.S. Abood, H. Kotb, A. Enayati, V. Khori, others, Chromenone-based GSK-3$β$ inhibitors as potential therapeutic targets for cardiovascular diseases: In silico study, molecular dynamics, and ADMET profiles, Arabian Journal of Chemistry 15 (2022) 104288.

[71] Y. Lee, S.-B. Yoon, H. Hong, H.Y. Kim, D. Jung, B.-S. Moon, W.-K. Park, S. Lee, H. Kwon, J. Park, others, Discovery of GSK3$β$ Inhibitors through In Silico Prediction-and-Experiment Cycling Strategy, and Biological Evaluation, Molecules 27 (2022) 3825.

[72]   K.K. Ojo, J.R. Gillespie, A.J. Riechers, A.J. Napuli, C.L.M.J. Verlinde, F.S. Buckner, M.H. Gelb, M.M. Domostoj, S.J. Wells, A. Scheer, others, Glycogen synthase kinase 3 is a potential drug target for African trypanosomiasis therapy, Antimicrob Agents Chemother 52 (2008) 3710–3717.

[73]   K.K. Ojo, T.L. Arakaki, A.J. Napuli, K.K. Inampudi, K.R. Keyloun, L. Zhang, W.G.J. Hol, C.L.M.J. Verlinde, E.A. Merritt, W.C. Van Voorhis, Structure determination of glycogen synthase kinase-3 from Leishmania major and comparative inhibitor structure--activity relationships with Trypanosoma brucei GSK-3, Mol Biochem Parasitol 176 (2011) 98–108.

[74]   M. Maydan, P.C. McDonald, J. Sanghera, J. Yan, C. Rallis, S. Pinchin, G.E. Hannigan, L.J. Foster, D. Ish-Horowicz, M.P. Walsh, others, Integrin-linked kinase is a functional Mn2+-dependent protein kinase that regulates glycogen synthase kinase-3$β$ (GSK-3$β$) phosphorylation, PLoS One 5 (2010) e12356.

[75]   A. Via, F. Ferre, B. Brannetti, M. Helmer-Citterich*, Protein surface similarities: a survey of methods to describe and compare protein surfaces, Cell Mol Life Sci 57 (2000) 1970–1977.

[76]   D. Talavera, D.L. Robertson, S.C. Lovell, Characterization of protein-protein interaction interfaces from a single species., PLoS One 6 (2011) e21053. https://doi.org/10.1371/journal.pone.0021053.

[77]   N. Blom, S. Gammeltoft, S. Brunak, Sequence and structure-based prediction of eukaryotic protein phosphorylation sites, J Mol Biol 294 (1999) 1351–1362.

[78]   Y. Xu, H. Wang, R. Nussinov, B. Ma, Protein charge and mass contribute to the spatio-temporal dynamics of protein--protein interactions in a minimal proteome, Proteomics 13 (2013) 1339–1351.

[79]   O. Peleg, J.-M. Choi, E.I. Shakhnovich, Evolution of specificity in protein-protein interactions, Biophys J 107 (2014) 1686–1696.

[80]   M.A. Castrosanto, A.T. Abrera, M.N. Manalo, A. Ghosh, In silico evaluation of binding of phytochemicals from bayati (Anamirta cocculus Linn) to the glutathione-s-transferase of Asian Corn Borer (Ostrinia furnacalis Guenée), J Biomol Struct Dyn (n.d.) 1–7.

[81]   M. Islam, A.M. Khan, M. Parves, M.N. Hossain, M.A. Halim, others, Prediction of deleterious non-synonymous SNPs of human STK11 gene by combining algorithms, molecular docking, and molecular dynamics simulation, Sci Rep 9 (2019) 1–16.

[82]   T. Imai, A. Kovalenko, F. Hirata, Solvation thermodynamics of protein studied by the 3D-RISM theory, Chem Phys Lett 395 (2004) 1–6.

[83]   P.F.B. Gonçalves, H. Stassen, New approach to free energy of solvation applying continuum models to molecular dynamics simulation, J Comput Chem 23 (2002) 706–714. https://doi.org/https://doi.org/10.1002/jcc.10076.

[84]   R. Majumder, M. Mandal, Screening of plant-based natural compounds as a potential COVID-19 main protease inhibitor: an in silico docking and molecular dynamics simulation approach, J Biomol Struct Dyn 40 (2022) 696–711.

[85]   P. Polakis, Wnt signaling and cancer., Genes Dev 14 (2000) 1837–1851.

[86]   J. Mao, J. Wang, B. Liu, W. Pan, G.H. 3rd Farr, C. Flynn, H. Yuan, S. Takada, D. Kimelman, L. Li, D. Wu, Low-density lipoprotein receptor-related protein-5 binds to Axin and regulates the

canonical Wnt signaling pathway., Mol Cell 7 (2001) 801–809. https://doi.org/10.1016/s1097-2765(01)00224-6.

[87]   H. Zhang, X. Nie, X. Shi, J. Zhao, Y. Chen, Q. Yao, C. Sun, J. Yang, Regulatory Mechanisms of the Wnt/β-Catenin Pathway in Diabetic Cutaneous Ulcers, Front Pharmacol 9 (2018). https://doi.org/10.3389/fphar.2018.01114.

[88]   S. Choi, M. Yoon, K.-Y. Choi, Approaches for regenerative healing of cutaneous wound with an emphasis on strategies activating the Wnt/$β$-catenin pathway, Adv Wound Care (New Rochelle) 11 (2022) 70–86.

[89]   S. Ikeda, S. Kishida, H. Yamamoto, H. Murai, S. Koyama, A. Kikuchi, Axin, a negative regulator of the Wnt signaling pathway, forms a complex with GSK-3$β$ and $β$-catenin and promotes GSK-3$β$-dependent phosphorylation of $β$-catenin, EMBO J 17 (1998) 1371–1384.

[90]   R. Dajani, E. Fraser, S.M. Roe, M. Yeo, V.M. Good, V. Thompson, T.C. Dale, L.H. Pearl, Structural basis for recruitment of glycogen synthase kinase 3beta to the axin-APC scaffold complex., EMBO J 22 (2003) 494–501. https://doi.org/10.1093/emboj/cdg068.

[91]   R.S. Jope, C.J. Yuskaitis, E. Beurel, Glycogen synthase kinase-3 (GSK3): inflammation, diseases, and therapeutics., Neurochem Res 32 (2007) 577–595. https://doi.org/10.1007/s11064-006-9128-5.

[92]   B. Calvo, M. Fernandez, M. Rincon, P. Tranque, GSK3β Inhibition by Phosphorylation at Ser389 Controls Neuroinflammation, Int J Mol Sci 24 (2023). https://doi.org/10.3390/IJMS24010337/S1.

[93]   O.C. Jorge-Torres, K. Szczesna, L. Roa, C. Casal, L. Gonzalez-Somermeyer, M. Soler, C.D. Velasco, P. Martínez-San Segundo, P. Petazzi, M.A. Saez, Inhibition of Gsk3b reduces Nfkb1 signaling and rescues synaptic activity to improve the Rett syndrome phenotype in Mecp2-knockout mice, Cell Rep 23 (2018) 1665–1677.

[94]   Y. Zheng, Y. Yang, Y. Li, L. Xu, Y. Wang, Z. Guo, H. Song, M. Yang, B. Luo, A. Zheng, Ephedrine hydrochloride inhibits PGN-induced inflammatory responses by promoting IL-10 production and decreasing proinflammatory cytokine secretion via the PI3K/Akt/GSK3β pathway, Cell Mol Immunol 10 (2013) 330–337.

[95]   L. Hoffmeister, M. Diekmann, K. Brand, R. Huber, GSK3: a kinase balancing promotion and resolution of inflammation, Cells 9 (2020) 820.

[96]   C. Skurk, H. Maatz, E. Rocnik, A. Bialik, T. Force, K. Walsh, Glycogen-synthase kinase3β/β-catenin axis promotes angiogenesis through activation of vascular endothelial growth factor signaling in endothelial cells, Circ Res 96 (2005) 308–318.

Chapter III

Fabrication and Characterization of Starch-Gelatin MAT loaded with commercially available Proanthocyanidin-Rich Grape Seed Extract

3.1 Background

Tissue engineering (TE) has utilized a wide range of biomaterials, including natural biopolymers, ceramics, and synthetic polymers [1] [2], as well as different manufacturing techniques to create scaffolds for several different purposes[3,4]. It's been a trending topic recently to incorporate sustainable methods to cope with some of the most pressing environmental challenges. TE scaffolds are now made using environmentally safe materials and techniques [5] to tackle the problem. Renewable biomaterials that are both green and non-toxic (such as keratin extracted from chicken feathers [6,7], hydroxyapatite derived from egg shells[8,9], and silk sericin obtained as an industrial byproduct) are gaining considerable attention as long-term substitutes to traditional biomaterials [10]. These materials are involved in producing biological, physicochemical, and mechanically stable devices [5].

Sustainable tissue engineering uses largely natural polymers or polymers from living organisms. Sustainable or renewable materials are biodegradable, natural, and non-toxic. [11]. Renewable polymers are mostly derived from natural sources, including plants and animals. Collagen, gelatin, starch, chitosan, etc., are naturally available polymers extracted from biomass [12]. These materials are of great interest as they are biocompatible, environment-friendly, biologically active, biodegradable, and adaptable [13].

Polymeric materials have accumulated in nature because they survive long after being abandoned. Plastic rubbish is usually discarded or burned [14]. Landfills contaminate groundwater, and harmful gases are released when the trash is burned [15]. Choosing the right polymer, however, allows for the creation of novel materials that might form the backbone of the manufacturing process with the principles of the circular economy [16].

Biomaterials are a fast-growing biomedical renewable materials sector. Renewable materials' bioactivity, compatibility, and mechanical qualities have improved, enabling tissue engineering, implants, and drug delivery systems. They're biocompatible, degradable, have controlled swelling, and are low toxicity. Tissue engineering biodegradable polymers usually degrade into non-toxic compounds [13]. Technological advancements have made biomaterials more versatile and acceptable in healthcare [13,17]. Nano and microscale sustainable material production adopt "green chemistry," especially in biomaterials, employing diverse methodologies. Using natural polymers and materials to synthesize biomaterials for tissue engineering has exploded [18]. Natural polymers have several advantages over synthetic ones.

Extracellular matrix proteins in biomaterials allow cells to connect and proliferate. Researchers must also build cell adhesion receptors for synthetic polymers since they lack epitopes for cell attachment. [19].

One of the main ways the circular economy tries to improve the use of resources in the environment is by using waste as a raw material [20]. When reusing raw materials, strategies from both the circular economy and sustainable design must be used [21]. Natural biodegradable polymers could enable green tissue engineering healthcare solutions. The EU's "Strategy for Plastics in the Circular Economy" emphasizes recycling plastics and stopping microplastics, as they are one of the most widespread causes of marine pollution [22]. Synthetic implants add to biomedical waste and harm the environment. Thus, the natural polymer could save us from this threat and enable sustainable tissue engineering.

Gelatin exhibits low immunogenic response *in vivo* applications[23]. However, if the gelatin is not pure after extraction, it can cause unexpected immune rejection [24]. Also, gelatin has low mechanical properties, so some other proteins or polysaccharides should be used together to improve their mechanical properties for biomedical applications [25]. Major polysaccharides are extracted from plants or other animal sources. Starch is a polysaccharide with important characteristics for biomedical applications, such as biocompatibility, biodegradability, and renewability [26]. Starch mimics the extracellular matrix and has low immunogenicity and excellent modifiability. Starch alone is undesirable since it has low mechanical characteristics and is water-sensitive [27]. Due to this, a composite of gelatin and starch might overcome the individual drawbacks of both materials.

This research, in brief, aims to synthesize a composite material using all-natural products and finally evaluate the composite film as a potential tissue engineering product to be used in the future as a sustainable product for multiple biomedical engineering applications. The effect of the natural polymers and extracts as a starting material for scaffold has been potentially evaluated using different in-vitro and in-vivo studies. Different Compositions of starch and gelatin were used to assess whether there is any compositional effect of the natural polymers on the physio-chemical and biological properties of the Mat, thus keeping the concentration of the extract constant, and different weight ratios of the polymers were used. The use of Gelatin and starch-based mats for packing agents are there in research, and there are composite hydrogels with UV-Crosslinking. Still, we tried to eliminate the use of any irradiation or synthetic chemical for the cross-linking process. We aim to use such compositions for

biomedical applications, bringing sustainable healthcare change. The study aims to channel edible food materials toward sustainable tissue engineering biomaterials and promote a circular economy using green materials.

3.2 Materials and Methods

Gelatin (from Cattle bone 110/120 bloom) was purchased from Loba Chemie. SAIPRO Potato Starch Powder food grade, B0779HRZ6S (PSP 250), was procured from SAIPRO AGROTECH. INLIFE Grape Seed Extract (Proanthocyanidins > 95%) Anti-oxidant 400 Mg B013UYJEJK (IL00111) was purchased from INLIFE Pharma Pvt. Ltd. Distilled water was prepared in Lab using a double distillation technique. Ethanol was procured from Merck. Cells were procured from NCCS Pune. DMEM (Dulbecco's Modified Eagle Medium), FBS (Fetal Bovine Serum) was procured from Thermo Fisher Scientific - IN, 3-(4,5-dimethylthiazol-2-yl)-2,5-diphenyl tetrazolium bromide (MTT) and penicillin-streptomycin were procured from HiMedia Laboratories Pvt. Ltd . Xylaxin, was bought from Indian Immunologicals, India and ketamine hydrochloride from Ketalar, Parke-Davis, India. Fluorescein Diacetate (FDA) was purchased from Thermo Fisher Scientific.

3.2.1 Preparation of malleable mat using Gelatin and Starch

Food-grade potato starch was added to water and heated up to 90 °C to get a homogenized solution. The temperature was decreased to 60 °C, and gelatin was added and was mixed for 30 mins to get a homogenized mixture. Daksha Beeja extract or grape seed extarct (95 % proanthocyanidin) was used at 2.5% and was mixed for another 30 mins to ensure complete mixing. The whole mixture was taken in a falcon, and an equal amount of ethanol was added. A soft polymer lump was deposited at the bottom on vigorous shaking, which was malleable and could be given any shape. Finally, the lump was pressed with the KBr Press Model MP-15 to give a circular film type of structure. The maximum concentration of starch and gelatin used was 5% w/v. Three different gelatin and starch composite compositions were made and are mentioned in Table 3.1. A schematic of material fabrication and characterization is given in Figure 3.1.

Table 3.1: Sample Composition ratio

Sample Name	Ratio of Gelatin	Ratio of Starch	Quantity of Gelatin: Starch (in gms)	Quantity of Solvent (mL)
Sample A	2	1	1.5:0.75	30
Sample B	1	1	1.5:1.5	30
Sample C	1	2	0.75:1.5	30
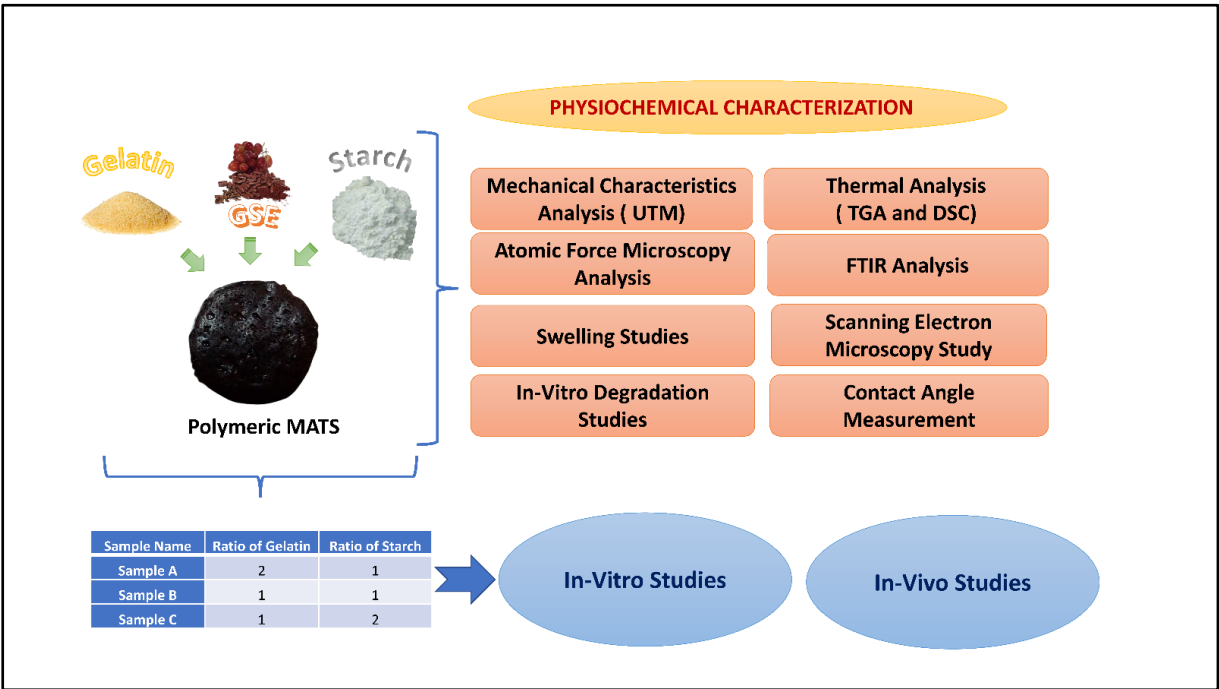
Figure 3.1: A Schematic for MAT fabrication, Characterization, and biological studies

3.2.2 Material Characterization

3.2.2.1FTIR Analysis

The composites were characterized using a PerkinElmer Frontier FT-IR instrumentation system to understand the molecular interactions. The FTIR spectra were measured between the ranges of 400-4000 cm^{-1}[28]. The obtained spectra were filtered carefully for noise reduction without losing major data.

3.2.2.2 Atomic Force Microscopy Analysis

Atomic Force Microscopic study (AFM) of the mats was carried out by scanning the samples in all three dimensions – x, y, and z using the 5500 Atomic Force Microscope (N9410S) from Agilent Technologies.

3.2.2.3 Scanning Electron Microscopy Study

SEM analysis was done using Hitachi's FlexSEM 1000 to analyze the surface morphology of the fabricated mats. An accelerating voltage of 10kV was selected for performing the tests. The images were captured in magnifications of 1.0K and 10K [29].

3.2.2.4 Mechanical Characteristics Analysis

The mechanical strength (tensile strength) was measured using the universal testing machine (Tinius Olsen 5 KT, Tinius Olsen, U.K.). The test utilized samples with dimensions of 50× 15× 0.1 mm and a tensile load of 125 N was applied at a rate of 0.1mm/min. The samples were grasped using a clip-type sample holder with a ten mm-long gripping zone. Three samples were evaluated for each mat. The nominal stress at which the specimens collapsed was considered the ultimate stress of the scaffolds [30].

3.2.2.5 Swelling Studies

The dried composite mats were pre-weighted and placed in a buffer solution of different pH of 4, 7, and 9, respectively, to check pH-dependent water intake and swelling index. The composite mats were kept in a buffer solution for 6 hrs, and the surface water was wiped off with filter paper and weighed. The equilibrium swelling capacity (Q) of the composite mats was measured using the following equation[31]:

$$Q = \frac{Wt - Wo}{Wo} \times 100$$

Wt and Wo are the final weights of the swollen and dry samples, respectively.

3.2.2.6 In-Vitro Degradation Studies

For testing in-vitro degradation of the polymer composite mats, the three samples were cut into a measurement of 10 ×10× 0.1 mm and put into 15 mL of Simulated body fluid (SBF) having a pH of 7.4 to mimic body-fluid conditions. The entire degrading process was carried out in a shaker at 100 rpm at a temperature of 37 °C throughout the study (21 days). SBF was changed at two days to avoid any chances of acceleration of hydrolysis [32]. The polymer mats were withdrawn from the SBF at regular intervals and dried in a 50 °C hot air oven until a constant weight was achieved and the water was evaporated. Every degradation experiment was conducted three times. The percentage of degradation (D) was computed using the following equation [32]:

$$D = \frac{Wt}{Wo} \times 100$$

Here, W_t is the weight of sample Mat at different time intervals after being taken out of SBF, and W_0 is the initial weight of the polymer sample.

3.2.2.7 Thermal Analysis

Thermo-gravimetric analysis (TGA) determines the thermal stability of all three samples. TGA was performed using TG 209 F1 Libra - NETZSCH. The composite mat specimens weighing 12-15 mg were heated from 30 to 600 °C at a heating rate of 10°C/min. The crucible used for the experiments was composed of Al_2O_3. Differential scanning calorimetry (DSC) was performed to analyze the thermal transition of the Mats. DSC was performed using the TA Instruments DSC Q20 Differential Scanning Calorimeter (DSC). Three samples were tested, each containing gelatin and starch in three different proportionate quantities, as indicated in Table 1. The samples were tested between 40 and 300 °C and 10°C/min using a copper pan in a nitrogen atmosphere.

3.2.2.8 Contact Angle Measurement and Analysis

The wettability and hydrophobicity of all three mats were tested by conducting contact angle tests. Using the sessile drop method, a goniometer SURFTENS 4.5 (OEG GmbH, Hessisch Oldendorf, Germany) was used to measure the polymeric Mats' static water contact angles. The

measurements were performed with a water droplet of the volume of 2 µL. For each sample, more than five measurements were taken in different places [33].

3.2.3 In Vitro Cell Culture on Polymeric Mats

The cell culture investigation was conducted to determine the cytocompatibility of the Mats by using the L929 mouse fibroblast cell line (purchased from NCCS, Pune). A 10% (v/v) heat-inactivated FBS and 1% penicillin-streptomycin antibiotics supplemented DMEM medium were used to cultivate the cells. Cells were kept at 37°C and 5% CO_2 and kept in a CO_2 incubator. At 70-80% confluency, the cells were subculture and employed in the experiment [34].

The effect of the material on fibroblast cells was tested using a conditioned medium. Briefly, each sample was prepared at a concentration of ~1% w/v of culture medium and incubated for 24 h and 72 h at 37°C before the experiments. The Conditioned media was then used for further toxicity tests. Briefly, Five millilitres of DMEM/FBS cell growth medium were added to 100 milligrams of Samples (SAMPLE A, SAMPLE B, and SAMPLE C), and the mixture was vortexed for 2.5 hours. The mixture was then cultured for four weeks under aseptic conditions. To further purify the conditioned media for cell culture assays, a PVDF, Sterile,30 mm, 0.22um-SF141 filter unit was used [35], [36]. The cells were harvested by trypsinization and resuspended in complete media to obtain a final concentration of 7500 cells per mL, and 100 µL of cells were seeded into each well of 96 well plates. The cells were incubated for 24h and 72h, then the media was taken out, and conditioned media (Media with the degraded material) was added to each of the wells. The conditioned media-treated cells and the Control (Complete media without any sample) were incubated for 24 h at 37°C. The cellular viability was checked through the 3-[4,5-dimethylthiazol-2-yl]-2,5-diphenyltetrazolium bromide (MTT) assay. The formazan crystals formed after 4 hrs. of incubation at a wavelength of 575nm using a BIORAD ELISA Plate Reader. The following formula was used to figure out the cell viability [37]:

Cell Viability (%) = [(Sample O.D) / (Control O.D)] × 100

We used fluorescein diacetate (FDA) labeling of cell-attached MATs to evaluate the cellular adherence efficacy of three different polymeric MATS (A, B, and C). Fluorescein diacetate staining confirmed the polymeric mats' capacity to sustain cellular viability. A nonspecific esterase in the cytoplasm hydrolyzes FDA, converting it to fluorescein. FDA is readily taken

up by live cells. The resulting "fluorescein" is highly luminous, accumulates intracellularly, and is maintained by the cell due to its polar nature. After 72 hours of cultivation on the mats, the wasted medium was discarded from the 24-well culture plates before live-cell imaging could begin. Polymeric mats loaded with cells were then treated with 10 mg/mL FDA (Sigma-Aldrich, USA) in serum-free Dulbecco's Modified Eagle's Medium (DMEM) for 5 minutes at room temperature. Mats were incubated for 24 hours, rinsed three times with sterile PBS, and then seen under a fluorescence microscope (Magnus)e with a 465 nm filter as soon as possible afterward

3.2.4 Hemocompatibility Assay

The hemolysis test was used to determine polymer mats' hemocompatibility. Hemocompatibility tests assess blood and blood component effects from blood-contacting medical devices or materials. The hemolysis test was carried out by the procedure outlined in a previous study [37][31]. Fresh rat blood in EDTA tubes is used to estimate the hemocompatibility of the composite MATs. A standard sample without sharp edges was incubated at 37 °C for 30 min in a centrifuge tube with 10 mL of normal saline. This was mixed gently with 0.2 mL of diluted blood and incubated for 60 min. For the positive control, 0.2mL of diluted blood was collected in 10 mL of 0.1 percent Triton X-100, and for the negative control, 0.2mL of the blood was taken in 10 mL of normal saline solution and incubated for 60 min at 37°C. The sample was incubated at 37 °C for 60 min. After 60 min of incubation, all test tubes were centrifuged for 5 min at 4000 rpm. The supernatant was carefully collected and transferred to the cuvette for readings at 545 nm wavelength and percentage hemolysis [14]. The tests were done in triplicate, and the percentage of hemolysis was calculated using

$$\text{Percentagezof hemolysis} = \frac{(\text{Sample} - \text{Negative Control})}{(\text{Positive Control} - \text{Negative Control})} \times 100$$

3.2.5 In-vivo cellular response and biocompatibility assay

Twelve Wistar female rats weighing 150–180 g were utilized in this experiment and divided into four groups consisting of three rats in each group. Before the experiment, animals were housed in a laboratory for seven days to get used to the environment. Laboratory settings include temperatures ranging from 20 to 24 degrees ⁰C and a 12h light-dark cycle for the animals housed in polypropylene cages. For the trial, the rats were fed a regular meal, given

water at will, and basic medication. Group-I was kept as the control without samples. Sample A, B, and C were administered to Groups II, III, and IV, respectively. The rats were anesthetized with 80 mg/Kg -ketamine and 10 mg xylazine hydrochloride /kg body weight as pre-anesthetic [38] before creating an incision wound model for tissue transplantation. A 1 cm long tissue wound incision was genrated using (no 10) using a surgical blade. Polymeric mats were transplanted into the tissue wound after the incision and remained in place with the required/necessary suturing. An injection of the painkiller meloxicam (Melnex; Intas-Polivet; India; @ 0.2 mg/kg O.D. for three days) was used to treat the discomfort caused by the wound's development. Each rat was housed in its well-ventilated cage, making it easier to keep an eye on the animals and better for their general health. The tissue of the incision area was collected after the prescribed period (14 days). All the experiments were conducted as per standard protocol and with proper ethical permission from the Institutional Animal Ethical Committee (IAEC) of the West Bengal University of Animal and Fishery Sciences, Kolkata, India (approval no.763/G0/Re/SL/O3/CPCSEA/05/2021-22 dated 26.04.2022) . The biomaterial-coated tissue specimens were placed in a 10% formalin solution for one hour. After that, the samples were frozen and sectioned with a microtome to produce 2 mm thick slices. It was then examined under a light microscope and stained with a hematoxylin-eosin stain [38,39]. The photographs were captured using a microscope and a Lecia camera.

3.2.6 Data analysis

For repeatability, all biological tests were carried out in triplicate, and the results are provided here as the mean value, the standard deviation (SD). *, **, ***, and ****were evaluated for p values 0.05, 0.01,0.001, and 0.0001, respectively, in a two-way ANOVA or one-way ANOVA statistical analysis as per the data set and representation.

3.3 Results and Discussion

3.3.1 Synthesis and Fabrication of Polymeric Composite MATs

The polymeric mats are fabricated using different compositions of Gelatin and Starch and cross-linked using Draksha Beeaj Extract(Grape Seed Extract,Inlife). After making a blend of the polymers, the mixture was mixed vigorously with ethanol (99.9%) in a ratio of 1:2. The resultant material was a polymeric composite lump with a brownish colour, which might be due to the incorporation of the extract. The whole procedure is depicted in Figure 3.2. The

ethanol in reaction with the polymeric mixture converts the starch and the gelatin to micro-structured granules [40] and precipitates the gelatin to induce intramolecular and intermolecular interactions to enhance the composite property [41,42]. The ethanol precipitation due to Hofmeister ion formation helps in the formation of a film-like structure for the composite [43]. When ethanol is added to a polymer solution, some strongly polar and macromolecular components become less soluble, which results in precipitation [44]. The fabricated mat showed some elasticity initially, but it got hard when kept in the air. The material, again in contact with water, gets soft and elastic. The Mats, when stored in a vacuum, maintained their normal integrity. The Draksha beeja extract added to the Mat enhanced the stability and mechanical strength by cross-linking the polymers owing to the presence of proanthocyanidins in the extract [45]. The proanthocyanidin along with ethanol precipitation results in more hydrogen bonds in the polymeric structure. All the Mats were synthesized under sterile conditions in an airflow hood to avoid major contamination during synthesis. Later during cell culture and animal study the Mats were sterilized using Ethanol and UV.

Sample Name	Gelatin	Starch
Sample A	2	1
Sample B	1	1
Sample C	1	2
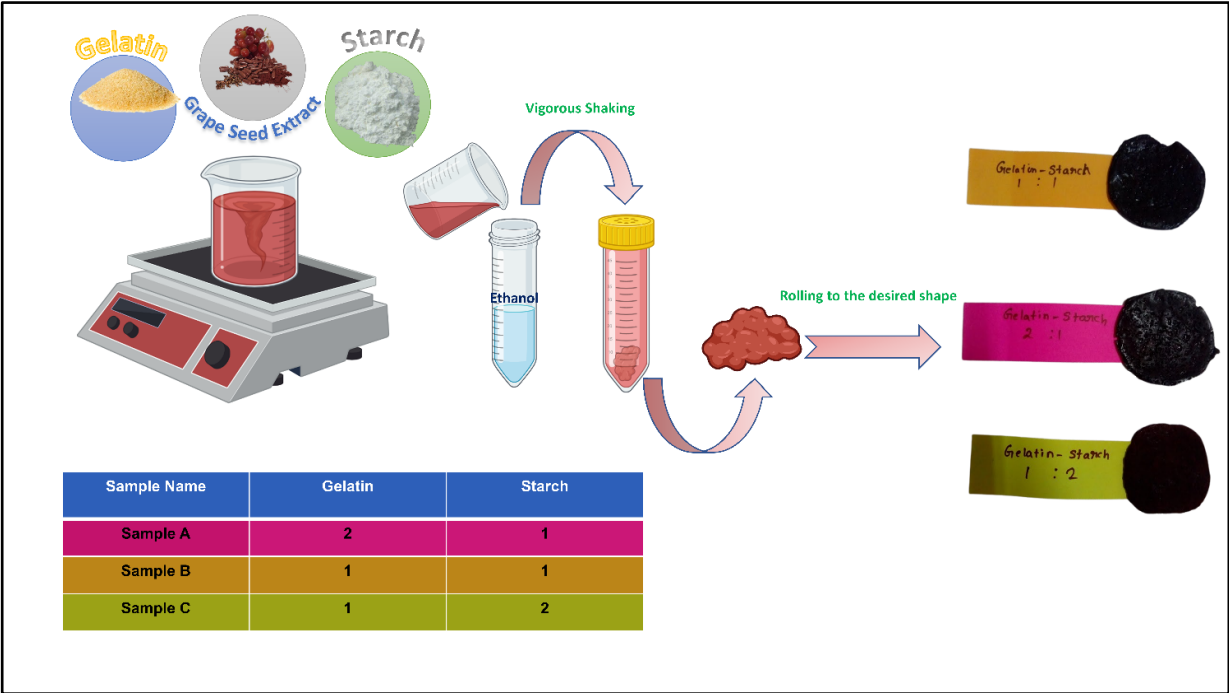
Figure 3.2: Schematic for the synthesis of Gelatin-Starch polymer composite

3.3.2 Material Characterization

FTIR analysis (Figure 3.3) was done to evaluate the presence of different functional groups, which finally contributed to the fabrication of the Mats. To evaluate the chemical effect of the draksha beeja supplement in the mat, a simple composite of starch and gelatin was compared

to that of the draksha beeja incorporated mats. The aim was to check whether the draksha beeja extracts impart any chemical change in the composite, although the major aim of the study is to evaluate the overall chemical functional group of the whole composite Mats. A distinct peak was observed for all three samples at around ~3400 cm^{-1}. At 3425 cm^{-1}, the absorption peak could be assigned to the O-H stretch of hydroxyl groups present in the sample. This region also corresponds to the presence of an amine. As the sample is composed of starch and gelatin and both -OH and -NH$_2$ groups are abundant in starch and gelatin, respectively, the high intensity of the peak in this region is justified. Samples with draksha beeja showed a peak at 2842 cm^{-1}, which was not significant in simple composite without draksha beeja; the peak at 2842 cm^{-1} typically corresponds to the C-H stretching vibration of aliphatic compounds. Amide I and II peaks in gelatin were observed at around 1650 and 1550–1500 cm^{-1}, respectively[46]. The peak of amide III in gelatin was seen around 1200 cm^{-1}. However, the samples with drkasha beeja showed a fine and distinct peak at 1635 and 1328 cm^{-1}. FTIR peak 1635 cm^{-1} is typically associated with amide I (C=O stretching vibration in peptide and protein). It is usually a strong peak and can be used to identify the presence of proteins and other biomolecules. The peak 1328 cm^{-1} is typically associated with amide III (N-H bending vibration in peptide and protein). It usually has a weaker peak than amide I and is sensitive to secondary structure and conformational changes in proteins and other biomolecules. The shifting in peak and presence of a distinct peak indicates the polymeric interaction between starch and gelatin, which can be facilitated due to the presence of Draksha beeja. The Draksha beeja is rich in proanthocyanidin and is also considered a crosslinking agent [45], which has possibly contributed to the interaction of the polymers. Due to the reaction between amino groups of gelatin and hydroxyl groups of starch, a slight shift of the peaks can be seen. This shifting points towards the involvement of amide groups in the cross-linking reaction. The incorporation of GSE helped in crosslinking of the composites, and the use of a natural product as a crosslinking agent could certainly promote sustainability and reduce the use of synthetic chemicals as crosslinking agents.
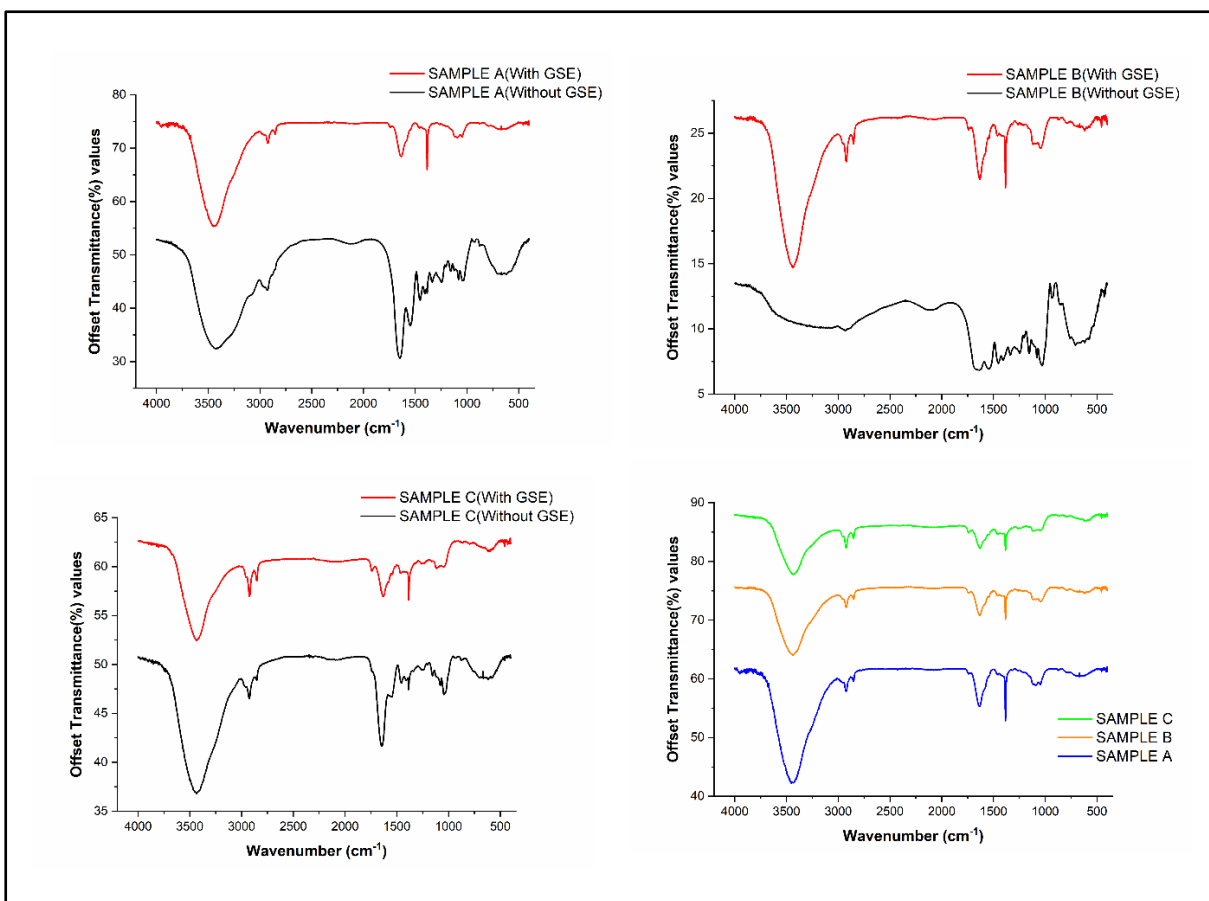
Figure 3.3: FTIR analysis of all the three polymeric composite MATS

The AFM results **(Figure 3.4)** show that sample B is the better material among the three in terms of smoothness. The root means square height (RMS) gives us an idea of the surface roughness of the sample (Table 3.2). Sample A (254 nm) and C (229 nm) have a high roughness value compared to sample B (56 nm). Also, the maximum peak height and pit height values are high for samples A and C. In both cases, we can say that the gelatin granules are not well embedded in the matrix and have higher roughness, resulting in a huge topological gradient. Sample C has a lower RMS value than sample A, indicating its higher surface smoothness. The overall characterization suggests that samples B and C possess a smoother surface with few irregularities compared to A, which can help in good cellular attachments. A smooth surface promotes cellular proliferation and is less allergic when used for biological applications [47,48]. The difference in roughness is due to different compositions of starch and gelatin. Sample B with 1:1 showed the best smoothness may be due to an equal proportion contribution of starch and Gelatin, which in turn avoided the presence of unreacted grains of gelatin or starch. The uneven blends for Sample A and Sample C caused poor miscibility and thus caused

phase separation of the components [49], while a homogenous surface morphology is observed for the blend with the same proportion mixing of Gelatin and Starch.
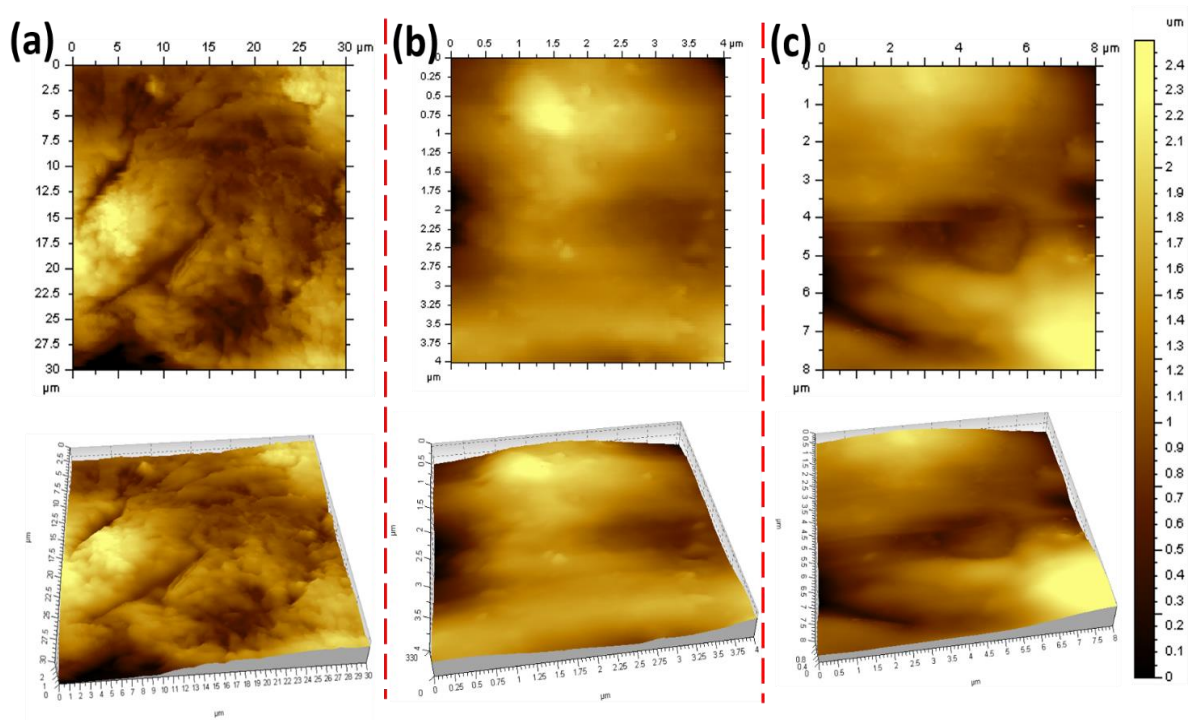
Figure 3.4: (a-c) AFM analysis of Sample A, B & C, respectively.

Table 3.2: AFM RMS values of each sample

Parameters	Sample A	Sample B	Sample C
RMS (Root mean square height) in nm	254	56	229
Sp (Maximum peak height) in nm	735	170	714
Sv (Maximum pit height) in nm	636	161	479

SEM images of the samples were analyzed to study the composite Mats's surface morphology and structure details at different magnifications (1000x and 5000x). Sample A shows a very high aggregation of gelatin granules in certain pockets. In figure **Figure 3.5 (a)** the doughnut-shaped gelatin granules are not properly embedded in the starch matrix which is because of the higher (2:1) gelatin: starch ratio. The higher surface roughness of the Mat is because of these gelatin granules, which is confirmed by the AFM Sq value (Table 3.2). The material also lacks pores because of its high inhomogeneity. Sample B shows well-dispersed gelatin granules in the starch matrix (fig. 3.5 b), and many pores are visible in Figure 3.5 (b). This composition

has the best blend of gelatin and starch (1:1), giving rise to a smooth surface structure which is confirmed by the low Sq value of AFM. Sample C shows well-embedded gelatin granules in the starch matrix Figure 3.5 (c). The number of gelatin granules is visibly more compared to sample B and has a higher roughness, as observed from the Sq value of AFM. Bigger pores are observed in this sample compared to sample B Figure 3.5 (c). The granule-like structure is mostly microparticles of gelatin and starch, which got precipitated due to agitation using ethanol. Structures of all the samples pointed to a self-assembled polymeric network pointing to the Inter-penetrating polymeric Network (IPPN).
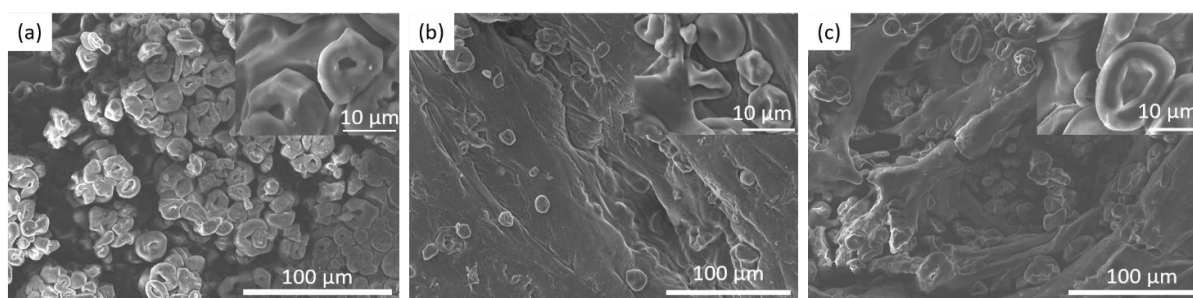
Figure 3.5: Scanning Electron microscope images of the polymeric MAT a) Sample A, b) Sample B, c) Sample C at different magnifications 1000x and 5000x.

In addition to the physio-chemical properties of composite polymers, it's also important to understand the polymer's mechanical characteristics. **Figure 3.6** points to the tensile stress-strain curve, Young'smodulus, ultimate stress, and ultimate strain (%) of the different compositions of the composite polymer. Figure 6(a) represents the characteristic stress-strain curve of the composite polymers at different compositions, i.e., different mixture ratios. Stress-strain curve confirmed the elastomeric nature of all Mats. Sample A (Gelatin: Starch →2:1) exhibited very poor mechanical properties with Young's modulus, ultimate stress, and ultimate strain of 1.137±0.146 MPa (Figure 6b), 0.129±0.15 MPa (Figure 5c), and 5.57±0.98 % (Figure 6d), respectively. The gelatin, in general, is unstable and contributes to poor mechanical properties when used in a hydrogel formulation. Thus, a greater proportion of gelatin might have affected the overall mechanical property of Sample A. Sample B showed better mechanical property with a young modulus value of 3.38±0.08 MPa. The ultimate stress and ultimate strain were observed to be 11.46±.91 MPa and 5.75±1.2 %, respectively. Sample B indicated considerable tensile strength due to the presence of an equal amount of gelatin and starch. Sample C exhibited a maximum young modulus among the three samples with a

calculated value of 3.60± .11 MPa. The presence of starch might have contributed to this increased mechanical strength. The ultimate stress and ultimate strain of Sample C were found to be 11.033±1.30 MPa and 4.19±0.24 %, respectively. The mechanical properties of Samples B and C were quite strong and closely resembled human tissues, such as soft collagenous tissue, cartilage, ligaments, etc. [50].
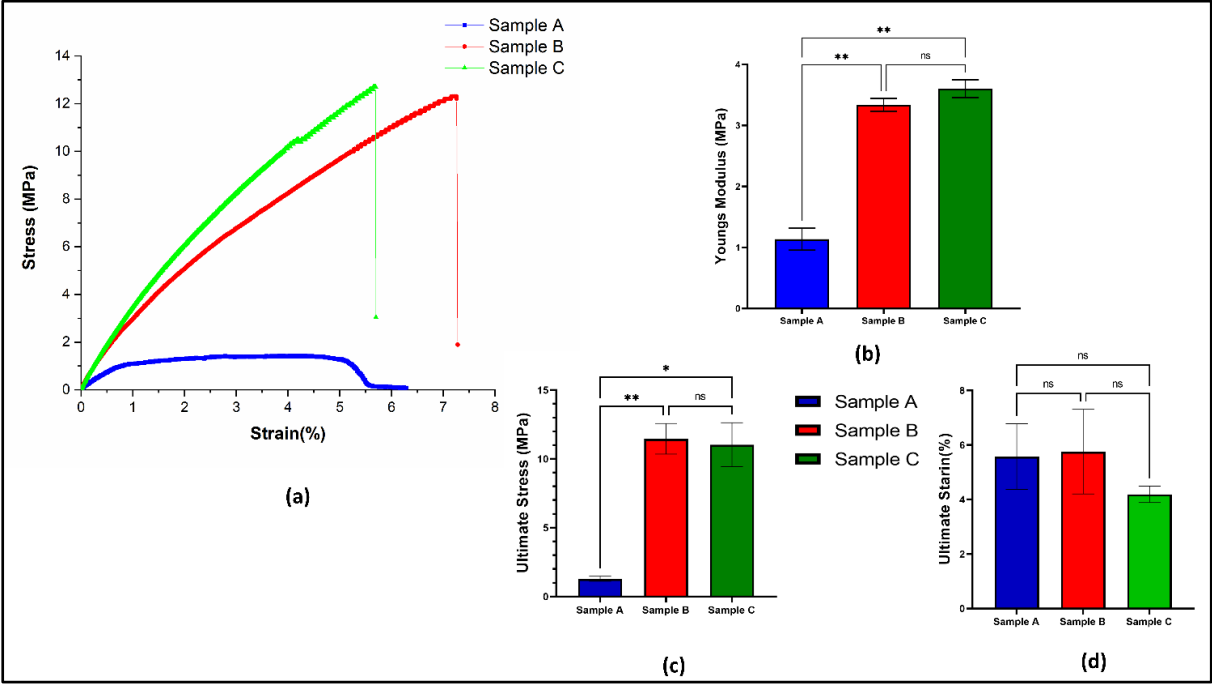
Figure 3.6: Mechanical Characterization of the three polymeric MATs (a) Stress-Strain Curve (b) Comparative Young's modulus (c) Comparative Ultimate Stress and (d) Comparative ultimate Starin

It's necessary to look at a scaffold's capacity to retain liquid in it while evaluating its suitability for tissue engineering. Structure, physical condition, the flexibility of the chain segment, and interactions between the molecules can all impact biomacromolecule swellability [51]. Figure 3.7(a) points to the swelling capacity at the equilibrium of all three polymeric composite Mats at three different pH levels. All three Samples with different compositions of gelatin and starch showed the lowest swelling at pH 4, i.e., in acidic conditions, followed by approx. doubling swelling at pH 7(Neutral) and maximum swelling at pH 9(Basic). Sample A showed maximum swelling among other samples in acidic conditions (pH 4) with a swelling index of 102.86 ± 1.9%. Samples B and C exhibited a swelling index of 100.64 ± 1.2 % and 72.68 ± 2.4 % at pH 4. In neutral pH (pH=7), both Sample A and B showed almost similar swelling properties with a swelling ratio of 229.06 ± 4.7 % and 224.9 ± 14.69%, whereas Sample C showed a

considerably less amount of swelling (144.87 ±2.6 %). At basic conditions, all three samples showed superior swelling capability. Sample A, Sample B, and Sample C showed a swelling index of 2050.15 ± 37.44%, 2022.54 ± 23.72 %, and 1890.34 ± 24.71%, respectively, at a pH of 9. The maximum swelling index at a pH of 9 might be due to leaching out of draksha beeja, which is more likely to diffuse out at basic conditions. The maximum swelling also indicates maximum release of the active component, i.e., draksha beeja extract, into the fluid; thus, it could be effective in delivering the draksha beeja extract to sites with higher or basic pH like infected sites[52]. Thus, this polymeric mat-based scaffold could be very helpful in healing tissues with infections.
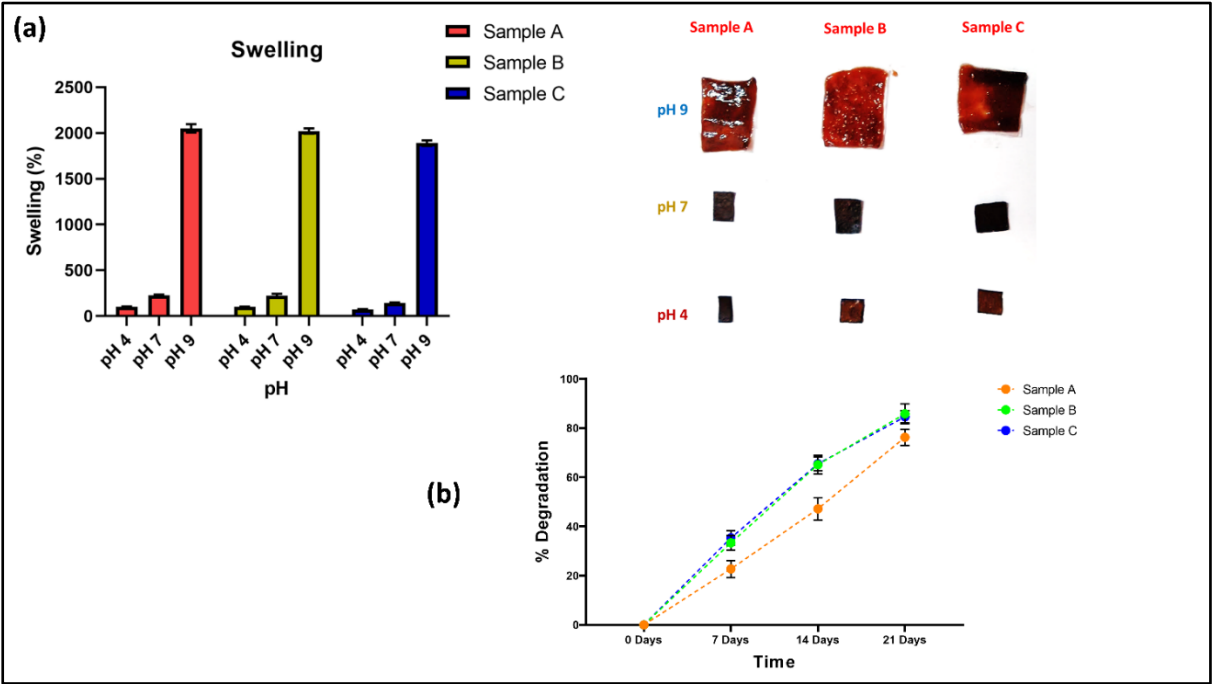
Figure 3.7: (a) The swelling percentage of all the three composite MATs in different pH, (b) Percentage degradation of polymeric MATs in SBF at a different time interval

One major drawback of a polymer-biomaterial for clinical application in tissue engineering can be its low degradation rate within a certain period. In the case of our samples, all three samples show optimal degradation after each time interval(Figure 3.7b). After an interval of 7 days, all the samples can be seen to have degraded by 22% to 35%. After an interval of 7 days, Sample C exhibited a degradation of 35.406 ± 2.38 %, and Sample B also showed similar degradation of 33.385 ± 2.46 %. Sample A, although, showed a lesser degradation rate of 22.73 ± 2.78 %. After the interval of 14 days, both samples B and C have shown almost the same degradation rate of 65.14 ± 3.07 % and 65.46 ± 2.33%. In this case, also Sample A has shown a slow

degradation of only 47.17 ± 3.69 % after 14 days. In the case of the final interval of 21 days, degradation of all the samples can be seen in the range of 76% to 85%. Sample A, as in earlier cases, showed a very slow degradation rate of 76.27 ± 2.70%. Sample B showed a maximum degradation of 85.19 ± 1.98%. In-vitro degradation of Sample B and C exhibited almost 80% degradation in just 21 days hence pointing to the effectiveness of these materials for various tissue engineering applications[53,54].

Thermal characterization is an important characterization for biomaterials to check their stability. All three polymeric composite Mats showed thermal stability up to a temperature of around 130 ºC. The TGA graphs (Figure 3.8(a)) show the weight loss of the polymeric composite through a temperature range of 30 -600 ºC. The initial dip in the thermograph is due to the evaporation of adsorbed water for all film samples. The weight loss at the second stage for Sample A is 11.427 %, for Sample B is 14.631 %, and for Sample C is 11.273 %. This weight loss can be attributed due to the polymer chain decomposition of Gelatin and Starch. Finally, at the third stage, a weight loss of 29.65 %, 27.22%, and 26.33% were observed for Samples A, B, and C, respectively. This weight loss might be due to the decomposition of polymeric chains and small carbon and hydrocarbon molecules present in the polymeric composite mats. All three mats exhibited good thermal stability, and this increase in thermal stability might be due to cross-linking of the -OH group of the starch and the amine group of the gelatin. Interestingly, it should also be noticed that Sample B had much less residue than Sample A and Sample C (more than 20%). This could be due to the optimum mixing of the ingredients that produced a completely biodegradable composite. For Samples A and C, the excess amount of gelatin and starch, respectively, would have caused more residue even after the temperature of 600ºC. The process of cleaving long polymer chains under heating, generally in the absence of air, is termed pyrolysis [55]. Pyrolysis temperature between 500-800 °C leads to forming biochar from biogenic wastes such as corn stover [56]. It has also been highlighted that extensive pyrolysis for cellulose-based samples initiates around 300 °C [57]. Hence, under an N_2 atmosphere, the TGA process at high temperature might have attributed forming of biochar that eventually contributes to the mass retention of samples beyond 500 °C. A similar three-stage thermal degradation up to 600 °C for pure starch of different origins has been observed by Pigłowska et al. A mass retention of around 20% has been observed in the temperature regime of 600 °C and beyond [58]. The sharp peak in DTG graphs for all the samples represents that the maximum mass loss rate occurred at the second stage of thermal degradation. Blending gelatin and starch improves thermal stability when compared to pure

gelatin films due to increased interaction between blend constituents, enhancing dissociation energy [59]. However, in the second stage of degradation, starch could disrupt the structure of gelatin and enhance degradation [60]. Furthermore, no significant conclusion could be drawn for enhanced mass loss of sample B at the third degradation stage. One possible explanation for the disparity could be the variation in inorganic impurities [61]. It is to be noted that mass loss (similar to sample B) has also been reported in the literature[62].
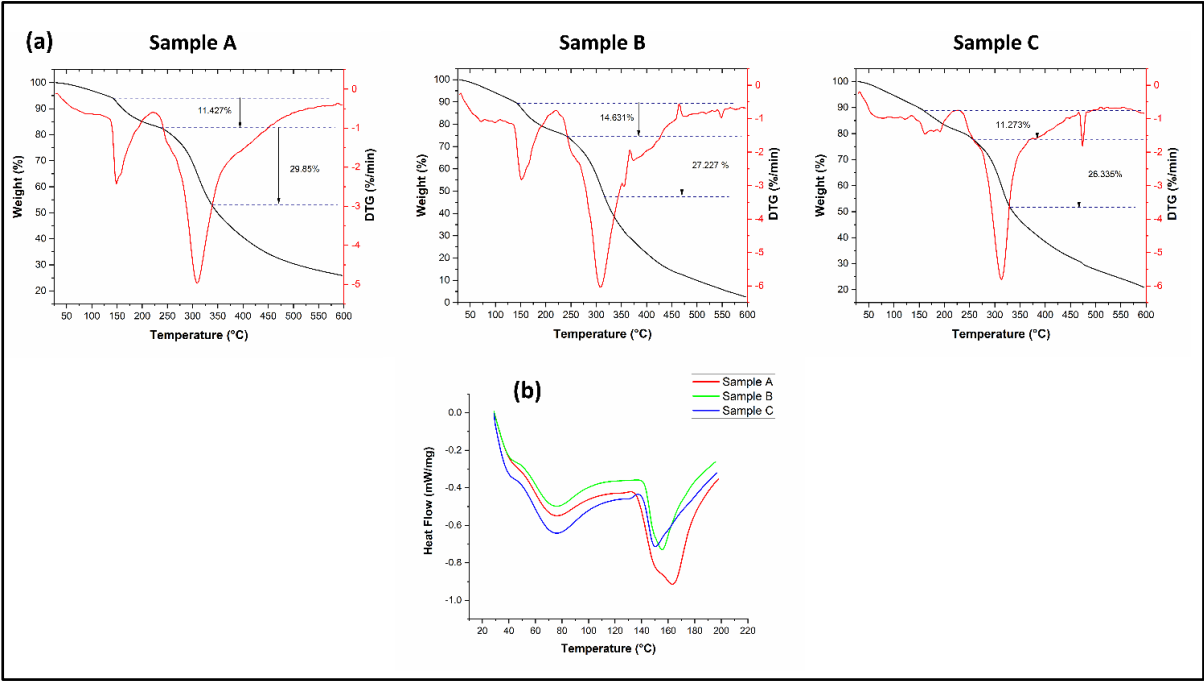
Figure 3.8: Thermal Characterization of the three Polymeric Mats (a) Thermogravimetric Analysis of the three Mats. (b) Differential Scanning Calorimetry of the Samples

We also carried out differential scanning calorimetry (DSC) and the corresponding DSC thermograms to learn additional details about the glass transition temperature (Tg) of the polymeric Mats and calculated the Tg of the three different Mats are shown in **Figure 3.8(b)**. For all three samples, obtained thermograms indicate that the first major endotherm peak was present at about 70° - 80°C. This temperature lies in the range of Tg of Starch. To be highly specific, the first major endotherm peak for Samples A, B, and C lies at 75.83, 75.25, and 76.07 °C, respectively. Two endothermic peaks corresponding to the Tg values could be observed for all the samples below 100°C, indicating the two constituents maintained their integrity in the composite systems. The Tg value around 80°C is contributed by gelatin [63], and Tg near 40°C is contributed by starch[64]. The Tg of Starch varies with moisture content. Above Tg of gelatin, the small exothermic peak could be attributed to the molecular relaxation of gelatin.

The peaks beyond 140° C correspond to the degradation, and it is to be noted that composite with high gelatin content displayed enhanced temperature for degradation that might be due to the denaturation. Hence, sample C displayed the highest degradation temperature, followed by samples B and A. The increase in the degradation temperature might be due to the restricted mobility of gelatin chains due to enhanced participation in cross-linking with grapeseed extract. Proanthocyanidin, one of the main ingredients of grape seed extract, successfully cross-links gelatin with amide and ester linkage[65]. Hence, an increase in gelatin content might have increased the cross-link density.

The contact angle measurement of the three polymeric Mats was done, and the results are depicted in **Figure 3.9**. Gelatin and starch are both hydrophilic polymers, and the composite Mats exhibited significant wettability properties. Sample A, B, and C showed a contact angle of 55.235°, 27.284°, and 55.299°, respectively. All the samples showed a contact angle below 60° hence indicating the hydrophilic nature of the mats. Sample B showed the lowest contact angle owing to its highly smooth surface, as indicated by AFM and SEM studies. A lower contact angle indicates higher hydrophilicity. It has been proposed that hydrophilicity is a critical factor in cell adhesion[66]. A range of cell activities, including cellular attachment, can be regulated by the adsorption of blood proteins, which are hydrophilic in nature. Contact angles have been utilized to identify non-thrombogenic surfaces, despite the lack of a correlation between the wettability of the surface and the thromboresistance. Good blood compatibility is more commonly found in materials that create tiny contact angles when in direct proximity to blood rather than in materials that produce high contact angles[67]. From the above fact, it can be assumed that the Mats will be biocompatible and hemocompatible in nature, considering the contact angle value. The equal combination of the polymers showed a better wettability property than that of the othernature, considering the contact angle value. The equal combination of the polymers showed a better wettability property than that of the others.
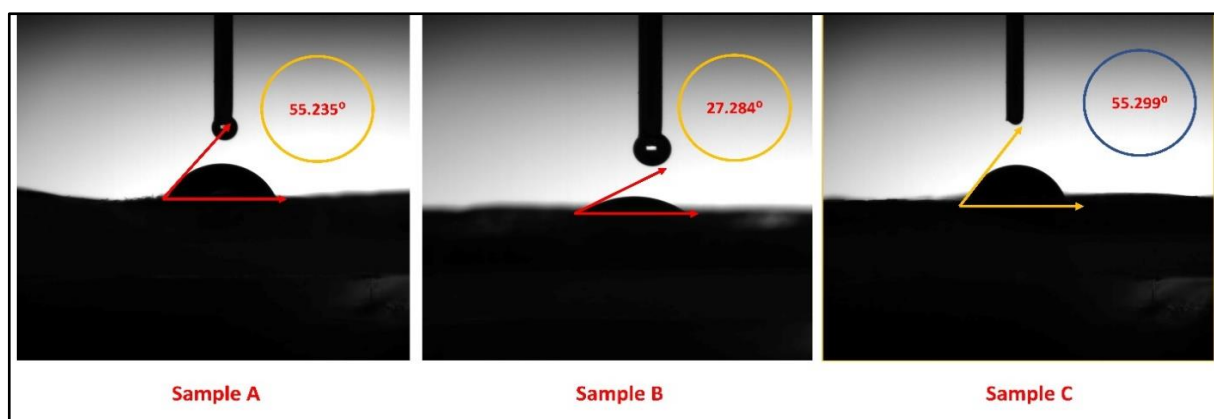
Figure 3.9: Contact Angle for all three polymeric composite MAT.

3.3.3 Cellular Morphology and Viability response of the Polymeric MATs

The in-vitro cytotoxicity assay of all three samples, i.e., Sample A, B, and C, was assessed using the L929 Cell line after 24 h and 72 h of treatment using conditioned media. **Figure 3.10** represents the MTT assay and the cellular pictographs of the cells after treatment with conditioned media. Here control means the cell with no treatment and is considered 100% viable. MTT assay results from both the time point showed that all three samples have superior cellular compatibility with cellular viability of over 90% for all the cases. Sample A showed cellular viability of 83.28 ± 3.3 % after a 1-day interval and 91.90 ± 1.51% after 72 h of treatment, and sample B showed cellular viability of 113.82± 9.14 % after 24h and 99.57 ± 2.05 % after 72 h, which was the maximum among all three samples. Sample C also showed a cell viability of 97.29± 6.35 after 24 h and 90.28 ± 1.50 % after 72h(3 days). Cellular images also pointed out that all the cells treated with conditioned media of respective samples maintained their normal integrity and structure. Cells that were in contact with Sample B conditioned media also showed some signs of proliferation for both time points (Figure 3.10 (c), (g)). Overall, in-vitro cytotoxicity assay using MTT and cellular images pointed out that all three Mats showed superior biocompatibility and hence could be used further in tissue engineering applications. Cells exhibited normal growth within the three-day interval, and all the cells treated with Samples A, B, and C showed no signs of toxicity. These Mats could also help in cellular attachment and enhance cellular proliferation. The Mats hence fabricated, could be a promising material for Tissue Engineering applications.
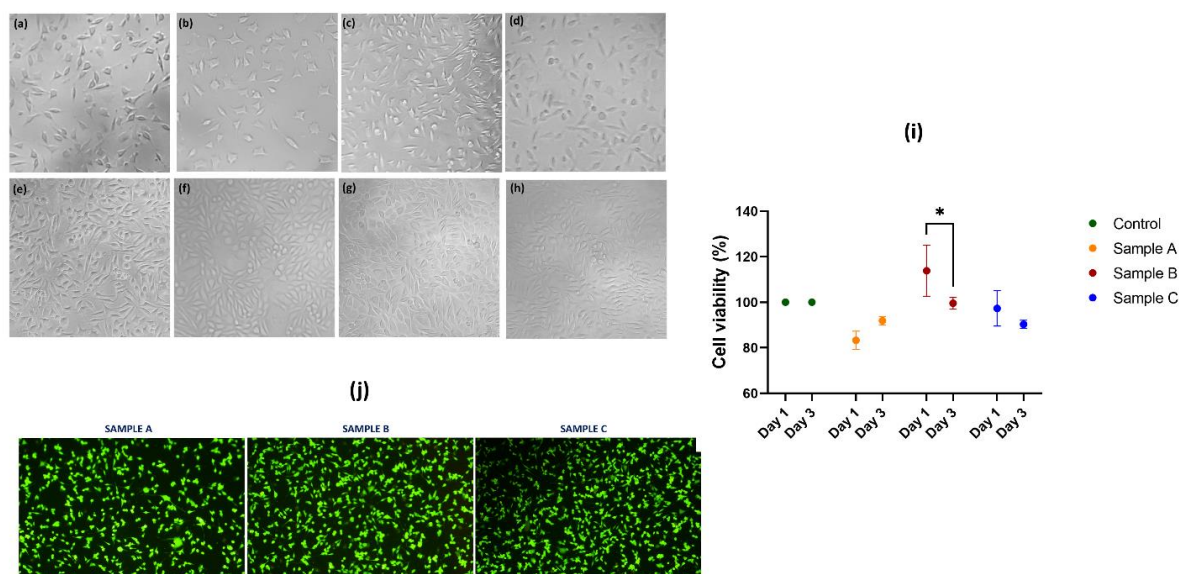
Figure 3.10: (a-d) Cellular Image of Control, Sample A-C respectively after one day. (e-h) Cellular Image of Control, Sample A-C, respectively, after three days. (i) MTT Assay Data (j) Fluorescence Image of L929 Cells attached to the Mats

Fluorescein diacetate (FDA) staining of the cell-attached mats was performed after 72 h of incubation to observe live cells/cell viability and the cell proliferation status on the Polymeric Mats. All three samples showed good cellular attachments with proliferating cells (Figure 3.10 (j)). Mat B and C also showed good cellular interconnection among each other's thus would promote good cell-to-cell communication [68]. The Cell population was found to be maximum in Mat B, followed by Mat C. Good cell adhesion was confirmed for all three samples.

3.3.4 In-vitro Hemocompatibility Assay

The average hemolytic index value of the three polymeric composite Mats is depicted in **Figure 3.11**. The hemolysis percentage of Samples A, B, and C were 2.543 ± 0.318 %, 1.546 ± 0.34 %, and 1.87 ± 0.25 %, respectively. The hemolysis percentage of Sample A was found to be significantly different from that of B and C. All the samples were hemocompatible, as the percentage of hemolysis for all the samples was less than 5%. Although Sample A had a higher hemolysis index than Sample B and C., Sample B showed minimum hemolytic effect with (%) hemolysis of around 1.5 %. Sample B could be considered close to being highly hemocompatible as per standard. Material can be categorized as highly hemocompatible, hemocompatible, or non-hemocompatible by ASTM F756-00 (2000) if its hemolytic index

values are less than 2%, within 2%–5%, and more than 5%, respectively [69]. A higher value of OD is associated with increased red blood cell (R.B.C) hemolysis because the materials put greater osmotic pressure on the blood cells. From the results, it could be easily pointed out that samples B and C are highly hemocompatible and could be used for proper biological applications.

Figure 3.11: Hemocompatibility index of the three polymeric composite MATs (SAMPLE A,

Sample	Average O.D at 545	Mean % Hemolysis	Remarks
+ve Control	0.5496	100%	
+-ve Control	0.0029	0%	
Sample A	0.0165	2.543 ± 0.318 %	Highly Hemocompatible
Sample B	0.0093	1.546 ± 0.34 %	Highly Hemocompatible
Sample C	0.0124	1.87 ± 0.25 %	Highly Hemocompatible
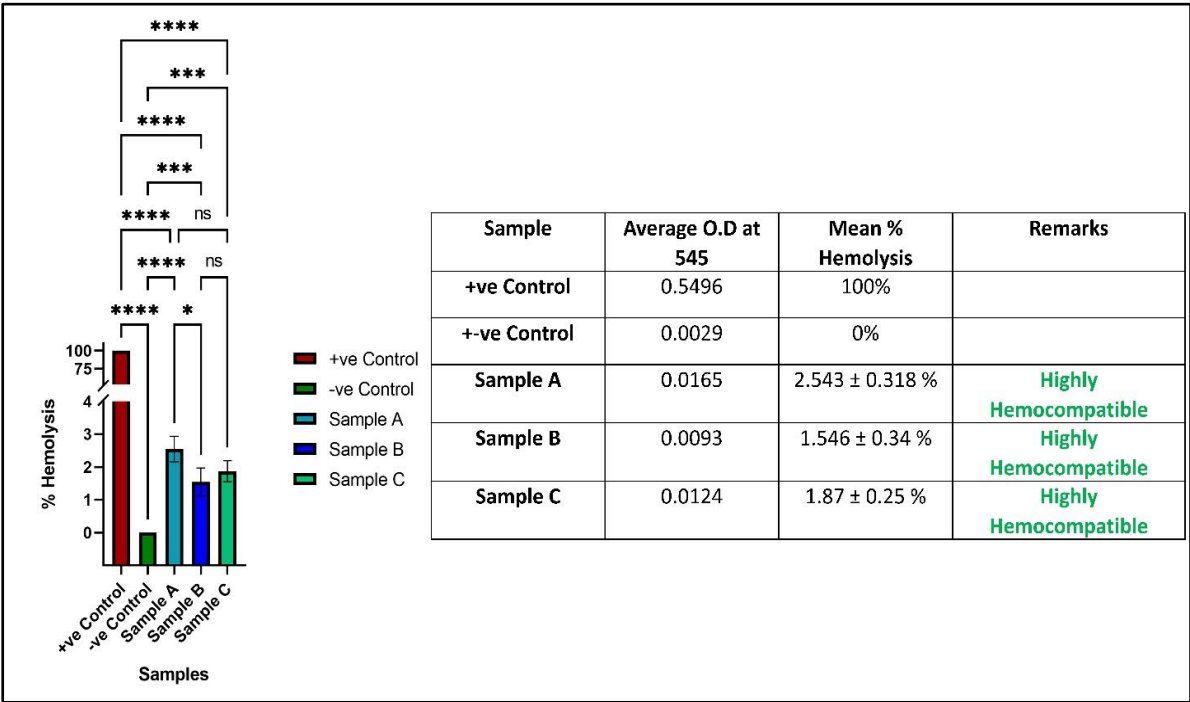
B & C)

3.3.5 In vivo Biocompatibility study

The biocompatibility and the in-vivo study of the Mats were performed by implanting the materials into the inner layer of skin rats. The implantation technique and the effect of the implantation after 14 days have been depicted in Figure 3.12(a). Tissues from the sacrificed rats were made into slides and were stained using hematoxylin and eosin dyes to observe (Figure 3.12b) the histology of the tissue.
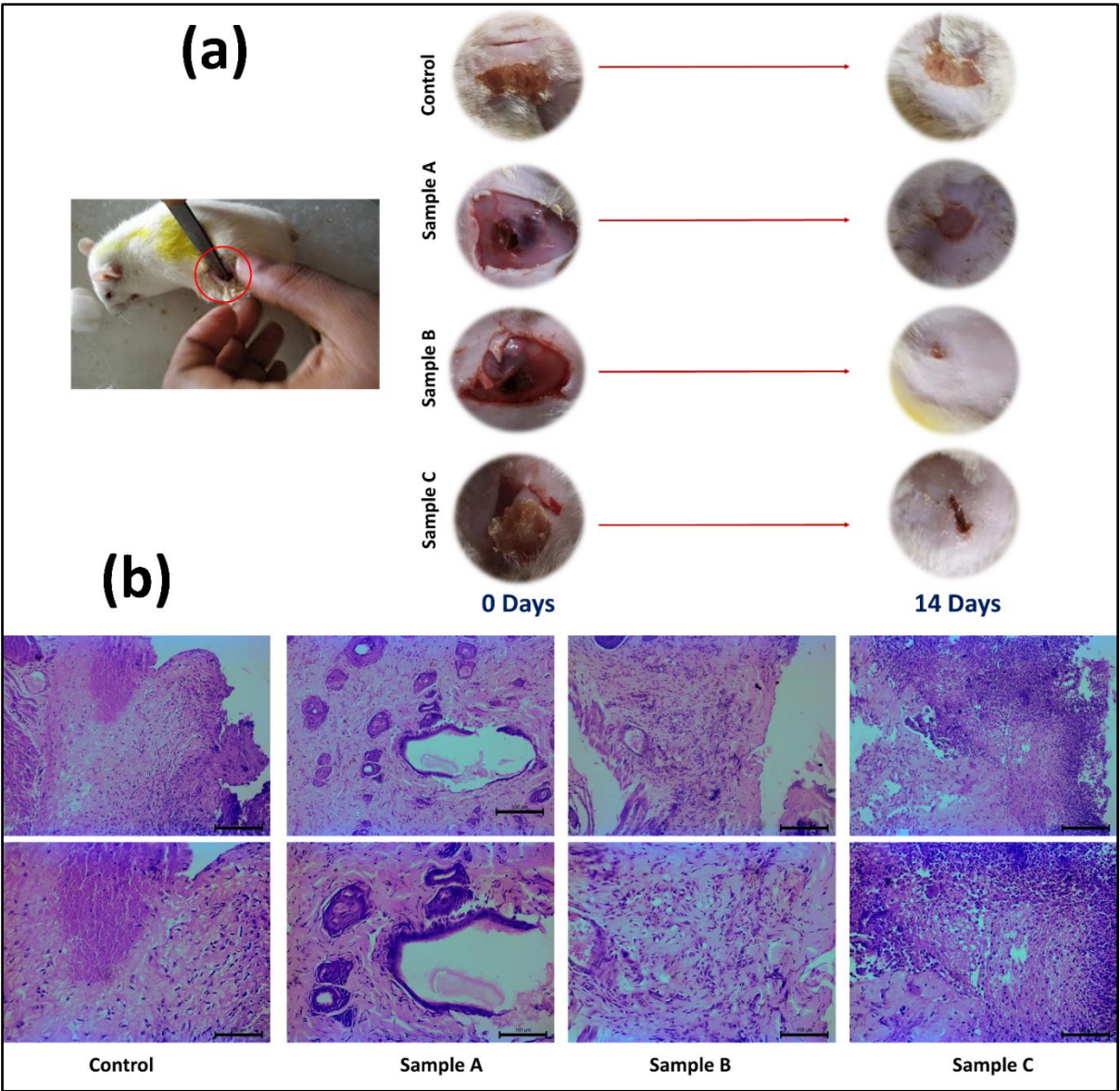
Figure 3.12: In-vivo studies of the Mats (a) Implantations of Mats underneath the rat skin. (b) Histopathology of the tissue samples from the site of implantation.

After the 14th day, it was examined that all the material had been degrading, and no such tissue-level infection in the implanted area was observed, and it was also observed and found that treated one with polymeric biomaterial MATs (Samples A, B and C) showed excellent biocompatibility and degradation than the control. Sample A showed almost 70% degradation, whereas Sample B and C showed complete degradation; notable tissue recovery was also seen in the Rats implanted with the Mats. To be highly specific, Rats treated with Sample B showed almost full healing, whereas the control and the other two samples did not show full closer of the wound created for implantation.

The histopathological analysis of sample A showed proliferation of blood vessels and hyalinization, with perivascular inflammatory cell infiltrate, and also the presence of edema was noted. Histologically, angiogenesis could be observed as the formation of small capillary buds, sprouts, or tubes extending from existing blood vessels into adjacent tissue areas. During angiogenesis, endothelial cells proliferated to form small buds or sprouts that penetrated the surrounding tissue. This sprout then lumenizes, forming a tube-like structure that could connect to other sprouts and form a functional network of blood vessels. The new blood vessels appear as small, thin-walled tubes or capillaries, often with a surrounding halo of proliferating endothelial cells. Hyalinization was the term used in histology to describe a condition where a normal cellular tissue or organ becomes more homogenous and appears glassy or eosinophilic under microscopic examination. It was associated with the accumulation of a proteinaceous substance called hyaline, characterized by the pinkish deposition deposited at the site, which had a glassy or translucent appearance under the microscope [70]. It could be composed of various proteins, including collagen, elastin, and other extracellular matrix proteins. Collagen production was moderate.

Sample B exhibited the proliferation of fibroblasts increased collagen production, and a clear indication was present pointing to the ongoing process of repair. Histopathological changes in the section of sample B were appreciated with abnormal deposition of collagen fibers in an unorganized or disordered manner. This could occur in various organs and was associated with chronic diseases or conditions. In this fibrosis, collagen fibers were deposited in a random and chaotic pattern without any clear direction or alignment. This led to the formation of dense and rigid scar tissue, which could impair the normal function of the affected organ. On a microscopic level, haphazard fibrosis was characterized by the presence of thickened collagen bundles, along with other changes such as the accumulation of inflammatory cells and the formation of normal tissue architecture.

Sample C showed chronic inflammatory granulation tissue formation with the presence of lymphocytes and plasma cells. On a microscopic level, tissue appeared as a highly vascularized and cellular tissue, with a loose and disorganized extracellular matrix. The tissue was composed of a variety of cell types, including fibroblasts, myofibroblasts, macrophages, neutrophils, and lymphocytes. Fibroblasts were responsible for producing collagen, which provided structural support to the wound, while myofibroblasts were specialized fibroblasts that could contract and were found to be in the middle of the reparative tissue. Macrophages were involved in the clearance of dead cells and debris, which were observed in the sub-peripheral region and

secreted growth factors that promoted tissue regeneration. Both monomorphic and polymorphic cell populations were seen to be infiltrated peripheral areas and moderately populated.

In control, mild chronic inflammatory cell infiltrate was noted along with mild fibroblast proliferation, and a focal area of necrosis was also seen. The inflammatory response in subcutaneous tissue was characterized by localized fluid accumulation preceding degenerative changes, although the extent of tissue damage and inflammation was limited. The presence of a limited number of inflammatory cells, especially the monomorphic population, which was distributed roughly in the lesion on histologic examination, was consistent with a mild inflammatory response. The desmoplastic reaction was noted by fibrocystic hyperplasia with spindle-shaped nuclei having moderate production of collagen surrounding the lesion.

3.3.6 Discussion

The development of tissue engineering techniques has cleared the path for the use of newly grown tissues in the treatment of a wide range of human health problems[71]. The Scaffold is the central part of tissue engineering, functioning both as a cell reservoir and a support system[72]. Though effective standards for these biomaterials have not been well-articulated for a long time, the necessity for biodegradability and prior FDA clearance for use in medical devices has dominated the material selection process[73]. Despite advances in scaffold construction techniques, significant challenges related to the immunogenicity, biocompatibility, and biodegradability of synthetic materials exist[74]. The solution to this pressing issue may be found in nature, specifically in the utilization of natural products as a scaffold for tissue engineering through the application of appropriate engineering techniques. In this study, we explore a natural product-based scaffold fabrication strategy for use in tissue engineering. Keeping the concept of circular economy and sustainability in mind, an all-natural product-based material has been fabricated. Starch is an important polysaccharide that the human body needs. This naturally abundant polymer is biocompatible and inexpensive, making it a promising candidate for use in tissue engineering[75]. Gelatin, on the other hand, is a denatured collagen-based protein that is biocompatible, biodegradable, non-immunogenic, non-toxic, and inexpensive[76,77]. Since both starch and gelatin are extremely hydrophilic, starch-based scaffolds were crosslinked to provide the best possible swelling and degradation properties. Three different compositions were prepared for different testing. The inclusion of Draksha Beeja from Inlife (Grape Seed Extract) worked dually: the phytochemicals present in

grape seed extract (95% Proanthocyanidins) acted as an anti-oxidant which would help in cellular proliferation, and on the other hand, Proanthocyanidins is also reported as a crosslinking agent that helped in crosslinking Starch and Gelatin naturally which any use of toxic chemicals. Morphological characterization of the Mats showed a smooth surface along with the presence of pores. Sample B showed a good porous structure along with large micropores. The scaffolds' porosity and microstructure reduce the mass transmission limitations, allowing enough nutrition and oxygen passage across the scaffold to affect cellular permeation and promote healthy cellular migration and regeneration[78]. Smaller pores allow for a more uniform distribution of nutrients over the scaffold, but their reduced surface area hampers cellular adhesion[79]. Here AFM data points out the large surface area of the scaffolds. All three Mats showed superior biocompatibility. MTT assay data revealed that all the Mats were capable of holding the cells, thus qualifying for being a proper scaffold. Over time, L929 cells were seen to attach and adhere effectively to the surface of all three Mats. Surface topography and substrate morphology are two particularly important aspects of biomaterials that affect how cells respond to them [80]. Importantly, microfibers' surface qualities determine whether fibroblast cells adhere and spread over the material [81]. Fibroblasts are known to prefer a hydrophilic and flat surface for optimal proliferation [82]. For this reason, L929 cells adhered well to and multiplied in abundance on a Gelatin and Starch-based medium. Hydrophilic substances, including gelatin and starch, and Proanthocyanidin [83], stimulated cell proliferation. The pours structure of the Mats, high surface-to-volume ratio owing to the formation of microstructure, and superior wettability all contributed to their efficacy as a medium for cell contact and proliferation. In terms of cellular proliferation, Sample B fared the best. In-vivo study also pointed to the biocompatibility of the Mats. Mat B and C exhibited complete degradation in 14 days and Mat A showed around 80% degradation. Degradation in a biological system is an important factor in Tissue Engineering. The period of 14 days is highly crucial as after tissue defect the fibroblast growth and tissue modeling start during this time point [84]. Thus, the scaffold would support the full fibroblast growth phase in any tissue reconstruction. Work with gelatin and starch is mostly limited to food packaging with very little focus on biocompatibility or biomedical application (Table 3.3), but this work extends further to the use of composite Mats for Biomedical applications.

Table 3.3: Details of Gelatin and starch-based MATS used for different applications (Some recent studies)

Materials used	Bio-Compatibility Assay or Test related to Biomedical Application	Application	Discussion	Reference
Native corn starch, native waxy corn starch, modified waxy corn starch, Gelatin type A, glycerol, sorbitol.	No such Study performed	The coating on refrigerated grapes	No Crosslinking agent was used, and no studies pointed to the Mats' biocompatibility.	[85]
Native manioc starch, acetylated and crosslinked manioc starch, Gelatin type A, glycerol, sorbitol	No such Study performed	Edible packaging	The use of natural plasticizers was indicated, with no indication of the biocompatibility of the films.	[86]
Cassava Starch powder, bovine gelatin glycerol, liquid sorbitol, Essential oil fennel, Nano TiO2, AbbasAli pistachio cultivar.	No Such Data was found	Novel packaging for raw fresh pistachio	Samples 3% FEO/5% Nano TiO2 were selected as the best sample for bio packaging, but no data was indicated regarding the biocompatibility of the films. Apart from this, there was no indication of further studies.	[87]
Gelatin, waxy starch, sodium periodate hydrochloric acid, glycerol.	No Data related to biomedical applications was found.	Packaging material in the food industry	The composite film was well characterized phytochemically and improved food shelf life and quality, although proper biological characterization	[88]

			was not indicated in the work.	
Furcellaran, local potato starch, gelatin, lavender essential oil S/F/G – Starch/ Furcellaran/ Gelatin OEL – Lavender Essential Oil	S/F/G films with OEL showed anti-oxidant and antimicrobial ability, which is an advantage to retard the oxidation reaction in food and can be used for prolonging the shelf life of packed foods	Food packaging material	The use of films containing S/F/G with OEL in food, preservation could be limited because of their physical properties, such as high values of solubility and low values of tensile strength The higher value of solubility of S/F/G films with OEL is disadvantageous for their application in foods with high water content.	[89]
Cassava starch, Sodium hydroxide, glacial acetic acid, gelatin extract from chickens, glycerol.	Test not done	Food packaging material	Overall no data was presented showing the prospect of the material being used as Biomaterials or in Tissue Engineering approaches.	[90]
Commercial cassava starch, Recycled gelatin, commercial glycerol.	No such biological test was investigated.	Packaging material instead of plastic	The work majorly focused on the characterization of the composite material without any indication related to its biocompatibility or any other biological properties.	[59]
Food-grade potato starch, citric acid, lithium chloride,	A primary Biodegradation study was done	Food packaging material	The composite film showed the possibility of	[91]

potassium acetate, magnesium chloride ammonium nitrate, magnesium nitrate, sodium chloride, potassium chloride gelatin, sorbitol.			being utilized as an eco-friendly composite films for food packaging and coating in the future. The study is majorly a basic fabrication and characterization-based study with no indication of its biocompatibility.	
Corn starch, citric acid, calcium chloride, gelatin, sorbitol.	Test not done	Coating material for fruits and vegetables	The composite films/coatings exhibited that coating materials potentially enhanced the shelf life of cucumbers, although their biocompatibility was not evaluated.	[92]

The brief literature review points out that most of the work done using gelatin and Starch was used majorly for food packing. This work would open a new horizon of using gelatin and starch-based mats for biomedical applications.

It is up to the future generation to make sustainability a mainstream topic of conversation [93], and it is the responsibility of the older generation to make clear the significance of the management of goods and existing resources in determining the quality of life for both the current and future generations [94]. So, understanding the results of a project isn't the only thing that's important after it's done. It's also important to evaluate and keep track of a series of actions that can lead to new research in the future, such as expanding and creating scenarios that help people learn more about how design affects different fields of knowledge and the great benefits that can be gained. In conclusion, the most important and fundamental suggestion of this study is to find new ways to ensure that information about sustainability, circular economy, and sustainable development pervades all demographics and communities around the globe [95]. This includes people of all ages and backgrounds.

This polymeric scaffold indeed showed various promising properties to qualify to be used in future tissue engineering, but few modifications and further study could make it closer to the goal. The degradability of the scaffold in the biological system should be tailored to support tissue growth for a longer time. The inclusion of some FDA-approved synthetic polymer could be thought of to attain the goal. A further detailed study could be done at the cellular level as well as organ-specific in-vivo could be carried out to evaluate the proper function of these polymeric biomaterials.

3.4 Inference

Herein, we developed a mat or film-like structure composed of starch, gelatin, and Draksha beeja extract (Grape seed extract). Detailed characterization of the film indicated that the phytochemicals from the extract would have played a key role in the cross-linking of the biopolymers. The film is also found to have a rough surface with macropores and was found to be hydrophilic in nature. The hemocompatibility assay indicated no blood toxicity and more than 80 % cell viability was noted for all the 3 Mats. In-vivo testing showed high biocompatibility and no toxic reactions. The mats degraded after 14 days, promoted cellular proliferation, and accelerated wound healing based on histological examinations. Most importantly, these films would be very effective for use as in-vivo tissue engineering scaffolds as they showed almost 100% cellular viability and thermo-mechanically resembled that of some soft tissues. Thus, it could be inferred that the fabrication of the gelatin and starch-based Mats loaded with Draksha Beeja Extract could pave the way towards sustainable tissue engineering using different food or non-food wastes with bioactive ingredients and hold immense potential in biomedical applications. This initial study although pointed various aspects of sustainability in biomaterials with the use of completely natural product,but the material fabricated had a lot of drawbacks like fast degradation, low structural stability and mechanical stability. Thus in the following work, we would first try to extract grape seed directly from the waste thus promoting a circular economy and finally fabricating a sustainable material using that grape seed extract and finally evaluating its effect on inflammatory cytokines hence nullifying the effect of dysregulated GSK-3β.

References

[1]   B.D. Ratner, A.S. Hoffman, F.J. Schoen, J.E. Lemons, Biomaterials science: an introduction to materials in medicine, Chemical Engineering (2004) 26.

[2]   A. Koyyada, P. Orsu, Natural gum polysaccharides as efficient tissue engineering and drug delivery biopolymers, J Drug Deliv Sci Technol 63 (2021) 102431.

[3]   P.X. Am, Scaffolds for tissue fabrication, 5th World Congress: Enabling Technologies and New Markets, Nanocomposites 2005 7 (2005) 30–40.

[4]   L. Moroni, T. Boland, J.A. Burdick, C. De Maria, B. Derby, G. Forgacs, J. Groll, Q. Li, J. Malda, V.A. Mironov, C. Mota, M. Nakamura, W. Shu, S. Takeuchi, T.B.F. Woodfield, T. Xu, J.J. Yoo, G. Vozzi, Biofabrication: A Guide to Technology and Terminology, Trends Biotechnol 36 (2018) 384–402. https://doi.org/10.1016/j.tibtech.2017.10.015.

[5]   H. Jahangirian, E.G. Lemraski, R. Rafiee-Moghaddam, T.J. Webster, A review of using green chemistry methods for biomaterials in tissue engineering, Int J Nanomedicine 13 (2018) 5953–5969. https://doi.org/10.2147/IJN.S163399.

[6]   G.M. Fortunato, F. Da Ros, S. Bisconti, A. De Acutis, F. Biagini, A. Lapomarda, C. Magliaro, C. De Maria, F. Montemurro, D. Bizzotto, P. Braghetta, G. Vozzi, Electrospun structures made of a hydrolyzed keratin-based biomaterial for development of in vitro tissue models, Front Bioeng Biotechnol 7 (2019) 174. https://doi.org/10.3389/fbioe.2019.00174.

[7]   X.C. Yin, F.Y. Li, Y.F. He, Y. Wang, R.M. Wang, Study on effective extraction of chicken feather keratins and their films for controlling drug release, Biomater Sci 1 (2013) 528–536. https://doi.org/10.1039/c3bm00158j.

[8]   S.C. Wu, H.K. Tsou, H.C. Hsu, S.K. Hsu, S.P. Liou, W.F. Ho, A hydrothermal synthesis of eggshell and fruit waste extract to produce nanosized hydroxyapatite, Ceram Int 39 (2013) 8183–8188. https://doi.org/10.1016/j.ceramint.2013.03.094.

[9]   E.M. Rivera, M. Araiza, W. Brostow, V.M. Castaño, J.R. Díaz-Estrada, R. Hernández, J.R. Rodríguez, Synthesis of hydroxyapatite from eggshells, Mater Lett 41 (1999) 128–134. https://doi.org/10.1016/S0167-577X(99)00118-4.

[10]   A. Lapomarda, A. De Acutis, I. Chiesa, G.M. Fortunato, F. Montemurro, C. De Maria, M. Mattioli Belmonte, R. Gottardi, G. Vozzi, Pectin-GPTMS-Based Biomaterial: Toward a Sustainable Bioprinting of 3D scaffolds for Tissue Engineering Application, Biomacromolecules 21 (2020) 319–327. https://doi.org/10.1021/acs.biomac.9b01332.

[11]   D. Fouad, M. Farag, Design for Sustainability with Biodegradable Composites, in: Design and Manufacturing, IntechOpen, 2020: pp. 1–7. https://doi.org/10.5772/intechopen.88425.

[12]   Y. Zhao, Y. Qiu, H. Wang, Y. Chen, S. Jin, S. Chen, Preparation of Nanofibers with Renewable Polymers and Their Application in Wound Dressing, Int J Polym Sci 2016 (2016). https://doi.org/10.1155/2016/4672839.

[13]   S. Malik, S. Sundarrajan, T. Hussain, A. Nazir, M. Ayyoob, F. Berto, S. Ramakrishna, Sustainable nanofibers in tissue engineering and biomedical applications, Material Design and Processing Communications 3 (2021) e202. https://doi.org/10.1002/mdp2.202.

[14]   H. Duan, G. Song, S. Qu, X. Dong, M. Xu, Post-consumer packaging waste from express delivery in China, Resour Conserv Recycl 144 (2019) 137–143.

[15]   N. Khatoon, A. Jamal, M.I. Ali, Lignin peroxidase isoenzyme: a novel approach to biodegrade the toxic synthetic polymer waste, Environ Technol 40 (2019) 1366–1375.

[16]   R. Dziuba, M. Kucharska, L. Madej-Kiełbik, K. Sulak, M. Wiśniewska-Wrona, Biopolymers and Biomaterials for Special Applications within the Context of the Circular Economy, Materials 14 (2021) 7704.

[17]   B.M. Size, Share, Analysis$\backslash$Industry Report, 2027, (2020).

[18]   T. Hyeon, L. Manna, S.S. Wong, Sustainable nanotechnology, Chem Soc Rev 44 (2015) 5755–5757. https://doi.org/10.1039/c5cs90072g.

[19]   B.S. Kim, D.J. Mooney, Development of biocompatible synthetic extracellular matrices for tissue engineering, Trends Biotechnol 16 (1998) 224–230. https://doi.org/10.1016/S0167-7799(98)01191-3.

[20]   C. Balaceanu, D.M. Tilea, D. Penu, others, Perspectives on Eco Economics. Circular Economy and Smart Economy, Academic Journal of Economic Studies 3 (2017) 105–109.

[21]   C. Antoine, S. Aránguiz, C. Montt, Formación para el Diseño Social. Percepciones y expectativas entre los estudiantes de la Facultad de Diseño de la Universidad del Pac{\'\i}fico, Chile, Cuadernos Del Centro de Estudios En Diseño y Comunicación. Ensayos (2018) 1–6.

[22]   A. Aguilar, T. Twardowski, R. Wohlgemuth, Bioeconomy for sustainable development, Biotechnol J 14 (2019) 1800638.

[23]   A.K. Lynn, I. V. Yannas, W. Bonfield, Antigenicity and immunogenicity of collagen, J Biomed Mater Res B Appl Biomater 71 (2004) 343–354. https://doi.org/10.1002/jbm.b.30096.

[24]   G.D. Mogoşanu, A.M. Grumezescu, Natural and synthetic polymers for wounds and burns dressing, Int J Pharm 463 (2014) 127–136. https://doi.org/10.1016/j.ijpharm.2013.12.015.

[25]   S. Afewerki, A. Sheikhi, S. Kannan, S. Ahadian, A. Khademhosseini, Gelatin-polysaccharide composite scaffolds for 3D cell culture and tissue engineering: Towards natural therapeutics, Bioeng Transl Med 4 (2019) 96–115. https://doi.org/10.1002/btm2.10124.

[26]   A. Alissandratos, P.J. Halling, Enzymatic acylation of starch, Bioresour Technol 115 (2012) 41–47. https://doi.org/10.1016/j.biortech.2011.11.030.

[27]   F. Mirab, M. Eslamian, R. Bagheri, Fabrication and characterization of a starch-based nanocomposite scaffold with highly porous and gradient structure for bone tissue engineering, Biomed Phys Eng Express 4 (2018) 55021. https://doi.org/10.1088/2057-1976/aad74a.

[28]   P. Basak, P. Pahari, P. Das, N. Das, S.K. Samanta, S. Roy, Synthesis and Characterisation of Gelatin-PVA/Hydroxyapetite(HAP) Composite for Medical Applications, in: IOP Conf Ser Mater Sci Eng, 2018: p. 12021. https://doi.org/10.1088/1757-899X/410/1/012021.

[29]   P. Das, S. Manna, A.K. Behera, M. Shee, P. Basak, A.K. Sharma, Current synthesis and characterization techniques for clay-based polymer nano-composites and its biomedical

applications: A review, Environ Res 212 (2022) 113534.
https://doi.org/10.1016/j.envres.2022.113534.

[30]   S. Datta, R. Sarkar, V. Vyas, S. Bhutoria, A. Barui, A. Roy Chowdhury, P. Datta, Alginate-honey
        bioinks with improved cell responses for applications as bioprinted tissue engineered
        constructs, J Mater Res 33 (2018) 2029–2039. https://doi.org/10.1557/jmr.2018.202.

[31]   P. Basak, P. Das, S. Biswas, N.C. Biswas, G.K. Das Mahapatra, Green Synthesis and
        Characterization of Gelatin-PVA Silver Nanocomposite Films for Improved Antimicrobial
        Activity, in: IOP Conf Ser Mater Sci Eng, 2018. https://doi.org/10.1088/1757-
        899X/410/1/012019.

[32]   K. Ghosal, U. Bhattacharjee, K. Sarkar, Facile green synthesis of bioresorbable polyester from
        soybean oil and recycled plastic waste for osteochondral tissue regeneration, Eur Polym J 122
        (2020) 109338. https://doi.org/10.1016/j.eurpolymj.2019.109338.

[33]   M.F. Ismail, M.A. Islam, B. Khorshidi, A. Tehrani-Bagha, M. Sadrzadeh, Surface characterization
        of thin-film composite membranes using contact angle technique: Review of quantification
        strategies and applications, Adv Colloid Interface Sci 299 (2022) 102524.
        https://doi.org/10.1016/j.cis.2021.102524.

[34]   E.R. Hahm, Y.S. Gho, S. Park, C. Park, K.W. Kim, C.H. Yang, Synthetic curcumin analogs inhibit
        activator protein-1 transcription and tumor-induced angiogenesis, Biochem Biophys Res
        Commun 321 (2004) 337–344. https://doi.org/10.1016/j.bbrc.2004.06.119.

[35]   B. Subramanian, A.P. Rameshbabu, K. Ghosh, P.K. Jha, R. Jha, S. Murugesan, S. Chattopadhyay,
        S. Dhara, K.C. Mondal, P. Basak, S.K. Guha, Impact of styrene maleic anhydride (SMA) based
        hydrogel on rat fallopian tube as contraceptive implant with selective antimicrobial property,
        Materials Science and Engineering: C 94 (2019) 94–107.
        https://doi.org/https://doi.org/10.1016/j.msec.2018.09.023.

[36]   M.V. Fedorchak, J. Krawiec, S.R. Little, K. Lorentz, D.A. Vorp, J. Weinbaum, Artificial Cells and
        Delivery Devices for Use in Tissue Engineering, and Related Methods, (2019).

[37]   P. Das, T. Dutta, S. Manna, S. Loganathan, P. Basak, Facile green synthesis of non-genotoxic,
        non-hemolytic organometallic silver nanoparticles using extract of crushed, wasted, and spent
        Humulus lupulus (hops): Characterization, anti-bacterial, and anti-cancer studies, Environ Res
        204 (2022) 111962. https://doi.org/10.1016/j.envres.2021.111962.

[38]   Z. Shen, C. Kang, J. Chen, D. Ye, S. Qiu, S. Guo, Y. Zhu, Surface modification of polyurethane
        towards promoting the ex vivo cytocompatibility and in vivo biocompatibility for
        hypopharyngeal tissue engineering, J Biomater Appl 28 (2013) 607–616.
        https://doi.org/10.1177/0885328212468184.

[39]   I. Chakraborty, C.M. Hossain, P. Basak, Synthesis and characterization of ester-diol based
        polyurethane: a potentiality check for hypopharyngeal tissue engineering application, Biomed
        Eng Lett 11 (2021) 25–37. https://doi.org/10.1007/s13534-020-00180-7.

[40]   B. Zhang, S. Dhital, E. Haque, M.J. Gidley, Preparation and characterization of gelatinized
        granular starches from aqueous ethanol treatments, Carbohydr Polym 90 (2012) 1587–1594.
        https://doi.org/10.1016/j.carbpol.2012.07.035.

[41]   A. Nikolaidis, T. Moschakis, On the reversibility of ethanol-induced whey protein denaturation, Food Hydrocoll 84 (2018) 389–395. https://doi.org/10.1016/j.foodhyd.2018.05.051.

[42]   A. Sholtei, M. Takanori, N. Tomoaki, Effects of pH and Salt Concentration on the Precipitability of Gelatin with Ethanol, The Journal of Photographic Science 43 (1995) 108–111. https://doi.org/10.1080/00223638.1995.11738629.

[43]   F. Hofmeister, Zur Lehre von der Wirkung der Salze - Zweite Mittheilung, Archiv Für Experimentelle Pathologie Und Pharmakologie 24 (1888) 247–260. https://doi.org/10.1007/BF01918191.

[44]   Y. Tai, J. Shen, Y. Luo, H. Qu, X. Gong, Research progress on the ethanol precipitation process of traditional Chinese medicine, Chin Med 15 (2020) 1–17.

[45]   S. Kim, M.E. Nimni, Z. Yang, B. Han, Chitosan/gelatin-based films crosslinked by proanthocyanidin, J Biomed Mater Res B Appl Biomater 75 (2005) 442–450. https://doi.org/10.1002/jbm.b.30324.

[46]   D.H. Lee, Y. Arisaka, A. Tonegawa, T.W. Kang, A. Tamura, N. Yui, Cellular orientation on repeatedly stretching gelatin hydrogels with supramolecular cross-linkers, Polymers (Basel) 11 (2019) 2095.

[47]   L. Ramaglia, L. Postiglione, G. di Spigna, G. Capece, S. Salvatore, G. Rossi, Sandblasted-acid-etched titanium surface influences in vitro the biological behavior of SaOS-2 human osteoblast-like cells, Dent Mater J 30 (2011) 183–192. https://doi.org/10.4012/dmj.2010-107.

[48]   H.-I. Chang, Y. Wang, Cell Responses to Surface and Architecture of Tissue Engineering Scaffolds, in: Regenerative Medicine and Tissue Engineering - Cells and Biomaterials, InTechOpen, 2011. https://doi.org/10.5772/21983.

[49]   J. Rydz, A. Šišková, A. Andicsová Eckstein, Scanning electron microscopy and atomic force microscopy: Topographic and dynamical surface studies of blends, composites, and hybrid functional materials for sustainable future, Advances in Materials Science and Engineering 2019 (2019).

[50]   Y.S. Lai, W.C. Chen, C.H. Huang, C.K. Cheng, K.K. Chan, T.K. Chang, The effect of graft strength on knee laxity and graft in-situ forces after posterior cruciate ligament reconstruction, PLoS One 10 (2015) e0127293. https://doi.org/10.1371/journal.pone.0127293.

[51]   A. Karimi, W.M.A. Wan Daud, Comparison the properties of PVA/Na+-MMT nanocomposite hydrogels prepared by physical and physicochemical crosslinking, Polym Compos 37 (2016) 897–906. https://doi.org/10.1002/pc.23248.

[52]   S. Ono, R. Imai, Y. Ida, D. Shibata, T. Komiya, H. Matsumura, Increased wound pH as an indicator of local wound infection in second degree burns, Burns 41 (2015) 820–824. https://doi.org/10.1016/j.burns.2014.10.023.

[53]   D. Das, Z. Zhang, T. Winkler, M. Mour, C. Gunter, M. Morlock, H.G. Machens, A.F. Schilling, Bioresorption and degradation of biomaterials., Adv Biochem Eng Biotechnol 126 (2012) 317–333. https://doi.org/10.1007/10_2011_119.

[54]   N.L. Davison, F. Barrère-de Groot, D.W. Grijpma, Degradation of Biomaterials, Tissue Engineering: Second Edition (2014) 177–215. https://doi.org/10.1016/B978-0-12-420145-3.00006-7.

[55]   P. Dwivedi, P.K. Mishra, M.K. Mondal, N. Srivastava, Non-biodegradable polymeric waste pyrolysis for energy recovery, Heliyon 5 (2019) e02198.

[56]   R. Chatterjee, B. Sajjadi, W.-Y. Chen, D.L. Mattern, N. Hammer, V. Raman, A. Dorris, Effect of pyrolysis temperature on physicochemical properties and acoustic-based amination of biochar for efficient CO2 adsorption, Front Energy Res 8 (2020) 85.

[57]   C. Zhang, L. Chao, Z. Zhang, L. Zhang, Q. Li, H. Fan, S. Zhang, Q. Liu, Y. Qiao, Y. Tian, others, Pyrolysis of cellulose: Evolution of functionalities and structure of bio-char versus temperature, Renewable and Sustainable Energy Reviews 135 (2021) 110416.

[58]   M. Pigłowska, B. Kurc, Ł. Rymaniak, P. Lijewski, P. Fuć, Kinetics and thermodynamics of thermal degradation of different starches and estimation the OH group and H2O content on the surface by TG/DTG-DTA, Polymers (Basel) 12 (2020) 357.

[59]   N.M. da Silva, F.M. Fakhouri, R.L.L. Fialho, E.C. de M. Cabral Albuquerque, Starch--recycled gelatin composite films produced by extrusion: physical and mechanical properties, J Appl Polym Sci 135 (2018) 46254.

[60]   K. Wang, W. Wang, R. Ye, J. Xiao, Y. Liu, J. Ding, S. Zhang, A. Liu, Mechanical and barrier properties of maize starch--gelatin composite films: Effects of amylose content, J Sci Food Agric 97 (2017) 3613–3622.

[61]   K. Villalobos, H. Rojas, R.J. González Paz, D. Brenes Granados, J. González Mas\'\is, J. Vega Baudrit, Y.R. Corrales Ureña, Production of starch films using propolis nanoparticles as novel bioplasticizer, (2017).

[62]   I.A. Channa, J. Ashfaq, M.A. Siddiqui, A.D. Chandio, M.A. Shar, A. Alhazaa, Multi-Shaded Edible Films Based on Gelatin and Starch for the Packaging Applications, Polymers (Basel) 14 (2022) 5020.

[63]   A. Salerno, M. Oliviero, E. Di Maio, S. Iannace, Thermoplastic foams from zein and gelatin, International Polymer Processing 22 (2007) 480–488. https://doi.org/10.3139/217.2065.

[64]   P. Liu, L. Yu, H. Liu, L. Chen, L. Li, Glass transition temperature of starch studied by a high-speed DSC, Carbohydr Polym 77 (2009) 250–253. https://doi.org/10.1016/j.carbpol.2008.12.027.

[65]   S. Kim, M.E. Nimni, Z. Yang, B. Han, Chitosan/gelatin-based films crosslinked by proanthocyanidin, J Biomed Mater Res B Appl Biomater 75 (2005) 442–450. https://doi.org/10.1002/jbm.b.30324.

[66]   K. Pal, A.K. Banthia, D.K. Majumdar, Biomedical evaluation of polyvinyl alcohol-gelatin esterified hydrogel for wound dressing, J Mater Sci Mater Med 18 (2007) 1889–1894. https://doi.org/10.1007/s10856-007-3061-2.

[67]   F.N. Parin, P. Terzioğlu, Y. Sicak, K. Yildirim, M. Öztürk, Pine honey–loaded electrospun poly (vinyl alcohol)/gelatin nanofibers with antioxidant properties, Journal of the Textile Institute 112 (2021) 628–635. https://doi.org/10.1080/00405000.2020.1773199.

[68]   D. Song, D. Yang, C.A. Powell, X. Wang, Cell--cell communication: old mystery and new opportunity, Cell Biol Toxicol 35 (2019) 89–93.

[69] A.M. Elbarbary, N.M. El-Sawy, Radiation synthesis and characterization of polyvinyl alcohol/chitosan/silver nanocomposite membranes: antimicrobial and blood compatibility studies, Polymer Bulletin 74 (2017) 195–212. https://doi.org/10.1007/s00289-016-1708-1.

[70] D. Augustine, R.S. Rao, S. Patil, Hyalinization as a histomorphological risk predictor in oral pathological lesions, J Oral Biol Craniofac Res 11 (2021) 415–422.

[71] J.R. Jones, Scaffolds for tissue engineering, Biomaterials, Artificial Organs and Tissue Engineering 14 (2005) 201–214. https://doi.org/10.1533/9781845690861.4.201.

[72] A.J. Janvier, Characterising Load-Induced Changes in 3D Cultured Mesenchymal Stem Cells Through Collagen Isoform Composition and Arrangement, The University of Liverpool (United Kingdom), 2021.

[73] D.F. Williams, Challenges With the Development of Biomaterials for Sustainable Tissue Engineering, Front Bioeng Biotechnol 7 (2019). https://doi.org/10.3389/fbioe.2019.00127.

[74] F.M. Chen, X. Liu, Advancing biomaterials of human origin for tissue engineering, Prog Polym Sci 53 (2016) 86–168. https://doi.org/10.1016/j.progpolymsci.2015.02.004.

[75] M. Jin, J. Shi, W. Zhu, H. Yao, D.A. Wang, Polysaccharide-Based Biomaterials in Tissue Engineering: A Review, Tissue Eng Part B Rev 27 (2021) 604–626. https://doi.org/10.1089/ten.teb.2020.0208.

[76] R. Chhabra, V. Peshattiwar, T. Pant, A. Deshpande, D. Modi, S. Sathaye, A. Tibrewala, S. Dyawanapelly, R. Jain, P. Dandekar, In Vivo Studies of 3D Starch-Gelatin Scaffolds for Full-Thickness Wound Healing, ACS Appl Bio Mater 3 (2020) 2920–2929. https://doi.org/10.1021/acsabm.9b01139.

[77] S. Petros, T. Tesfaye, M. Ayele, A Review on Gelatin Based Hydrogels for Medical Textile Applications, Journal of Engineering (United Kingdom) 2020 (2020). https://doi.org/10.1155/2020/8866582.

[78] M. Abedin Zadeh, M. Khoder, A.A. Al-Kinani, H.M. Younes, R.G. Alany, Retinal cell regeneration using tissue engineered polymeric scaffolds, Drug Discov Today 24 (2019) 1669–1678. https://doi.org/10.1016/j.drudis.2019.04.009.

[79] A. Marques, G. Miranda, F. Silva, P. Pinto, Ó. Carvalho, Review on current limits and potentialities of technologies for biomedical ceramic scaffolds production, J Biomed Mater Res B Appl Biomater 109 (2021) 377–393. https://doi.org/10.1002/jbm.b.34706.

[80] F. Liu, J. Xu, L. Wu, T. Zheng, Q. Han, Y. Liang, L. Zhang, G. Li, Y. Yang, The Influence of the Surface Topographical Cues of Biomaterials on Nerve Cells in Peripheral Nerve Regeneration: A Review, Stem Cells Int 2021 (2021). https://doi.org/10.1155/2021/8124444.

[81] Y. Jiao, X. Li, J. Chen, C. Li, L. Liu, X. Liu, F. Wang, G. Chen, L. Wang, Constructing Nanoscale Topology on the Surface of Microfibers Inhibits Fibroblast Fibrosis, Advanced Fiber Materials 4 (2022) 1219–1232. https://doi.org/10.1007/s42765-022-00165-4.

[82] M. Jurak, A.E. Wiącek, A. Ładniak, K. Przykaza, K. Szafran, What affects the biocompatibility of polymers?, Adv Colloid Interface Sci 294 (2021) 102451. https://doi.org/10.1016/j.cis.2021.102451.

[83] D. Wang, Z. Du, F. Mighri, Z. Xu, L. Wang, Z. Zhang, Proanthocyanidins Promote Endothelial Cell Viability and Angiogenesis, J Cardiovasc Pharmacol 79 (2022) 719–729. https://doi.org/10.1097/FJC.0000000000001231.

[84] S. Ather, K.G. Harding, S.J. Tate, Wound management and dressings, in: S. Rajendran (Ed.), Advanced Textiles for Wound Care, Second Edi, Woodhead Publishing, 2019: pp. 1–22. https://doi.org/10.1016/b978-0-08-102192-7.00001-1.

[85] F.M. Fakhouri, S.M. Martelli, T. Caon, J.I. Velasco, L.H.I. Mei, Edible films and coatings based on starch/gelatin: Film properties and effect of coatings on quality of refrigerated Red Crimson grapes, Postharvest Biol Technol 109 (2015) 57–64.

[86] F.M. Fakhouri, S.M. Martelli, L.C. Bertan, F. Yamashita, L.H.I. Mei, F.P.C. Queiroz, Edible films made from blends of manioc starch and gelatin--Influence of different types of plasticizer and different levels of macromolecules on their properties, LWT 49 (2012) 149–154.

[87] N. Chavoshi, M.M. Marvizadeh, N. Fallah, N. Rezaei-savadkouhi, A. Mohammadi Nafchi, Application of Novel Nano-biopackaging Based on Cassava Starch/Bovine Gelatin/Titanium oxide nanoparticle/Fennel Essential Oil to Improve Quality of the Raw Fresh Pistachio, Journal of Nuts 14 (2023) 19–31.

[88] P. Wang, Y. Wang, P. Hong, C. Zhou, Di-aldehyde starch crystal: A novel bio-crosslinker for strengthening the structure and physio-chemical properties of gelatin-based films, Food Biosci 43 (2021) 101308.

[89] E. Jamróz, L. Juszczak, M. Kucharek, Investigation of the physical properties, antioxidant and antimicrobial activity of ternary potato starch-furcellaran-gelatin films incorporated with lavender essential oil, Int J Biol Macromol 114 (2018) 1094–1101.

[90] J.I. Castro, D.P. Navia-Porras, J.A. Arbeláez Cortés, J.H. Mina Hernández, C.D. Grande-Tovar, Synthesis, characterization, and optimization studies of starch/chicken gelatin composites for food-packaging applications, Molecules 27 (2022) 2264.

[91] R. Kumar, G. Ghoshal, M. Goyal, Synthesis and functional properties of gelatin/CA--starch composite film: excellent food packaging material, J Food Sci Technol 56 (2019) 1954–1965.

[92] R. Kumar, G. Ghoshal, M. Goyal, Biodegradable composite films/coatings of modified corn starch/gelatin for shelf life improvement of cucumber, J Food Sci Technol 58 (2021) 1227–1237.

[93] H.N.J. Schifferstein, Changing food behaviors in a desirable direction, Curr Opin Food Sci 33 (2020) 30–37.

[94] B. Hricova, H. Nakatova, M. Badida, Principles of design for the life-cycle, in: Ann. DAAAM Proc. Int. DAAAM Symp, 2011: pp. 165–166.

[95] A.A. Zorpas, Sustainability behind sustainability, Nova Publishers, 2014.

Chapter IV

Development of winery waste-derived Proanthocyanidin-Rich Grape Seed Extract-Based Gel for Modulating Inflammatory Responses in Wound Healing

4.1 Background

"The *Grapes are sour*" is a famous idiom adopted from the Greek writer Aesop's famous fable about a fox that cannot reach some grapes on a tall vine and declares that they are sour[1]. From stories to science, grapes (*Vitis vinifera*) have always been in discussion for ages. Grapes are rich in phytochemicals and have high nutritional value, so it is widely used in our daily lives for their health-beneficial properties. The use of grapes ranges from the wine industry to the food industry, and not only that, grapes play a significant role in pharmaceuticals [2]. In addition, grapes are rich sources of polyphenols, vitamins, and minerals[3]. Grape seeds are even good polyphenols and are also used as a rich source of proanthocyanidins[4]. Therefore, grape seed extracts are being commercially sold in markets for their health benefits property. Grape Seed extracts are super-rich antioxidants, including phenolic acids, anthocyanins, flavonoids & oligomeric proanthocyanidins complexes (OPCs), providing 360-degree health benefits [4]. These extracts are primarily used for their anti-inflammatory and antioxidant activity. In addition, regular uptake of these extracts may boost the body's overall immunity. Due to the presence of various phytochemicals, proanthocyanidin-rich grape seed extracts could play a significant role in curing various diseases and supporting multiple health issues. Recently Grape seed proanthocyanidins have gained substantial attention owing to their extensive range of biological and pharmacological properties [5]. Although research indicates that around 75% of global grape output goes toward the wine business[6].

Wine business is financially profitable[7–9]. The public has not looked down on the business because of the large amounts of garbage it produces, the significant quantity of water resources it uses, or the extensive amount of land it occupies. Because of this, it has flourished, leading to increased garbage production[10].

Recycling food, energy, synthetic materials, and chemicals will be a major trend in the next decade as people seek out more eco-friendly ways of doing things. One of the most important steps in developing sustainable energy sources is finding creative ways to recycle and reuse materials, such as biochemical wastes for medical purposes[11][12].

Grape seeds are widely used in various disease models, from cancers to cardiovascular diseases[13,14]. Some studies also showed its potential as a wound-healing agent[15–17] , but only a few studies are done at the cellular level in-vitro, and the molecular mechanism of these proanthocyanidin-based extracts in wound healing yet needs much attention.

Wounds are life-threatening physiological conditions. Wound healing process is the mending of skin or soft tissue injuries[18].

Chronic wounds do not heal despite receiving adequate and proper treatment. Managing such wounds is not an easy task. Debridement, irrigation, antibiotics, tissue grafts, and proteolytic enzymes are currently utilized to treat chronic wounds[19,20]; however, they all have significant limitations and unpleasant side effects. In the era of natural treatment, scientists are finding alternatives to treat various diseases without any major side effects[21].

Topical, systemic, and antibacterial treatments help heal surgical and traumatic wounds [22]. These topicals may cause oversensitivity, resistance, and re-epithelialization[23,24]. Thus, several treatments are under investigation. Plant remedies help heal wounds. Grape seed extract containing proanthocyanidins treats wounds, cancer, cardiovascular disease, stomach ulcers, obesity, and skin irritation[25]. Collagen, and elastin, formation is promoted by proanthocyanidins[26]. Proanthocyanidins accelerate wound healing by reducing edoema and increasing blood flow[27]. Grape seed extract volatility and bio-absorption are still the key difficulties. Proanthrocyanidin-based extract can be delivered using an appropriate agent.

This work attempts to bridge the gap between alternative treatment and conventional treatment by finding the effect of proanthocyanidin-rich grape seed extract as a potential wound healing agent. This work also aims to promote sustainable technology by using waste to formulate therapeutic agents. Grape seeds, in general, are not edible, but many people use them as a supplement to boost health and hence can be considered a non-conventional plant product. Thus, this study aims to use this waste material directly derived from the Indian winery and optimize its extraction process to check its efficacy as a potent wound healing agent both in-vitro and in-vivo . In order to deliver it topically a Starch Glycerite based gel was formulated for easy delivery of the extract loaded Gel directly to the wound site. The Glycerite based gel would potentially help in better absorption of the extract at the wound site . Few studies pointed to the use of proanthocyanidin as a potential crosslinking agent. Hence, this study could find a potential dose that could help in designing biocompatible material for many research studies and could point out the multi-functionality of these extracts.

4.2 Materials and Methods

4.2.1 Extraction and Optimization

The grape pomace waste from the Vinsura Winery Pvt.Ltd, Nasik was collected and the seeds were sorted and cleaned. The dried seeds were crushed and the extraction procedure was carried

out at different gradients of ethanol (Merck) solution (40% to 90 %). Ethanol was chosen above any other solvent because is relatively safer (less toxic) and has a polarity index value of 5.2 which makes it very suitable for extracting different phytocompunds from the seeds[28]. Briefly, around 2 gms of crushed seed was added to 20 mL of different percentage (40-90 %) of ethanol solutions. The mixtures were agitated in a shaking incubator (BOD Shaker INC) at 37° C for 1h and then the mixtures were kept in a 4º C freezer for the cold maceration process for 48 hours. After 48 hours the mixtures were taken out and centrifuged at 10000 rpm for around 10mins to precipitate down any undissolved or suspended particles. Finally, the supernatant from each was scanned from 200 nm to 800nm using a UV-VIS spectroscopy (Carry 60) to identify the maxima peak of proanthocyanidins which in the literature is mentioned to be at around 270nm[29]. The gradient in which the maximum peak was obtained was taken into consideration. The extract was concentrated using a rotary evaporator and finally lyophilized to get powder form.

4.2.2 Total Proanthocyanidin Content Assay

The proanthocyanidin contents of the selected extract were determined by the vanillin - H_2SO_4 method [30][31]. Briefly, an extract solutions of 200 µL was added to 500 µL of 1.2% vanillin(SRL) solution and 500 µL of 20% H_2SO_4 (Merck) solution in methanol. The reaction was carried out in the dark at room temperature for 20 min, and then absorbance was measured at 500 nm. Proanthocyanidin contents were expressed as a (+)-catechin (Sigma-Aldrich) equivalents (mg CE/g extract). The standard curve of catechin was prepared using different known concentrations of catechin hydrate.

4.2.3 Total Phenol Content

The total phenolic contents of the ethanolic extracts of Grape Seed were estimated using the Folin Ciocalteau reagent as described elsewhere[32]. The calibration curve (**Figure 1**) was plotted by mixing 0.5 mL aliquots of 100, 200, 400, 800 µg/mL Gallic acid solutions with 2.5 mL of Folin Ciocalteu reagent (diluted tenfold) and 2.0 mL of sodium carbonate solution (7.5 %). The absorbance was measured after 30 min at 765 nm. The phenolic content of the extract was estimated by performing a similar experiment and the phenolic concertation was calculated from the standard curve.
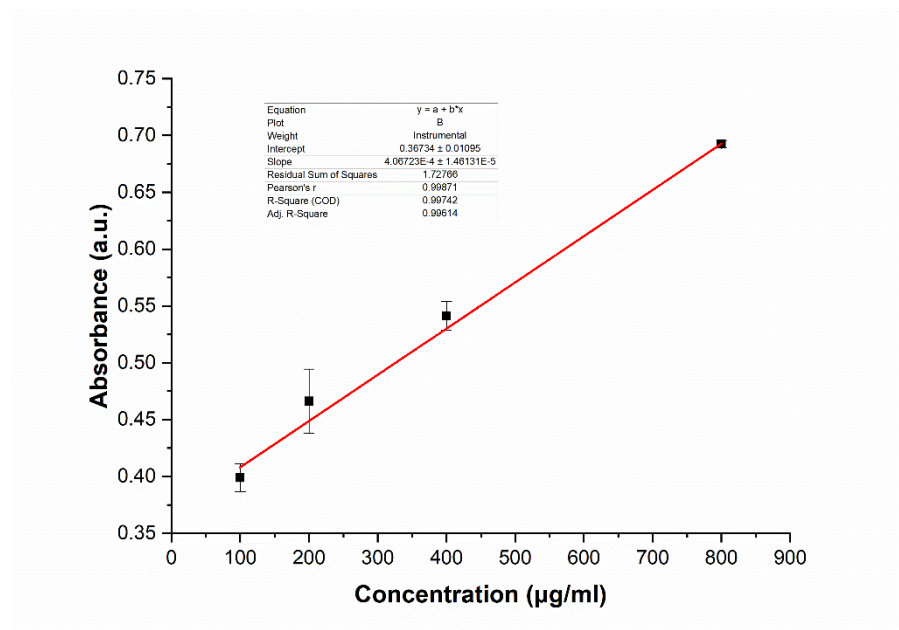
Figure 4.1: Standard Curve for Gallic Acid for detection of Phenol

4.2.4 FTIR analysis

The Fourier transform infrared (FTIR) spectrophotometer is the gold standard for determining the nature of chemical bonds (functional groups) in a given substance[33]. The FTIR spectrum was obtained from the powdered extract that had been dried. Translucent sample discs were prepared by encapsulating 5 mg of the dried extract powder in 100 mg of KBr pellet. Using a Shimadzu FTIR Spectroscope (IR Affinity1, Japan) set to scan from 400 to 4000 cm^{-1}, powdered samples of each extract and catechin (reference sample) were analysed.

4.2.5 LCMS/MS analysis of the Extract

In order to predict the probable phytochemicals the extract was subjected to LCMS analysis using Eclipse Plus C18 (150 x 2.1mm-5 MICRON). The mobile phase was composed of solvent A: water +0.1 % of formic acid, solvent B: 90% Acetonitrile + 0.1 % of formic acid. The flow rate was 0.3mL. The elution was performed starting at 5% of B increased up to 100% B after 30 min. The injection volume was 5 μL for the measurement in negative mode. The library search was performed by using the software

4.2.6 Dosage Preparation

The main aim of the study is to prepare a selective dose which would be highly effective for wound healing in the cellular level. The extract was freeze-dried to obtain powder form and finally, a stock of 1mg/mL was prepared to be used for further experiments.

4.2.7 Cell Viability Assay

L929- A mouse fibroblast cell line was used to assess the cell viability (MTT) assay. The L929 cells were maintained in DMEM High Glucose media supplemented with 10 % FBS alongwith the 1% antibiotic-antimycotic solution and 1% L-Glutamine (200mM) in atmosphere of 5% CO_2 , at 37° C temperature maintained in the CO2 incubator and sub-cultured for every 2days. Cell viability was assessed by measuring the mitochondrial reductase activity of the viable cells. Grape seed extract at different concentration of 500, 250, 100, 50, 25 and 10 µg/mL was used respectively to treat the cells grown in 96 well plates. After incubating the plate for 24, 48 and 72 hours at 37°C in a 5% CO2 atmosphere respectively, the spent was removed followed by adding MTT solution into the wells @5 mg/mL concentration, there after incubating the plates for 3 more hours. Then all the solutions were removed followed by addition of the DMSO to dissolve the MTT formazan crystals. The absorbance was then read on a spectrophotometer or an ELISA reader (BIORAD) at 595 nm wavelength. % cell viability was calculated by using following formula[34],

$$\% \ Cell \ Viability = \frac{Abs. \ of \ the \ sample \ treated \ cell}{Abs. \ of \ the \ control \ untreated \ cell} \times 100$$

By labelling the GSE-treated cells with fluorescein diacetate(FDA), we could see whether or not the (Grapes seed extract) GSE was able to keep the cells alive. FDA is degraded by a cytoplasmic esterase to create fluorescein. "Fluorescein" stays attached to the cell and emits intense fluorescent light due to its polarity[35]. Before live cell imaging could begin, the wasted medium from the 24 well culture plates had to be removed after cells had been cultured with GSE at a concentration of 100µg/mL for predetermined time periods of 1, 2, and 3 days. The cells that had been pretreated with GSE were then incubated with 10 µg/mL of freshly produced FDA (Sigma-Aldrich, USA) in serum-free Dulbecco's Modified Eagle's Medium (DMEM) for 5 minutes at room temperature. The FDA-treated Cells were washed for 3 times and then seen under a fluorescent microscope with a 465 nm filter (Magnus Fluorescence Microscope).

4.2.8 Scratch Assay

The capability of migration for L929- mouse fibroblast cell line was evaluated by using cell scratch assay to measure the augmentation of the cell population on surfaces. Seeding of the

cells was done into 12 well cell culture plates in DMEM high glucose growth medium with added fetal bovine serum, where the cell concentration was 0.25 million cells per well. Almost 70-80 % of confluent cell monolayers were formed by maintaining all optimum conditions. A linear wound was made on the monolayer by using a 200 µl pipette tip by holding the long axial of the tip perpendicular to the bottom of the well. Cellular debris was removed by D-PBS washing. The growth medium containing grape seed extract (100 µg/ml) was added followed by incubation for 24 hours. An inverted biological binocular microscope was used to photograph the scratched areas at 0, 12- and 24-hour intervals. Areas between the scratch edges were calculated by image J, processing software. The closure rate of the layers was calculated by the following formula,

$$\% \text{ of Wound Healing } = (^{\text{Initial Area} - \text{Final area}}/_{\text{Initial area}}) \times 100$$

Where the initial area is the area value at 0 hours and the final area is the area value at 12h and 24h. A triplicate experiment was done which was finalized by calculating the mean value.

4.2.9 Assessment of Cellular Morphology using Cytoskeleton and Nucleus staining

L929 Cells were cultured in glass slides placed in 12 well plates with a density of 105 cells/mL and incubated in a CO2 incubator at 37°C for 24 hours to achieve 70-80% confluence. Cells were treated with a selected dose of Grape Seed Extract (GSE) and the control was left blank with no treatment. The whole system was incubated for 24hrs. After incubation, the cells were washed and fixed with a 4% paraformaldehyde solution and permeabilized using 0.1% Triton-X 100. After washing the cells 2-3 times with PBS and stained with 10µL of Fluorescein Phalloidin and incubate for 90mins at room temperature and counter-stain the cells with 10µL of DAPI solution (1ug/ml) for 10min in the absence of light before imaging. The cells were observed in ZEISS LSM 880 Fluorescence live cell imaging system (Confocal Microscopy) with filter cube with Excitation 341 nm and Emission 452 nm for DAPI stain for blue channel and for Fluorescein Phalloidin with Excitation/Emission: 496/516 nm.

4.2.10 Cell Cycle Analysis

The cells were seeded at a density of 2 x 10^5 cells/2 ml in a 6-well plate before being incubated in a CO2 incubator at 37°C for 24 hours. A control group of cells was not treated and allowed to grow for 24 hours before being treated with GSE extract at 100 µg/mL. The cells were centrifuged at 2000 rpm for 10 minutes after treatment and washing. The cells were resuspended and then fixed in 70% ethanol at 4 °C for two hours. The cells were fixed, then

washed twice with PBS, centrifuged at 2000 rpm for 10 minutes, and finally plated. After 30 minutes in the dark, the pellet was broken up by vertexing and resuspended in 400 L of PI/RNase staining buffer. The cells were then analyzed by flow cytometry (BD FACS Calibur, BD Biosciences, USA).

4.2.11 ROS Analysis and Antioxidant Study

ROS were analysed by generating them with hydrogen peroxide and then detecting them with a stain made from 5-(and-6)-carboxy-2′,7′-dichlorodihydrofluorescein diacetate (DCFDA). The cells were grown in Dulbecco's modified Eagle medium (DMEM) at 37 °C for one night after being seeded at a density of 2×10^5 cells/2 ml on a coverslip in a 12-well plate. The cells were adhered for 24 hours, then pre-incubated with GSE (100 μg/mL), and finally exposed to H2O2 (0.75 mmol/L) for 1 hour. After being exposed to DCF-DA (10 μM), L929 cells were incubated in DMEM devoid of FBS for 30 minutes at 37 °C in the dark. Fluorescence microscopy was used to analyse the results following two washes in phosphate-buffered saline (PBS) to remove the unreacted probe (Magnus). Images were taken, and the software Image J was used to calculate mean density values.

The free radical scavenging activity (RSA) was performed using DPPH method. Different concentration of the GSE extracts (25, 50, 100, 250, 500, 1000, 2500 μg/mL) were used. A volume of 2.5 mL of 0.04% DPPH solution was mixed with 0.5 mL of all concentrations of extracts separately. After 30 min incubation at room temperature in dark, the absorbance was taken at 517 nm in triplicates for each concentration. Ascorbic acid was used as a standard antioxidant. Water was used as a control. The percent inhibition of free radical formation was calculated as follows:

$$RSA(\%) = \left(\frac{\{Abs\ Control - Abs\ Sample\}}{Abs\ Control} \right) \times 100$$

4.2.12 CAM assay

To conduct the chorio-allantoic membrane assay (CAM assay), fertilised chicken eggs were incubated for 7 days. White chicken eggs were fertilised and collected from the State Poultry farm in Tollygaunge. The eggs were disinfected in 70% alcohol and then placed in an incubator set between 37 and 38 ºC and 70 and 80% humidity. Two to three millilitres of albumin were removed using a hypodermic needle of 18 gauge through a tiny hole bored in the narrow end on the second day of incubation. Again, the window was taped over and put into the incubator. On day three of incubation, a little square hole was drilled into the shell. Sterile normal PBS

(pH-7.0), and 100µg/ml GSE were used to impregnate in the vehicle of control group and test group, respectively. The eggs were put back into the incubator and left there for another 48 hours. Upon removing the eggs from the incubator at the end of the incubation period, CAM-treated eggs were photographed and analysed for the presence of blood vessels. Careful count was taken of how many vessel forks was there in the photographs.

4.2.13 In-vitro anti-Inflammatory Assay using RAW Cells in an LPS-induced inflammation model

4.2.13.1 Cell Viability assay using RAW cells

Raw 264.7- Mouse monocyte/ macrophage cell line (NCCS, Pune) was used to assess the cell viability (MTT) assay. The RAW 264.7 cells were maintained in DMEM High Glucose media supplemented with 10 % FBS along with the 1% antibiotic-antimycotic solution and 1% L-Glutamine (200mM) in atmosphere of 5% CO_2, at $37^\circ C$ temperature maintained in the CO_2 incubator and sub-cultured for every 2 days. Cell viability was assessed by measuring the mitochondrial reductase activity of the viable cells. Grape seed extract at a concentration of 100 µg/ml was used to treat the cells grown in 96 well plates. After incubating the plate for 24hrs at 37°C in a 5% CO_2 atmosphere, the spent was removed followed by addition of the MTT solution (0.5 mg/ml) into the wells and incubated the plates for 3 more hours. Then all the solutions were removed following by adding DMSO to dissolve the MTT formazan crystals. The absorbance was then read on a spectrophotometer or an ELISA reader at 570nm wavelength. % cell viability was calculated by using following formula,

$$\% \ Cell \ Viability = \frac{\text{Abs. of the sample treated cell}}{\text{Abs. of the control untreated cell}} \times 100$$

4.2.13.2 Nitric Oxide Inhibition Assay

Cultured cells upon 70-80% confluency, seeded in 96 well plates with a density of 20,000 cells/well were incubated for 24 hours followed by removing the spent media. Stimulation of the cells was done with 1ug/ml of Lipopolysaccharide (LPS) for 2 hours in all the wells except in untreated well and cells were with the different concentrations (100-400 ug/mL) of given test compound i. e. GSE, and thereby incubation at 24 hours. After the incubation, the supernatants from all the wells were collected and washed by using PBS. 100 µl of culture supernatants mixed with Griess reagent followed by incubation at 37°C in the 5% CO_2 incubator for 2 hours. The absorbance was measured at 580 nm in a Multimode Microplate

Reader. Values of total Nitric oxide for each sample from the standard curve were calculated by using the following formula,

$$\text{Total NO inhibition study} = [(\text{Corrected Absorbance} - \frac{(y - \text{intercept}))}{\text{Slope}}]$$

4.2.13.3 ROS Estimation

Cells were seeded in a 6-well plate at 0.5 x 10^6 cells per 2 ml of growth media. The plate was then incubated overnight in a 37°C CO2 incubator. On day 2, the spent media was aspirated and the cells were rinsed with 1 ml of 1X PBS. The cells were treated with 1μg/mL lipopolysaccharide (LPS) for 2 hours to produce inflammation. Next, the GSE extract was added to the culture media in separate wells, and the cells were incubated for 24 hours. One well was untreated as a control and in another well there was no LPS treatment. The media was collected from all wells and the cells were rinsed with PBS after treatment. The cells were detached with trypsin-EDTA solution and harvested and centrifuged. The cells were resuspended in 2',7'-dichlorodihydrofluorescein diacetate (H2DCFDA) working solution and incubated at 37°C for 30 minutes after discarding the supernatant. The cells were resuspended in DPBS for flow cytometric measurement of reactive oxygen species (ROS) levels after centrifugation and washing (488 nm).

4.2.13.4 Assessment of the key inflammatory cytokines like TNF-alpha, IL6, and NF-kB

Cells were seeded in a 6-well plate at 0.5 x 10^6 cells per 2 ml of growth media. The plate was then incubated overnight at 37°C in a CO2 incubator. On day 2, the spent media was aspirated and the cells were rinsed with 1 ml of 1X PBS. The cells were treated with 1μg/mL lipopolysaccharide (LPS) for 2 hours to produce inflammation. Next, the GSE extract was added to the culture media in separate wells, and the cells were incubated for 24 hours. One well was untreated as a control and another well only LPS treatment with no drug were performed which acted as a Positive control for Anti-inflammatory marker expression. The media was collected from all wells and the cells were rinsed with PBS after treatment. The cells were detached with trypsin-EDTA solution, harvested and centrifuged. Reading for three sets for **TNF-alpha, IL6, and NF-kB** were taken in triplicate for each**.**

For checking the expression of TNF-alpha cells were fixed with 1ml cold 70% ethanol and incubated for 30 minutes and finally centrifuged. The cells were washed twice with PBS and 10μL TNF a - FITC Antibody (Cat No: 562082, BD Biosciences) was added and incubated for

30 minutes in the dark at room temperature (20° to 25°C)[36]. The cells were then analyzed by flow cytometry (BD FACS Calibur, BD Biosciences, USA, Cell quest pro software).

For checking the expression of IL-6, cells were fixed with 1ml cold 70% ethanol and incubated for 30 minutes and finally centrifuged. The cells were washed twice with PBS and 10µL IL 6 - PE Antibody (Cat No:554545, BD Biosciences) was added and incubated for 30 minutes in the dark at room temperature (20° to 25°C)[37]. The cells were then analyzed by flow cytometry (BD FACS Calibur, BD Biosciences, USA , Cell quest pro software).

The expression of the NF-KB was analyzed using Fluorescence microscope technique. Keeping the basic cell culture procedure same the only difference was that the cells were cultured on glass slides. One well was untreated as a control and in another well only LPS treatment with no sample kept for treatment which acted as positive control and one well with both LPS and GSE. After the treatment for 24hrs the cells were washed for 2times using PBS and cells were fixed using 0.5 mL BD Cytofix/Cytoperm solution (RRID:AB_2869008, BD Biosciences). After proper washing cells were stained using 10µL of PE anti-NFkB p65 antibody (#558423, BD Biosciences) for 30mins and counter stained with 100µL of DAPI solution (1ug/ml) for 10min under the absence of Light before imaging. Cells were analysed under ZEISS LSM 880 Fluorescence live cell imaging system (Confocal Microscopy). Images were analysed by ZEN Blue Software and recorded and the expression of NFkB-p65 is measured using Image J software.

4.2.14 Formulation of Starch -Glycerite Gel loaded with Grape Seed Extract

For topical delivery of the GSE at the wound site Starch -Glycerite gel was chosen. Firstly, Starch Glycerites are purely natural with zero use of synthetic polymers and are also highly biocompatible. The Starch-Glycerite Gel was created in accordance with the standard protocol [38]. Briefly, 10 gm of starch were weighed and combined with 20 ml of cold water until a homogenous mixture was created. 70 ml of glycerine was poured into the mixture, the entire volume was agitated until homogeneity was once again achieved. The beaker and its contents were then transferred to an electric hot plate with an accurate temperature controller. The temperature was so precisely controlled that the heat rose very slowly, and the dish was stirred continuously. The hottest temperature recorded within the evaporating dish was 110 ºC . After some hours, a transparent, viscous liquid was formed, which was then cooled and loaded with the grape seed extract. The final GSE concentration in the gel was made to 1mg/ml so that after 10x dilution with media, the effective concentration obtained will be 100 ug/ml.

4.2.15 Rheological Characterization of the Starch -Glycerite Gel

The rheological measurements of ointment sample was performed using rheometer device (RheolabQC, Anton Paar). All experiments were performed in rotation mode with parallel plate–plate with each plate diameter of 25 mm. 10 ml of ointment sample put onto lower plate of the rheometer and the gap size between two plates was adjusted at 1 mm. The rheological tests were carried out in shear rate control mode to determine shear stress (σ) and viscosity (η) as a function of shear rate (γn). The shear rate was raised linearly from 1 to 1000 s^{-1} for 300s.

4.2.16 In-vitro Cytocompatibility of the Starch-Glycerite Gel

In vitro, the cellular response was observed by separately culturing L929 (NCCS Pune) on contact with the ointment. Before proceeding with the cell culture studies, the ointment/gel was exposed to UV light for 20 min . Around 5000 cells were seeded on a 96-well plate and around 20ul of the gel was added to the well so that the final concentration of the extract remained as 100ug/ml. The whole system was maintained at 37 °C, 5% CO2, and 95% relative humidity for the required time. The cellular viability of the was analysed using MTT assay and FDA staining assay at three different time points i.e 1,3 and 7days.The detailed protocol of MTT assay and FDA staining is already mentioned in the earlier sections.

4.2.17 In-vitro Hemocompatibility of the Starch -Glycerite Gel

Hemolysis Studies using fresh rabbit blood in an EDTA tube are used to estimate the hemocompatibility of the prepared **Starch-Glycerite Gel**. A 25ul prepared sample was incubated at 37 °C for 30 min in a centrifuge tube with 1 mL of normal saline. 0.2 mL of diluted blood was added, mixed gently, and incubated for 60 min for the negative control. 0.02 mL of diluted blood was collected in 1 mL of 0.1 per cent sodium carbonate solution for the positive control and incubated for 60 min at 37 °C. In a similar manner, the sample material was incubated for 60 min at 37 °C. After 60 min of incubation, all test tubes were centrifuged for 5 min at 4000 rpm, and the supernatant was carefully collected and transferred to the cuvette for readings at 540 nm wavelength to compute % haemolysis[39]. The hemolysis percentage is computed from three replicate averages.

4.2.18 In-Vivo Animal Experiments

Animal models were used to study the biological effects of the GSE-loaded Starch-Glycerite Gel according to the rules of the Institutional Animal Ethical Committee (IAEC) at the West Bengal University of Animal and Fishery Sciences in Kolkata, India

(763/GO/Re/SL/03/CPCSEA/05/2021-22 dated 26.04.2022 approval no. of IAEC of West Bengal University of Animal and Fishery Sciences.). We looked at how skin wounds healed on rabbits, both male and female, that weighed between 1.5 and 1.8 kg. The animals were put into three groups randomly, and their skin wounds were checked at three different times: on day 7, day 14, and day 21. Before the wounds were made, the animals were anesthetized with xylazine hydrochloride (6 mg/kg body weight; Xylaxin, Indian Immunologicals, India) and ketamine hydrochloride (33 mg/kg body weight; Ketalar, Parke-Davis, India) injected into their muscles. Before making wounds, betadine lotion was put on the rabbits' backs and the dorsal surface of their mid-thoracolumbar area was cut off under sterile conditions.

According to the procedure, three full-thickness wounds (each 20 mm in diameter) were produced on the dorsal mid thoracolumbar region of all the rabbits to evaluate the wound healing process in an animal model. Two wounds were used as controls; one was closed with the commercial ointment Topicure Gel (Vea Impex), while the other was treated with GSE-loaded Starch-Glycerite Gel and the third was left untreated. Every other day, a new outfit was worn. Meloxicam (Melex, IntasPolivet, India; @ 0.2 mg/kg O.D. for 3 days) was injected as an analgesic to help with the pain associated with wound development. Each rabbit was provided with its own spacious cage in a clean, well-lit home so that its health could be monitored more easily. Photographs of the wounds were taken at 0, 3, 7, 10, 14, and 21 days to evaluate the healing process. After analysing the images with ImageJ software, we determined the wound closure rate using the equation below:.

$$\text{Wound Area}(\%) = \frac{\text{Wound Size at Day zero}}{\text{Wound Size at specific time}}$$

Tissues from the wound site were taken on days 7, 14, and 21 for histological, immunohistochemistry, and biochemical analysis of ECM component to determine the success of the healing process.

The hydroxyproline estimation of the tissues of 7 ,14 21 days were done using Hydroxyproline estimation kit (Hydroxyproline (HYP) Colorimetric Assay Kit (Acid Hydrolysis Method), E-BC-K062-M) following the protocol provided by the manufacturer.

Following their removal from the wound bed on days 7, 14, and 21, the recovered tissues were cleaned in normal saline and stored in 10% neutral buffered formalin until they could be processed for tissue sectioning. Tissues were dried in a series of ethanol concentrations, paraffin-embedded, and sliced using microtome into 5μm slices, and then mounted on glass

slides for examination. Tissue slices were stained with Haematoxylin and Eosin for a histological evaluation. Masson's trichrome technique[40] and Verhoeff's Van Gieson method [41] were used to stain collagen and elastin, two additional connective tissue components of the ECM. The bright-field microscope was used to take the pictures (Leica DM 2000, Germany).

Immunohistochemistry of tissue sections was further carried out to evaluate the synthesis of collagen type I and CD 31/PECAM 1, a marker of angiogenesis in the wound bed using Vectastain ABC kit, Vectors lab, U.K . Immunohistochemistry was performed following the protocol discussed elsewhere [42]. The CD31 positive signal was used to calculate the microvascular density. Blood vessel development was defined as the appearance of brown, lumen-containing endothelial structures and the separation and clustering of endothelial cells. We saw and measured at least three distinct domains in each group. The data was presented as a mean ± standard deviation.

4.3 Results and Discussion

4.3.1 Extraction and Optimization

Preparing plant extracts in an ethanol-water combination is advised since it is safe for human consumption[43]. However, there is no such report were a proper cproportion of ethanol: water is given which can extract maximum proanthrocyanidin (a condensed tannins and flavonoids derived from flavan-3-ols) from grape seeds[44]. It is well proven that grape seeds are rich in proanthrocyanidin however this study showed that the proanthrocyanidin content of grape seed extract vary with the ethanol: water ratio. Catechins and Proanthocyanidins have a lambda max of around 278nm in the UV range when scanned from 200-800nm[45]. Because of these features, we were able to determine the optimal solvent extraction ratio that would allow for the maximal extraction of proanthocyanidin from grape seeds. After extraction, the solutions were centrifuged and the finally extorted phytochemicals in the solvent were scanned in the UV-Vis spectrophotometer. The extraction with 70% ethanol-water showed the maximum absorbance at around 278 nm (**Figure 4.2a**) after 2 days of cold maceration. As absorbance is directly proportional to the concentration it could be well established that 70% ethanolic solvent extracted maximum proanthrocyanidin. The extraction mixture was then concentrated using a rotary evaporator and finally lyophilized to get powder extract. The powdered sample was then dissolved in solvent (70% ethanol) and was scanned in an UV-VIS spectrophotometer to confirm the peak. A sharp peak was observed at 278nm (**Figure 4.2b**) confirming the presence of proanthocyanidin.

4.3.2 Total Proanthocyanidin Content Assay

The total amount of proanthocyanidin in the GSE was found to be maximum in the 70% ethanolic extract (203.4111 ± 7.545 mg CE/g extract). The 60% ethanolic extract had similar value but slightly lacking behind with a proanthocyanidin content of 186.802 ± 5.044 mg CE/g extract (**Figure 4.2c**).

4.3.3 Total Phenol Content

Total phenolic content of GSE extract was found to be 435.2217 µg/mL Gallic acid equivalent from the Gallic acid standard curve [**Figure 4.1**] hence reflecting the effectiveness of the plant in scavenging free radicals.

4.3.4 FTIR analysis

The FTIR spectra of both grape seed extract and catechin are same, suggesting the existence of functional groups or chemical bonds that are comparable between the two compounds (**Figure 4.2D**). The peaks at 3357 cm^{-1}, 1618 cm^{-1}, 1523 cm^{-1}, 1448 cm^{-1}, 1365 cm^{-1}, 1286 cm^{-1}, 829 cm^{-1}, 970 cm^{-1}, and 1286 cm^{-1} and the 771 cm^{-1} were common in both the spectra of catechin and grape seed extract which indicates the presence of molecular components with similar functional group.

In contrast to grape seed extract, the FTIR spectrum of catechin shows extra peaks at 1228 cm^{-1}, 1074 cm^{-1}, and 1020 cm^{-1}.

The stretching vibration of O-H (hydroxyl) groups is often related with 3357 cm^{-1}, suggesting the presence of alcohol or phenolic chemicals in both grape seed extract and catechin. The C=C stretching vibration at 1618 cm^{-1} correlates to the presence of aromatic rings in both samples. It indicates the presence of aromatic chemicals like flavonoids or phenolic compounds. The C=C stretching vibration in aromatic rings is responsible for 1523 cm^{-1}, which supports the existence of aromatic chemicals in both grape seed extract and catechin. The bending vibrations of -CH2 groups at 1448 cm-1 are connected with the existence of aliphatic chains or saturated hydrocarbons. The bending vibrations of -CH3 groups account for 1365 cm^{-1}, showing the existence of methyl groups or aliphatic chemicals in both samples. The stretching vibration of C-O bonds is often related with 1286 cm^{-1}, suggesting the presence of esters, carboxylic acids, or other oxygen-containing functional groups in both samples. The bending vibrations of C-H bonds dominate at 970 cm^{-1}, indicating the presence of aliphatic molecules or saturated hydrocarbons in both grape seed extract and catechin. The existence of aromatic chemicals in

both samples is further supported by the fact that 829 cm^{-1} is frequently connected with the rocking vibrations of aromatic C-H bonds. The bending vibrations of C-H bonds are commonly assigned to 771 cm^{-1}, indicating the presence of aliphatic molecules or saturated hydrocarbons[46][47].
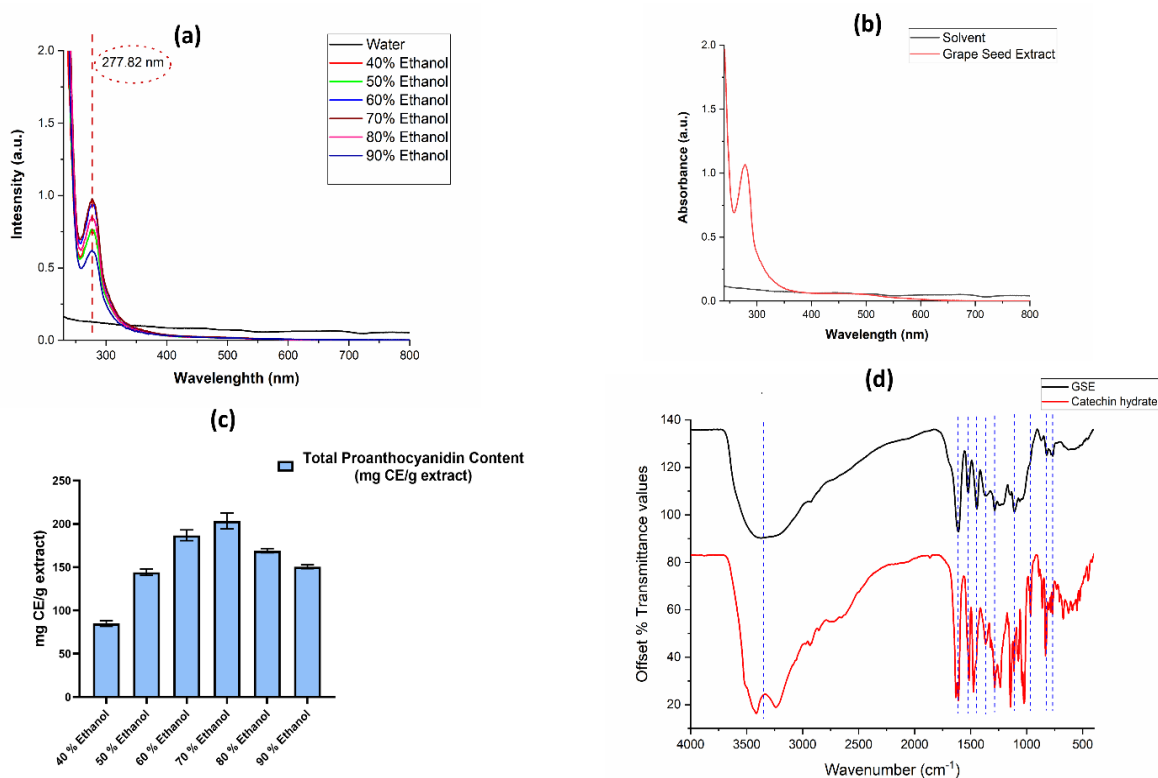
Figure 4. 2 : UV-VIS scan of GSE extract , extracted with different ethanolic solvent ratio(a) , The UV-VISIBLE scan of the dried extract in solvent (b) ; Total proanthrocyanidin content of different extracts of Grape seeds(c); FTIR of catechin and GSE.

4.3.5 LCMS/MS analysis : The extract was subjected to LCMS analysis with ESI/MS coupled to the system. Since negative ion mode (ESI) has less interference from the environment, it was selected. The LC-MS Total Ion Chromatogram(TIC) and mass spectrum of the negative ionization mode is in shown (**Figure 4.3**) by summing up intensities of all phytochemical mass spectral peaks belonging to the full scan. 3 major compounds were detected using the database with two duplicates. The first and third compounds correspond to the same compound, procyanidin B6(Proanthocyanidin) , which has the formula $C_{30}H_{26}O_{12}$. The score values for this compound are relatively high (99.12 and 98.94), indicating a strong match with the expected chemical structure. The RT value estimated was 3.925 for compound 1 and 4.559 for compound 3 [Table 1]. The second compound corresponds to (-)-epicatechin, a flavon, which

has the formula $C_{15}H_{14}O_6$. The score value for this compound was calculated to be 97.76 with a RT value of 4.206. Epicatechin is also abundant in grapes, therefore, it could directly present as an analyte but chances are there that this is a fragment of procyanidin B6 (Proanthocyanidin)[48,49]. The fourth and fifth compound correspond to N-undecylbenzenesulfonic acid, which has the formula $C_{17}H_{28}O_3S$. The score values for this compound were somewhat lower than that of the epicatechin and proanthrocyanidin. N-Undecylbenzenesulfonic acid is an arenesulfonic acid that is found in waste water amongst bioactive compounds[50].
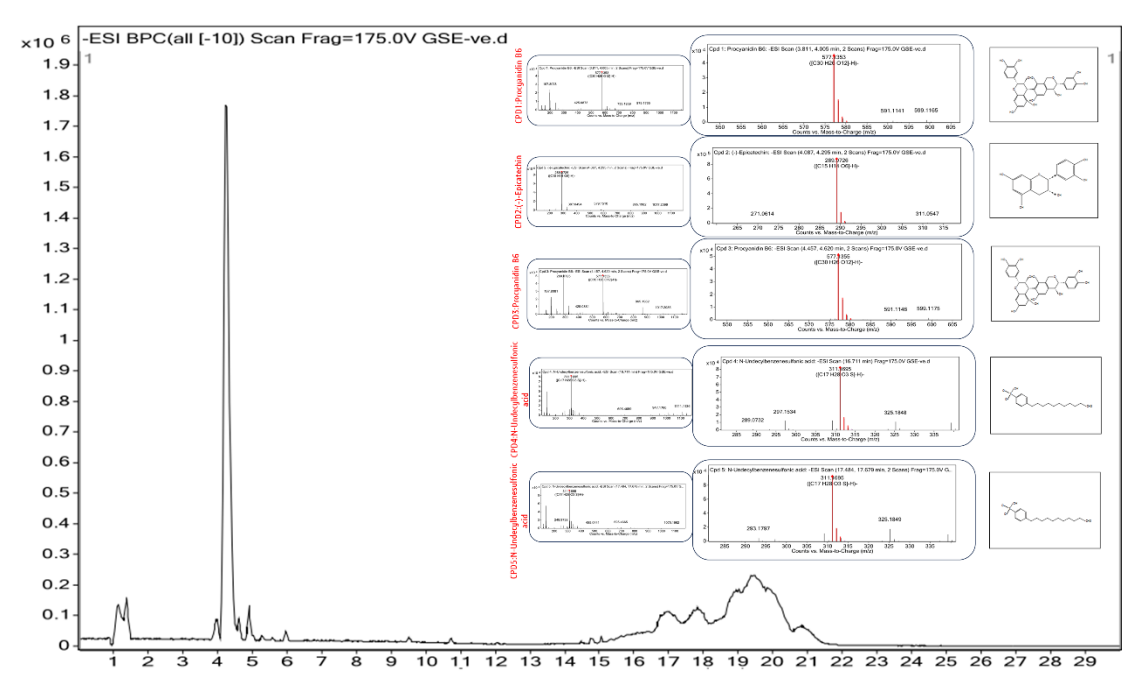
Figure 4.3: LCMS analysis of the optimized Grape seed extract from winery sources.

Table 4.1: List of Compounds with Score, Mass, m/z and RT detected by LCMS/MS

Name	Formula	Score	Mass	m/z	RT
Procyanidin B6	$C_{30}H_{26}O_{12}$	99.12	578.1425	577.1353	3.925
(-)-Epicatechin	$C_{15}H_{14}O_6$	97.76	290.0798	289.0726	4.206
Procyanidin B6	C30 H26 O12	98.94	578.1428	577.1355	4.559
N-Undecylbenzenesulfonic acid	C17 H28 O3 S	94.53	312.1768	311.1695	16.725
N-Undecylbenzenesulfonic acid	C17 H28 O3 S	96.14	312.1768	311.1695	17.595

4.3.6 Cytotoxicity assay

Assessing the toxicity of the applied extract is one of the important studies for consideration of its potentiality. To appraise the cytotoxicity of the applied grape seed extract (GSE), 3- (45-dimethylthiazol-2-yl)-2,5-diphenyltetrazolium bromide (MTT) assay was performed on an L929 cell line [51]. Exposure of these cells was done in different concentrations starting from 10 mcg/ml, followed by 25, 50, 100, 250, and 500 µg/ml for 24, 48, and 72 hours. The bar diagram of cells in different exposures has been pointed out in **Figure No. 4.4(a)**. The result pointed, out that up to 100µg/ml the cells did not show any significant toxicity, whereas in increasing the concentration from 250µg/ml onwards, the cytotoxicity was more as shown in **Figure no. 4.4(a)**. Among all the concentrations, the highest concentration where cell viability was seen above 90 percent (highly cyto- compatible) for 100µg/ml, which was 94.34+1.5, 99.72+1.16, and 94.73+2.81 in 24, 48, and 72 hours respectively. In this mentioned concentration, the cells did not show any significant changes compared to the control group. The image of the 24, 48, and 72 hours of exposure has been shown in **Figure no 4.4 (c, e, and g)**. The natural product extract shows toxicity at higher concentrations because, beyond 100 µg/mL, bioactive components can overwhelm cellular protective mechanisms, leading to oxidative stress, mitochondrial dysfunction, or toxic metabolite accumulation. This concentration-dependent cytotoxicity is common with many natural compounds[52,53].

Fluorescein diacetate assay (FDA) Staining

FDA is an esterase substrate that can be used as a viability probe. It yields fluorescein when hydrolyzed by intracellular esterases [35]. The cells treated with GSE at a concentration of 100 µg/ml were subjected to the FDA, and result pointed that there were no significant changes observed compared to the control group in all the three-time durations, i.e. 24, 48, and 72 hours. The FDA images are displayed in **Figure no. 4.4 (h)**, thus pointing to the cellular viability at the selected dose. The result also showed some increase in cell proliferation in the GSE-treated samples compared to the control.
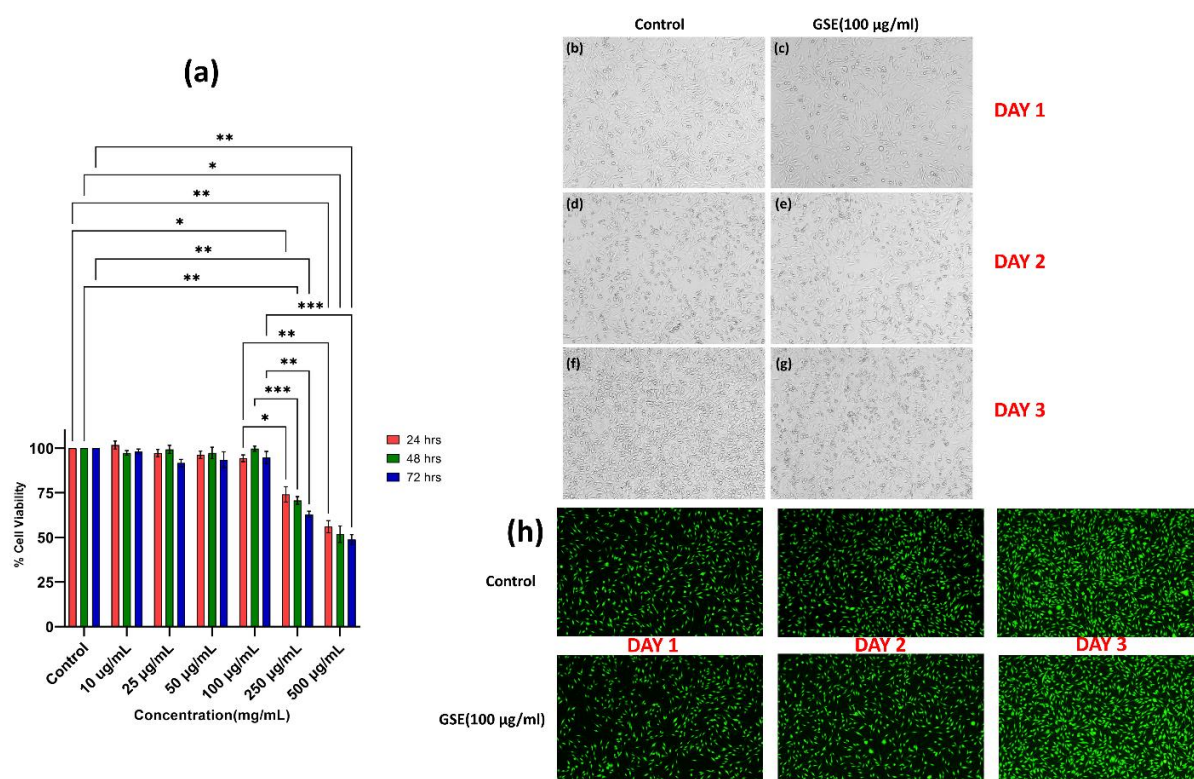
Figure 4.4: MTT assay of GSE treated cells at different concentrations (a); Microscopic pictographs of control and GSE treated cells at different time points (b-g); Representative fluorescence microscopy images of L929 cells treated with 100ug/ml of GSE at 3 different time points (h).

4.3.7 Scratch assay

Cell migration was assessed with the help of scratch assay. In this technique, the L929 cell monolayer was scraped in a straight line to create a scratch with the help of a p200 pipet tip, followed by applying GSE 100 µg/ml [54]. The migration of cells from both sides of the scratch was evaluated. In **Figure no. 4.5 (a)**, it can be seen that at 0 hours, there are minimal numbers of the cells being migrated through the scratch, whereas, in the sample-treated cells at 24 hours there was a 69.57% of scratch closure. And finally, at 48 hours, 98.68% of wound closure have been observed in the sample-treated cells. It indicates that the migration potential of GSE-treated cells reaches its maximum value at 48 hours of treatment, whereas the control group still showed minimal migration of cells through scratch (% closing value). The graphical representation of the wound closure has been pointed out in **Figure no. 4.5(b)**.

4.3.8 Cell Cycle Analysis

The cell cycle is the process through which a single parent cell replicates and divides into two daughter cells. There are four phases in this process: G1 (Gap 1), S (Synthesis), G2 (Gap 2), and M (Mitosis)[55]. A lot can be learned about how therapy affects cell proliferation and differentiation by looking at how cells are distributed across the various stages of the cell cycle. Using fluorescence-activated cell sorting (FACS), we observed significantly fast cell cycle progression in proanthocyanidin-rich GS extracts than that of blank control (**Figure 4.5c ,4.5d)**) Comparatively, the proportion of treated cells in the G0/G1 phase is significantly lower and the percentage in the S and G2/M phases is significantly higher than in control cells. This data indicates that the use of GSE stimulates cell proliferation and division. The S phase showed 4.31 ± 0.22 % cells in control cells whereas GSE treatment showed 10.81 ± 0.23 % of cells which is significantly high. The GSE treatment also showed almost a 5% increase in the percentage of cells G2/M phases compared to the control (**Figure 5e**). This suggests that the treatment with GSE has a stimulatory effect on cell proliferation and division, which can have a positive effect on wound healing. Increased DNA synthesis can be inferred from the greater proportion of treated cells in the S phase. As it may stimulate more cell growth and tissue regeneration, this may aid in wound healing.
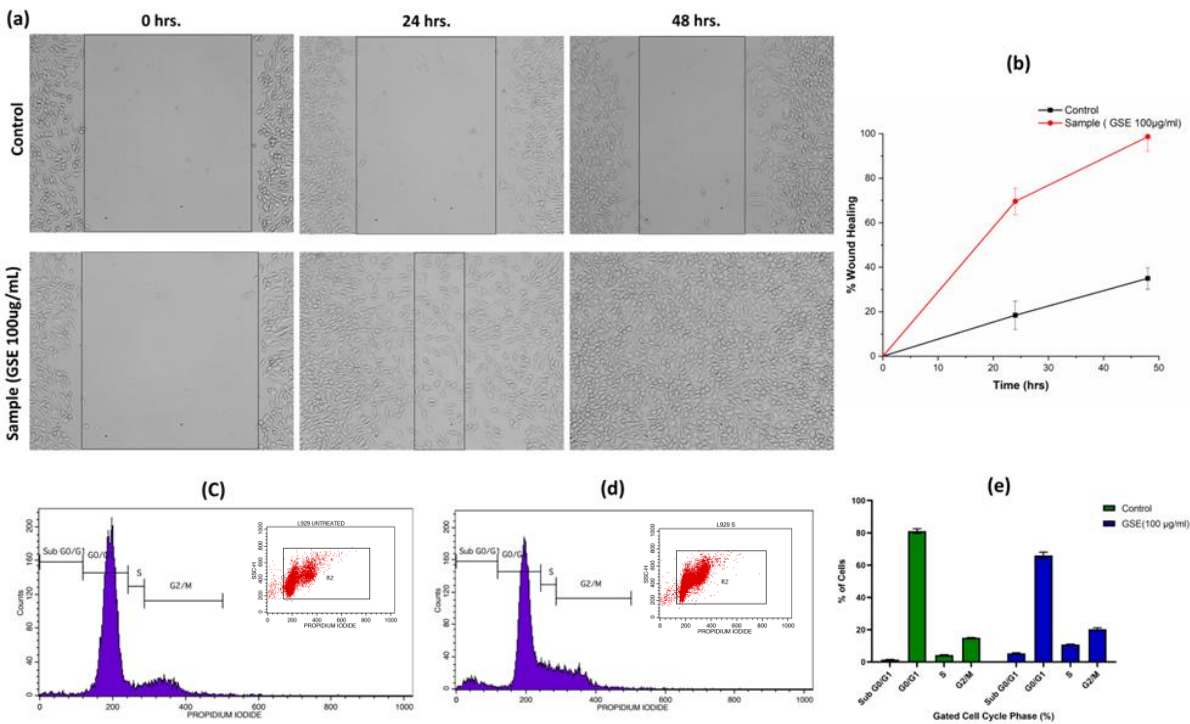
Figure 4.5 : Wound Healing scratch assay on L929 cells of control and sample treated group(a) ; Percentage wound healing from wound healing scratch assay for control and GSE treated

cells(b); Cell Cycle[: G1 (Gap 1), S (Synthesis), G2 (Gap 2), and M (Mitosis)] analysis of control(no treatment cells) (c) , GSE treated cells (d) ; percentage of cells expressed in different phases of cell cycle for control and GSE treated Cells(e).

4.3.9 Cellular Morphology (Fluorescence Staining of Cells)

The Control Cells and the treated cells were stained with Alexa Fluor 488 Phalloidin dye along with Hoechst 33342 solution to stain the cytoskeleton and the nucleus of the cells respectively (**Figure 4.6(a)**). Most often, phalloidin is employed to stain actin filaments, which acted as a marker for the cell's overall perimeter. The nucleus was mostly round in shape in both control as well as treated samples, thus indicating no nucleus degradation. The phalloidin-stained cells showed normal cytoskeletal morphology indicating healthy cells with a well-defined nucleus inside it. Overall, the data points to the fact that the sample GSE at a concentration of 100 ug/ml had no adverse effects on the cells and maintained its healthy structure as compared to normal cells with no treatment.

4.3.10 CAM assay

The development of new blood vessels is known as angiogenesis, and one popular model for assessing this process is the Chick CAM (chorioallantoic membrane) experiment[56]. In this assay, substances are examined for their potential to stimulate or inhibit the development of new blood vessels. Fertilized chicken eggs are incubated for many days until the growing chick embryo and the chorioallantoic membrane are visible through the eggshell, completing the experiment. The CAM is exposed to the test material, and the subsequent effects on new blood vessel formation are monitored and quantified[57].

The overall result (**Figure 4.6b**) indicates an overall increase in blood vessel branching in terms of sample application than that of the control. The significant rise in the blood vessel indicates the potential of the GSE to induce neovascularization and promote angiogenesis.
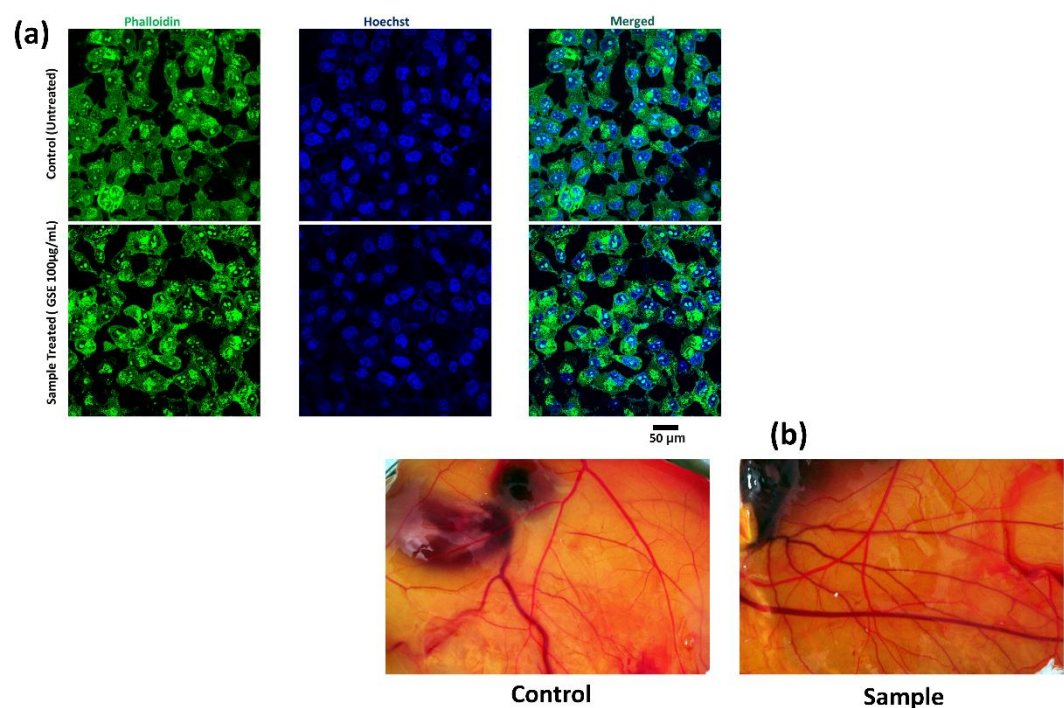
Figure 4.6: Cellular morphology of L929 cells on treatment with GSE (a); Pictographs of the GSE treated and Control groups in CAM assay(b).

4.3.11 Cytotoxicity assay (RAW cells)

The toxicity of the GSE was evaluated using RAW 264.7 cell line, which is macrophage-like, Abelson leukaemia virus-transformed loosely adhered rounded viable cells derived from BALB/c mice [58]. Cells were treated with 1μg/ml of lipopolysaccharide (LPS) and 25, 50, 100, 200, 400 μg/ml of GSE respectively. The LPS-treated cells lost their viability at almost 50 %, showing their toxicity to the cell line. Whereas the cells treated with 100 μg/ml GSE, showed a good cell viability which is 86.68+1.62. The different concentrations of GSE till 100 μg/ml (25, 50, 100 μg/ml) did not show any significant cytotoxicity. The cell viability at different concentrations has been graphed in **Figure no. 4.7a**. The highest concentration with no significant toxicity was chosen for further experiments.

4.3.12 Nitric oxide (NO) inhibition assay

NO production by RAW 264.7 macrophage was determined by measurement of the accumulated nitrite an indicator of NO in the supernatant [59]. NO is a signalling molecule produced by iNOS (inducible nitric oxide synthase), that exerts an essential inflammatory

response and its production depends upon the degree of inflammation or injury [60]. More the injury, the more will be the production of NO. To assess the anti-inflammatory effect of GSE in LPS-stimulated RAW 264.7 cell line, the amount of NO in the culture medium was quantified. 100% NO production was seen in cells treated with LPS, whereas pre-treatment with GSE (6.25, 12.5, 25, 50 and 100 μg/mL) significantly inhibited NO production in a dose-dependent manner, and among these concentrations, cells treated with 100 μg/ml of GSE showed lowest NO production which is 31.96+1.32. The NO production in different GSE-treated cells including the LPS treatment has been showed in **Figure No.4.7b**.
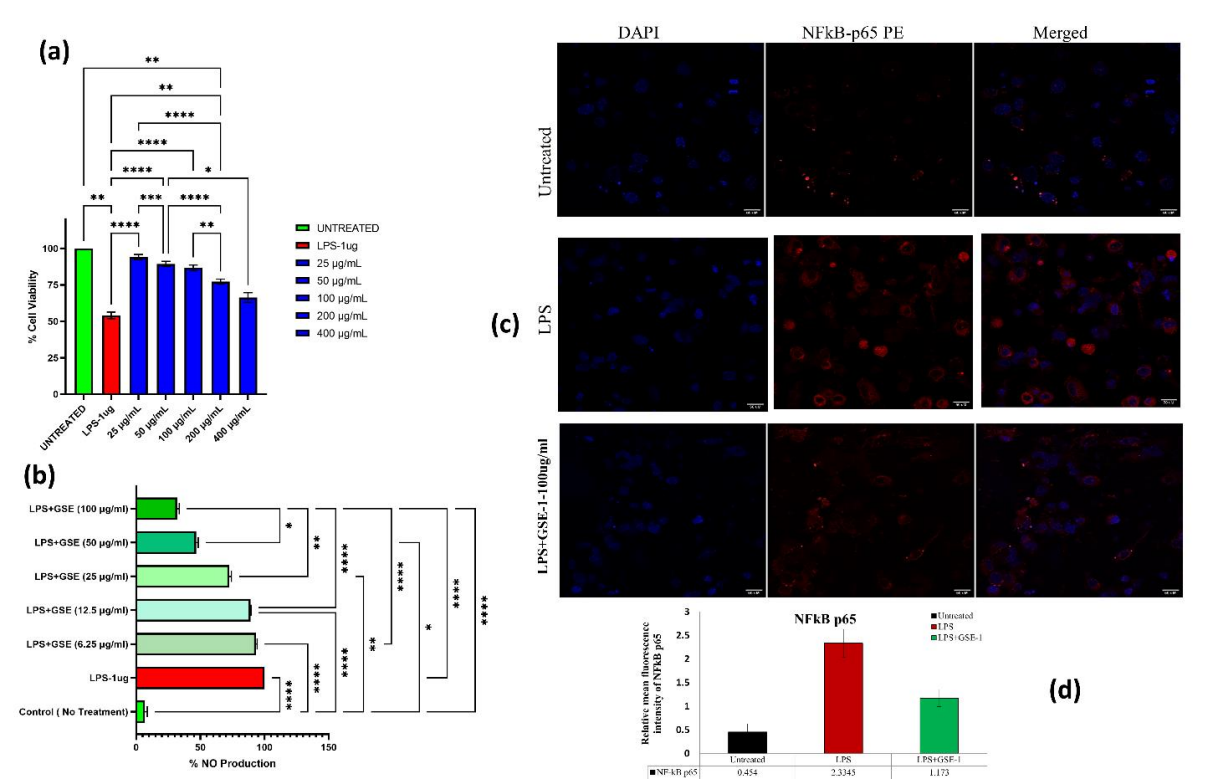
Figure 4.7: MTT assay of different concentration of Grape Seed extracts on RAW cell line(a); Effect on nitric oxide (NO) production in RAW 264.7 cells. Production of NO was measured in the medium of RAW 264.7 cells cultured with LPS (1μg/mL) and different concertation of GSE (b), Fluorescence-Microscopic image for detection of NF-kB expressing RAW cells with LPS induced inflammation on Treatment with GSE(c); Quantification of relative fluorescence for detection of NF-kB expressing RAW cells

4.3.13 Evaluation of the key inflammatory cytokines like NF-kB TNF-alpha, and IL-6,

It has been suggested that the transcription factor NF-κB regulates the production of inflammatory proteins in response to microglial/macrophage activation. When bacterial endotoxin enters active macrophages, it may trigger NF-κB activation, which in turn controls

the release of NO, iNOS, TNF-α, IL-6, and other inflammatory mediators[61,62]. In this view, we examined the effect of GSE extract on the activation of NF-κB in LPS-stimulated RAW cells and the cell expressing NF-κB are represented in **Figure 4.7c**. Cells treated with GSE (100μg/ml) after pre-stimulation with LPS(1g/ml) showed 1.173 in terms of Mean fluorescence intensity of NFkB p65 while LPS (1ug/ml) alone exhibited 2.34 in terms of Mean fluorescence intensity of NFkB p65 respectively (**Figure 4.7d**). Overall, the observations strongly suggest that the Test compound, GSE-1 exhibited significant Anti-inflammatory potency compared to the LPS-stimulated Murine macrophages by suppressing the expression of NFkB, p65 respectively. However further preclinical studies need to be evaluated to confirm its mechanism of action related to the anti-inflammatory activity.

The percentage of Raw 264.7 cells expressing IL-6 ranged from 6.39±1.33 percent in untreated cells upto 33.31±2.13 % in cells stimulated with lipopolysaccharide (LPS), and from 19.92±2.03 % in cells treated with LPS and GSE (100 ug/ml) which was recorded using flow cytometry to examine anti-inflammatory effects (**Figure 4.8a**).

Comparatively, 4.74 ±1.69 % of untreated normal cells expressed TNF-alpha, 68.05 ±1.54 % of LPS-treated cells expressed TNF-alpha, and 31.55 ± 3.11 percentage of LPS and GSE treated cells expressed TNF-alpha (**Figure 4.8b**).

Since the expression levels of IL-6 and TNF-alpha are lowered by about 50% with its use in LPS-treated cells, the results suggest that Grape Seed Extract (GSE) may have anti-inflammatory capabilities.

The anti-inflammatory experiment showed a reduction in IL-6 and TNF-alpha levels, which may be indicative of a protective effect against inflammation. Pro-inflammatory cytokines are essential for both the development and maintenance of inflammation and examples include interleukin-6 (IL-6) and tumour necrosis factor-alpha (TNF-alpha). Slower healing and more protracted inflammation are common outcomes of increased production of these cytokines.
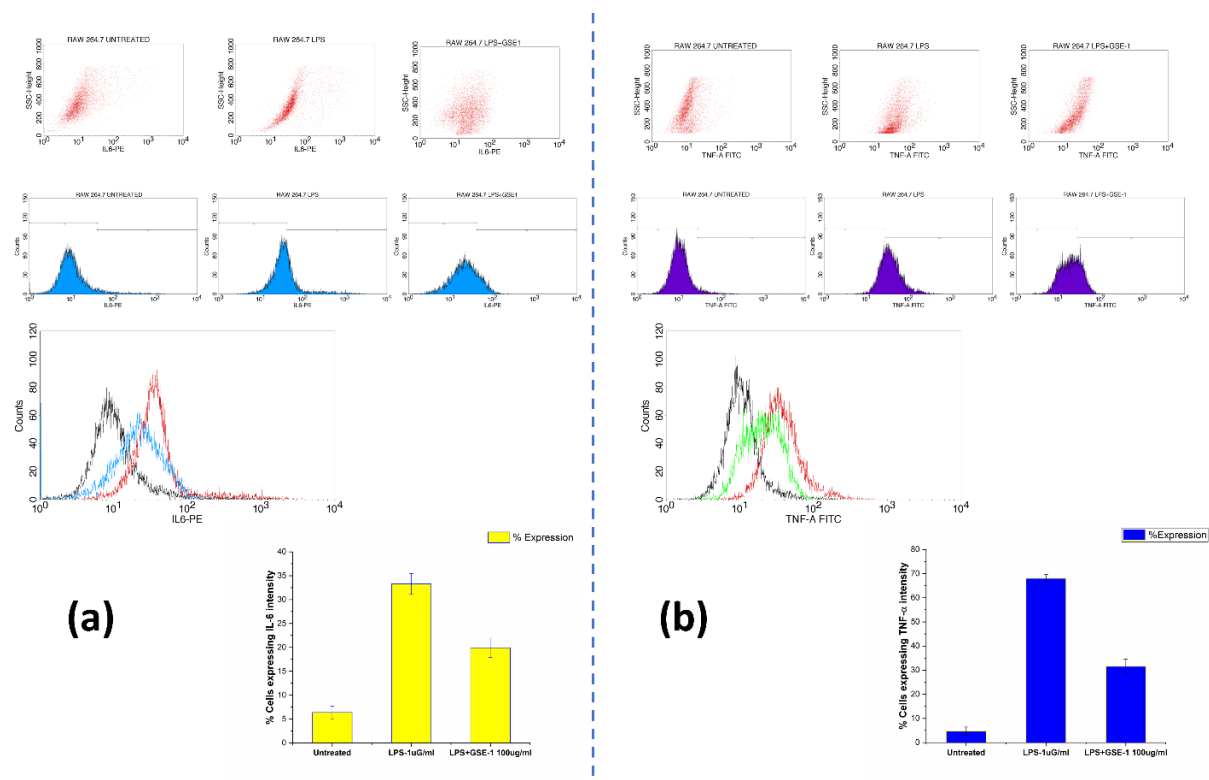
Figure 4.8: Fluorescence-Activated Cell Sorting analysis for detection of IL-6 (a) and TNF-α (b) expressing RAW cells with LPS induced inflammation on Treatment with GSE.

4.3.14 ROS Analysis and Antioxidant Study of GSE extracts

The purpose of this study was to examine the effect of Grape Seed Extract (GSE) on oxidative stress caused by inflammation in RAW cells. Lipopolysaccharide (LPS) was used to initiate inflammation in the cells. Fluorescence-Activated Cell Sorting was used to determine what fraction of cells expressed DCFDA (a marker for intracellular reactive oxygen species) (FACS). The expression of DCFDA increased by 44.68 ± 2.97 percentage after LPS treatment. However, DCFDA expression was drastically reduced to $29.21 \pm 2.06\%$ when LPS-treated cells were co-treated with GSE (**Figure 4.9a**). The fact that GSE has reduced inflammation and increased antioxidant capacity is promising. These results suggest that GSE may aid in wound healing by reducing the oxidative stress caused by inflammation. Since GSE therapy has been shown to reduce intracellular ROS, this may suggest that it aids in wound healing. Healing may proceed more smoothly if oxidative stress is mitigated and cellular function and tissue restoration are improved. It's possible that GSE's ability to modulate immunological responses is responsible for the observed decline in DCFDA expression. Inflammation and oxidative stress interact to affect immune cell function, which plays a critical role in wound healing. In

the context of wound healing, GSE's effect on ROS levels indicate that it may affect the behaviour of immune cells, too.

It has been proven that the GSE extract has the ability to scavenge DPPH radicals. The GSE extract showed greater radical scavenging activity in the assay, almost similar with the reference standard, Ascorbic acid (**Figure 4.9b**). The EC50 value for both the compound i.e. standard Ascorbic acid and GSE extract was calculated from the data and the estimated EC50 value for Ascorbic Acid is 41.49 µg/mL and for GSE extract estimated EC50 value is 50.98 µg/mL.

To further investigate the effect of GSE as an antioxidant agent, test was carried out using H_2O_2 induced L929 cells. There are three distinct stages of wound healing: the inflammatory, proliferative, and remodelling phases. During the inflammatory phase, neutrophils penetrate the wound site, where they secrete H2O2 and proteases to kill bacteria and sweep away dead cells. Overproduction of H2O2 causes non-healing wounds by weakening fibroblast, the cell most closely associated with the wound-healing process. DCFH-DA staining was used to measure ROS levels, and **Figure 4.9C** displays the results for control cells, H2O2-induced cells treated without GSE (100 µg/mL), and H2O2-induced cells treated with GSE (100 g/mL). The presence of ROS is represented here by green fluorescence in the figure. In this work, ROS levels were found to be lower in the GSE-treated group than in the H2O2-induced cells without GSE treatment. The amount of reactive oxygen species produced was also measured with image J. (Figure 9c). The levels of reactive oxygen species (ROS) in H2O2-induced L929 cells treated with GSE were lower than in untreated cells.
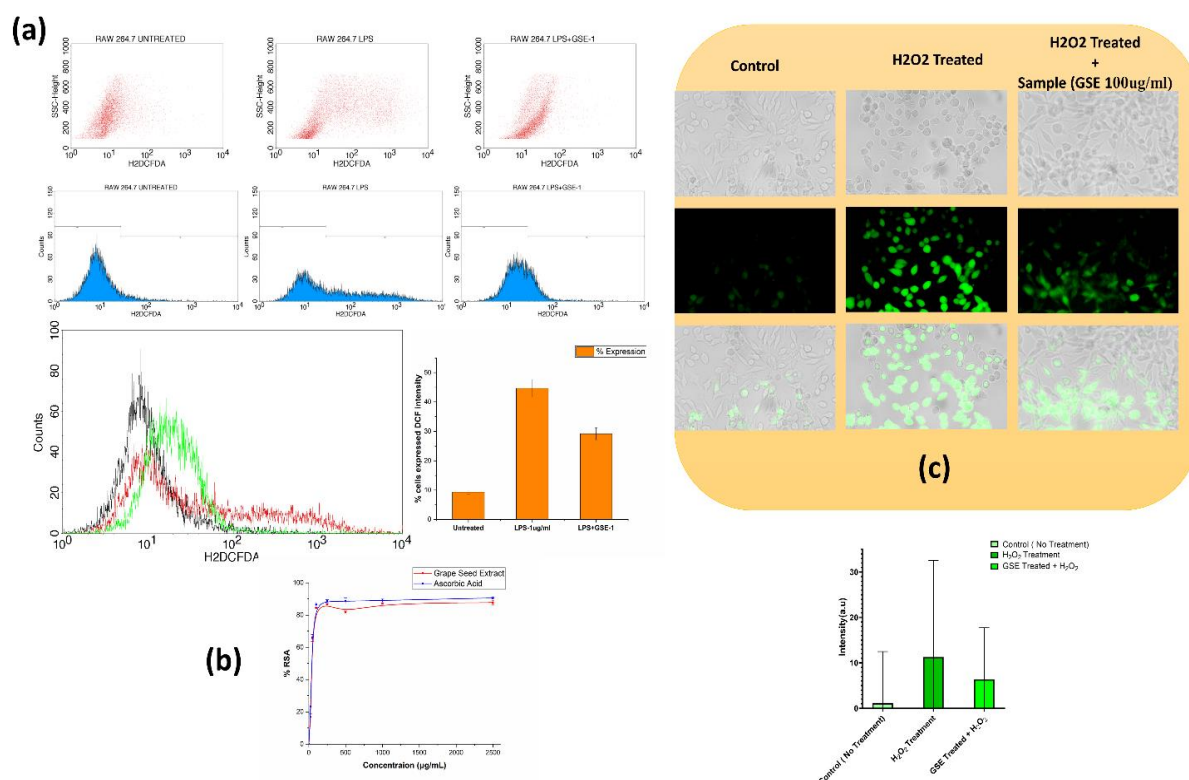
Figure 4.9: Fluorescence-Activated Cell Sorting analysis for detection of DCFDA expressing RAW cells with LPS induced inflammation(a); DPPH Free Radical Scavenging Assay(b) Fluorescence microscopic images of L929 cells for detection of DCFDA expressing cells treated with H_2O_2 and Samples(c).

4.3.15 Mechanical and Biological Characterization of the GSE-loaded Starch Glycerite Gel

The rheological data for GSE-Gel demonstrates a time-dependent decrease in viscosity accompanied by a rise in both shear rate and shear stress (**Figure 4.10a**). Data was obtained for 300 seconds (5 min). It is evident from the data collected that the GSE-Gel displays shear-thinning behaviour, which is typically similar to most ointments and cosmetics[63]. As the shear rate consistently increases, the viscosity concurrently decreases, indicating that GSE-Gel becomes less resistive to flow as more shear force is applied which is a common characteristic of shear-thinning materials. This rheological feature may have practical significance in a variety of contexts, such as the formulation of cosmetics, where getting the right texture and ease of application is essential.

To assess the cyto-compatibility of the GSE Gel, cell viability or MTT assay have been performed on L929 cell line. Where at the intervals of 1, 3 and 7th day the viability has been

studied. In all the interval points, the sample has shown to be biologically compatible. The viability found in each time point i.e., 1, 3 and 7th, were 95.26 ± 2.20, 99.86 ± 1.15 and 98.40 ± 2.97 respectively. The viability is shown in the **Figure No. 4.10b**.

The fluorescein diacetate (FDA) assay is used in this assay as a viability indicator. In this study, at time intervals of 1, 3 and 7th day, the GSE Gel showed similar viability as to the controls, suggesting the gel to be highly bio-compatible. At 7th day the GSE gel-treated cells showed even cellular proliferations. There was no significant difference between the control groups and the gel applied samples at all the time points. The FDA images are shown in the **Figure 4.10c**.

The results show that GSE (Grape Seed Extract) gel has a good haemolysis index, with a mean of around 0.547 and a standard deviation of 0.139 (**Figure 4.10d**). This is consistent with the goal of minimising red blood cell disruption in clinical settings and implies that the gel has no adverse effect on blood samples[64]. The modest standard deviation in findings is more evidence that GSE gel is reliable for analysing blood samples.
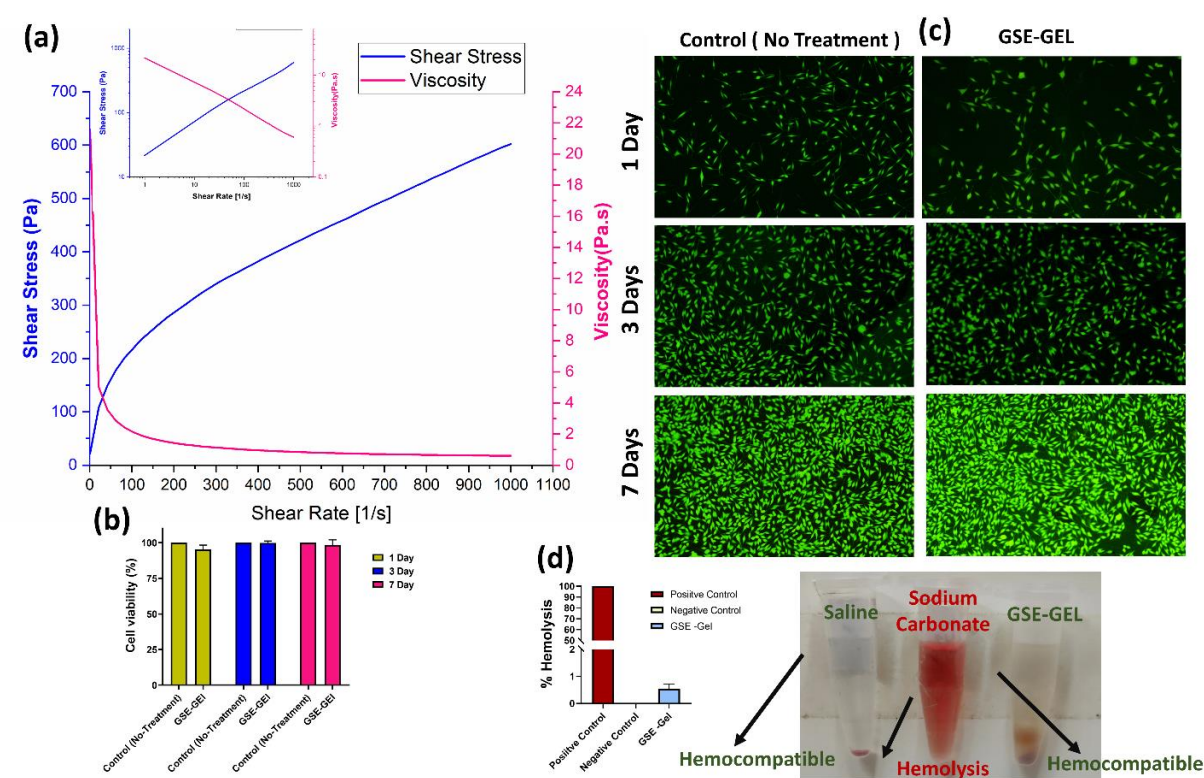
Figure 4.10 : Rheological analysis of the formulated GSE-Gel (Shear Rate vs Shear Stress and Shear Rate vs Viscosity) (a);MTT assay of the GSE gel at 3differnt time points (1,3,7 days)(b); Representative fluorescence microscopy images of L929 cells treated with GSE gel and stained with fluorescein diacetate (FDA) after 1,3 and 7 days of incubation(c); Analysis of hemocompatibility of the GSE-gel by using rabbit blood.

4.3.16 Evaluation of the In-Vivo Wound Healing in Rabbit Model

The wound healing efficacy of the GSE-Gel was assessed by application of the ointment on full-thickness critical cutaneous wounds (Around 20mm) in the rabbit model as shown in **Figure 4.11a.** The healing efficacy of the formulated gel was evaluated by measuring the average wound area of the treatment and control groups as the healing progressed. A sharp decline in the average wound area was observed in the GSE- gel and the standard topicure gel treated groups in comparison to the control group. The average wound area of GSE- gel treated group (77.84 ± 1.25 %) on day 7 was significantly ($p < 0.01$) reduced in comparison to control (84.83 ± 3.56 %) and the standard topicure gel treated group (63.49 ± 2.08 %). A sharp reduction in the average wound area was observed on day 14 of healing whereby the GSE- gel treated group (16.81 ± 4.48 %) and the standard topicure gel treated group (19.84 ± 1.65 %) showed a significantly ($p < 0.0001$) and ($p < 0.01$) lesser wound area than control group (75.24 ± 0.51 %) respectively. By day 21 complete healing was achieved in the GSE- gel (3.63 ± 5.12 %) and standard topicure (2.23 ± 3.16 %) treated groups, the control still showed an unhealed wound area (58.32 ± 6.86 %) that was significantly ($p < 0.01$) greater than the other groups(**Figure 4.11b**).

4.3.17 Hydroxyproline quantification

The quantification of hydroxyproline can directly indicate the progression of wound healing by the deposition of ECM components. In this study we observed a gradual increasing trend in the deposition of hydroxyproline from day 7 to day 21 in all the groups except the control group which showed a decline in hydroxyproline concentration even on day 21(**Figure 4.11c**). The mean hydroxyproline concentration of the GSE-Gel treated group (6.899 ± 0.027 µg/mg) was significantly greater ($p < 0.05$) than control group (5.67 ± 0.23 µg/mg) on day 21 of study indicating the positive impacts of the formulated gel in influencing hydroxyproline turnover during the healing process.
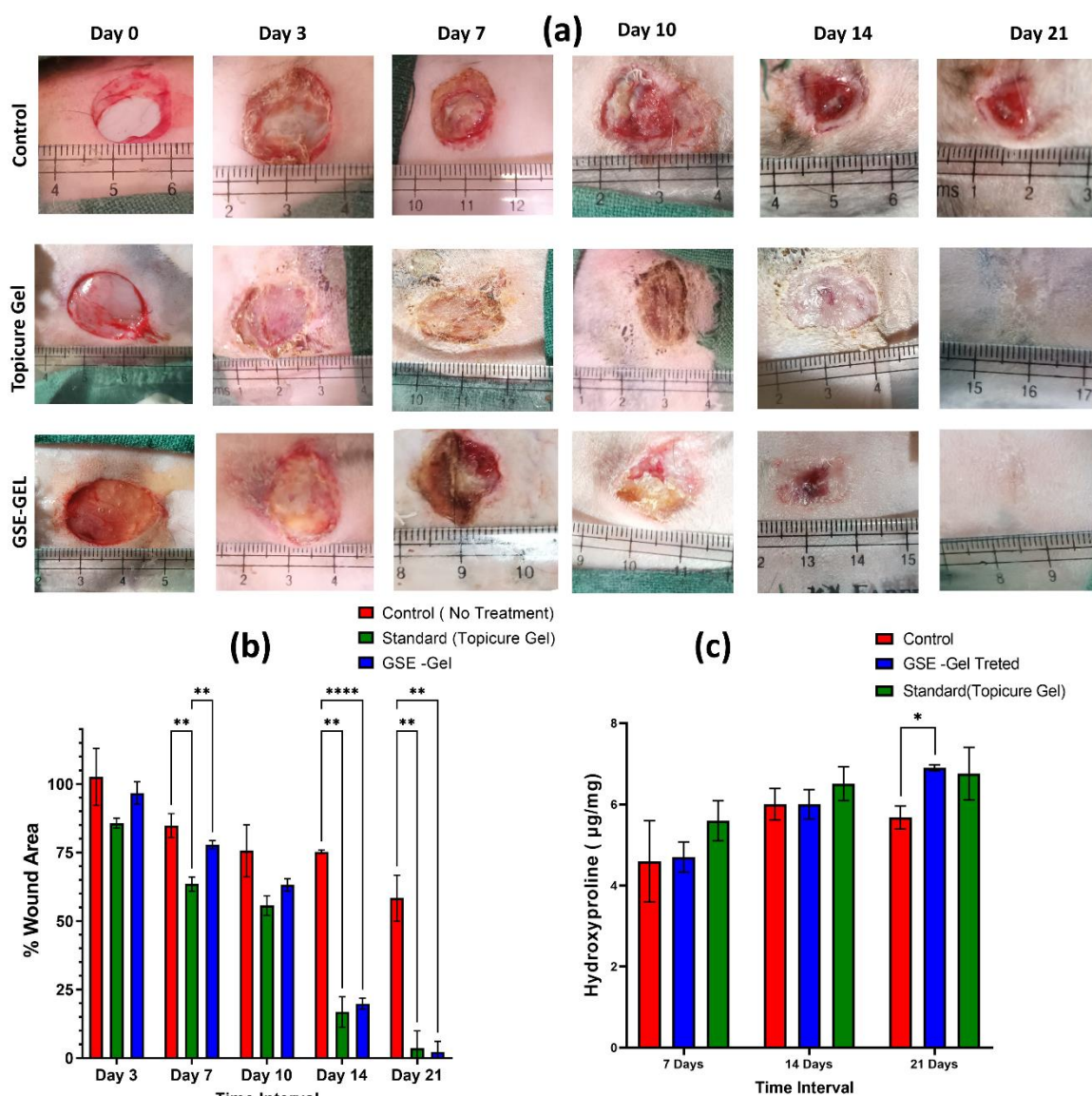
Figure 4.11: Representative gross pictures of full-thickness cutaneous wounds in the rabbit model demonstrating wound healing by various treatments at certain time points, i.e. days 3, 7, 10, 14, and 21.(a) ; graphical representation of the average wound area (%) at the corresponding day points determined by using ImageJ software demonstrating the efficacy of wound closure by the treatments (b); Quantification of hydroxyproline in wound-healing tissues on days 7, 14, and 21 after wound creation. (c)

4.3.18 Histological study

4.3.18.1 H & E staining:

To assess the morphological changes associated with the healing process induced GSE gel as well as control groups, the H&E stained sections at various daypoints were examined carefully (**Figure 4.12a**).In the control wounds a marked infiltration of polymorphous phagocytes was evident on day 7, dermal edematous lesions along with eschar was present. The epidermal migration was not observed and epidermis was still not formed. While granulation tissue was poorly generated, dermal collagenization was evident in the dermal matrix. With the topicure standard gel application, the tissue sections depicted a marked subsidence in inflammatory infiltration, the healing was progressed with the appearance of epidermal closure with the advancement of neo-epidermal migration. Few clots in blood vascular system was also evident. Dermal collagenization has begun. In the GSE-Gel treated wound, inflammatory infiltrates were seen within the blood vassels and the upper region of the dermis. Few clots were also observed. The epidermis formation was not seen but dermal collagenization was marked in the dermis region.

In the control wound, epithelial coverage was not seen, inflammation was prevent with large amount of polymorphous phagocytes dominating the wound bed. Granulation tissue formation was observed but cellular reaction was still prominent. In the standard topicure gel group, inflammatory cellular reaction was evident on day 14 along with the appearance of granulation tissue rich in angiogenic vessels, fibroblasts and precollagen bundles. Epidermal closure was complete with the appearance of rete pegs. In the GSE-Gel treated group, histiocytes and macrophages invasion was observed in the healing wound bed. Epidermal closure and generation of a fibroblastic-collagenous granulation tissue matrix with neo vascularization was seen.

By day 21, the control wounds depicted epidermal closure but the presence of accessory skin appendages was scanty. Histiocytes and macrophages were observed in the collageous matrix. In the standard topicure gel treated group, an abundant of skin appendages ; sweat glands, sebaceous glands and hair follicles were observed. Dermal region depicted mature collagen tissues along with a few cellular infiltration. Thus, complete skin renewal with dermal differentiation was achieved here. In the GSE-Gel treated group, complete neo-epidermal regeneration was observed along with the appearance of accessory skin appendages. Cellular infiltration was evident in the dermis region. complete skin regeneration was seen.

4.3.18.2 ECM assessment

The deposition of ECM components was closely examined by staining the tissue sections of control and treatment groups with Masson's trichrome staining method (**Figure 4.12b**).

On day 7, control wound was mostly occupied with eschar and inflammatory cellular infiltration with a hint of scattered early collagenization in the wound bed. The immature collagen in the lesion lacked specific organization and orientation. With the topicure standard gel application, the tissue sections depicted inflammatory cellular debris with exudates. Collagen deposition, mostly in its primitive stage comprising of immature strands of early collagen were found to appear in the reticular dermis. In the GSE-Gel treated wound, the inflammatory reaction appeared to have subsided by day 7 favouring the deposition of collagenous matrix in the healing wound lesion. The early collagen, mostly immature type filled up the entire wound bed with spaces in between occupied by fluid which showed no inflammatory reaction.

The control group on day 14 of healing presented a substantial amount of pre-collagen deposition in the reticular dermis region. The collagen appeared to be loosely arranged with spaces having thin and long structural pattern representing early immature type of collagen synthesis. Rete pegs was not visible but distinctive epidermis and dermis could be appreciated. With the standard topicure gel application compactly packed strands of early collagen deposition were abundantly visible in both the papillary and reticular dermis region. While the papillary dermis precollagen fibres were loosely arranged, an abundance of rete pegs were also observed. In the GSE-Gel treated wound, the healing matrix was evidenced with an abundant appearance of precollagen fibres compactly filling up the entire papillary and reticular dermis region. The appearance of collagen fibers in bundles and rete pegs had begun by day 14. While the collagen was mostly immature type with thin fibers in the papillary dermis, the reticular dermis still presented a more mature type of collagen fibers indicating early collagen maturation in this group.

On day 21, the control wound depicted the presence of immature type of collagen strands in the papillary dermis while a more mature type was seen in the reticular dermis region. The collagen bundles were slackly arranged without any definite pattern being filled up with spaces within the matrix. The rete ridges had appeared by this time suggesting its slow healing progression. In the standard topicure gel group, mature collagen bundles were seen in day 21 of healing arranged anisotropically. However the matrix was loosely segregated in its fiber arrangement. The adnexal structures forming the structural and functional elements of the skin

tissues were well appreciated in this group by 21 of healing. In the GSE-Gel treated wound, isotropically arranged group of mature collagen bundles were seen occupying the dermis region. The thick fibres arranged themselves in a basket-weave pattern suggestive of mature type of collagen deposition supporting the structural elements of the extra-cellular matrix. Along with mature type of collagen, adnexal structures were abundantly renewed in the healing skin.

The deposition of Elastin fibers were analysed qualitatively by staining the tissue sections with Verhoeff–Van Gieson stain (VVG) method to investigate the role of the developed gel in remodelling the ECM during wound healing (**Figure 4.12c**).

After 7 days in the control wound, short, thin and scattered segments of elastin fibers were observed in papillary dermis region. The elastin fibres appeared immature, and randomly present in the dermis. In the standard topicure gel group, elastosis was minimal within this time period with the appearance of clustered spots of elastic tissue randomly occupying scattered spots of the dermis. In the GSE-Gel treated group, small thin, immature strands of elastic fibers were appreciated at scattered spots of the epidermo-dermal section.

In the control group elastosis was moderate on day 14 of healing with only scattered spots of elastic tissue occupying the wound bed. The thin immature fibres lacked the interlacing pattern and dispersed over the matrix without definite orientation. In the standard topicure group fine fibers of elastin were arranged isotropically in close association with the immature collagen fibres in the granulation tissue matrix. An even distribution of fibres with spacing pattern was observed in the dermis region. In the GSE-Gel treated group, an even distribution of isotropically spaced elastin fibres in close association with the collagen fibers were seen the dermis region. Elastic fibers was securely placed and abundantly latticed in the matrix in both; the standard topicure and GSE-Gel treated groups

A significant amount of thick elastic fibers were observed in the control group on day 21 of healing. The fibers appeared matured and dispersed over the dermis, however the fibers lacked any specific arrangement and orientation making them slackly organized. In the standard topicure group, dense elastois was evident on day 21 of healing. Thick, robust and mature fibers of elastin tissue in close association with mature collagen bundles were observed in the reticular and papillary dermis; however the fibers lacked the definite arrangement in the ECM and randomly oriented. A copious deposition of thick, mature and robust elastic fibers were observed in the GSE-Gel treated group. The fibers secured themselves with the mature collagen

bundles that were interlaced in the ECM. The thick fibers sew themselves firmly within the protein fibrous structural basement in a definite organizational pattern conducive to efficient ECM rebuilding in the skin tissues.

4.3.19 Immunohistochemistry analysis

To assure the expression of mature collagen (type 1) in the healing tissue, an immunohistochemistry examination was conducted in the retrieved tissue sections (**Figure 4.12d**). On day 14 of healing we observed a positive expression of collagen type 1 in all the groups under study. However, a dense deposition was observed in standard topicure and GSE-Gel treated groups in comparison to the control group. Similar observation followed on day 21, where the control group expressed collagen type 1 prominently in the reticular dermis region whereas in the standard topicure and GSE-Gel treated groups, we observed a copious expression in both the papillary and reticular dermis emerging into the epidermis too.

Neovascularization is an essential factor in wound healing as new tissue growth is dynamically regulated by the blood vascular supply that serves multifactorial functions in replenishing nutrients, oxygen, and growth factors to the repairing cells and draining out metabolites thereby conditioning the microenvironment for cellular and ECM turnover. To assess the extent of neovascularization in the healing tissues, CD 31, an endothelial cell marker was identified by immunohistochemical methods(**Figure 4.12e**). On day 7, we observed that positive expression for CD31 was scanty in all the treatment and control groups. By day 14 of treatment an intense positive expression for the marker was noted in GSE-Gel treated group that was significantly ($p < 0.05$) higher than the standard topicure and control groups. The markers were situated intensively as random distributed spots covering the vast stretches of the granulation tissue and also around sprouting blood vessels. This intense neovascularity feature by the formulated GSE- gel is a unique feature of promoting tissue renewal by way of stimulating angiogenesis as validated from the present study.
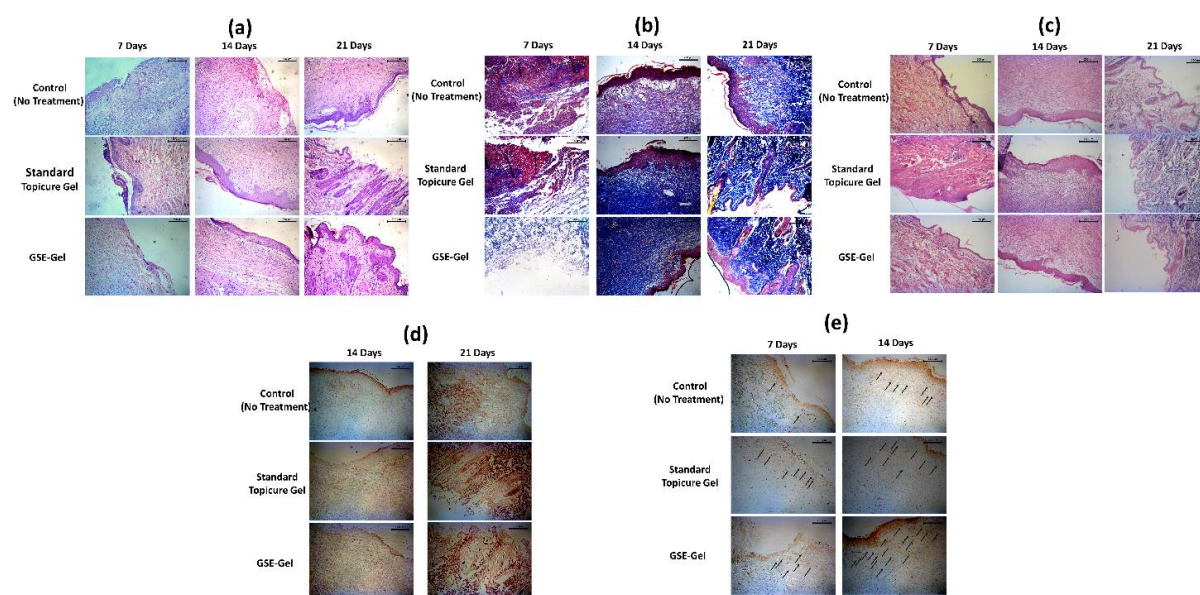
Figure 4.12: Histological assessment of H&E-stained tissue slices from sample treatment and control groups on healing days 7, 14, and 21.(a); Histological slices of wound tissues stained using Masson's trichrome technique on days 7, 14, and 21 post-wounding to demonstrate collagen fibres in the healing tissues.(b); Histological slices of injured tissues illustrating elastin fibres at various time periods throughout the healing process stained by Verhoeff–Van Gieson stain (VVG) method (c); Images of collagen type 1 deposition in the ECM by immunohistochemistry on days 14 and 21 after healing.(d). Immunohistochemistry pictographs depicting the distribution of CD 31/PECAM 1 over the first 7 and 14 days of wound healing. Neovascularization is indicated by the black arrows pointing to CD 31-positive findings.(e).

Cellular functions play a key role in regulating the outcomes of any healing process wherein the intricate functions of cellular recruitment, migration, proliferation and maturation are intertwined sequentially for progression towards functional healing [65]. In this perspective, the GSE-gel designed as a wound healing agent showed immense potential in the healing of cutaneous wounds through an activated cellular response and an efficient ECM stacking in the wound bed. GSE-gel treated wounds represented an early wound closure as compared to both the controls, by an effective growth of neo-epidermis and underlying tissue matrix. It stimulated cell recruitment, enhanced angiogenesis, collagenization and ECM reconstruction (**Fig4.12b and Figure 4.12c**). These functional implications could be attributed to the synergistic roles of bioactive ingredients richly present in the GSE-gel viz the polyphenols such as (−)-epicatechin, (+)-catechins, and (−)-epicatechin-3-o-gallate and proanthocyanidins [66].

These bioactives exert potent anti-inflammatory, anti-oxidant, and antibacterial effects that favourably induced the wound microenvironment towards achieving a healing state [67]. Enhanced neovascularization by positive expression of CD31 is a notable feature of wound healing by GSE-gel (**Figure 4.12e**). This could be ascribed to Proanthocyanidins mediated upregulation and secretion of vascular endothelial growth factor, a key cytokine that regulates angiogenesis and sprouting of new blood vessels for efficient wound rebuilding as reported in some previous study [68].

Thus, this simplistic bioactive gel-based wound healing approach has remarkable features in terms of cost, availability, efficacy and applicability and therefore could hold surprising benefits for the biomedical front in the future years.

4.4 Inference

This study demonstrates the potential use of a by-product of the wine industry - grape seed extract - as a sustainable and viable resource for biomedical applications. Extraction resulted in a proanthocyanidin-rich extract that showed great biocompatibility in vitro. In addition, the extract showed significant anti-inflammatory and antioxidant activities, suggesting its potential in the field of wound healing therapeutics. When this extract was incorporated in a starch glycerite gel, the formulation showed superior wound healing properties than the commercially available ointment and control when evaluated on a wound defect model in rabbits. The GSE gel supported angiogenesis and attenuated inflammation, which translated into improved healing compared with untreated control mice. This approach not only reduces agricultural waste but also adds value to a byproduct of the winemaking industry and at the same time aligns with sustainable and environmentally friendly practices. Utilization of grape seed extract will reduce waste and promote the development of eco-friendly medical treatments. This study opens new paths for the conception of effective, sustainable wound healing therapies, signifying the potential for integrating natural, renewable resources into medical applications. This GSE-Gel also shows a potential effect on pro-inflammatory cytokines thus it can also act as potential therapy for GSE dysregulation as well as the high proanthocyanidins content could act as a good crosslinking agent.

References

[1] H.J. Blackham, The fable as literature, A\&C Black, 2014.

[2] M. Bordiga, F. Travaglia, M. Locatelli, Valorisation of grape pomace: an approach that is increasingly reaching its maturity--a review, Int J Food Sci Technol 54 (2019) 933–942.

[3] S.H. Abu Hafsa, S.A. Ibrahim, Effect of dietary polyphenol-rich grape seed on growth performance, antioxidant capacity and ileal microflora in broiler chicks, J Anim Physiol Anim Nutr (Berl) 102 (2018) 268–275.

[4] F. Pasini, F. Chinnici, M.F. Caboni, V. Verardo, Recovery of oligomeric proanthocyanidins and other phenolic compounds with established bioactivity from grape seed by-products, Molecules 24 (2019) 677.

[5] A. Smeriglio, D. Barreca, E. Bellocco, D. Trombetta, Proanthocyanidins and hydrolysable tannins: occurrence, dietary intake and pharmacological effects, Br J Pharmacol 174 (2017) 1244–1262. https://doi.org/10.1111/bph.13630.

[6] C. Beres, G.N.S. Costa, I. Cabezudo, N.K. da Silva-James, A.S.C. Teles, A.P.G. Cruz, C. Mellinger-Silva, R. V Tonon, L.M.C. Cabral, S.P. Freitas, Towards integral utilization of grape pomace from winemaking process: A review, Waste Management 68 (2017) 581–594.

[7] B. Ahmad, V. Yadav, A. Yadav, M.U. Rahman, W.Z. Yuan, Z. Li, X. Wang, Integrated biorefinery approach to valorize winery waste: A review from waste to energy perspectives, Science of the Total Environment 719 (2020) 137315.

[8] M.A. Bustamante, C. Paredes, R. Moral, J. Moreno-Caselles, A. Pérez-Espinosa, M.D. Pérez-Murcia, Uses of winery and distillery effluents in agriculture: characterisation of nutrient and hazardous components, Water Science and Technology 51 (2005) 145–151.

[9] K.P.M. Mosse, A.F. Patti, E.W. Christen, T.R. Cavagnaro, Winery wastewater quality and treatment options in Australia, Aust J Grape Wine Res 17 (2011) 111–122.

[10] M.-P. Zacharof, Grape winery waste as feedstock for bioconversions: applying the biorefinery concept, Waste Biomass Valorization 8 (2017) 1011–1025.

[11] M.-P. Zacharof, R.W. Lovitt, Adding value to wastewater by resource recovery and reformulation as growth media: current prospects and potential, Journal of Water Reuse and Desalination 5 (2015) 473–479.

[12] P.K. Sarangi, A.K. Singh, R.K. Srivastava, V.K. Gupta, Recent Progress and Future Perspectives for Zero Agriculture Waste Technologies: Pineapple Waste as a Case Study, Sustainability 15 (2023) 3575.

[13] T. Ariga, The antioxidative function, preventive action on disease and utilization of proanthocyanidins, Biofactors 21 (2004) 197–201.

[14] V. Lobo, A. Patil, A. Phatak, N. Chandra, Free radicals, antioxidants and functional foods: Impact on human health, Pharmacogn Rev 4 (2010) 118.

[15] S. Khanna, M. Venojarvi, S. Roy, N. Sharma, P. Trikha, D. Bagchi, M. Bagchi, C.K. Sen, Dermal wound healing properties of redox-active grape seed proanthocyanidins, Free Radic Biol Med 33 (2002) 1089–1096. https://doi.org/10.1016/S0891-5849(02)00999-1.

[16]   A.A. sghar Hemmati, M. Foroozan, G. Houshmand, Z.B. eigom Moosavi, M. Bahadoram, N.S. hakiba Maram, The topical effect of grape seed extract 2% cream on surgery wound healing, Glob J Health Sci 7 (2015) 52–58. https://doi.org/10.5539/gjhs.v7n3p52.

[17]   G. Carullo, F. Sciubba, P. Governa, S. Mazzotta, L. Frattaruolo, G. Grillo, A.R. Cappello, G. Cravotto, M.E. Di Cocco, F. Aiello, Mantonico and pecorello grape seed extracts: Chemical characterization and evaluation of in vitro wound-healing and anti-inflammatory activities, Pharmaceuticals 13 (2020) 97. https://doi.org/10.3390/ph13050097.

[18]   V.Y.A. Barku, Wound healing: contributions from plant secondary metabolite antioxidants, Wound Heal Curr Persp (2019).

[19]   E. Eriksson, P.Y. Liu, G.S. Schultz, M.M. Martins-Green, R. Tanaka, D. Weir, L.J. Gould, D.G. Armstrong, G.W. Gibbons, R. Wolcott, others, Chronic wounds: Treatment consensus, Wound Repair and Regeneration 30 (2022) 156–171.

[20]   V. Falanga, R.R. Isseroff, A.M. Soulika, M. Romanelli, D. Margolis, S. Kapp, M. Granick, K. Harding, Chronic wounds, Nat Rev Dis Primers 8 (2022) 50.

[21]   A. Syahidah, C.R. Saad, H.M. Daud, Y.M. Abdelhadi, Status and potential of herbal applications in aquaculture: A review, (2015).

[22]   L.L. Bolton, W. Oleniacz, B. Constantine, B.O. Kelliher, D. Jensen, B. Means, D. Rovee, Repair and antibacterial effects of topical antiseptic agents, Models in Dermatology 2 (1985) 145–158.

[23]   D.G. Greenhalgh, Topical antimicrobial agents for burn wounds, Clin Plast Surg 36 (2009) 597–606.

[24]   C.D. Brown, J.A. Zitelli, A review of topical agents for wounds and methods of wounding: guidelines for wound management, J Dermatol Surg Oncol 19 (1993) 732–737.

[25]   M. Gupta, S. Dey, D. Marbaniang, P. Pal, S. Ray, B. Mazumder, Grape seed extract: Having a potential health benefits, J Food Sci Technol 57 (2020) 1205–1215.

[26]   L. Baumann, Skin ageing and its treatment, The Journal of Pathology: A Journal of the Pathological Society of Great Britain and Ireland 211 (2007) 241–251.

[27]   S. Soorgi, A.M. Izadpanah, G.R. Sharifzadeh, M. Torshizi, Z. Khazaye, M. Hasanpour, The effects of grape seed extract ointment on approximation of cesarean section wound, Modern Care Journal 13 (2016).

[28]   N.P.E. Hikmawanti, S. Fatmawati, A.W. Asri, The effect of ethanol concentrations as the extraction solvent on antioxidant activity of Katuk (Sauropus androgynus (L.) Merr.) leaves extracts, in: IOP Conf Ser Earth Environ Sci, 2021: p. 12060.

[29]   B. Guo, K. Lv, Y. Hu, J. Du, Y. Lv, Study on Optical Properties and Biological Activity of Proanthocyanidins at Different pH and Alkalinit, in: IOP Conf Ser Earth Environ Sci, 2021: p. 12040.

[30]   H.-R. Lee, M.-J. Bak, W.-S. Jeong, Y.-C. Kim, S.-K. Chung, Antioxidant properties of proanthocyanidin fraction isolated from wild grape (Vitis amurensis) seed, J Korean Soc Appl Biol Chem 52 (2009) 539–544.

[31] S. Upanan, S. Yodkeeree, P. Thippraphan, W. Punfa, R. Wongpoomchai, P. Limtrakul, The proanthocyanidin-rich fraction obtained from red rice germ and bran extract induces HepG2 hepatocellular carcinoma cell apoptosis, Molecules 24 (2019) 813.

[32] N. Siddiqui, A. Rauf, A. Latif, Z. Mahmood, Spectrophotometric determination of the total phenolic content, spectral and fluorescence study of the herbal Unani drug Gul-e-Zoofa (Nepeta bracteata Benth)., J Taibah Univ Med Sci 12 (2017) 360–363. https://doi.org/10.1016/j.jtumed.2016.11.006.

[33] S. Sravan Kumar, P. Manoj, P. Giridhar, Fourier transform infrared spectroscopy (FTIR) analysis, chlorophyll content and antioxidant properties of native and defatted foliage of green leafy vegetables., J Food Sci Technol 52 (2015) 8131–8139. https://doi.org/10.1007/s13197-015-1959-0.

[34] P. Das, T. Dutta, S. Manna, S. Loganathan, P. Basak, Facile green synthesis of non-genotoxic, non-hemolytic organometallic silver nanoparticles using extract of crushed, wasted, and spent Humulus lupulus (hops): Characterization, anti-bacterial, and anti-cancer studies, Environ Res 204 (2022) 111962. https://doi.org/10.1016/j.envres.2021.111962.

[35] S. Jana, P. Datta, H. Das, P.R. Ghosh, B. Kundu, S.K. Nandi, Engineering Vascularizing Electrospun Dermal Grafts by Integrating Fish Collagen and Ion-Doped Bioactive Glass, ACS Biomater Sci Eng 8 (2022) 734–752.

[36] A.S. Mørkholt, O. Wiborg, J.G.K. Nieland, S. Nielsen, J.D. Nieland, Blocking of carnitine palmitoyl transferase 1 potently reduces stress-induced depression in rat highlighting a pivotal role of lipid metabolism, Sci Rep 7 (2017) 2158.

[37] T. Baranek, R. Debret, F. Antonicelli, B. Lamkhioued, A. Belaaouaj, W. Hornebeck, P. Bernard, M. Guenounou, R. Le Naour, Elastin receptor (spliced galactosidase) occupancy by elastin peptides counteracts proinflammatory cytokine expression in lipopolysaccharide-stimulated human monocytes through NF-$κ$B down-regulation, The Journal of Immunology 179 (2007) 6184–6192.

[38] F.L. Geiler, A method of preparing glycerite of starch, J Am Pharm Assoc 23 (1934) 810–811.

[39] P. Basak, P. Das, S. Biswas, N.C. Biswas, G.K. Das Mahapatra, Green Synthesis and Characterization of Gelatin-PVA Silver Nanocomposite Films for Improved Antimicrobial Activity, in: IOP Conf Ser Mater Sci Eng, 2018. https://doi.org/10.1088/1757-899X/410/1/012019.

[40] J. Goldner, A modification of the Masson trichrome technique for routine laboratory purposes, Am J Pathol 14 (1938) 237.

[41] K.R. Percival, Z.A. Radi, A modified Verhoeff-van Gieson elastin histochemical stain to enable pulmonary arterial hypertension model characterization, Eur J Histochem 60 (2016).

[42] S. Jana, P. Datta, H. Das, S. Jaiswal, P.R. Ghosh, D. Lahiri, B. Kundu, S.K. Nandi, Copper and cobalt doped bioactive glass-fish dermal collagen electrospun mat triggers key events of diabetic wound healing in full-thickness skin defect model, J Mech Behav Biomed Mater 134 (2022) 105414.

[43] K. Waszkowiak, A. Gliszczyńska-Świgło, Binary ethanol--water solvents affect phenolic profile and antioxidant capacity of flaxseed extracts, European Food Research and Technology 242 (2016) 777–786.

[44] C. Rodr\'\iguez-Pérez, B. Garc\'\ia-Villanova, E. Guerra-Hernández, V. Verardo, Grape seeds proanthocyanidins: An overview of in vivo bioactivity in animal models, Nutrients 11 (2019) 2435.

[45] L.-Z. Lin, J.M. Harnly, Quantitation of flavanols, proanthocyanidins, isoflavones, flavanones, dihydrochalcones, stilbenes, benzoic acid derivatives using ultraviolet absorbance after identification by liquid chromatography--mass spectrometry, J Agric Food Chem 60 (2012) 5832–5840.

[46] M.S. Maoela, O.A. Arotiba, P.G.L. Baker, W.T. Mabusela, N. Jahed, E.A. Songa, E.I. Iwuoha, Electroanalytical determination of catechin flavonoid in ethyl acetate extracts of medicinal plants, Int J Electrochem Sci 4 (2009) 1497–1510.

[47] R. Yadav, D. Kumar, A. Kumari, S.K. Yadav, Encapsulation of catechin and epicatechin on BSA NPs improved their stability and antioxidant potential, EXCLI J 13 (2014) 331.

[48] A. Rauf, M. Imran, T. Abu-Izneid, S. Patel, X. Pan, S. Naz, A.S. Silva, F. Saeed, H.A.R. Suleria, others, Proanthocyanidins: A comprehensive review, Biomedicine \& Pharmacotherapy 116 (2019) 108999.

[49] X. Lan, X. Han, Q. Li, J. Wang, (-)-Epicatechin, a natural flavonoid compound, protects astrocytes against hemoglobin toxicity via Nrf2 and AP-1 signaling pathways, Mol Neurobiol 54 (2017) 7898–7907.

[50] M. Bayati, H.-Y. Hsieh, S.-Y. Hsu, C. Li, E. Rogers, A. Belenchia, S.A. Zemmer, T. Blanc, C. LePage, J. Klutts, others, Identification and quantification of bioactive compounds suppressing SARS-CoV-2 signals in wastewater-based epidemiology surveillance, Water Res 221 (2022) 118824.

[51] L.-J. Li, M.-Z. Wang, T.-J. Yuan, X.-H. Xu, H.A. Dad, C.-L. Yu, J. Hou, L.-H. Peng, The crude ethanol extract of Periplaneta americana L. stimulates wound healing in vitro \& in vivo, Chin Med 14 (2019) 1–9.

[52] T. Somarathna, M.G. Thammitiyagodage, K. Ranaweera, G.A.S. Premakumara, M.A. Akbarsha, B. Kadalmani, N.S. Weerakkody, In vivo and in vitro toxicity profiles of hexane extract of Alpinia malaccensis rhizome in rat and cell line models, J Toxicol 2021 (2021) 9578474.

[53] V. Nemudzivhadi, P. Masoko, In vitro assessment of cytotoxicity, antioxidant, and anti-inflammatory activities of Ricinus communis (euphorbiaceae) leaf extracts, Evidence-Based Complementary and Alternative Medicine 2014 (2014) 625961.

[54] S. Ghayempour, M. Montazer, M.M. Rad, Encapsulation of Aloe Vera extract into natural Tragacanth Gum as a novel green wound healing product, Int J Biol Macromol 93 (2016) 344–349.

[55] A. Ligasová, I. Frydrych, K. Koberna, Basic Methods of Cell Cycle Analysis, Int J Mol Sci 24 (2023) 3674.

[56] S. Vimalraj, S. Renugaa, A. Dhanasekaran, Chick embryo chorioallantoic membrane: a biomaterial testing platform for tissue engineering applications, Process Biochemistry (2022).

[57] A. Laborda-Illanes, L. Sánchez-Alcoholado, D. Castellano-Castillo, S. Boutriq, I. Plaza-Andrades, L. Aranega-Mart\'\in, J. Peralta-Linero, E. Alba, A. González-González, M.I. Queipo-Ortuño, Development of in vitro and in vivo tools to evaluate the antiangiogenic potential of melatonin to neutralize the angiogenic effects of VEGF and breast cancer cells: CAM assay and 3D endothelial cell spheroids, Biomedicine \& Pharmacotherapy 157 (2023) 114041.

[58] M.A. Eissa, Y.Z.H.Y. Hashim, S.S.S. Abdul Azziz, H.M. Salleh, M.L.M. Isa, N.M. Abd Warif, F. Abdullah, E. Ramadan, D.M. El-Kersh, Phytochemical Constituents of Aquilaria malaccensis leaf extract and their anti-inflammatory activity against LPS/IFN-$γ$-stimulated RAW 264.7 cell line, ACS Omega 7 (2022) 15637–15646.

[59] D.R. Dwijayanti, S. Puspitarini, N. Widodo, Piper betle L. Leaves Extract Potentially Reduce the Nitric Oxide Production on LPS-Induced RAW 264.7 Cell Lines, The Journal of Experimental Life Science 13 (2023) 78–83.

[60] R.T. Ruhee, S. Ma, K. Suzuki, Sulforaphane Protects Cells against Lipopolysaccharide-Stimulated Inflammation in Murine Macrophages., Antioxidants (Basel) 8 (2019). https://doi.org/10.3390/antiox8120577.

[61] K.-J. Yun, J.-Y. Kim, J.-B. Kim, K.-W. Lee, S.-Y. Jeong, H.-J. Park, H.-J. Jung, Y.-W. Cho, K. Yun, K.-T. Lee, Inhibition of LPS-induced NO and PGE2 production by asiatic acid via NF-$κ$B inactivation in RAW 264.7 macrophages: Possible involvement of the IKK and MAPK pathways, Int Immunopharmacol 8 (2008) 431–441.

[62] C.-Y. Chen, W.-H. Peng, K.-D. Tsai, S.-L. Hsu, Luteolin suppresses inflammation-associated gene expression by blocking NF-$κ$B and AP-1 activation pathway in mouse alveolar macrophages, Life Sci 81 (2007) 1602–1614.

[63] L. Gilbert, C. Picard, G. Savary, M. Grisel, Rheological and textural characterization of cosmetic emulsions containing natural and synthetic polymers: relationships between both data, Colloids Surf A Physicochem Eng Asp 421 (2013) 150–163.

[64] V. Albright, A. Marin, P. Kaner, S.A. Sukhishvili, A.K. Andrianov, New family of water-soluble sulfo--fluoro polyphosphazenes and their assembly within hemocompatible nanocoatings, ACS Appl Bio Mater 2 (2019) 3897–3906.

[65] L. Yildirimer, N.T.K. Thanh, A.M. Seifalian, Skin regeneration scaffolds: a multimodal bottom-up approach, Trends Biotechnol 30 (2012) 638–648.

[66] M. Nassiri-Asl, H. Hosseinzadeh, Review of the Pharmacological Effects of Vitis vinifera (Grape) and its Bioactive Constituents: An Update. Phyther Res. 2016; 30 (9): 1392–1403, (n.d.).

[67] A. Ajit, A.G. Vishnu, P. Varkey, Incorporation of grape seed extract towards wound care product development, 3 Biotech 11 (2021) 261.

[68] A.A. Hemmati, G. Houshmand, Z.B. Moosavi, M. Bahadoram, N.S. Maram, The topical effect of grape seed extract 2% cream on surgery wound healing, Glob J Health Sci 7 (2015) 52.

Chapter V

Fabrication and Characterization of Starch-PVA Thin Films Crosslinked with Proanthocyanidin-Rich Grape Seed Extract for wound healing application

5.1 Background

The use of sustainable technologies in the field of healthcare is transforming the industry by significantly reducing the harmful impact towards the environment while maintaining high-quality care towards the patient. The integration of sustainable technologies into health care is creating positive economic, social, and environmental impacts[1]. The recent advances include the use of renewable energies, the implementation of energy-efficient designs and comprehensive waste management systems[2].Along with this the inclusion of newer technologies like telemedicine, electronic health records, and green pharmaceuticals is making a big impact in reducing the carbon footprint and hence promoting eco-friendly practices[3]. All these together contribute to creating a more sustainable and health-conscious future, ensuring superior and advanced healthcare facilities to treat patients without any harm to the environment.

One of the biggest concerns in the field of healthcare is promoting sustainable routes for fabricating various devices and biomaterials. Fabrication of green and effective wound dressing material is one of the current fields of research in which scientists are focusing deeply. The largest organ in the body is the skin which is made up of three layers called the epidermis, dermis, and hypodermis[4]. It serves as a barrier of defence against pathogens, UV radiation and other harmful substances as well as mechanical, thermal, physical, and chemical elements. It also permits the perception of heat, touch, and cold and aids in controlling body temperature[5]. However, damage or injury in the skin's normal structure results in the destruction of the skin, resulting in the loss of skin tissue and integrity[6]. The process of treating a wound continuously involves preventing skin deterioration and creating an environment that is conducive to healing through both direct and indirect means. A wound is defined as an injury or damage to the skin's epidermis caused by a burn or physical injury. Wound recovery is a dynamic procedure that necessitates an ideal environment for the healing process to take place in an extremely complex phenomenon[7]. There are three different kinds of wounds: acute, chronic and burn. Tissue damage from resection injuries or unconscious trauma is what causes an acute infectious wound. Depending on the extent and depth of the skin wound, it takes around 12 weeks to heal. Chronic infectious wounds refer to wounds that do not heal according to a regular time frame rather healing process is a very slow, and takes a lot longer to recover completely[8]. Burn wounds are regarded as a distinct kind of injury because of their particular pathophysiology, which has the potential to permanently damage blood vessels and nerves deep within the body. One or more of the following effects of this

damage may impede the healing process: decreased cell influx, restricted nutrient and oxygen supply, and impaired signalling. Burn injuries therefore increase the risk of infection and scarring and may also result in reduced sensation[9]. Managing wound care is one of the very challenging tasks, emergency wounds need to be treated right away to reduce the risk of permanent disability, infection, deformity, morbidity, and death. Before their evacuation to a hospital, patients' conditions are considerably improved when prompt wound care management is provided during the "golden hour"[10]. The "golden hour" in wound healing refers to the critical period immediately following an injury, typically within the first hour, during which prompt medical intervention can significantly improve the chances of optimal healing and reduce complications such as infection. Early treatment during this period maximizes the potential for tissue repair and minimizes scarring or further damage.

Traditional wound dressings have been around since the 19th century and have been widely used because of their low cost, ease of application, and straightforward manufacturing. This category of dressings includes gauze, bandages, plasters, and lint. Despite protecting the wound from outside infections, they are unable to regulate the amount of moisture they absorb from the wound, making it too dry for quick healing. Furthermore, if there is excessive wound drainage, dressings might stick to the wound, making removal painful and difficult. As a result, traditional dressings are typically applied as secondary dressings or to wounds with mild extrusion[11]. Current wound dressings use a variety of multifunctional polymer-based systems that have the potential to significantly accelerate wound healing[12]. Polymers are of two types natural and synthetic polymers. Since the use of synthetic polymers is associated with environmental issues, natural polymers that are eco-friendly and renewable are being used in an effort to reduce the risks and high costs of plastic recycling and disposal. When using both synthetic and natural polymers to create composites, there will inevitably be a transitional phase. Using synthetic and natural polymer combinations offers feasible methods to improve the biodegradability of synthetic polymers[13]. The goal of both traditional and modern research in the field of biocomposite films for biomedical applications is to create blends that are low-cost, simple to fabricate, and highly biodegradable with suitable combinations of characterization parameters[14].

Various research is currently being done on transforming wastes into biomaterials that are affordable, safe for the environment, and economically feasible for use in biomedical applications like wound healing, tissue engineering, and drug delivery. Because biomaterials made from these extracted raw materials are found to satisfy most or all of these requirements,

they are being used extensively in the biomedical fields[15]. One such product is winery waste. Wine is the product of the chemical fermentation of must, or grape juice (*Vitis vinifera L.*), which is carried out by yeasts that use the sugars in the grapes to produce CO_2 and ethanol. Because of their medicinal qualities, grapes and grape residues (pomace or marc), such as lees and seeds, are interesting products in the winemaking industry. Byproducts like oil seeds and pomace yeasts are natural sources of bioactive compounds as reported. Because of this, wineries have used natural bio-products to increase their influence on the environment and the economy[16,17]. Bioactive compounds with pharmacological importance can be found in abundance in grapes and grapes seed. Bioactive compounds, or secondary metabolites that plants produce in response to stress, are abundant in grapes and their byproducts. Approximately 70% of the bioactive molecules among these constituents are composed of phenolic compounds[18]. These compounds also contain other advantageous qualities, such as antibacterial, anti-inflammatory, and antioxidant activities, which may facilitate wound healing. Previous research has demonstrated that grape extracts enhance the hemostatic properties of graphene oxide aerogels reinforced with PVA and chitosan[19].

Many materials are being employed for the fabrication of modern wound dressing. Both synthetic and natural polymers are being well employed to create effective and degradable dressing mats. Starch is one of the most cost-effective natural polymers since it can be readily made from sustainable natural biological resources like corn, potatoes, wheat, and rice[14]. It is frequently utilized in biomedical applications because it is biodegradable and biocompatible[20]. Polyvinyl Alcohol(PVA)on the other hand have many advantages, including excellent film formation, non-toxicity, biocompatibility, and non-carcinogenicity, they have already been used in a wide range of biomedical and pharmaceutical applications[21]. Hydrophilic, non-toxic, and easily scalable composite biomaterials based on starch and PVA are widely employed as scaffolding support materials in tissue engineering. In comparison to all other synthetic polymer-derived materials, the starch-based/PVA composite films show superior biodegradability, mechanical and pH stability, flexibility, and semi-permeability[14,22–24]. This allows nutrients and oxygen to be delivered to the wound bed area, which is essential for the survival of biological cells[25].

Along with the creation and fabrication of effective wound dressing materials concerns related to biomedical waste and waste generation due to bioproducts should also be considered. The idea of the circular economy altered how processes are perceived. Utilizing feedstocks to their utmost potential and processing wastes produced during the transformation process are

essential components of the "zero waste" challenge[26]. Pre-clinical and clinical evaluation of grape seed extracts produced encouraging results, supporting their potential application in wound healing. Notably, the use of grape seeds, an enological by-product, ensures environmental sustainability in the supply chain and represents the basis for an "intelligent" reconversion of waste achieved through eco-compatible "green technologies"[27].

Thus, this work tries to incorporate sustainable technology to fabricate a wound dressing material using PVA and Starch loaded with grape seed extract derived from winery waste which would not only promote healing but also the proanthocyanidin in the extract might have a strong effect in crosslinking the material. The use of the selected polymers would help to heal wounds and at the same time, these polymers are highly biocompatible and have no adverse effect towards the environment. This work aims to fill in the drawbacks of the earlier work i.e fabrication of sustainable wound dressing materials for wound healing materials. This work uses waste-derived grape seed extract by replacing commercially available grape seed extract.

5.2. Materials and Method

5.2.1 Materials

Modified Starch powder (Allwyn Chem Industries, ALW600-I50) , Polyvinyl Alcohol (Loba Chemie, Mol Wt-1,15,000 approx.) .L929 cells were procured from NCCS Pune. The purchase of DMEM (Dulbecco's Modified Eagle Medium) and FBS (Fetal Bovine Serum) required for cell culture Media was accomplished from Thermo Fisher Scientific - IN, on the other hand, Penicillin-streptomycin and 3-(4,5-dimethylthiazol-2-yl)-2,5-diphenyltetrazolium bromide (MTT) were obtained from HiMedia Laboratories Pvt. Ltd.Poly Vinlyl Alcohol (PVA) was procured from Loba Chemie. Xylaxin(20mg/ml) was purchased from Indian Immunologicals in India, whereas ketamine hydrochloride(50mg/ml) was obtained from Ketalar, a product of Parke-Davis in India. The purchase of Fluorescein Diacetate (FDA) was procured from Thermo Fisher Scientific. Plasticware was mostly procured from Tarsons.

5.2.2 Preparation and Fabrication of Polymeric Composite Film:
The fabrication of biopolymer-based composite films was carried out using the conventional solvent casting method. In brief, Polyvinyl alcohol (PVA) and Food grade starch were mixed in distilled water and stirred for 45-60mins to get a homogenized solution. The grape seed extract was prepared by extracting the phytochemicals of winery waste-derived grape seed using a 70% ethanol solution. The extract was then concentrated using a rotary evaporator and finally was lyophilized to make a formulation dosage("Intellectual Property India," 2023, Application

Number: 202331073970). 2.5%(w/v) of the grape seed was finally added to the polymer mixture after cooling and the mixture was again stirred for another 2 hours for proper mixing. Finally, the whole mixture was poured into Glass Petri dishes and was left for drying. After 48 hours of air drying at room temperature, the thin films were peeled off and stored in desiccators for further use. The starch and PVA were employed at a maximum concentration of 5% w/v. Three separate PVA and starch composites were developed and are listed in Table 5.1.

Table 5.1: Sample Composition and coding

Sample Code	PVA: Starch	Amount of PVA: Starch (in gms)	Amount of Solvent (mL)
PS@2:1	2:1	1.5:0.75	30
PS@1:1	1:1	1.5:1.5	30
PS@1:2	1:2	0.75:1.5	30

5.2.3 Material characterization

5.2.3.1. Fourier Transform Infrared Spectroscopy (FT-IR) analysis:

The molecular interactions and the evaluation of functional groups of the three mats were analysed using a FT-IR equipment system(PerkinElmer Frontier). The FTIR spectra were obtained within the wavelength range of 400–4000 cm^{-1}[29]. The acquired spectra were meticulously filtered to reduce noise without compromising significant data.

5.2.3.2 X-ray Diffractometric Analysis (XRD)

The X-ray diffractometer (Rigaku MiniFlex 600) was used to evaluate the crystallinity of the three distinct compositions of MATs, utilizing a Cu Kα radiation source. The data were gathered by scanning within a range of 2–80° (2θ), using a current of 15 mA and a voltage of 30 kV.

5.2.3.3 Scanning Electron microscope (SEM)

Scanning Electron microscopic analysis was done using ZEISS EVO LS 10 to analyse the surface morphology and film thickness of the different types of fabricated polymeric mats. The accelerating voltage which was employed during the experiment was 30kV. The images were acquired at magnifications of 1.0 K, 2.5 K and 250 x.

5.2.3.4 Atomic Force Microscope (AFM)

The mats were analysed using Atomic Force Microscopy (AFM), (Innova SPM Atomic Force Microscope). The samples were scanned in all three dimensions - x, y, and z using tapping mode.

5.2.3.5 Thermal Analysis

The thermal characteristics were assessed by thermogravimetric analysis (TGA). The thermogravimetric analysis (TGA) was conducted using a TG 209 F1 Libra - NETZSCH thermogravimetric analyzer. The temperature spanned from 25 to 600 °C, with a heating rate of 10 °C/min in a nitrogen atmosphere. This investigation was conducted to measure the temperature at which the polymeric biomaterials undergo breakdown. Subsequently, the results were fitted into derivative analysis to obtain the derivative thermogravimetry (DTG). The crucible utilized for the research was made of Al2O3. The thermal transition of all the Mats was analyzed using Differential Scanning Calorimetry (DSC). The TA Instruments DSC Q20 Differential Scanning Calorimeter (DSC) was used to perform the DSC analysis.

5.2.3.6 Tensile Strength Analysis

The tensile strength properties of three distinct polymeric mats were examined using the Tinius Olsen 5 KT universal testing equipment, manufactured by Tinius Olsen in the United Kingdom. The test employed samples measuring $50 \times 15 \times 0.1$ mm and subjected them to a tensile force of 125 N at a rate of 0.1 mm/min. A clip-type sample holder with a 10-millimetre-long gripping zone was used to hold the samples in place. Nominal stress upon specimen collapse was used to calculate the matting' ultimate stress.. The tensile test was used to compute the mechanical parameters of elastic modulus (EM), ultimate stress, and ultimate strain[30].

5.2.3.7 Contact Angle Analysis

Contact angle experiments were conducted to evaluate the wettability and hydrophobicity of all three mats. The polymeric Mats' static water contact angles were measured using the sessile drop method with a goniometer SURFTENS 4.5 (OEG GmbH, Hessisch Oldendorf, Germany). The experiments were carried out utilizing a 10-microliter water droplet. The droplets on the mats were screened using an image analyzer and the average values were obtained.

5.2.3.8 Nano-indentation Analysis

Nanoindentation tests were conducted to measure the hardness (H) and effective Young's modulus (E*) of the coating using a Hyistron TI 950 (Bruker, Germany). This system provides in-situ indentation load versus indent depth curves. Samples were tested in load constant mode with a maximum nanoindentation load of 1000 μN. A Berkovich diamond indenter was employed. For each specified sample load, five indents were performed and the average values for hardness and modulus were reported in this study.

5.2.3.9 Swelling Index

To evaluate the fluid holding capacity of the sample, the swelling ratio of the film was measured, the films were cut into uniform sizes of area 1 cm^2 and their initial dried weight was recorded. Then, the specimen was immersed in a phosphate buffer solution (PBS) of pH 7.4. The samples were weighed by removing excess moisture at regular intervals of 15, 30, 45, 60, 120 and 180 minutes. In another experiment, the samples were again measured at three different pH buffer solutions of pH 4, pH 7, pH 9 to assess the response of the biomaterial to varying pH, i.e. in acidic, neutral and alkaline conditions. The swelling ratio can be calculated using the formula:

Swelling ratio (%) = (W$_i$-W$_f$)/W$_i$ × 100

where W$_i$ is the initial weight of the sample and W$_f$ is the final weight of the sample measured.

5.2.3.10 Degradation studies

The hydrogel samples were cut into square pieces measuring 1 cm^2. These samples were then immersed in PBS (phosphate-buffered saline) at a temperature of 37°C. Subsequently, the hydrogel samples were taken out from the PBS solution at particular times of day 1, 3, 7, 14, 21, and 28. The samples were dried in the incubator at a temperature of 60°C until they reached a stable weight. The dried hydrogels were measured by weight. The weight loss (%) or degradation of hydrogel can be determined using the following equation:

$$Degradation\ (\%) = \frac{Initial\ weight\ (W0) - Final\ weight\ (W1)}{Initial\ weight\ (W0)}\ X\ 100$$

5.2.4 Anti-bacterial Assay

To assess surface antibacterial activity, gram-positive bacterial strain, Staphylococcus aureus, and gram-negative bacterial strain, Escherichia coli (DH5-α), were selected (1). The hydrogel samples PS@2:1, PS@1:1, and PS@1:2 were evaluated for their antibacterial properties using the direct contact method. Each sample was first cut into a square of 1 cm², placed in a sterilized Petri dish, and then exposed to an UV light for 20 minutes. A sterile Luria Broth (LB) culture of Escherichia coli and S.aureus was grown overnight at 200 rpm and at 37 °C. The bacterial suspension turbidity was adjusted to 0.4-0.5 optical density (OD) at 600 nm by diluting the culture. The sterilized samples were placed in polystyrene plates containing 12 wells. A bacterial suspension (0.5 OD) containing 200 μL was added to the surface of every sample. For two hours, plates were incubated at 37 °C. After that, the films were repeatedly washed with sterile 0.9% saline solution to get rid of the non-adherent bacteria after the cell suspension was removed. Samples were shifted to a centrifuge tube filled with 2 mL of saline solution. The tubes were bath-sonicated for ten minutes in order to remove the adhered bacteria from the sample surface. A vortex mixer was used for 10 seconds to dilute and mix the bacterial suspension. 50 μL of each diluted E. Coli suspension were spread out, plated on LB agar plates, and then incubated for 24 hours at 37 °C. Colonies of E. Coli and S.aureus on agar plates were counted and photographed[31].

5.2.5 Hemolysis Study

The hemocompatibility of three kinds of polymeric films was evaluated using a hemolysis assay, as previously described. Briefly, blood was drawn from a healthy rabbit as per guidelines and was diluted in a ratio of 2:3 with normal saline. All the samples in 1 ml saline, along with Positive control (0.1 % Na_2CO_3) and Negative Control (Saline) were incubated for 30 mins in a 37 C incubator. Subsequently,20ul of the diluted blood was added to all the tubes and the tubes were incubated for 60 mins. Finally, after incubation, the tubes were centrifuged and the absorbance of the supernatants was measured at 540 nm in a spectrophotometer (Carry 60, Agilent). The %Hemolysis was calculated using the below formula[32]:

$$\%Hemolysis = \frac{\text{Absorbance value of Sample} - \text{Absorbance value of negative control}}{\text{Absorbance value of positive control} - \text{Absorbance value of negative control}} \times 100$$

5.2.6 In-Vitro Cell Culture and Compatibility Analysis

The cytocompatibility of the three different mats was tested using L929 fibroblast cells (purchased from NCCS, Pune). Two different types of tests were conducted, firstly the indirect method in which the sample conditioned media was used for evaluation and secondly cells were directly seeded onto the mats at 3 different time points. The conditioned media was prepared using a similar protocol mentioned in previous chapter [33]. Around 5000 cells were seeded into 96 well plates grown overnight using DMEM media along with 10 % FBS. Cells were kept in a CO2 incubator at 37°C. On the next day, the media was discarded and the cells were treated with 3 different conditioned media prepared using the three different polymeric mats. The cells were incubated for 3 different time points i.e. 24hrs,48hrs and 72hrs to finally evaluate the cellular proliferation[34].

The 3-[4,5-dimethylthiazol-2-yl]-2,5-diphenyltetrazolium bromide assay(MTT assay) was used to determine the cell viability. After 4 hours of incubation and crystal dissolution in DMSO, formazan crystals were identified at a wavelength of 575 nm using a BIORAD ELISA Plate Reader. The cellular viability was determined using the following equation.

$$\% \, Cell \, Viability \, = \frac{O.D \; of \; Samples(\; Condtioned \; Media \; Samples)}{O.D \; of \; the \; Control(No \; Treatment} \times 100$$

The in-vitro scratch assay was performed to analyse the healing effects of the polymeric mats. The cells were seeded onto a 12-well plate and a scratch was generated using the tip of the microtip[35]. Following the generation of scratch, the cells were incubated with conditioned media and pictures were taken to evaluate the scratch area. Images were acquired at 0hrs,12hrs and 24hrs.

To evaluate the structure of the cells after the treatment with conditioned media the cells were stained using Rhodamine Phalloidin and 4',6-diamidino-2-phenylindole (DAPI). Cells were seeded onto coverslips and incubated with conditioned media for 24 hours before evaluation. After incubating for 24 hours, the spent medium was promptly taken from the wells and washed twice with PBS (pH 7.4). The cells were then fixed with 4% formaldehyde in PBS for 30 minutes at 37 °C. Subsequently, the cells were exposed to a PBS solution containing 0.1% Triton-X100 for 5 minutes to facilitate cellular permeabilization. The cells were then treated with actin imaging dye, namely a 1:1000 dilution of Rhodamine-phalloidin in PBS with 1% BSA, for 30 minutes. Finally, following thorough washing, the cells were incubated for an

additional 5 minutes with the nucleus staining dye, DAPI[36]. Following incubation and subsequent washing in phosphate-buffered saline (PBS), the mats were examined using a fluorescence filter-enabled microscope (Leica DM 2000, Germany).

The L929 cells were also cultured on the mats to assess the impact of direct contact between the mats and the cells, as well as to analyze the morphological structure of the cells. The cells were cultivated for a certain duration, namely 1, 2, and 3 days, and then prepared for observation of cellular structure, morphology and attachment using a scanning electron microscopy (SEM). Following the specified date, the medium that had been used was removed from the mats containing the cells. The mats were then treated with a solution of 2.5% glutaraldehyde (Grade I, Sigma-Aldrich, USA) in phosphate buffer, with a pH of 7.4. This treatment was carried out at a temperature of 37 °C for 30 minutes. Afterwards, the mats were washed in the same buffer and then dehydrated using a sequential gradient of ethanol (40-100%). Finally, it was dried overnight in a desiccator. The desiccated mats containing cells were coated with a layer of gold-palladium using a sputter-coating technique. The mats were then examined using a scanning electron microscope (Phenom ProX, Phenom-World B.V., Netherlands) at magnifications of 1000× and 2500×.

The cell-seeded mats were also stained using fluorescein diacetate (FDA) to evaluate the cellular viability of the cells while attaching to the mats. The polymeric mats containing cells were exposed to a solution of FDA (Sigma-Aldrich, USA) at a concentration of 10 μg/mL in FBS-free Dulbecco's Modified Eagle's Medium (DMEM) media for 5-7 minutes at room temperature. After incubation, the polymeric mats along with attached cells were rinsed thoroughly three times with newly made sterile PBS and were observed immediately using a fluorescence microscope(Magnus Fluorescence microscope) with a 465 nm filter.

5.2.7 In-Vivo Wound Healing Experiments in Rabbit Model

5.2.7.1 Design of the experiment

The research was conducted with prior consent from the Institutional Animal Ethics Committee (IAEC) WBUAFS, Kolkata-37, India. Nine mature rabbits weighing between 1.8 and 2.0 kg were employed in the current study (763/GO/Re/SL/03/CPCSEA/05/2021-22 dated 26.04.2022 approval no. of IAEC of West Bengal University of Animal and Fishery Sciences.). Before the start of the research, the rabbits both male and female were accommodated in

separate cages and randomly distributed into three groups with alternating 12-hour light and dark cycles in a room with regulated humidity and temperature for 10 days to help acclimatize them to their newly acquired unfamiliar environment. During this period, activities such as feeding schedules and health status were monitored frequently. They were fed consistent, well-balanced food and had unrestricted access to water. After it was established that each rabbit was capable of participating in the experimental procedure, the study on skin wound healing got started. Anesthesia was induced by administering two intramuscular injections of ketamine hydrochloride (at a dosage of 33 mg/kg body weight; KETMIN® 50, Themis Medicare Limited, Uttarakhand, India) and xylazine hydrochloride (at a dosage of 6 mg/kg body weight; XYLAXIN®, Indian Immunologicals Limited, Telangana, India) in a ratio of 11:2 (mg/kg body weight)[37]. Twenty millimeters in diameter full-thickness surgical incisions were created on each side of the mid-thoracolumbar area after aseptically cutting off immobile animals from the thoracolumbar region. Each animal received a total of five wounds in accordance with the experimental protocol, three of which were treated with polymeric films. The other two were maintained as controls, with the negative control receiving no treatment and the positive control receiving Tegaderm Dressing patches. Following surgery, wounds had to be dressed on alternate days, surgical tape and protective gauge bandages was used, as well as intramuscular injections of antibiotics Enrofloxacin @5 mg/kg body weight (Floxidin® VET, Intervet India Pvt. Ltd, Thane, India) and anti-inflammatory drugs Meloxicam @0.6 mg/kg body weight (MELONEX®, INTAS PHARMACEUTICALS LTD, Gujarat, India)[38,39].

Photographs of the wound healing process were taken on the first, third, seventh, tenth, fourteenth, and twenty-first days. On the appropriate days, the wound closure rate was ascertained.

5.2.7.2 Histological examinations

On research days 7, 14, and 21, the healing wound tissues were removed from the experimental animals and immediately cleaned in normal saline to eliminate any debris and blood. They were then stored in 4% neutral buffer formalin until further processing. Before the tissue fragments were implanted in paraffin blocks to create tissue slices, they were first dried with ethanol at a concentration that was graduated in steps. Glass slides were adhered to after the tissue containing paraffin blocks was sectioned into 5 μm thick slices using a microtome. Before performing the histological analyses, the sections were deparaffinized using xylene and

rehydrated by gradually immersing the slides in downgrade ethanol concentrations in descending order. Standard Hematoxylin and Eosin (H&E) staining was then carried out.

The other ECM components were assessed using Masson's trichrome staining , to get the collagen deposition on during the wound healing phases.

5.2.7.3 Immunohistochemistry

Use of immunohistochemistry (IHC) on tissue slices allowed for evaluation of collagen type I production and CD 31/PECAM 1, a marker of blood vessel development. The IHC was assessed using the Vectastain ABC kit, Vectors lab, U.K.[40]

In brief, the tissue slices, which had been preserved in formalin and embedded in paraffin, were soaked in a solution to restore their moisture and then subjected to a temperature of 95°C for 20 minutes. This process was carried out to facilitate the retrieval of antigens through the application of heat, specifically for the purpose of conducting immunohistochemistry (IHC) analysis of collagen type 1 and CD 31. The temperatures were adjusted to citrate buffer with a pH of 6.1 for collagen type 1 and EDTA buffer with a pH of 8 for CD31. Following 3% H_2O_2 peroxidase blocking, the sections were blocked with blocking horse serum for 30 minutes at 37 °C and then cleaned with PBS-Tween 20. The primary antibodies (1:100 dilutions in PBS; monoclonal antibody against collagen type I, Sigma-Aldrich, USA; and monoclonal anti-PECAM 1/anti-CD 31, Sigma-Aldrich, USA, respectively) were then added to the tissue sections and incubated for overnight at 4 °C in a humidified room. The sections were then covered with biotinylated secondary antibodies the following day, and they were allowed to sit at room temperature for half an hour. After the slices were washed and incubated at 37 °C for 30 minutes, the ABC reagent was added. A brown reaction result was eventually obtained after 10 minutes of adding 3,3′-diaminobenzidine (DAB) peroxidase substrate (ImmPACT DAB, peroxidase substrate kit, vector lab, U.K.). Following dehydration through graded alcohol and xylene wash, the sections were mounted using DPX and then examined under a bright field compound microscope. The density of micro blood vessels was measured using DAB positive signals for CD 31, focusing on newly developing blood vessels with a lumen and organized endothelial cells.

5.3. Results and Discussion

The polymeric Films were fabricated using conventional solvent casting techniques and the films were finally peeled off from the glass plates and were used for various characterization and testing.

5.3.1 Analysing Material Characterization

5.3.1.1 FTIR analysis

The FTIR data of six samples, including PVA, starch, grape seed extract, and different PVA-starch mixtures (PS@2:1, PS@1:1, PS@1:2)(**Figure 5.1(a)**), reveal key functional group vibrations and interactions. The spectra exhibit characteristic peaks for PVA and starch, such as O-H stretching (3300-3500 cm^{-1}) , C-H stretching (2900 cm^{-1}:), and C-O stretching vibrations of carbohydrates (1000cm^{-1}:)., Broad peaks in the 3300-3500 cm^{-1} region indicate the presence of hydrogen-bonded hydroxyl groups. Different alcohol and phenol groups provide peaks in the region of 1000-1400cm^{-1}. The vibrations at 1240 and 1082 cm^{-1} can be considered to be the stretching vibrations of C–O in C–O–H groups, the vibration at 1020 cm^{-1} directs to the C–O stretching vibration of C–O–C groups of the glucose unit in starch. This characteristic C-O stretching peak of carbohydrates is more prominent in starch and PS@1:2, where amount of starch is maximum compare to other two samples. The characteristic prominent sharp absorption peak of the carbonyl group of gallets is observed at 1600 cm^{-1} in grape seed extract, which is not so much intense in samples. This may be due to the fact that gallates are not so much involved in physical cross-linking of the starch and PVA compared to Proanthocyanidin. Again there is a peak of C-S stretching at 1250 cm^{-1} present in grape seed extract which may be due to sulphonic acid present in grape seed extract as indicated in LCMS data reported previously in our published patent (Indian Patetnt, Application Number : 202331073970). This C-S stretching peak is again absent in samples as possibly it does not take part in the physical crosslinking reaction of starch and PVA. The characteristic aliphatic C–H stretching vibration band of alkanes appeared at 2937 cm^{-1} [41] in both starch and PVA but absent in grape seed extract, which indicates the absence of alkane chains in grape seed extract. This alkane stretching vibration is present in all of the samples indicating the presence of both starch and PVA in all samples. An intense peak for cyclic ether is present in grape seed extract at 1400 cm-1. A sharp peak corresponding to aryl-OH is present in all the graphs in the region of 1100-1200 cm-1. A broad peak of –OH in the region of 3000-3500 cm-1 indicates

the presence of H-bonding. Cyclic ether group and OH groups of grape seed extract make hydrogen bonding with –OH group starch and PVA resulting in physical crosslinking of them.

There is an indication of slight shifts or changes in the intensity of these peaks compared to pure PVA and starch, suggesting interactions. The C-O stretching region (1000-1100 cm^{-1}) may show changes, indicating possible crosslinking. Oligomeric proanthocyanidin enhances the amount of aliphatic and phenolic hydroxyl groups in the gel, resulting in the creation of new hydrogen bonds between the phenolic hydroxyl groups in the proanthocyanidin molecules and the hydroxyl groups in the PVA/Starch hydrogel. This strengthens the interactions between them [42].

5.3.1.2 XRD analysis

The XRD data of all three samples are presented in **Figure 5.1(b).** The XRD data pointed to 3 major semi-crystalline peaks with a hump. For all the blends peaks at 17.4°, 20.2°, and 22.4° were common. Sample PS@1:2 exhibits the most prominent peak. The three semi-crystalline peaks majorly indicate the presence of starch. X-ray diffraction peaks at 2Ө values of 17.4°, 18.1°, 23.3° and 26.7° majorly indicate A-type of starch [43] ,whereas 12.9°, 19.8° and 22.6° are the characteristics of a Vh crystalline type structure [44,45]. The peak located at 2Ө = 17.4° is due to the existence of a very small amount of residual A-type crystalline structure [46] .The presence of a small hump at 40° is also the characteristic peak of PVA indicating its amorphous nature.
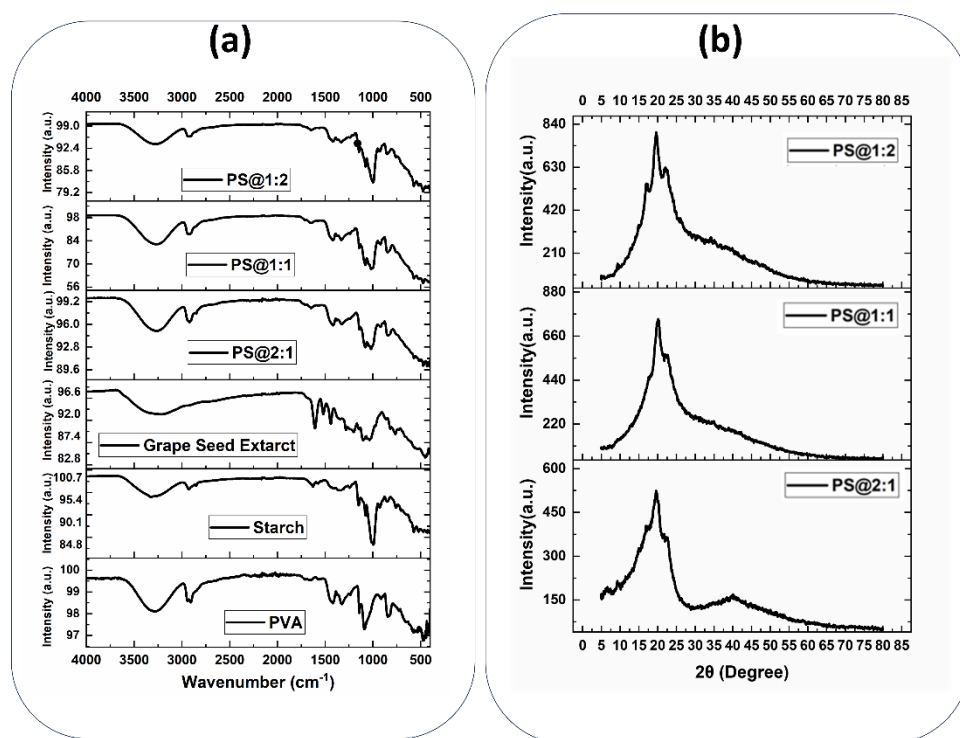
Figure 5.1: FTIR of the three different samples PS@2:1, PS@1:1 and PS@1:2 along with all the raw materials used(a) ; XRD of the 3 film samples PS@2:1,PS@1:1 and PS@1:2 (b)

5.3.1.3 SEM Analysis for Morphological Characteristics

To analyse the surface morphology and cross-sectional characteristics of each sample, al three samples were subjected to SEM analysis(**Figure 5.2(a)**). Sample PS@2:1 and Sample PS@1:1 exhibited relatively smooth surfaces with some scratches or minor irregularities. No significant particles or contaminants are observed. Samples PS@1:2 showed a relatively rough surface, this might be due to the excess presence of starch which can contribute to the roughness. Overall, all the samples showed a continuous structure with a mostly smooth surface. The cross-sectional view of the samples was taken to analyse the thickness of the films. The thickness of sample PS@2:1 was measured to be approximately 184.1 µm and 194.4 µm in different regions. Sample PS@1:1 exhibited a consistent thickness of about 162.0 µm and 164.5 µm in different regions. Sample @PS@1:2 showed a thickness is around 119.3 µm and 120.7 µm, which is thinner compared to the other two samples.

Based on the SEM analysis, PS@2:1 exhibited the smoothest surface, making it ideal for applications requiring minimal surface friction with a smooth finish, and it also has the maximum thickness, offering high protection or insulation but potentially adding significant weight.PS@1:1 has a moderately rougher surface than that of PS@2:1 which makes it suitable for applications needing a balance between surface texture and smoothness, and a moderate

thickness that balances protection and material usage. PS@1:2 exhibited the roughest surface among all the three samples, which makes it useful for applications requiring higher surface area or better adhesion properties, and has the lowest thickness, which may be ideal for lightweight applications but might compromise protection or durability[47,48].

5.3.1.4 AFM analysis

The AFM analysis was done to evaluate the roughness of the films. The AFM data is presented in **Figure 5.2 (b)**. The AFM data shows similar trends to SEM analysis. Sample PS@2:1 has a relatively smooth surface with some peaks and valleys. Sample PS@1:1 sample exhibited a more textured surface with pronounced peaks and valleys. Sample PS@1:2 showed the roughest surface among the three samples. The Rmax values of the PS@2:1(183nm) show that it has the lowest roughness compared to the Rmax values of PS@1:1(251nm) and PS@1:2(459nm). The Ra and Rq values of the sample also confirm this. The Ra i.e. the the arithmetic average of the absolute values of the profile heights over the evaluation length. values for PS@2:1, PS@1:1, and PS@1:2 was found to be 10.3nm. 19.4nm and 41.3 nm respectively. RMS Roughness, Rq, is the root mean square average of the profile heights over the evaluation length. For samples PS@2:1, PS@1:1, and PS@1:2 the Rq value was found to be 14.6nm , 25.9nm and 54.6 nm respectively. PS@2:1 has the smoothest surface, ideal for applications requiring a smooth finish and minimal friction. PS@1:1 offers a balanced texture for moderate adhesion, while PS@1:2 has the roughest surface, suitable for high surface area and improved adhesion which is also supported by the SEM data.
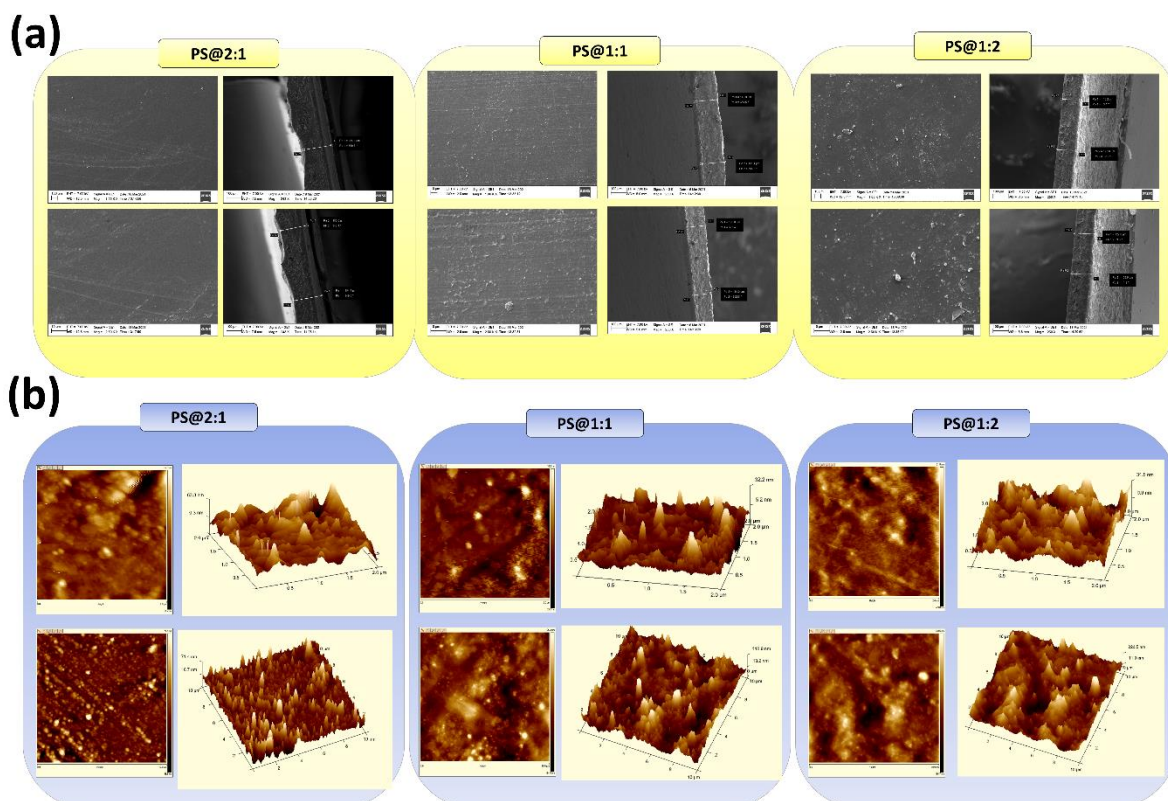
Figure 5.2: Scanning Electron Microscope analysis of the 3 samples PS@2:1, PS@1:1, and PS@1:2 (a); Atomic Force microscope analysis of 3 samples PS@2:1, PS@1:1, and PS@1:2(b)

5.3.1.5 Thermal Analysis

The thermogravimetric analysis (TGA) and derivative thermogravimetry (DTG) graphs show the thermal degradation behaviour of the three samples: PS@2:1, PS@1:1, and PS@1:2 starch(**Figure 5.3(a)**). All samples show initial mass loss around 80°C, indicating moisture evaporation. The initial loss ranged from 5-10 % with the PS@1:2 sample having the highest initial mass loss, suggesting higher moisture content due to the increased proportion of starch, which is more hygroscopic. The initial loss ranged from 5-10 %. For Sample PS@1:2 a significant mass loss of about 50% around 300°C was noted, indicating the primary degradation phase where both starch and the initial PVA components decomposed. This degradation starts around 250-300°C for all samples, which is more than the melting temperature of both PVA (around 200°C)[49] and Starch(around 257°C) [50,51]. This indicates physical crosslinking of PVA and Starch increases the temperature of melting in the crosslinked samples. A second major degradation event was noted at around 450°C, accounting for an additional 30% mass

loss, corresponding to the complete degradation of the remaining polymer components. By the end of the analysis at 600°C, the residual mass is around 10 %. For sample PS@1:1 the first major degradation event was noted around 300°C, with an approximate mass loss of around 60%. At around 450°C the second phase of degradation occurred with a further 25% mass loss, leading to degradation of the polymer components compared to PS@1:2, resulting in around 5-10% residual mass. Lastly for sample PS@2: 1 the major degradation occurred at around 300°C with a mass loss of approximately 55%, which corresponds to the degradation of both the primary polymers. At 400°C an additional 30% mass loss was detected. Around 500°C again a small mass loss takes place. As a result after 600°C there was no residual mass present. From these results, it can be observed that with more amount of PVA in the sample total thermal degradation occurs within the 600°C. This may be due to the reason PVA has less molecular weight than starch. An additional peak at around 500°C in the sample PS@2:1 results in total degradation of the sample.

The DSC analysis results of the three samples representing the various ratios of PVA (Polyvinyl Alcohol) to Starch, PS@2:1, PS@1:1, and PS@1:2, showed different thermal behaviours (**Figure 5.3(b)**). One main endothermic peak was visible in all samples; 180-200° C (related to the melting of crystalline PVA domains and/or starch decomposition[52]). The intensity of the peaks is lower with the increase in the amount of starch present. Conversely, the PS@2:1 sample with the highest PVA content displays the highest maximum heat flow ($_{max}$ = −1.20 W/g) than the other sample PS@1:2 ($_{max}$ = −0.50 w/g) and PS@1:1 ($_{max}$ = −0..35 w/g) data. This suggests that starch interferes with PVA crystallization and has a lower heat capacity, reducing the overall heat absorption of the composite. Although the peaks were majorly observed in similar positions, the differences in intensities for these blends reflected the thermal properties which are profoundly changed with the PVA content i.e. higher the PVA content, the more intense the heat absorption action.
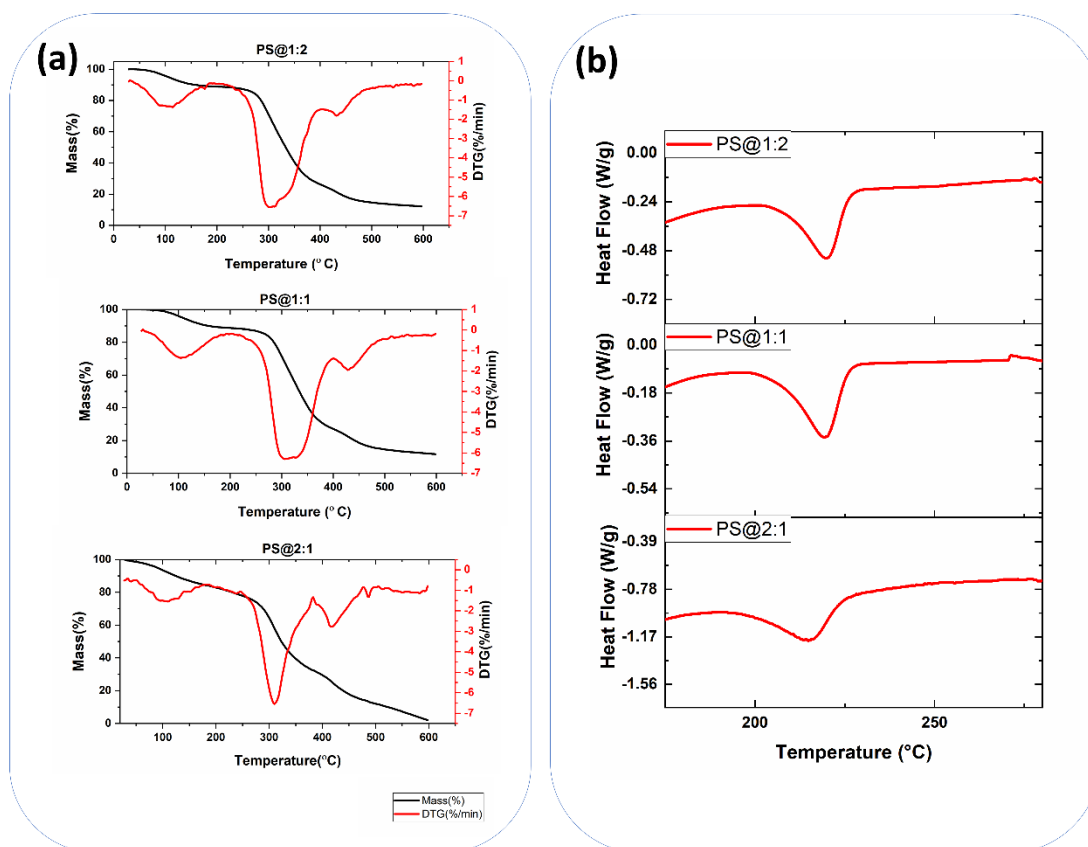
Figure 5.3: TGA-DTG curve representing thermal decomposition of PS@2:1, PS@1:1, and PS@1:2 (a) ; Differential scanning calorimetry plot for PS@2:1, PS@1:1, and PS@1:2 (b).

5.3.1.5 Mechanical Property Analysis

Evaluating the mechanical properties of the polymeric mats is crucial for its application. Some important characteristics like durability, softness, flexibility, pliability, stress resistance, and elasticity, are highly desirable in wound dressing material[53]. Fig.5.4 exhibits the different mechanical characteristics of the 3 different polymeric films. From the stress-strain curve (Figure 5.4(a)) it is quite evident that the sample PS@1:2 showed a different pattern than that of the Sample PS@2:1 and PS@1:1. Sample PS@2:1 and PS@1:1 exhibited a more ductile property than that of PS@1:2. The stress-strain curve although indicated the elastomeric nature of all the films. The Young's modulus (**Figure 5.4(b)**) although showed a different perspective. Sample PS@2:1 exhibited a Young's modulus of 5.231± 0.226 MPa The Young's modulus of sample PS@1:1 and PS@1:2 was observed to be 11.235 ± 1.295 and 8.101 ± 0.521 MPa respectively. It was quite evident that an equal mixture of both polymers showed the maximum Young's modulus and the increase in Young's modulus might be due to the increase in the concentration of starch[54]. Young's modulus values indicate that PS@2:1 is the more flexible,

PS@1:1 is the stiffest, and PS@1:2 has intermediate stiffness. The Ultimate stress (**Figure5.4(c)**) and Strain (**Figure 5.4(d)**) data have also been pointed out to give more details regarding the material strength. The Ultimate Stress and Starin of PS@2:1 was found to be 22.466 ±2.380 MPa and 101.7 ± 14.787% respectively, for PS@1:1 it was found to be 29.93 ± 1.603 MPa and 8.01 ± 1.126% respectively, and for PS@1:2 it was observed to be 17.86 ± 5.758 MPa and 4.03 ± 1.06% respectively. PS@2:1 showed moderate stress, high strain capacity and a good balance of strength and flexibility. PS@1:1 with its high stress capacity but low strain came out be the toughest material among all although flexibility could be a concern in terms of application. PS@1:2 showed moderate stress capacity with very low strain capacity with moderate flexibility. Overall all the films showed good strength along with flexibility which could make these a possible candidate for wound dressing material.
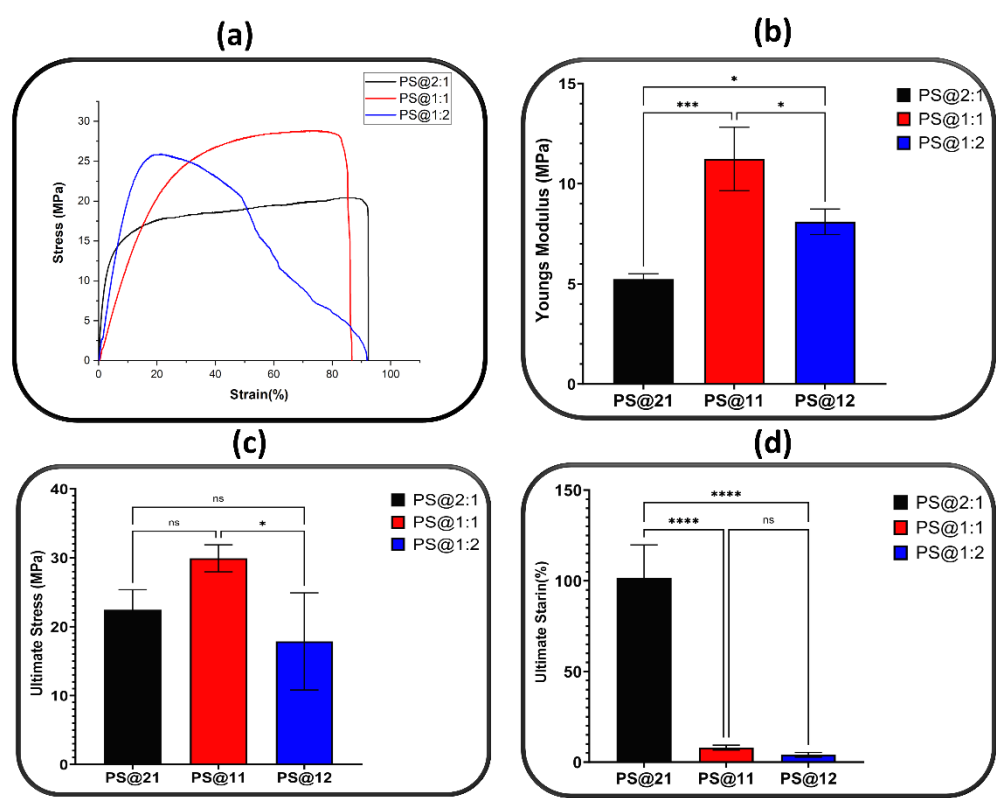
Figure 5.4: Mechanical Characterization of the three polymeric films PS@2:1, PS@1:1, and PS@1:2: Stress-Strain Curve (a); Comparative Young's modulus (b); Comparative Ultimate Stress (c); Comparative ultimate Starin(d).

5.3.1.6 Evaluating Contact Angle

The Contact angle of the samples was measured to check the wettability of the samples (**Figure 5.5(a)**). All the samples exhibited an initial water contact angle of less than 90° thus making an

acute angle. All the samples showed mostly closely related data with PS@2:1, PS@1:1, and PS@1:2 making an angle of $76.27 \pm 1.438°$, $82.23 \pm 1.225°$ and $83.3595 \pm 1.78°$ respectively. All the samples showed a contact angle of less than 90 ° indicating that all these formulations exhibit good wettability. These findings indicate that each of these samples has the ability to cling well to the wound surface and provide a moist environment, which is essential for promoting good wound healing in wound dressing applications[55]. Starch samples with higher amylose content have possibly lower wettability properties[56], which was also prominent from the above results.

5.3.1.6 Nano-indentation test to analyse the hardness

The load versus displacement of the synthesized samples is shown in **Figure 5.5(b)(1)**. It can be seen that the indentation depths of samples PS@2:1 and PS@1:1 are comparably similar. However, sample PS@1:2 exhibits a significantly decreased indentation depth under the same load. This result corresponds to the Stress vs strain curve in UTM analysis. This indicates that sample PS@1:2 has a higher resistance to penetration, demonstrating reduced susceptibility to plastic deformation compared to samples A and B. The hardness (H) and effective Young's modulus (E*) of the samples are presented in Figure 5.5(b)(2). Samples PS@2:1 and PS@1:1 display notably lower mechanical properties than sample PS@1:2. The highest hardness of 2.90 GPa and a reduced Young's modulus of 6.98 GPa was observed in sample PS@1:2.

5.3.1.7 Analysis of Sample Degradation

Figure 5(c)(1) represents the degradation rate over a period of 28 days for all the samples. All the samples showed a consistent degradation pattern with the increase in time points. PS@2:1 showed an initial degradation of 22.21 ± 0.3707 % on Day 1 to a maximum degradation of 29.31 ± 1.338 % on Day 28. Sample PS@1:1 showed an initial low degradation of 13.86 ± 1.833 % on Day 1 to a final degradation of 22.66 ± 6.169 % on the final 28th day. For sample PS@1:2 started degradation with an initial rate of 18.20 ± 1.596 % to a final 24.32 ± 0.503 %. PS@2:1 consistently exhibited the highest values, signifying that it possessed the highest initial integrity and degraded steadily over time. PS@1:1 initially exhibited the lowest values but witnessed a substantial increase, implying that despite its initial state of degradation, it followed a noticeable trend of degradation. PS@1:2 exhibited intermediate values but displayed a continuously increasing trajectory similar to PS@2:1 and PS@1:1. PVA is used as a film is highly hydrophilic and that makes the film more wettable. This may lead to the greater degradation observed in the PS@2:1 composite, as also the moisture absorption can contribute

to accelerating the polymer chain breakdown. This amounted to higher moisture uptake and hence a higher rate of degradation was observed over time due to higher abundance of PVA in this proportion. The degradation is also highly influenced by the interaction between the proanthocyanidin and polymer.

5.3.1.8 Evaluation of Swelling Index

The swelling investigations involved precise measurement of the weight of the dry films, which were then submerged in a pH 7.4 PBS buffer at a temperature of 37°C. The outcomes of these experiments are presented in **Figure 5.5(C)(2)**. Data was recorded at various time intervals until equilibrium was reached. After the 1st interval i.e. 15mintues it was observed that Sample PS@2:1 showed maximum swelling (242.163 ± 9.8075 %) compared to the other two samples. However, samples PS@1:1 and PS@1:2 exhibited a steady rise in swelling from the initial 15 minutes to 2hrs. PS@1:1 showed an initial swelling of 139.028 ± 6.346 % with a final swelling of 164.9035 ± 7.3425 % in 3hrs. Similarly, PS@1:2 exhibited an initial swelling of 128.748 ± 4.265 and finally swelled up to 153.7105 ± 0.1845% in 3 hrs. Overall all the films showed a steady welling ratio. It was quite evident that the swelling came into equilibrium after 2hrs.

To evaluate the effect of swelling in different pHs, swelling of the films was studied in different pHs i.e. pH4,7,9. Figure 5(C)(3) shows the effect of different pHs on the swelling of the films. Data was recorded after 2hrs as mostly after 2hrs the swelling was coming to an equilibrium. Sample PS@2:1 showed a swelling index of 437.473 ± 6.244 % , 421.976 ± 19.014% and 1477.649 ± 25.010 % in pH 4, pH 7and pH 9 respectively. The PS@1:1 and PS@1:2 samples exhibit similar swelling percentages at pH 4 and pH 7, but at pH 9, the PS@1:1 sample swelled significantly more (512.54 ± 8.171 %) compared to the PS@1:2 sample (330.49 ± 19.735 %). The swelling behaviour of these samples is highly dependent on both the pH of the environment and the ratio of PVA and Starch, with the PS@2:1 ratio exhibiting the highest sensitivity to pH changes. This behaviour can be attributed to the increased ionization of functional groups in the polymer matrix at higher pH, leading to greater water uptake[57].
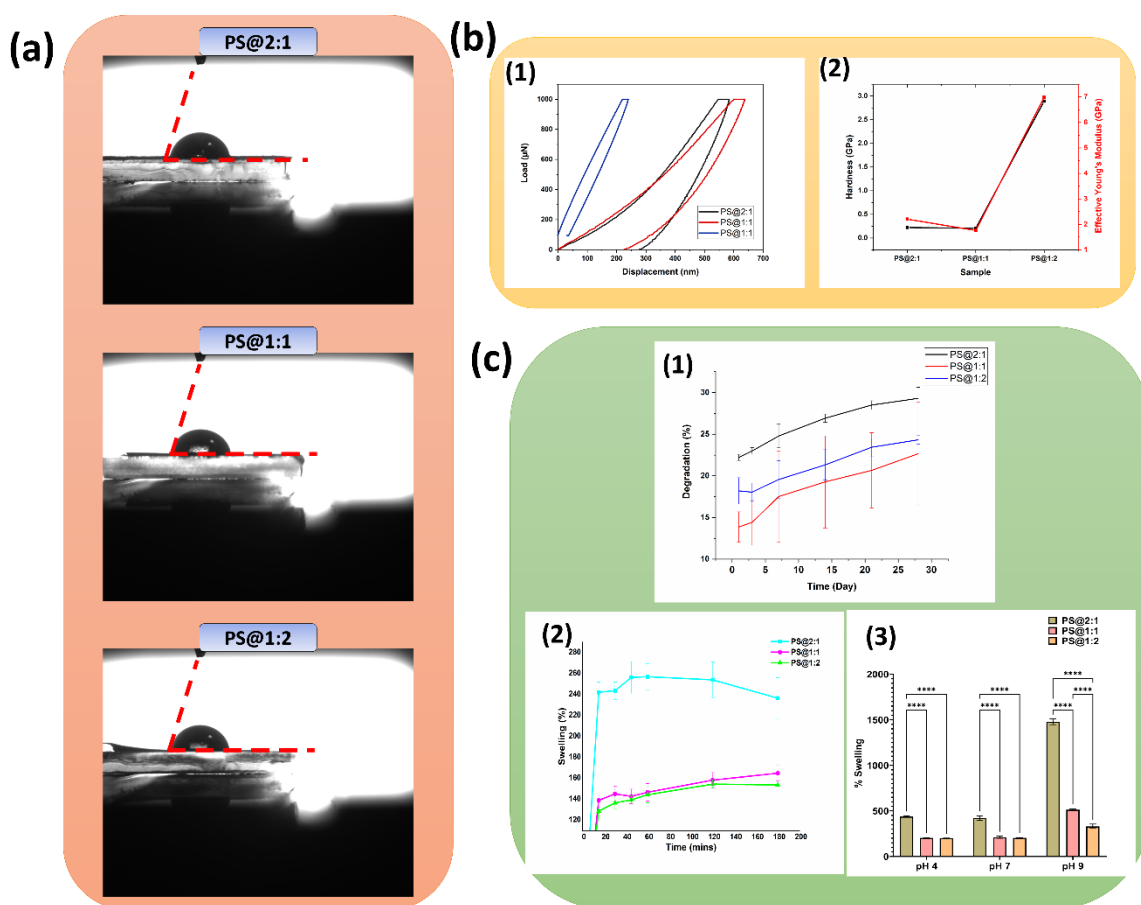
Figure 5.5: Analysis of Contact angle using water for samples PS@2:1, PS@1:1, and PS@1:2(a); Nanoindentation testing for analysis of hardness of the samples(b); Evaluating the degradation of the samples (c)(1), Times based swelling index(c)(2), and pH-dependent swelling index (c)(3)

5.3.2 Evaluating Antibacterial Efficacy

Antibacterial properties of the different PVA/Starch blends were tested against one gram-negative bacterium i.e. *E. coli* and one gram-positive bacterium i.e. *S. aureus* (**Figure 5.6(a)**). The positive control (standard material) was a commercial band-aid available in the market. Both the bacteria showed no growth in the presence of the positive control. The PS@21 showed the best results among the tested samples for both bacterial strains. For E. coli PS@21 showed only the growth of 4 colonies, whereas for S. aureus the same material inhibited the growth of the bacterium showing the growth of only a single colony. The other two samples, PS@12 and PS@11 also showed good results concerning E. coli. PS@12 showed the same effectiveness as PS@21 against E. coli inhibiting bacterial growth only to 4 colonies. PS@11 inhibited the E.

coli growth, but not as effectively as PS@21 and PS@12, allowing the growth of 31 colonies. PS@12 and PS@11 were proven to be not very effective against S. aureus allowing the growth of numerous colonies all over the media.

The study revealed that PS@2:1 exhibited superior antibacterial properties against both E. coli and S. aureus, and is highly effective in preventing bacterial growth, making it an excellent candidate for wound dressing materials. Its smooth surface likely contributes to its efficacy thus providing a protective barrier that minimizes infection risks[58]. The effectiveness of PS@1:2 against E. coli also suggests potential for specific antibacterial applications. The antibacterial activity of these PVA/Starch blends highlights their potential to enhance wound healing and reduce infection rates. PVA and Starch do not have in general antibacterial effect, the grape seed extract loaded in the film might also contribute to the antibacterial effect.

5.3.3 Evaluation of Hemocompatibility of the Films

The haemolysis study was conducted to evaluate the biocompatibility of the prepared films. The hemolysis study is majorly performed to evaluate the thrombotic response of the testing material when it is subjected to contact with blood[59] .The percentage Hemolysis of PS@2:1, PS@1:1, and PS@1:2 was found to be 2.89±0.20%, 1.63±0.34% and 0.92±0.15% respectively (**Figure5.6(b)**). These results suggest that all the films have hemolysis values well in the accepted range (<5%). According to the American Society for Testing and Materials (ASTM), a hemolysis value below 5% is considered to be null[60]. All the samples were well beyond the 5% mark thus indicating no hemolytic effect and hence can be considered as biocompatible.
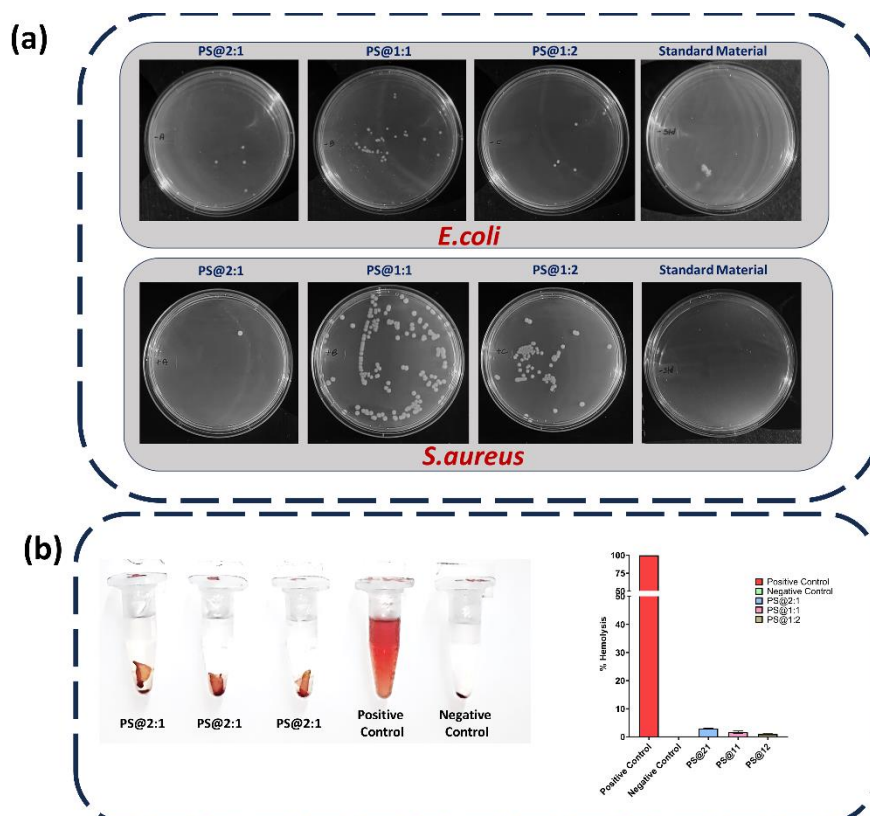
Figure 5.6: Antibacterial study showing colony count of E. coli and S.aureus on the different composites with respect to Standard material(a); Evaluation of % haemolysis of the 3 different composites(b)

5.3.4 Evaluation of cytocompatibility of the Composite films

The MTT assay was performed to evaluate the cytotoxicity of all three 3 samples i.e. PS@2:1, PS@1:1, PS@1:2 using sample conditioned media at 3 different time points 1 day,2 days and 3 days. **Figure 5.7(a)** depicts the MTT assay result where the control or the untreated group is considered to have 100% viable cells. All the 3 samples showed superior cytocompatibility along with some cellular proliferations. On day 1 all three 3 samples exhibited cellular viability of over 98%, with PS@1:1 & PS@1:2 showing cellular viability over 100% and thus pointing to cellular proliferation. A similar trend was observed on day 2 where all the samples showed cellular viability over 100 %, with sample PS@1:2 showing the maximum cellular proliferation. Similar Observation was noted on day 3 where all the samples showed cellular viability slightly more than that of the control. From the MTT assay, it was evident that all the samples had no toxic effect on normal fibroblast cells and also showed good signs of cellular proliferation. The % cellular viability showed no significance among the various groups within the same time point.

Scratch assay was performed to analyse the in-vitro wound healing capacity of all the samples in the fibroblast cell line. **Figure 5.7(b)** shows the figure of the starch assay on L929 at 3 different time points i.e. 0hrs, 12hrs and 24hrs. Sample-conditioned media of all the 3 samples was supplemented to the scratched cells along with one control set where no treatment was done and microscopic images were captured at regular intervals to evaluate the wound closure. After 12 hrs of treatment sample PS@1:2 exhibited superior wound closure followed by PS@1:1 and PS@2:1 as compared to the control where the wound size was much bigger. After 24 hrs of treatment sample PS@1:2 and PS@1:1 showed complete closure of the scratch wound with cellular proliferation. A small scratch area was still noticed for cells treated with PS@2:1 conditioned media. The untreated samples still showed a large scratched area. Hence the results pointed to the fact that all the samples can promote cellular proliferation and heal cellular wounds.

As the cellular proliferation and healing were achieved within 24 hours of the initiation of the assay the cellular structure was analysed at an interval of 24hrs using Rhodamine phalloidin and DAPI staining for the control (untreated) group and the sample-treated group. The sample treated group consisted of treatment using conditioned media of all the 3 samples i.e. PS@2:1, PS@1:1, PS@1:2. The assessment of cellular morphology predominantly the actin filaments and nucleus was achieved using this assay. As illustrated in **Figure 5.7(c)**, distinct actin filaments and well-organized nuclei were identified in all samples, including the Control Group. It is noteworthy that the group treated with samples (all three samples) exhibited robust proliferation and showed improved cytoskeletal and nuclear organization, suggesting their cytocompatibility and promotion of cellular proliferation.
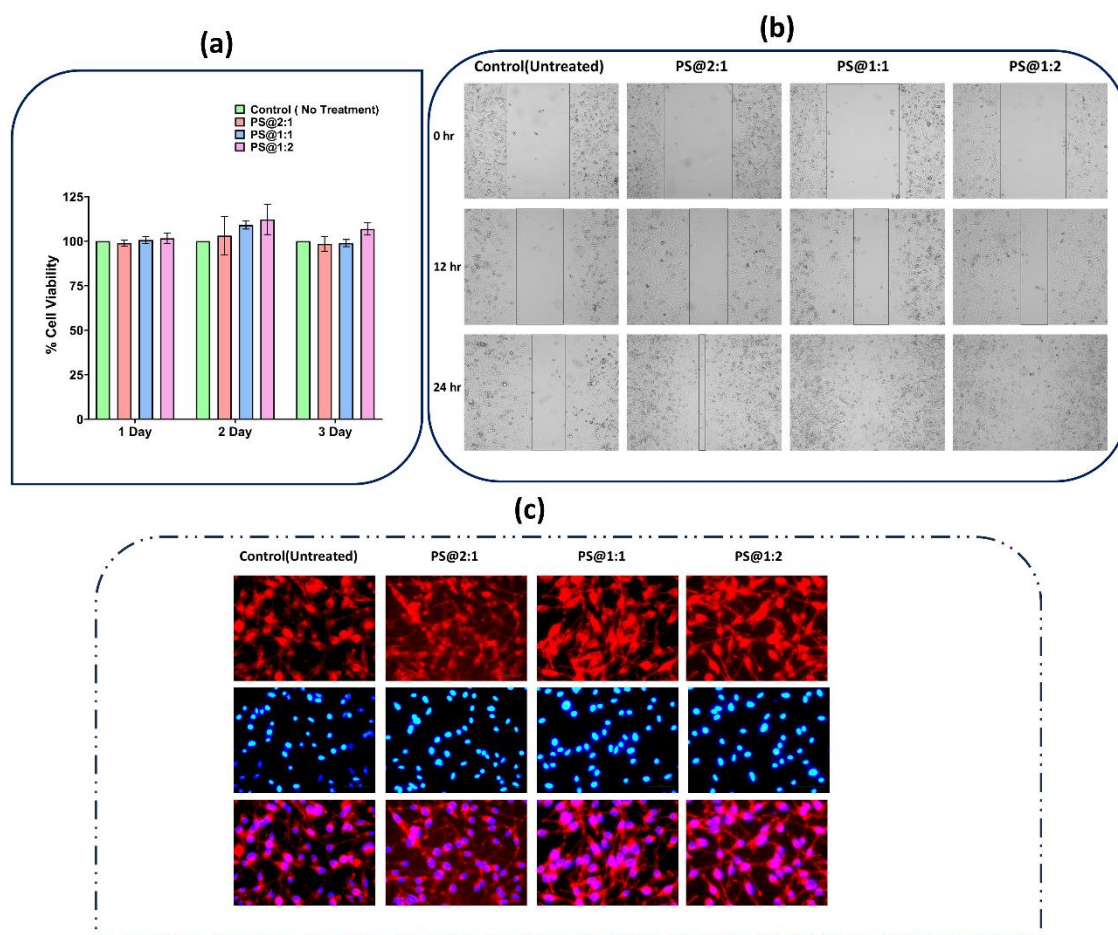
Figure 5.7: MTT assay of the 3 composite films PS@2:1, PS@1:1, PS@1:2(a); Scratch assay of using conditioned media of PS@2:1, PS@1:1, PS@1:2(b); Fluorescence staining of cellular structures with treatment with conditioned media of PS@2:1, PS@1:1, PS@1:2(c).

For evaluating the tissue engineering ability of the Mats the SEM images of the cells seeded on the different mats were accessed at 3 different time points. As observed in **Figure 5.8(a)** the cells were able to anchor and attain some fibroblast morphology after Day 1. The spreading of the cells had just started with most of the Mat portions being blank. A similar trend of cellular spreading and attachment was observed for all the 3 Mats. On Day 2 the cells were observed to proliferate over the mats and showed a matured cellular structure. L929 are heterogenous cell lines thus mixed cellular morphology was observed. An intact morphology of the cells was observed and the cells were randomly distributed over the mats. On the third day of observation, the images revealed that the cells exhibited successful attachment and acquired an elongated, slender form. Observations were made that the cells experienced a process of extending cellular projections called filopodia to boost their adhesion to the substrate, indicating that the surface topography of the microfibers was advantageous for cellular adhesion. Since the inception of the seeding process, the cells have undergone a progressive

transformation in their morphology, transitioning from a slender form to an enlarged state, exhibiting enhanced adhesion capabilities on the surface of the mats.

At 1,2, and 3 days after seeding cells on the mats, the polymeric mats were stained with fluorescein diacetate (FDA) to reveal the number of living cells, cell viability, and cell proliferation status. (**Figure 5.8(b)**). Green structure indicated live cells and a background greenish colour was observed due to sample fluoresce. Initially, the cells were less in number over the mats with a gradual increase in cell numbers from Day 1 to Day 3 thus pointing to the ability of the mats to support cellular proliferation. It is clear from the vivid green coloration that the mats included evenly dispersed live cells.. The illustration distinctly demonstrates the progressive rise in viable cell numbers from the first day to the third day on all the mats. This signifies the proliferation of the cell population over the duration and the sustenance of their viability on the mats. A comparable cellular population was noted in all three polymeric mats at every time interval.
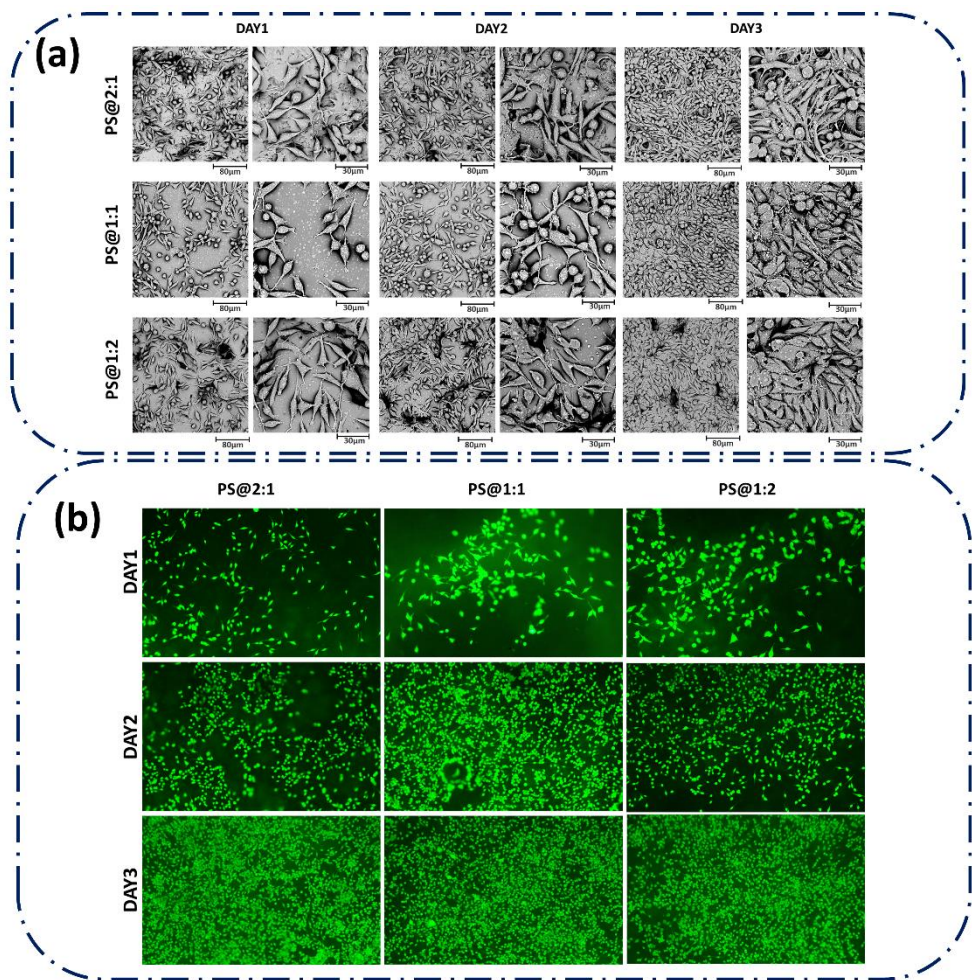
Figure 5.8: SEM images exhibiting cells attached to polymeric mats at different time intervals (a) ; FDA stating to analyses live cell proliferation over the three samples PS@2:1, PS@1:1, PS@1:2(c).

5.3.5 Evaluation of in-Vivo Wound Healing Efficacy in Rabbit Model

5.3.5.1 Evaluation of the Gross wound healing

The effectiveness of the three 3 different samples (PS@2:1, PS@1:1, PS@1:2) as a wound dressing and healing material was accessed by creating a critical size wound on the rabbit and applying the mats on the wound areas along with a standard material Tegaderm and keeping one no treatment control to get a comparative result (**Figure 5.9(a), (b)**). There were no significant differences among the treatments on Day 3(**Figure 5.9(b)**). By Day 7, % wound area was significantly lower for PS@1:1 (40.56 ± 2.06%) by comparison to PS@2:1 (65.17 ± 2.88%, $p<0.01$), PS@1:2 (46.40 ± 3.43%, $p<0.05$), Tegaderm (46.10 ± 2.23%, $p<0.05$), and Control (48.18 ± 3.12%, $p<0.05$).

On Day 10, PS@1:1 (40.74 ± 0.48 %) and PS@1:2 (40.52 ± 4.17%) continued to have significantly lower % wound areas compared to Control (65.34 ± 1.05%) ($p<0.001$ and $p<0.05$, respectively), while Tegaderm (51.98 ±0.37) also showed significant improvement ($p<0.05$). At Day 14, % wound area for PS@1:1 (13.58 ± 2.13%) was significantly less than the Control (24.76 ± 1.67%, $p<0.05$) with PS@1:2 (1.35 ± 0.23%, $p < 0.05$) with the most significant decrease in wound area. All treated groups exhibited significantly lower % wound areas compared to Control (14.26 ± 1.68%, $p<0.05$) on Day 21 including PS@2:1 (3.63% ± 0.46%), PS@1:1 (2.58% ±0.47%), PS@1:2 (1.05% ±0.05%), and Tegaderm (6.52% ± 1.08%). Specifically, PS@1:1 and PS@1:2 showed significant improvements over Control ($p<0.05$).

Overall, all films showed a significant reduction in wound area than that of the control (No treatment).
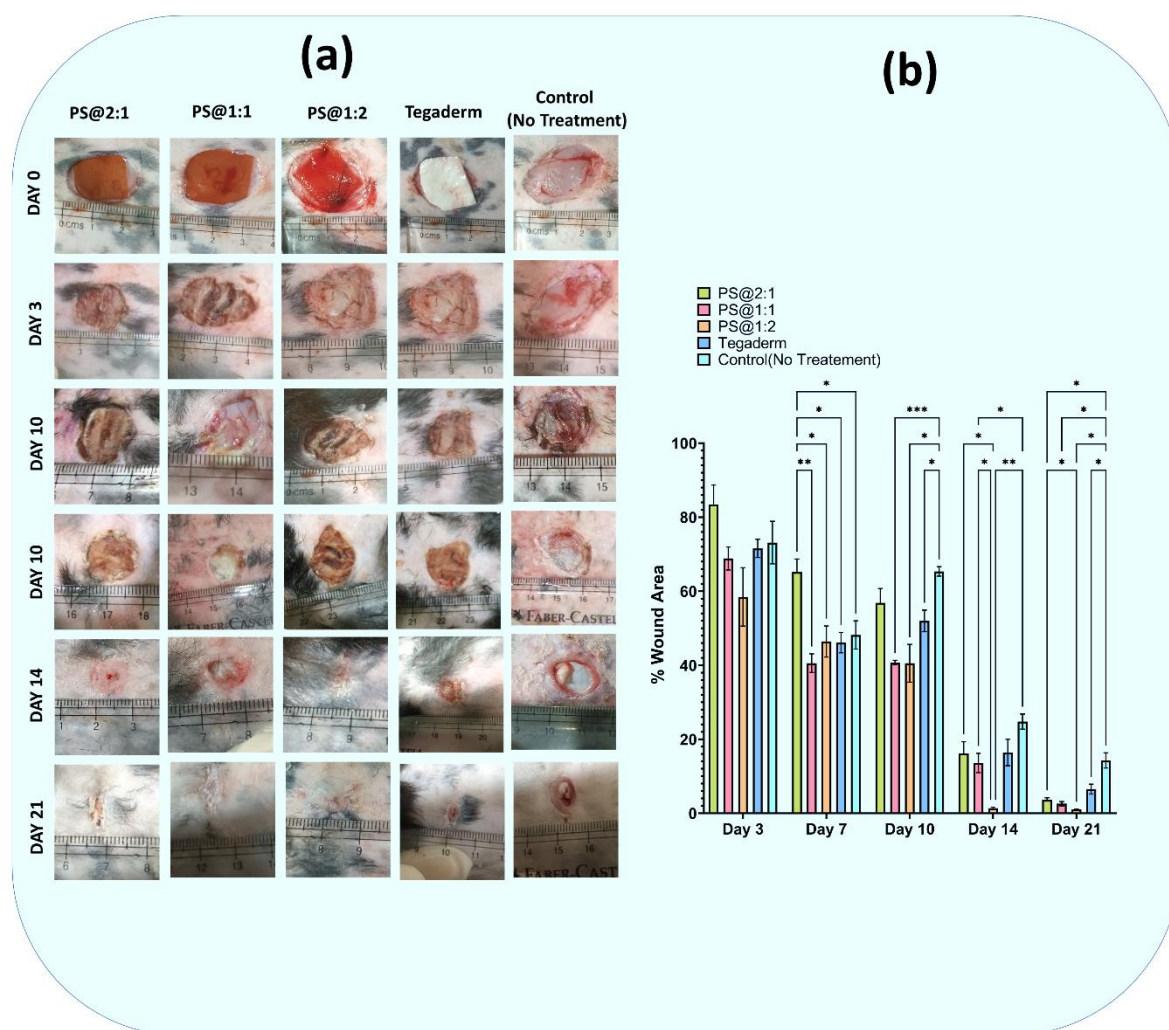
Figure 5.9: Gross pictures of wound healing phases at different time points of the treated and untreated wounds (a); Graphical representation of the % wound area of the different groups (b)

5.3.5.2 Histopathological examination of the wound tissue

To further evaluate the physiological condition and the morphology of the wound the tissue samples were H&E stained at various time points (**Figure5.10 (a)**). After 7 days post wound creation all the samples showed formation of granulation tissue. The wound with no treatment showed no re-epithelialization with focal infiltration. The presence of multifocal angiogenesis was observed with very low fibrocyte count. The wound treated with commercial treatment showed scab formation with inflammation. Fibrous hyperplasia was observed at the edge of the wound along with focal tightly packed fibrocytes. All the samples showed moderate to low re-epithelialization with PS@1:1 having the least. All the samples showed disorganized collagen fibres. Sample PS@1:2 and PS@11 showed good angiogenesis along with the presence of fibroblasts. Sample PS@2:1 also exhibited spindle-shaped nuclei. On Day 14 tissue

samples indicated complete closure of wounds for all the samples along with control. Although the control sample showed the presence of granulation tissue, mild infiltration and the production was in a concentric form. The Tegaderm-treated tissue showed moderate differentiation of squamous epithelial cells with low keratinocyte turnover. Extravasation of blood and fibrocytes was moderately spotted with sufficient collagen deposits. Epidermal differentiation was not the same all along. All the samples showed complete re-epithelialization of the epidermis. The collagen samples in all the samples were mostly immature and disorganized. Sample PS@1:2 treated wound exhibited minimal infiltration of mononuclear cells such as macrophages and lymphocytes indicating a resolving inflammatory response. Active fibroblasts were present producing collagen and other extracellular matrix proteins essential for wound strength and integrity. Myofibroblasts characterized by their spindled properties were also observed contributing to wound contraction. Numerous small blood vessels were present within the granulation tissue. The process of epidermal regeneration was near completion with the formation of new epidermal layers over the wound site. A similar trend was also observed in samplePS@1:1 the dermis underneath the re-epithelialized area showed granulation tissue, characterized by a dense network of new capillaries active fibroblasts and an extracellular matrix rich in collagen fibres. Active fibroblasts were present in the dermis producing collagen and other extracellular matrix components essential for wound strength and integrity. Myofibroblasts were also observed. Numerous small blood vessels were present within the granulation tissue. The process of epidermal regeneration was near completion with the formation of new epidermal layers over the wound site. Focal infiltration of mononuclear cells such as macrophages and lymphocytes were present indicating an ongoing inflammatory response. Similar focal infiltration of mononuclear cells was also noted in wound treated with PS@2:1. Other than that adnexal structures such as hair follicles and minute sebaceous glands began to regenerate signifying advanced healing and the restoration of the skin's specialized functions. Day 21 marked a fully closed wound for all the tissue samples although the epidermis of the control and standard material was thinner than that of the samples. All three film-treated wounds showed normal and well-differentiated epidermis. The control tissue still exhibited focal infiltration of mononuclear cells especially lymphocytes, indicating ongoing but diminishing inflammation and tissue remodelling. The adnexal structures like hair follicles and sebaceous glands were increasingly evident reflecting advanced healing and the restoration of skin's specialized structures. The Tegaderm-treated tissue showed that the dermis still contained granulation tissue characterized by loosely packed immature collagen fibres and a reduced number of fibrocytes. Neovascularization was

persistent although the number of budding vasculature was found to be decreasing as healing progressed. Like the control focal infiltration of mononuclear cells persisted signifying continued but resolving inflammation and tissue remodeling. Skin adnexal structures like hair follicles and sebaceous glands were becoming more evident reflecting advanced stages of healing and the re-establishment of specialized skin structure. All the film-treated tissues showed advanced healing and reasonable keratin production suggesting active cell proliferation. The presence of skin adnexal structures further indicated the advanced stage of healing, where both the epidermis and dermis were actively regenerating and restructuring to restore skin integrity. The collagen fibers were also tightly packed with more density in sample PS@1:2. Overall the H&E staining pointed the efficiency of the polymeric films in treating critical wounds with superior healing abilities.

All the composite films of PVA and Starch loaded with proanthocyanidin-rich grape seed extract showed superior healing capabilities with PS@1:2 with a slightly better efficacy. Grape seed extract contains antioxidants and anti-inflammatory phytochemicals that assist in decreasing inflammatory reactions and oxidative stress, which can be crucial to creating a perfect environment for the healing of wounds[27]. The films also played a major role in cellular attachment which was also evident from in-vitro studies thus promoting tissue regeneration. Moreover, the ability of the composite to maintain a moist wound environment may improve cellular metabolism and collagen formation in the wound area, which will contribute to effective wound healing and recovery of skin architecture and function.

To access the deposition of other ECM components majorly collagen all the wound samples at different points were stained using Masson's trichrome stain (**Figure 5.10(b)**). A progression of collagen formation and deposition was noticed during the wound-healing phase. The untreated wound on day 7 showed minimal granulation tissue with minimal collagen deposition. On the other hand, the Tegaderm-treated wound showed a wound area predominantly filled with granulation tissue characterized by uneven and irregular collagen deposition. For both the untreated and Tegaderm treated wound active fibroblasts were noticed synthesizing collagen that appeared as thin, immature, and irregularly distributed fibers. All the sample-treated wounds showed signs of immature collagen deposition with highly active fibroblasts synthesizing collagen fibers. The collagens were mostly loosely arranged and uneven in thickness. Although PS@1:1 showed some indications of matured collagen deposition indicating an initial transition from the proliferative phase to the remodeling phase.

On the 14th day, the control sample showed loosely arranged blue fibers indicating early and immature collagen formation. The Tegaderm-treated wounds revealed mature granulation tissue characterized by a denser and more organized network of capillaries and fibroblasts compared to day 7. Masson's trichrome stain showed collagen fibers prominently in blue colour indicating a transition of collagen of greater tensile strength. Samples PS@1:2 exhibited loosely arranged collagen fibers in the dermoepidermal junction indicating ongoing remodeling and the transition of collagen. The rest of the wound area exhibited thick and densely packed collagen deposition highlighted in bluish staining signifying more mature and organized collagen which would enhanced the wound's tensile strength and structural integrity. This combination of loose collagen at the junction and thick collagen deposition reflected a transitional and advanced stage of wound healing[61].Sample PS@1:1 and PS@2:1 showed moderate collagen maturation. Collagen fibers as stained blue by the trichrome stain were present but appeared mildly loose-packed and disorganized reflecting ongoing matrix deposition[62].

Day 21 marked the maturation of collagen for all the samples than that of day 14 with the untreated sample dermis showing significant remodeling with fibroblasts actively producing collagen, which was highlighted by the blue staining of Masson's trichrome and was disorganized and loosely packed at this stage contributing to scar tissue formation. The Tegaderm-treated tissues exhibited fibroblasts actively producing closely packed collagen fibers which seemed to be mature collagen. Samples PS@1:1 and PS@1:2 showed superior healing with the presence of matured collagen. These collagen fibers were closely packed and exhibited a proper horizontal arrangement. The Granulation tissue had been decreased signifying the wound maturation and the inflammatory response was greatly reduced with fewer inflammatory cells present. The PS@2:1 still showed active collagen production and the dermis exhibited multifaced response signifying remodeling although there were loosely packed mature collagen fibers.
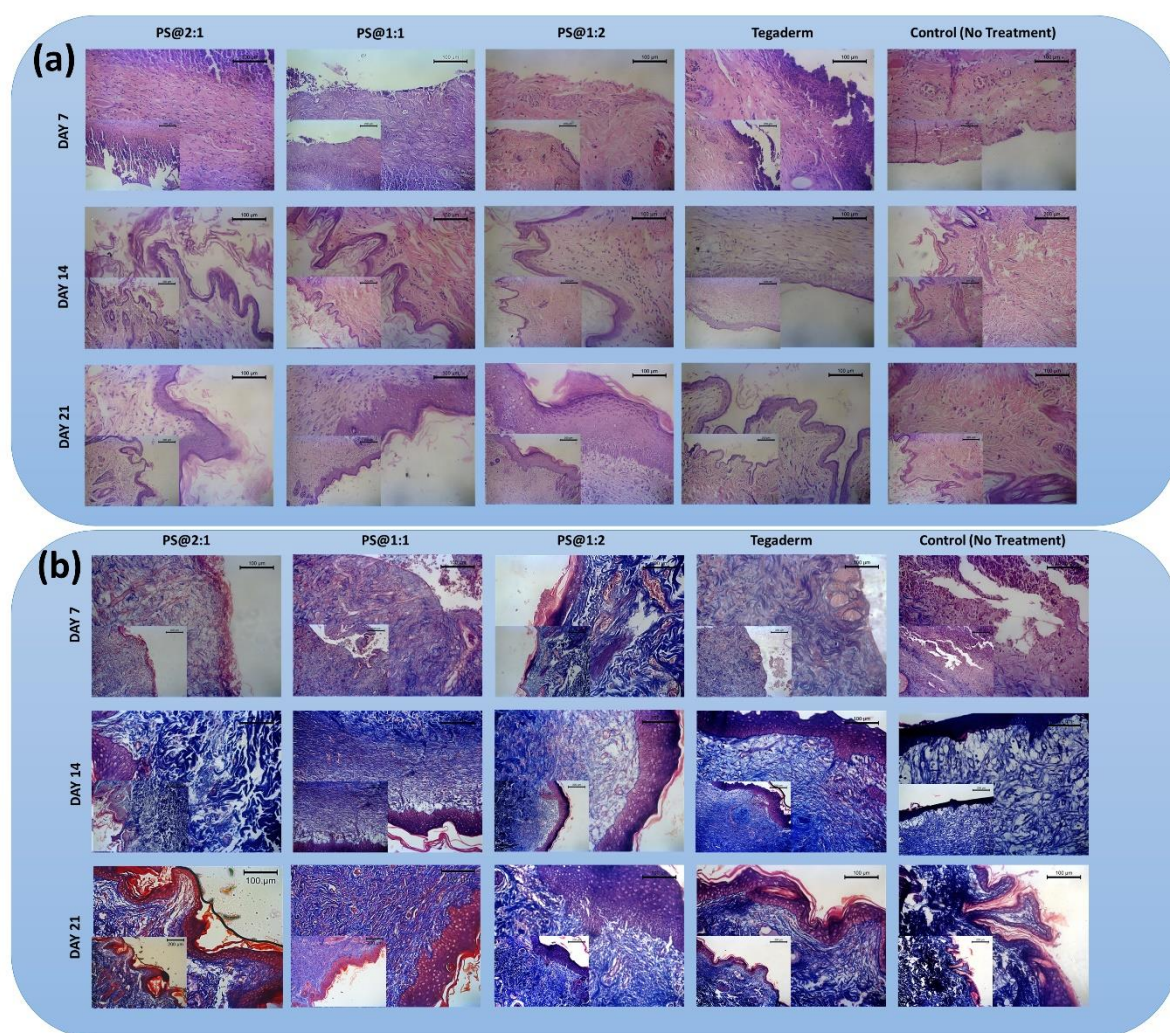
Figure 5.10: Assessment of histological sections stained with H&E from different treatment and control groups on 7, 14, and 21 days after healing(a); Samples of wound tissues stained with Masson's trichrome at 7,14, and 21 days post-incision showing the presence of collagen fibres in the healing tissue.

5.3.5.3 Immunohistochemistry Assessment of the wound tissue

The immunohistochemistry study was done to assess the presence of particular markers like CD-31 and collagen type-I. The presence of collagen type-I was noted in wounds treated with polymeric films. The collagen type -I was accessed on days 14 and 21 as the formation of mature collagen starts from that time point(**Figure 5.11(a)**). The collagen type-I synthesis and deposition were found to be better in all the polymeric mats when compared to control and Tegaderm-treated tissue sections. Collagen type 1 was abundant in the dermis region during

the remodelling phase, indicating that the polymeric materials facilitated the organization of the healing matrix in the extracellular matrix (ECM)[40].

The healing of a wound involves several initial steps, among which the process of neovascularization plays a major role in the formation of micro-blood vessels and hence contributes to the healing process by efficient remodelling. Both the chemical and structural characteristics of a dressing material must be taken into account to ensure enough blood flow to the injured area. There can be cell death and tissue necrosis due to inadequate blood circulation , which can delay the overall healing process[63]. In order to evaluate the degree of neovascularization in the healing tissues, immunohistochemistry staining of the tissue sections was done on day 7 and day 14 after treatment with polymeric mats and compared it with the standard material Tegaderm and control with no treatment **(Figure 5.11(b))**. Specifically, the endothelial cell marker CD 31 was examined. The Control and the standard Tegaderm showed quantitively lesser angiogenic markers than that of the samples. Wounds treated with PS@12 and PS@11 showed the formation of matured blood vessels by the end of 21 days thus pointing to signs of healing via epithelization. PS@2:1 also showed numerous CD-31 positive signals. The markers were evenly dispersed throughout both newly formed and fully developed blood vessels, as well as in solitary and grouped areas throughout the healing tissues. This study thus validated that PVA/Starch composite loaded with grape seed extract, holds potential for efficient neovascularization.
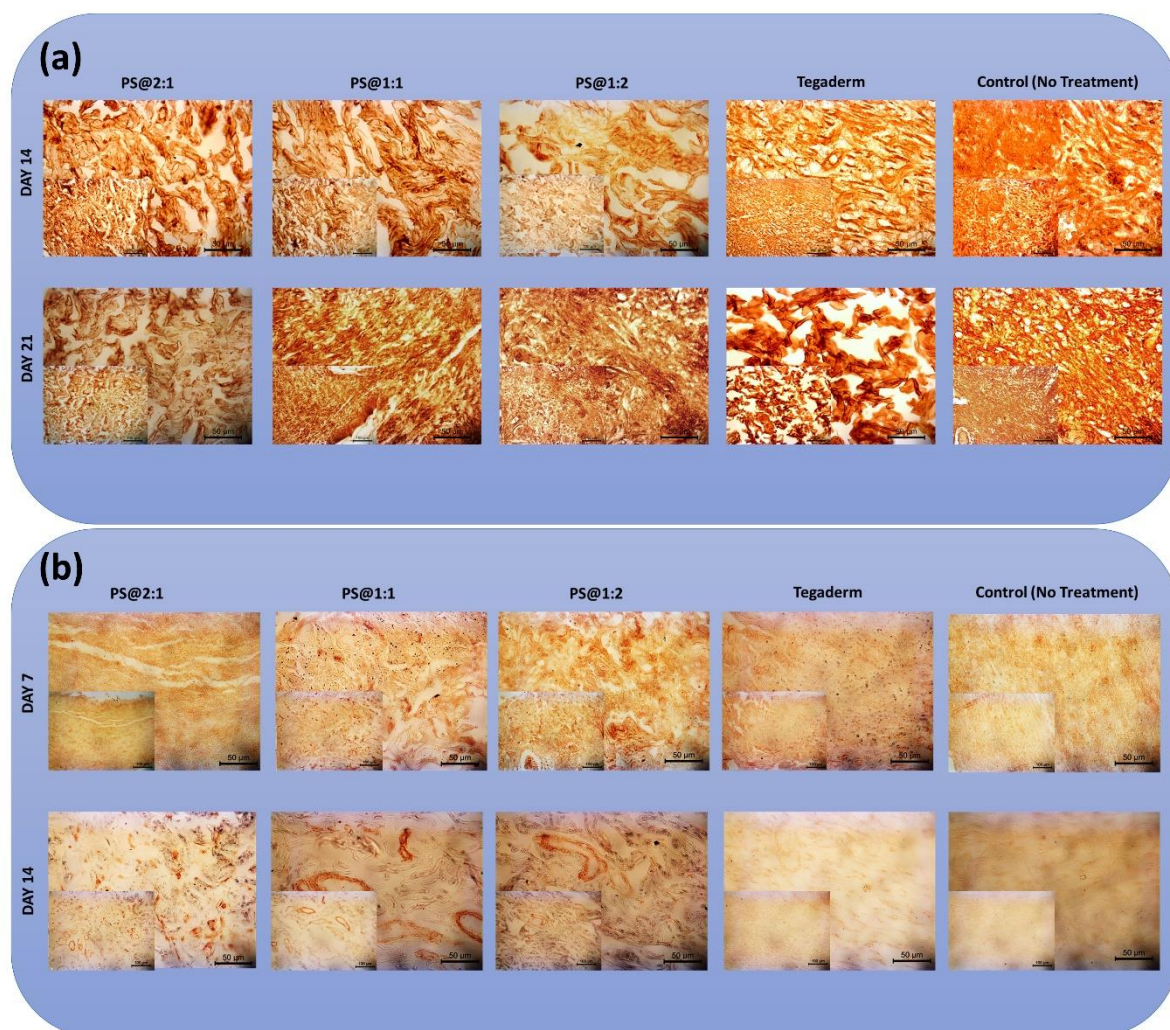
Figure 5.11: Using immunohistochemistry labeling, we examined collagen type 1 deposition in the extracellular matrix on days 14 and 21 after healing. (a). Immunohistochemistry pictographs illustrating the distribution of CD 31/PECAM 1 markers throughout the initial phases of wound healing (days 7 and 14) (b).

5.4 Inference

In this study, 3differnt types of polymeric film(PS@2:1, PS@1:1, and PS@1:2) were designed using PVA and Starch and incorporating grape seed extract rich in proanthocyanidins. The grape seed extract not only acted as a bioactive compound but also contributed to the crosslinking of the PVA starch blend by hydrogen bonding. The FTIR and XRD of the samples

revealed successful incorporation of all the components. The SEM and AFM analysis pointed out that all the prepared polymeric films were mostly smooth with very few irregularities. All the polymeric films exhibited good thermal stability, and mechanical properties with PS@1:1 showing maximum Youngs's modulus. The biocompatibility of the samples was confirmed, with all hemolysis values well below the 5% threshold, indicating suitability for medical applications. All the samples showed reasonable degradation along with good swelling which will allow the grape seed extract to diffuse to the site of a wound. The antibacterial study also pointed out that all the polymeric films somehow resisted the formation of bacterial colonies over them which can be highly beneficial for wound dressing application. The smooth and stable surface of the polymeric films aided cellular adhesion and proliferation in vitro. Also, the rabbit model showed that these polymeric mats were quite effective in healing wounds. To be precise PS@1:1 and PS@1:2 showed the best wound healing efficacy with the reduction in inflammation and controlled wound tissue regeneration by improved angiogenesis, re-epithelization, and arranged deposition of ECM components such as collagen. The polymeric films primarily facilitate scarless healing, which is a key goal in the production of wound dressing materials. Moreover, these polymeric films provide an ecologically responsible and sustainable approach to healthcare products. The application of renewable resources such as starch and the inclusion of natural bioactive substances like grape seed extract derived from winery waste is in accordance with the concepts of green chemistry and sustainability. These biomaterials are biodegradable, which helps to minimize their negative effects on the environment and provides a sustainable alternative to synthetic polymers. In addition, the method used for fabrication also reduces the utilization of toxic substances, making it a green synthesis. These polymeric films offer a sustainable and eco-friendly choice for healthcare supplies, in line with the objectives of sustainable healthcare and environmental preservation.

References

[1]   M. Cripps, H. Scarbrough, Making Digital Health "Solutions" Sustainable in Healthcare Systems: A Practitioner Perspective, Front Digit Health 4 (2022) 727421. https://doi.org/10.3389/FDGTH.2022.727421.

[2]   J. Kaur, Towards a Sustainable Triad: Uniting Energy Management Systems, Smart Cities, and Green Healthcare for a Greener Future, in: Emerging Materials, Technologies, and Solutions for Energy Harvesting, IGI Global, 2024: pp. 258–285.

[3]   D. Bevere, N. Faccilongo, Shaping the Future of Healthcare: Integrating Ecology and Digital Innovation, Sustainability 16 (2024) 3835.

[4]   H. Yousef, M. Alhajj, S. Sharma, Anatomy, Skin (Integument), Epidermis, in: StatPearls, StatPearls Publishing, Treasure Island (FL), 2024. http://www.ncbi.nlm.nih.gov/books/NBK470464/.

[5]   A. V Nguyen, A.M. Soulika, The Dynamics of the Skin's Immune System, Int J Mol Sci 20 (2019) 1811. https://doi.org/10.3390/ijms20081811.

[6]   A. Nourian Dehkordi, F. Mirahmadi Babaheydari, M. Chehelgerdi, S. Raeisi Dehkordi, Skin tissue engineering: wound healing based on stem-cell-based therapeutic strategies, Stem Cell Res Ther 10 (2019) 111. https://doi.org/10.1186/s13287-019-1212-2.

[7]   D. Bhattacharya, B. Ghosh, M. Mukhopadhyay, Development of nanotechnology for advancement and application in wound healing: a review, IET Nanobiotechnol 13 (2019) 778–785.

[8]   S. Hasan, M.A. Hasan, M.U. Hassan, M. Amin, T. Javed, L. Fatima, Biopolymers in diabetic wound care management: A potential substitute to traditional dressings, Eur Polym J 189 (2023) 111979. https://doi.org/10.1016/j.eurpolymj.2023.111979.

[9]   R.C. Op 't Veld, X.F. Walboomers, J.A. Jansen, F.A.D.T.G. Wagener, Design Considerations for Hydrogel Wound Dressings: Strategic and Molecular Advances, Tissue Eng Part B Rev 26 (2020) 230–248. https://doi.org/10.1089/ten.teb.2019.0281.

[10]   L. Mehra, S. Mehra, N. Tiwari, T. Singh, H. Rawat, S. Belagavi, A. Jaimini, G. Mittal, Fabrication, characterization and evaluation of the efficacy of gelatin/hyaluronic acid microporous scaffolds suffused with aloe-vera in a rat burn model, J Biomater Appl 36 (2022) 1346–1358. https://doi.org/10.1177/08853282211061821.

[11]   E. Rezvani Ghomi, M. Niazi, S. Ramakrishna, The evolution of wound dressings: From traditional to smart dressings, Polym Adv Technol 34 (2023) 520–530. https://doi.org/10.1002/pat.5929.

[12]   M.B. Dreifke, A.A. Jayasuriya, A.C. Jayasuriya, Current wound healing procedures and potential care, Mater Sci Eng C Mater Biol Appl 48 (2015) 651–662. https://doi.org/10.1016/j.msec.2014.12.068.

[13]   S. Bhatia, S. Bhatia, Natural polymers vs synthetic polymer, Natural Polymer Drug Delivery Systems: Nanoparticles, Plants, and Algae (2016) 95–118.

[14] M.M. Delavari, I. Stiharu, Preparing and Characterizing Novel Biodegradable Starch/PVA-Based Films with Nano-Sized Zinc-Oxide Particles for Wound-Dressing Applications, Applied Sciences 12 (2022) 4001. https://doi.org/10.3390/app12084001.

[15] S. Jana, P. Das, J. Mukherjee, D. Banerjee, P.R. Ghosh, P.K. Das, R.N. Bhattacharya, S.K. Nandi, Waste-derived biomaterials as building blocks in the biomedical field, J Mater Chem B 10 (2022) 489–505. https://doi.org/10.1039/D1TB02125G.

[16] M.J. Jara-Palacios, Wine Lees as a Source of Antioxidant Compounds, Antioxidants 8 (2019) 45. https://doi.org/10.3390/antiox8020045.

[17] M.E. Martin, E. Grao-Cruces, M.C. Millan-Linares, S. Montserrat-de la Paz, Grape (Vitis vinifera L.) Seed Oil: A Functional Food from the Winemaking Industry, Foods 9 (2020) 1360. https://doi.org/10.3390/foods9101360.

[18] G.N. Mattos, R. V Tonon, A.A.L. Furtado, L.M.C. Cabral, Grape by-product extracts against microbial proliferation and lipid oxidation: a review, J Sci Food Agric 97 (2017) 1055–1064.

[19] J. Borges-Vilches, J. Poblete, F. Gajardo, C. Aguayo, K. Fernández, Graphene oxide/polyethylene glycol aerogel reinforced with grape seed extracts as wound dressing, J Mater Sci 56 (2021) 16082–16096. https://doi.org/10.1007/s10853-021-06297-z.

[20] S. Ceylan, D. Demir, Polyvinyl alcohol: Starch based membrane scaffolds for tissue transparency requirements: Fabrication, characterization and cytotoxicity studies, Next Materials 3 (2024) 100148. https://doi.org/10.1016/j.nxmate.2024.100148.

[21] N. Kemençe, N. Bölgen, Gelatin-and hydroxyapatite-based cryogels for bone tissue engineering: synthesis, characterization, in vitro and in vivo biocompatibility, J Tissue Eng Regen Med 11 (2017) 20–33.

[22] A. Das, R. Uppaluri, C. Das, Feasibility of poly-vinyl alcohol/starch/glycerol/citric acid composite films for wound dressing applications, Int J Biol Macromol 131 (2019) 998–1007. https://doi.org/10.1016/j.ijbiomac.2019.03.160.

[23] A. Das, S. Bhattacharyya, R. Uppaluri, C. Das, Optimality of poly-vinyl alcohol/starch/glycerol/citric acid in wound dressing applicable composite films, Int J Biol Macromol 155 (2020) 260–272. https://doi.org/10.1016/j.ijbiomac.2020.03.185.

[24] M.M. Delavari, I. Stiharu, Preparation and Characterization of Eco-Friendly Transparent Antibacterial Starch/Polyvinyl Alcohol Materials for Use as Wound-Dressing, Micromachines (Basel) 13 (2022) 960. https://doi.org/10.3390/mi13060960.

[25] M.-C. Popescu, B.-I. Dogaru, M. Goanta, D. Timpu, Structural and morphological evaluation of CNC reinforced PVA/Starch biodegradable films, Int J Biol Macromol 116 (2018) 385–393. https://doi.org/10.1016/j.ijbiomac.2018.05.036.

[26] D. Evtuguin, J.P.S. Aniceto, R. Marques, I. Portugal, C.M. Silva, L.S. Serafim, A.M.R.B. Xavier, Obtaining Value from Wine Wastes: Paving the Way for Sustainable Development, Fermentation 10 (2024) 24. https://doi.org/10.3390/fermentation10010024.

[27] A. Ajit, A.G. Vishnu, P. Varkey, Incorporation of grape seed extract towards wound care product development, 3 Biotech 11 (2021) 261. https://doi.org/10.1007/s13205-021-02826-4.

[28] Intellectual Property India, (n.d.). https://iprsearch.ipindia.gov.in/PublicSearch/PublicationSearch/PatentDetails (accessed June 4, 2024).

[29] N. Rashid, S.H. Khalid, I. Ullah Khan, Z. Chauhdary, H. Mahmood, A. Saleem, M. Umair, S. Asghar, Curcumin-Loaded Bioactive Polymer Composite Film of PVA/Gelatin/Tannic Acid Downregulates the Pro-inflammatory Cytokines to Expedite Healing of Full-Thickness Wounds, ACS Omega 8 (2023) 7575–7586. https://doi.org/10.1021/ACSOMEGA.2C07018/ASSET/IMAGES/LARGE/AO2C07018_0005.JPEG .

[30] K. Ghosal, U. Bhattacharjee, K. Sarkar, Facile green synthesis of bioresorbable polyester from soybean oil and recycled plastic waste for osteochondral tissue regeneration, Eur Polym J 122 (2020) 109338. https://doi.org/10.1016/J.EURPOLYMJ.2019.109338.

[31] S. Kumar, S. Raj, K. Sarkar, K. Chatterjee, Engineering a multi-biofunctional composite using poly(ethylenimine) decorated graphene oxide for bone tissue regeneration, Nanoscale 8 (2016) 6820–6836. https://doi.org/10.1039/C5NR06906H.

[32] P. Das, T. Dutta, S. Manna, S. Loganathan, P. Basak, Facile green synthesis of non-genotoxic, non-hemolytic organometallic silver nanoparticles using extract of crushed, wasted, and spent Humulus lupulus (hops): Characterization, anti-bacterial, and anti-cancer studies, Environ Res 204 (2022) 111962. https://doi.org/10.1016/j.envres.2021.111962.

[33] P. Das, T. Chakravarty, A.J. Roy, S. Manna, S.K. Nandi, P. Basak, Sustainable development of Draksha- Beeja extract loaded gelatin and starch-based green and biodegradable mats for potential tissue engineering applications, Sustain Chem Pharm 34 (2023) 101134. https://doi.org/10.1016/J.SCP.2023.101134.

[34] Maciej Serda, F.G. Becker, M. Cleary, R.M. Team, H. Holtermann, D. The, N. Agenda, P. Science, S.K. Sk, R. Hinnebusch, R. Hinnebusch A, I. Rabinovich, Y. Olmert, D.Q.G.L.Q. Uld, W.K.H.U. Ri, V. Lq, W.K.H. Frxqwu, E. Zklfk, L. V Edvhg, R.Q. Wkh, F.G. Becker, N. Aboueldahab, R. Khalaf, L.R. De Elvira, T. Zintl, R. Hinnebusch, M. Karimi, S.M. Mousavi Shafaee, D. O 'driscoll, S. Watts, J. Kavanagh, B. Frederick, T. Norlen, A. O'Mahony, P. Voorhies, T. Szayna, N. Spalding, M.O. Jackson, M. Morelli, B. Satpathy, B. Muniapan, M. Dass, P. Katsamunska, Y. Pamuk, A. Stahn, E. Commission, T.E.D. Piccone, Mr.K. Annan, S. Djankov, M. Reynal-Querol, M. Couttenier, R. Soubeyran, P. Vym, E. Prague, World Bank, C. Bodea, N. Sambanis, A. Florea, A. Florea, M. Karimi, S.M. Mousavi Shafaee, N. Spalding, N. Sambanis, ح. فاطمی, In Vitro Evaluation of Wound Healing Property of Hemigraphis Alternata (Burm. F) T. Anders Using Fibroblast and Endothelial Cells, Biosci Biotechnol Res Asia 8 (2016) 185–193. https://doi.org/10.2/JQUERY.MIN.JS.

[35] J. Yang, A. Chen, X. He, S. Lu, Fabrication of baicalein-encapsulated zeolitic imidazole framework as a novel nanocomposited wound closure material to persuade pH-responsive healing efficacy in post-caesarean section wound care, Int Wound J 20 (2023) 1921–1933.

[36] A.P. Roy, S. Jana, H. Das, P. Das, B. Chakraborty, P. Mukherjee, P. Datta, S. Mondal, B. Kundu, S.K. Nandi, Stimulated Full-Thickness Cutaneous Wound Healing with Bioactive Dressings of Zinc and Cobalt Ion-Doped Bioactive Glass-Coated Eggshell Membranes in a Diabetic Rabbit Model, ACS Biomater Sci Eng (2024). https://doi.org/10.1021/acsbiomaterials.4c00691.

[37] M. Vinayak, S. Jana, P. Datta, … H.D.-J. of D.D., undefined 2023, Accelerating full-thickness skin wound healing using Zinc and Cobalt doped-bioactive glass-coated eggshell membrane,

Elsevier (n.d.). https://www.sciencedirect.com/science/article/pii/S1773224723001259?casa_token=2XugW 0uF_XAAAAAA:ZvIbXHzu7SkNpapampzxoxvnM5HGcaV3ixpAvKtUYOuXi2kDHqd3kEX8UeI8V4 Wa0XR3gVSIKg (accessed June 4, 2024).

[38]   V. M.N, S. Jana, P. Datta, H. Das, B. Chakraborty, P. Mukherjee, S. Mondal, B. Kundu, S.K. Nandi, Accelerating full-thickness skin wound healing using Zinc and Cobalt doped-bioactive glass-coated eggshell membrane, J Drug Deliv Sci Technol 81 (2023) 104273. https://doi.org/10.1016/J.JDDST.2023.104273.

[39]   P. Kayal, S. Jana, P. Datta, H. Das, B. Kundu, S.K. Nandi, Microfibers of fish waste-derived collagen and ion-doped bioactive glass in stimulating the healing sequences in full-thickness cutaneous burn injury, J Drug Deliv Sci Technol 83 (2023). https://doi.org/10.1016/j.jddst.2023.104429.

[40]   S. Jana, P. Datta, H. Das, P.R. Ghosh, B. Kundu, S.K. Nandi, Engineering Vascularizing Electrospun Dermal Grafts by Integrating Fish Collagen and Ion-Doped Bioactive Glass, ACS Biomater Sci Eng 8 (2022) 734–752.

[41]   E. Negim, R. Rakhmetullayeva, G. Yeligbayeva, P. Urkimbaeva, S. Primzharova, D. Kaldybekov, J. Khatib, G. Mun, C. W., Improving biodegradability of polyvinyl alcohol/starch blend films for packaging applications, International Journal of Basic and Applied Sciences 3 (2014). https://doi.org/10.14419/IJBAS.V3I3.2842.

[42]   J. Song, S. Zhang, L. Du, C. Gao, L. Xie, Y. Shi, L. Su, Y. Ma, S. Ren, Synthesis, characterization and application of oligomeric proanthocyanidin-rich dual network hydrogels, Scientific Reports 2023 13:1 13 (2023) 1–10. https://doi.org/10.1038/s41598-023-42921-5.

[43]   N. Leblanc, R. Saiah, E. Beucher, R. Gattin, M. Castandet, J.M. Saiter, Structural investigation and thermal stability of new extruded wheat flour based polymeric materials, Carbohydr Polym 73 (2008) 548–557. https://doi.org/10.1016/J.CARBPOL.2007.12.034.

[44]   N. Leblanc, R. Saiah, E. Beucher, R. Gattin, M. Castandet, J.-M. Saiter, Structural investigation and thermal stability of new extruded wheat flour based polymeric materials, Carbohydr Polym 73 (2008) 548–557.

[45]   R. Saiah, P.A. Sreekumar, N. Leblanc, M. Castandet, J. Saiter, Study of wheat-flour-based agropolymers: influence of plasticizers on structure and aging behavior, Cereal Chem 84 (2007) 276–281.

[46]   J.J.G. Van Soest, S.H.D. Hulleman, D. De Wit, J.F.G. Vliegenthart, Crystallinity in starch bioplastics, Ind Crops Prod 5 (1996) 11–22.

[47]   G. Wypych, Handbook of Surface Improvement and Modification, Elsevier, 2023.

[48]   B.P. Dyett, A.H. Wu, R.N. Lamb, Mechanical Stability of Surface Architecture◌ Consequences for Superhydrophobicity, ACS Appl Mater Interfaces 6 (2014) 18380–18394.

[49]   H. Pingan, J. Mengjun, Z. Yanyan, H. Ling, A silica/PVA adhesive hybrid material with high transparency, thermostability and mechanical strength, RSC Adv 7 (2017) 2450–2459.

[50]   J. Kapusniak, P. Siemion, Thermal reactions of starch with long-chain unsaturated fatty acids. Part 2. Linoleic acid, J Food Eng 78 (2007) 323–332.

[51]   Starch, (n.d.). https://www.chembk.com/en/chem/Starch (accessed June 17, 2024).

[52] Y. Garavand, A. Taheri-garavand, F. Garavand, F. Shahbazi, D. Khodaei, I. Cacciotti, Starch-Polyvinyl Alcohol-Based Films Reinforced with Chitosan Nanoparticles: Physical, Mechanical, Structural, Thermal and Antimicrobial Properties, Applied Sciences 2022, Vol. 12, Page 1111 12 (2022) 1111. https://doi.org/10.3390/APP12031111.

[53] K. Tenorová, R. Masteiková, S. Pavloková, K. Kostelanská, J. Bernatonienė, D. Vetchý, Formulation and Evaluation of Novel Film Wound Dressing Based on Collagen/Microfibrillated Carboxymethylcellulose Blend, Pharmaceutics 14 (2022). https://doi.org/10.3390/PHARMACEUTICS14040782.

[54] N.N. Nasir, S.A. Othman, The Physical and Mechanical Properties of Corn-based Bioplastic Films with Different Starch and Glycerol Content, Journal of Physical Science 32 (2021) 89–101. https://doi.org/10.21315/JPS2021.32.3.7.

[55] G. Xia, D. Zhai, Y. Sun, L. Hou, X. Guo, L. Wang, Z. Li, F. Wang, Preparation of a novel asymmetric wettable chitosan-based sponge and its role in promoting chronic wound healing, Carbohydr Polym 227 (2020) 115296.

[56] T. Białopiotrowicz, Wettability of starch gel films, Food Hydrocoll 17 (2003) 141–147.

[57] J. Singh, P. Nayak, pH-responsive polymers for drug delivery: Trends and opportunities, Journal of Polymer Science 61 (2023) 2828–2850.

[58] A. Abram, A. Zore, U. Lipovž, A. Košak, M. Gavras, Ž. Boltežar, K. Bohinc, Bacterial Adhesion on Prosthetic and Orthotic Material Surfaces, Coatings 2021, Vol. 11, Page 1469 11 (2021) 1469. https://doi.org/10.3390/COATINGS11121469.

[59] P. Mulinti, J.E. Brooks, B. Lervick, J.E. Pullan, A.E. Brooks, Strategies to improve the hemocompatibility of biodegradable biomaterials, Hemocompatibility of Biomaterials for Clinical Applications: Blood-Biomaterials Interactions (2018) 253–278. https://doi.org/10.1016/B978-0-08-100497-5.00017-3.

[60] A. E2524-08, Standard test method for analysis of hemolytic properties of nanoparticles, (2013).

[61] N. Mayet, Y.E. Choonara, P. Kumar, L.K. Tomar, C. Tyagi, L.C. Du Toit, V. Pillay, A comprehensive review of advanced biopolymeric wound healing systems, J Pharm Sci 103 (2014) 2211–2230.

[62] A.M. Barnes, W.A. Cabral, M. Weis, E. Makareeva, E.L. Mertz, S. Leikin, D. Eyre, C. Trujillo, J.C. Marini, Absence of FKBP10 in recessive type XI osteogenesis imperfecta leads to diminished collagen cross-linking and reduced collagen deposition in extracellular matrix, Hum Mutat 33 (2012) 1589–1598. https://doi.org/10.1002/HUMU.22139.

[63] I. Negut, G. Dorcioman, V. Grumezescu, Scaffolds for Wound Healing Applications, Polymers (Basel) 12 (2020) 1–19. https://doi.org/10.3390/POLYM12092010.

Chapter VI

Conclusion and Future Perspective

6.1 Conclusion

This comprehensive study highlights the multifaceted potential of sustainable technologies in biomedical applications, integrating bioinformatics, biopolymer development, and optimized extraction methods. By identifying harmful nsSNPs in the GSK-3β protein, critical mutations that affect protein stability and function were highlighted, offering potential therapeutic targets. GSK-3β has a negative impact on wounds by modulating inflammatory responses, with deleterious mutations potentially altering the binding/active site structure and inhibiting inhibitors' effectiveness. This dysregulation can lead to increased pro-inflammatory cytokines and reduced angiogenic response during wound healing. Destabilized or hyperactive GSK-3β enhances NF-κB activity, driving inflammation and tissue damage. Various GSK-3β inhibitors, such as TDZD-8, LiCl, and SB216763, have been shown to mitigate inflammatory responses and promote tissue healing. Furthermore, GSK-3β plays a role in angiogenesis by controlling vascular cell migration and differentiation through the Wnt/β-catenin pathway. The aim was to create therapeutic agents that control inflammatory cytokines post-wound and promote angiogenesis and neovascularization, countering the effects of dysregulated GSK-3β.

The development of a mat composed of starch, gelatin, and grape seed extract (GSE) demonstrated biocompatibility, degradability, and effective wound healing, positioning it as a promising tissue engineering scaffold. Optimized proanthocyanidin extraction from grape seeds yielded a potent antioxidant extract, which, when formulated into a GSE-Gel, showed significant wound healing and anti-inflammatory properties both in vitro and in vivo. Polymeric films incorporating GSE exhibited excellent mechanical properties, thermal stability, biocompatibility, and antibacterial efficacy, making them suitable for sustainable wound dressing applications.

The molecular dynamics simulations revealed structural instability in the A83T mutant and structural stability in F67C and T138I mutants, with variations in flexibility, solvent accessibility, solvation energy, and total energy, indicating distinct structural and stability profiles compared to the native GSK-3β protein. These results have important implications given GSK-3β's extensive involvement in cellular and metabolic networks.

Overall, this study expands our understanding of complex molecular mechanisms contributing to disease vulnerability and cellular malfunction, offering new diagnostic and therapeutic approaches targeting harmful missense SNPs in GSK-3β. The incorporation of natural, renewable resources like grape seed extract into biomedical materials underscores the potential

for eco-friendly and sustainable healthcare solutions. The formulations and the biomaterials also promoted angiogenesis and controlled inflammation which might be caused due to the dysregulation of GSK-3β.

6.2 Future Scope

In vitro Analysis of GSK-3β on Wound Healing:

Investigate the specific effects of GSK-3β on wound healing using in vitro models. This would involve observing the modulation of inflammatory responses, cytokine production, and angiogenic processes in wound healing environments with varying levels of GSK-3β activity.

Effect of Proanthocyanidin on GSK-3β Regulation:

Assess the impact of proanthocyanidin, extracted from grape seeds, on the regulation of GSK-3β. This could involve studying its potential to modulate GSK-3β activity, reduce inflammatory responses, and promote angiogenesis in wound healing scenarios.

Deep analysis of the mechanism of action and effect biodegradation process for the wound dressing materials

Future research could focus on the detailed molecular mechanisms by which bioactive compounds in wound dressing materials, such as grape seed extract (GSE), interact with key regulatory pathways like GSK-3β. Specifically, studies could explore how GSK-3β inhibitors incorporated into wound dressings modulate inflammatory responses and promote angiogenesis at a cellular level. Additionally, further biodegradation studies of materials like starch, gelatin, and GSE can be conducted to assess their long-term biocompatibility and degradability in vivo, particularly in relation to their interaction with body fluids and tissues. Analyzing the release profiles of active components over time, combined with the impact of degradation products on wound healing, will provide insights for optimizing material performance in clinical settings.

Clinical Trials for Product Testing:

Conduct clinical trials to evaluate the safety, efficacy, and therapeutic potential of the developed wound healing products, including the starch, gelatin, and GSE-based mat and GSE-Gel formulations. Human trials would provide critical insights into the products' performance in real-world medical settings, paving the way for their potential use in clinical practice.

These future directions aim to validate the findings of this study, explore new therapeutic avenues, and ultimately translate these innovations into effective and sustainable healthcare solutions.

Finding the mechanism of action of wound healing and also the biodegradation process for the wound dressing materials

Report

7%

SIMILARITY INDEX

PRIMARY SOURCES

---

1   Sonali Jana, Pradyot Datta, Himanka Das, Prabal Ranjan Ghosh, Biswanath Kundu, Samit Kumar Nandi. "Engineering Vascularizing Electrospun Dermal Grafts by Integrating Fish Collagen and Ion-Doped Bioactive Glass", ACS Biomaterials Science & Engineering, 2022
Crossref

817 words — 1%

---

2   opus4.kobv.de
Internet

376 words — < 1%

---

3   dokumen.pub
Internet

374 words — < 1%

---

4   "Encyclopedia of Signaling Molecules", Springer Nature, 2018
Crossref

273 words — < 1%

---

5   Vinayak M.N, Sonali Jana, Pradyot Datta, Himanka Das et al. "Accelerating full-thickness skin wound healing using Zinc and Cobalt doped-bioactive glass-coated eggshell membrane", Journal of Drug Delivery Science and Technology, 2023
Crossref

217 words — < 1%

---

6   Pallabi Kayal, Sonali Jana, Pradyot Datta, Himanka Das, Biswanath Kundu, Samit Kumar Nandi. "Microfibers of fish waste-derived collagen and ion-doped bioactive glass in stimulating the healing sequences in

119 words — < 1%

phenotype: Fueling a wound that never heals", Mechanisms of Ageing and Development, 2021
Crossref

166 Tarique J, S.M. Sapuan, Khalina A, S.F.K. Sherwani, J. Yusuf, R.A. Ilyas. "Recent developments in sustainable Arrowroot (Maranta arundinacea Linn) starch biopolymers, fibres, biopolymer composites and their potential industrial applications: A review", Journal of Materials Research and Technology, 2021
6 words — < 1%
Crossref

167 Xin Zhou, Yanling Guo, Kun Yang, Peng Liu, Jun Wang. "The signaling pathways of traditional Chinese medicine in promoting diabetic wound healing", Journal of Ethnopharmacology, 2022
6 words — < 1%
Crossref

EXCLUDE QUOTES   ON   EXCLUDE SOURCES   OFF
EXCLUDE BIBLIOGRAPHY ON   EXCLUDE MATCHES   OFF